UNIVERSITÀ
DEGLI STUDI
DI PADOVA

Sede Amministrativa: Universita degli Studi di Padova

Dipartimento di Ingegneria Industriale

CORSO DI DOTTORATO DI RICERCA IN: INGEGNERIA INDUSTRIALE
(EVENTUALE) CURRICOLO: INGEGNERIA CHIMICA, DEI MATERIALI E MECCANICA
CICLO XXIX

MICRO-CUTTING OF DIFFICULT-TO-CUT-MATERIALS

Tesi redatta con il contributo finanziario della Fondazione Cassa di Risparmio di Padova e Rovigo (Cariparo)

Coordinatore: Ch.mo Prof. Paolo Colombo
Supervisore: Ch.mo Prof. Stefania Bruschi

Dottorando: Zdenka Rysava

PREFACE

Activities described in this work are the outcomes of three years Ph.D. studies at the University of Padova in Italy.

The tutorial of the study is guaranteed by the department of the Industrial engineering and the majority of activities have been carried out in the TE.SI. laboratory for precision and micro manufacturing which is situated in Rovigo.

First of all I would like to thank to my supervisor prof. Stefania Bruschi for her support, help and valuable advices during my research work, because without her this work would not be possible.

I would like also to thank to prof. Enrico Savio, Simone Carmignato and whole metrology group for their collaboration during the study.

My thanks belong too to prof. Leonardo De Chiffre and all the people at the Technical University of Denmark for their kind hospitality and support during my three moths stay in Lyngby.

This Ph.D. study would never be possible without prof. Miroslav Piska from Brno University of Technology and David Prat, Laurent Laboureau from Art et Metiers ParisTech, which were there during my previous academic studies, so I would like to express to them my sincere acknowledgments.

And obviously my thanks belongs also to all my colleagues from TE.SI. laboratory and laboratories in Padova.

Last but not least my greatest thanks belongs to my family, my friends and all the people, that I had chance to meet in my life and who helped me along the way and shaped me into who I€m now and without them I would be incomplete.

Thus I would like to dedicate this work to them. Thank you my beloveds.

Rovigo 15 November 2016 Zdenka Rysava

ABSTRACT

The objective of this Ph.D. thesis is to study the micro-cutting (micro-milling) of difficult-to-cut materials, devoted to the biomedical applications.

In the first part of this work the interest is aimed to the process and understanding the cutting mechanisms at this scale, in order to choose the most suitable cutting conditions on the basis of the final application.

The actual state-of-the-art in the micro-manufacturing technologies with the target to the micro-milling process was investigated, with the aim of a better understanding of the cutting process and its mechanisms at micro-level.

In particular, up to now, the machinability of difficult-to-cut metals have not been deeply investigated under micro-milling conditions, especially in combination with additive manufacturing (AM) technologies, such as Electron Beam Melting (EBM) and Direct Laser Sintering (DLS), which are more and more used in industry, especially in a biomedical field.

In the second part of this thesis different AM techniques will be studied and their influence on the final material properties especially in relation to the biomedical implants and their function.

Third part of this work consists of the micro-cutting experiments conducted on Ti6Al4V biomedical alloy produced by different AM techniques. Their performances in micro-cutting world are studied and compared especially in the regards of the final applications, thus the most relevant parameters are studied as the quality of the surface finish, burrs formation, microstructural alterations, surface defect, tool state after machining etc.

CONTENT

LIST OF FIGURES AND TABLES

1 STATE-OF-THE-ART

1.1 INTRODUCTION TO THE MICRO-MILLING

1.1.1 What is micro-manufacturing / micro-milling?

In the literature can be found some different definitions of micro-machining /micro-milling, since first research attempts till the latest interested in micro-technology when the definitions start to be more consolidated.

As a first intuitive definition we can imagine the micro-machining process as process of creating something very small.

Masuzawa in 2000 define micro-machining as the foundation of the technology to realize miniaturize products, where the size are in the range of 1 pm to 999 pm and the products are so small that they can€t be fabricated easily [1].

Later Dornfeld et al. mentioned again the definition of parts †too small to be machined easily‡ but then they determine micro-machining as †cutting of features with tool defined as mechanical engagement less than 1 mm with geometrically defined cutting edges‡[2].

Aramcharoen et al. mention the definition of the †nano/micro-scale cutting as the removal of undeformed chip thickness range from a few nanometre to a few microns‡[3].

In 2012 Cˆmara et al . come in their review with more consolidated and widely used definition of micro-machining based on the dimensions of the cutting tool (tool€s diameter) which is within the range from 1 to 1000 …mand in addition they add probably the most relevant aspect which defines micro-machining. It is the fact that the uncut chip thickness and work material grain size have dimensions comparable to the cutting edge radius [4].

1.1.2 Advantages and the characteristics of micro-milling process

With the development in the industry parts are becoming smaller and smaller, thus a demand on minimization is increasing for a wide range of components [2], [5]• [7]

There are many different reasons of miniaturizations: from demand or reducing weight, dimensions, batches, costs etc. [2].

All these miniaturized components have common requirements on small complex features with reliable and high accuracy and precision at the micro scale, while also ensuring high surface quality [2], [5], [6].

Based on these requirements micro-machining is becoming very promising technology, because offer a big potential in production of complex micro components with high tolerances [1], [2], [8].

It is due to the main advantages of micro-milling process a high flexibility which can be seen in the production of different size, shapes, features, creation of complex three dimensional features, 3D cavities, any possible curvatures, also high aspect ratio feature, micro-channels etc. [3], [9]• [11].

The flexibility is not only limited in the terms of geometrical characteristics of the components but also in terms of the material, because micro-milling technique can be use in very wide range of materials to be machined, almost unlimited choice is available, such as metallic alloys, ceramics, polymers and so on [4], [10]• [12].

Another unexceptionable advantages are the ease of the use, low set-up costs, high removal rates especially compared to other unconventional techniques (especially micro-electro-mechanical system based methods), and high relative precision [9]• [11].

In fact widely used electrochemical machining and electro discharge machining (EDM) is very limiting method compared to micro-milling because workpiece material selection is very restricted, process is characterized by poor productivity with low material removal rate and high cost [7], [13].

Further advantage of cutting process comes from its nature and it is direct contact between the tool with defined, known geometry and the workpiece surface itself [1].

Additional very interesting and maybe not so evident and unexpected advantage of micro-milling process it is ability of machining of brittle materials. In fact it was found that any material regardless its ductility can be machined under certain conditions in ductal mode with sufficiently small depth of the cut. In other words when cutting below a critical depth of the cut, [2], [5] and also taking into account the relative negative rake angle and promoting high hydrostatic stress thus brittle materials as glass can be machined in a ductile mode and achieved a good surface finish [4].

1.1.3 Typical applications of micro-machining / micro-milling process

As described in previous part, micro-milling has many of advantages so the range of applications is very wide.

Regarding geometrical features which can be machined, we can found micro-holes in case of micro-drilling, microgrooves and micro 3D

shapes in the case of micro-milling, micro-pins in micro-turning and micro-convex structures in the case of fly cutting [1].

In general an application of micro-machining is some of microsystem technologies [14].

If we want to talk about industrial fields we have to mention mainly:

- electronics [4], [7], [13], [15]
- biomedical, biotechnology and medical [1], [4], [7], [13], [15], [16]
- defence [16]
- aerospace [4], [7], [15]
- transportation [13]
- optics [7]
- communication and telecommunication [16] [13]

And here are stated some of most typical final product examples:

- Integrated circuits with micro-holes [1]
- fuel injections nozzles [1]
- microelectromechanical systems, [4]
- micro-moulds and dies [4], [13]
- biomedical components [4]
- micro-turbines and pumps [4]
- micro-motors [4]
- optical devices [4]
- photolithographic masks [4]
- measuring devices [4]
- heat sinks [4]

1.1.4 System requirements, main limitations and issues related to the micro-milling process

Particular challenge in micro-milling process is to fully understand its nature [5].

In micro-milling, many factors that are normally neglected in macro-milling become more important as vibration, deflection, temperature, microstructure of workpiece [10], [11], tool edge geometry, grain size and orientation [2] .

Micro-milling is not simple scaling down from conventional, macro-milling [6], [14]. Some of parameters can€t be scaled down analogically [14] and thus it has its own characteristics and several problems related to size effects and minimum chip thickness [6], [9]. The size effect has a significant role in process physics, which are closely related to the cutting mechanism [2].

Ploughing cutting and shearing are observed in micro-milling, beside simple shearing in macro-milling [7].

Thus controlling of micro- milling process is much more difficult [10].

In micro-milling, tools are very important but their fabrication is challenging. The geometry from †macro‡ tools is simplified, with many imprecisions and irregularities influencing the final ultraprecision of the machining process [2].

Another point is radius reduction of the tool edge to be able to realize small thicknesses of the cut [1]. The tool edge in micro-milling has greater effect on performances compared to macro-milling [7].

In general actual tools dispose the cutting edge radius between 1 and 3 …m[4]. Further decrease in cutting tool edge radius is limited by actual manufacturing technologies and the available grain size of the tool material [12].

Poor stiffness of the tool will promote tool run-out and thus the accuracy of the micro-milling process [2] even the run-out of few microns will have extensive impact on the process [7] leading in some cutting conditions (due to low feed) than some of the cutting teeth will not be in contact with the workpiece [12].

Also tool deflection become significant compared to macro-milling [7]. The deflection affects chip formation and accuracy of the desired surface [17].

Moreover the behaviour of the tools used in micro-milling is in general unpredictable with rapid tool wear [3], [7], [9], [11], [13], [16], often the catastrophic failure occurs due to chip clogging leading to fatigue failure promoted by high spindle speed. Also with increasing tool wear cutting forces will increase and leading to extreme load on tool shaft. In addition the chipped and cracked cutting edges will also influence the surface finish and burr [4]. Unlikely to conventional milling the premature tool failures happen at very low depths of cut and thus tool life increases with increase in axial depth-of-cut to a certain extent [15].

Regarding the machine itself there can be found many special requirements starting from ultraprecision in positioning accuracy [1] and precision of linear guides, spindles bearings, with high resolution of linear and rotary motions ensured by special motors and encoders

[2] with short response time, and also compensation of static and dynamic positioning errors. [4].

Obviously high dynamic and static stiffness of the machine is necessary [4].

Other requirement will be high thermal stability of the machine, because in this scale even a very small thermal distortion could lead in significant errors. This is also valid for thermal dilation of the spindle in Z axis and thus the axial depth of the cut can be strongly affected. [2], [4].

Spindles are integral part of the machine and obviously as the tool diameter is going down the ultra-high speed spindles are required in micro-milling to ensure sufficient cutting speed during cutting process. This is of course related also to dynamic characteristics of the spindle and for example even a small run-out will influence significantly the precision of the cutting [2].

Another big issue in micro-milling is severe burr formation, maybe it is the most critical aspect [4], [7], [9], [11], [16], [17], because it is one of main damages on micro-milled surface, moreover further removal is not really possible due to technical (position and tolerances) and economic reasons [4], [16].

Other limitations are chatter, tool alignment errors, high friction, quality [7], poor surface quality [7], [9], [11], tolerances and precision that can be achieved [16], as well as low material removal rate compared to conventional macro-machining [3], supported by low cutting sped limits [16].

1.2 MAIN PRINCIPLES AND LAWS OF MICRO-MILLING

1.2.1 Scaling down and size effect

As already mentioned at previous pages the sample scaling down of laws applicable in macro-machining into micro-machining is not possible.

And many researchers in recent years have been interested in the study of so called size effect [6].

A general definition of size effect could be found in a work of Vollertsen et al. where is mentioned that in fact it is not possible to ensure all rules and laws while up or down scaling and thus these limitations can be called size effects [18].

In the case of micro-milling, the main difference between micro and macro-manufacturing is in the cutting mechanism which differs even that the kinematic is same depending on the degree of size effect [2], [17], [19].

The size effect is primordial characteristics of the micro-milling process and will be more promoting while the down-scaling of the process is increasing [4], [6], [12], [19], [20].

In fact the downscaling starts to be highly significant when the ration of the dimensions to be produced, compared to the tool dimensions or to the size of microstructure becoming too small, in the range of units [2].

In other words the cutting edge radius becomes significant compared to the material thickens to be removed and in some cases the uncut chip thickness can reach dimensions comparable also to grain size of the material [3].

Therefore we can talk about two aspects of the size effect: (1) tooling/feature • comparable dimensions of the tool (cutting edge radius) to the features to be machined (layer to be removed) and (2) material • grain size comparable to the tool edge [2], [4], [6].

In this case the milling process starts to change in comparison to macro-milling and the previously stated assumptions (based on Marchant research) are violated. The tool can€t be any more supposed to be perfectly sharp. The †no contact‡ between the cutting tool and workpiece along clearance face is not ensure due to the spring back and also the chip is not always formed [3], [4], [7].

The Marchant€s assumption would ensure material removal mainly predominant by shearing process but as they are now violated, the machining process itself is becoming more complicated and no more simple shearing of the material is presented [3].

Tool edge radius becomes a very significant [20] and the process is thus influenced by introducing highly negative effective rake angle which prevails for small depth of the cut and will implement the ploughing mechanism into the cutting process followed by high spring back of the material due to elastic recovery and also the phenomena of minimum uncut chip thickens [2]• [4], [7], [9], [20], [21].

The most widespread definition of size effect in the case of micro-milling in the literature is the dramatic non-linear increase of the specific cutting energy while decreasing undeformed chip thickness [3], [6], [12], [14], [15], [18], [20].

Find possible explanation of the radical increase of the specific cutting energy is not easy. The high effective rake angle will increase difficulty in material separation, by promoting plastic-elastic deformations [9],

[18] and high shear flow will be present [4], [12], due to affected dislocation density in multi-phase materials [11]

Lai et al. found that the maximum effective stress with regard of size effect is much higher than in the case without considering size effect [6].

Ploughing in fact will contribute to the higher to strain rate. [2] [21], thus size effect increases strain and strain rate [18].

Lai et al. studied the specific shear energy and they have found that the size effect of micro-milling process is caused by the material strengthen behaviours [6]. Which is in concordance of statement made by Fleischer et al., they mention that due to work hardening at each single machined layer, the specific cutting forces will rise with each hardened layer [14]. Also Vollertsen et al. are promoting the material strengthening as the reason of the size effect, material strengthening is due to the increase of strain rate in the primary deformation zone for decreasing undeformed chip thickness [18].

In fact the mechanisms in the case of very small undeformed chip thickness is similar and can be modelled by indentation size effects [18], when a strong material strengthening is also present [6].

Afazov et al., also explain the size effect by the material strengthening mechanisms and they add the possible causes of this strengthening (1.) the decreasing number of defects in microstructure, (2.) the increasing strain rate at the primary shear zone, (3.) the effect of thermal softening and (4.) the effect of strain gradient plasticity at the deformation zones at low uncut chip thickness [12].

For the material which is at conventional milling scale considered to be homogenous and isotropic, while the uncut chip thickness and depth of cut will be decreased, grain boundaries, crystal defects and impurities will become significant for cutting process by affecting the slip process [4]. In some literature material inhomogeneity is also described as the origin of size effects [18]. In fact there is lowest probability to meet any material inhomogeneity or defects, which would help to decrease shear stress and strain when decreasing the size of the removed material [20].

To conclude, the size effect has great impact to micro-milling process and primarily will influence the cutting force, chip thickness, chip formation and quality of machined surface [3], [12].

It can be seen that the roughness is not corresponding to the mechanism where only geometrical consideration are taken into account but also some other mechanisms, especially minimum chip thickness, ploughing, and elastic recovery effects have to be considered too [21].

Another problem is strong burr formation promoted by ploughing mechanism [12], [19] and we can€t forget to mention also increased and dramatic tool wear [12].

Cutting edge radius and multiple machining are thus very important parameters influencing the size effect [14].

1.2.2 Minimum chip thickness phenomenon

As it has been mentioned in previous chapters, the micro-milling process is different from conventional milling and it is not just a simple scaling down, the machining mechanism differs. In fact in micro-milling the chip will not be always formed, not at each tooth pass and we talk about the criteria of minimum chip thickness [3], [17], [22].

Moreover the sharpness of the tool is an big issue as also discussed before. In Fig. 1. we can see in the case (a) is shown example in conventional cutting where the tool can be supposed to be perfectly sharp and in (b) due to the small uncut chip thickness the highly negative rake angle is introduced and will be determining the minimum chip thickness phenomena [4], [21]• [23].

In other words the cutting edge radius is in the same range of dimensions as the uncut chip thicknesses [2], [3], [17], [20], [22], [23].

Cutting edge radius of the tool is one of the most significant parameter in micro-machining. And it is believed to be also the main parameter influencing the minimum chip thickness [3], [6], [17], [22]• [24], the material properties are secondary [2].

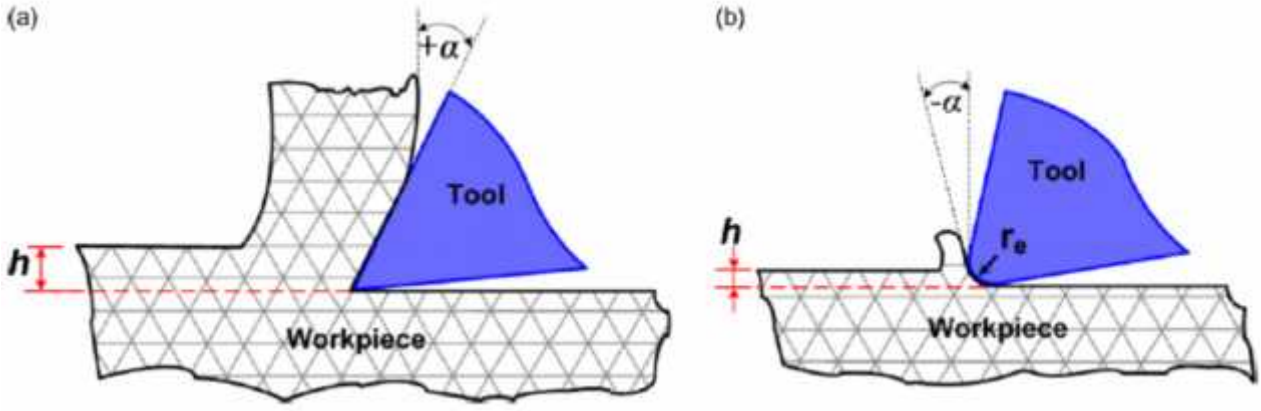

Figure 1 (a) Conventional cutting vs. (b) micro-cutting [3]

The minimum chip thickness is a boundary/limit between two phenomena, ploughing and shearing mechanism [3], [12]. In fact it can be related to the resistivity of the material to plastic deformation, similar as in the case of indentation hardness tests, or scratching [21], [22]. Liu et al., states that minimum uncut chip thickness reflects the behaviour of the material under extreme mechanical condition [23].

The minimum chip thickness can be defined as formation of chip when the uncut chip thickness becomes greater than a minimum chip thickness [17], [19], [22], [24].

Normalized minimum chip thickness can be expressed also as ration of the uncut chip thickness to cutting edge radius and if the value of the uncut chip thickness is lower ten this critical value, no chip will be formed [3], [22]• [24], depending also on the relation of the tool/material [21] as explained in the chapter dedicated to size effect.

We can deference 3 stages (as shown in the Fig. 2): (1) when the uncut chip thickens (h) is smaller than minimum chip thickens (h_m) the chip is not formed. The material is manly pushed and pressed under the tool without forming the chip and once the tool is passed by, the material springs back due to the elastic recovery, property of the material. This mechanism is called ploughing. (2) second stage corresponds to the uncut chip thickness (h) equal to minimum chip thickness (h_m) and at this moment the chip start to be formed, shearing process start to occur, but still a portion of elastic recovery is presented in the process. Finally at the stage (3) when the uncut chip thickens (h) is bigger than then minimum chip thickness (h_m) the chip is formed and shearing process is predominant [2]• [4], [6], [12], [17], [20]• [24].

In the case of orthogonal cutting, the uncut chip thickness is corresponding to the axial depth of the cut [23].

In the micro-slot milling the uncut chip thickness is a function of the rotation angle as shown in Fig. 3. The instantaneous uncut chip thickness varies from zero when the tool enters into the material to the maximal value approximately located in the middle of the slot, which is equal to the feed per tooth and then the thickness is again progressively decreased to the zero at the exit from the material. The chip will not be formed until the tool will rotate to a certain angle at which instantaneous chip thickness will reach the minim chip thickness value [3], [9], [11], [17], [19], [21], [24].

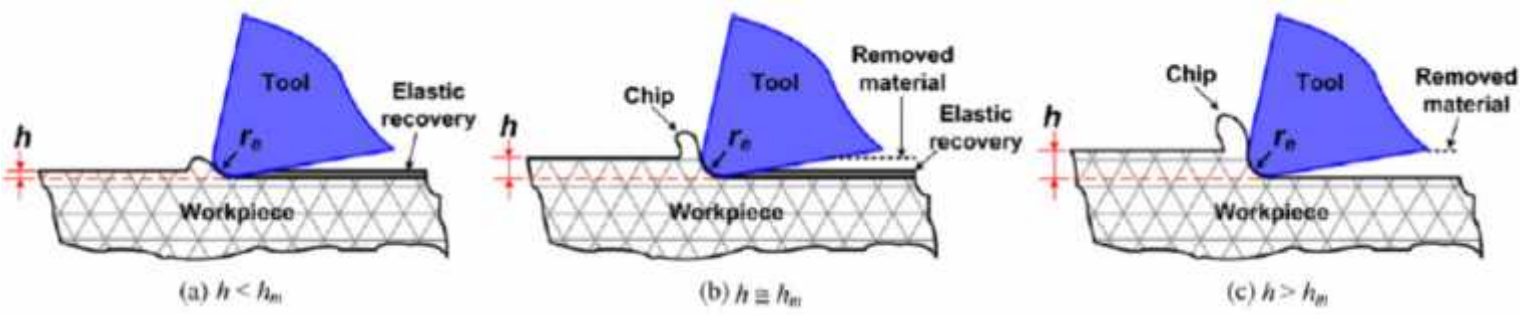

Figure 2 Different stage of micro-cutting (a) uncut chip thickness is smaller than minimum chip thickness, (b) uncut chip thickness is equal to minimum chip thickness and (c) uncut chip thickness is higher than minimum chip thickness [3]

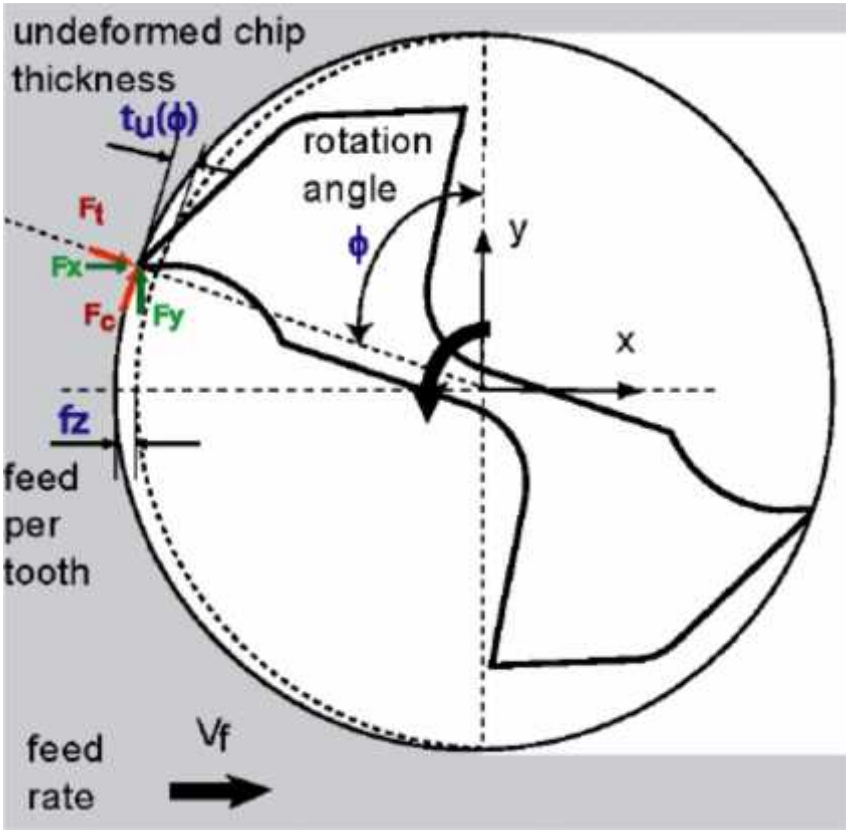

Figure 3 Instantaneous chip thickness in micro-slot milling [19]

The determination of minimum chip thickness is essential in the micro‰milling, as the minimum chip thickness will determine which cutting mechanism is predominant (shearing or ploughing) and consequently also the quality of the final product. So it is important to know the minimum chip thickness to choose appropriate cutting conditions [2], [3], [22]• [24].

When the feed per tooth is smaller than the cutting edge radius, and thus the minimum chip thickness criteria is not ensured, chip will not be formed [3], [9], [22], smaller edge radius causes early formation of minimum chip thickness and thus minimizing ploughing and conversely bigger or worn cutting edge radius will result in ploughing of the workpiece [3], [4], [17], [19], [24].

It should be also mentioned that a larger cutting edge could prevent rapid tool wear, which might be preferable and thus the choice of appropriate cutting edge radius should be question of compromise [20].

The switching between the two mechanisms is followed by deterioration of the workpiece quality. It is especially due to ploughing regime, that itself is accompanied by many negative aspects as damaged surfaces due to forces, vibrations, plastic deformation, higher burrs formation [3], [9], [12], [22], [23], tool wear, poor surface integrity and poor process stability [9], [22], [24].

The roughness itself is playing important role and is influenced by many parameters, firstly tool, its cutting edge radius, its sharpens, obviously sharper tool, smaller radius, better surface finish can be achieved, another important factor is the material characteristics itself as the microstructure, grain size, hardness [3].

Regarding the behaviour of the roughness we can split it into two regions. First when the ration of uncut chip thickness to the cutting edge radius is less than 1 (the minimum chip thickness criterion is not ensured) the roughness will decrease with increasing the load. In fact while increasing the load (feed pert tooth), the ploughing is minimizing thus elastic recovery of the material is minimised [2], [3], [10], [11], [20]• [23] and shearing becomes to be more and more present in the process until the boundary condition is reached when the ration is equal to 1 and shearing is becoming predominant. When the ration is bigger, the minimum chip thickness is ensured and with further increasing of the load/feed per tooth the roughness is increased too, which is well known from conventional cutting process [3], [4], [11], [22].

Liu et al., as well as later other authors state even that the minimum chip thickens is the main limiting factor while achieving desired roughness because the ploughing process will strongly deteriorate the

surface when the uncut chip thickness will be below the critical value [3], [4], [8], [17], [19], [22]• [24].

Aramcharoen and Mativenga [3] have been studied the trend of roughness and specific cutting force as the function of the ration of uncut chip thickness. In the Fig. 4 we can see the trend of the surface roughness in function of the ration of uncut chip thickness to the cutting edge radius, with clearly visible minimum when the ration is equal to 1 and the two different regions where the roughness behaviour is opposite, as described in previous paragraph.

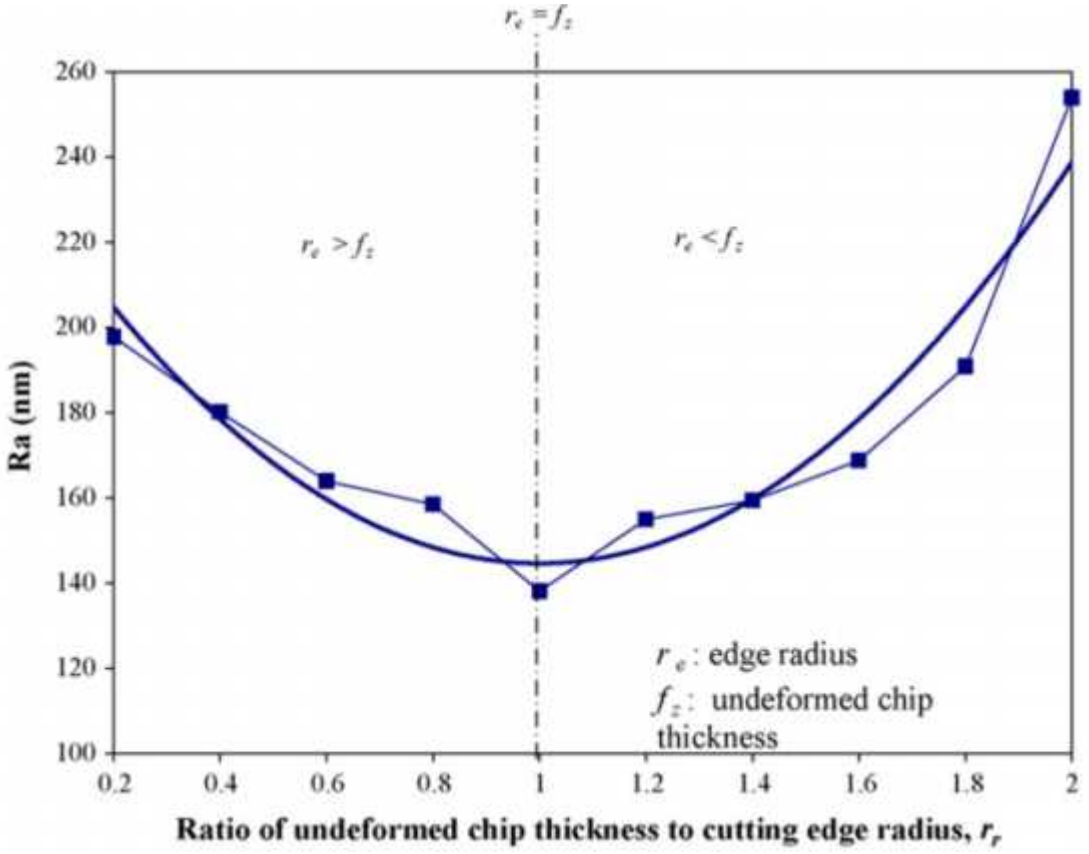

Figure 4 Roughness in function of ration of uncut chip thickness to cutting edge radius [3]

In the Fig. 5 there is shown the graph of the specific cutting force as the function of the ration of uncut chip thickness. We can see a clear increase of specific cutting force for the case when the ration is smaller then 1, in fact when the thickness is less then minimum chip thickness.

Lai et al., [6] explain the increase by the ploughing phenomenon and accumulation of the actual chip thickness. Birermann and Dornfeld [2], [20] arrive to the same conclusion that the specific cutting force increase is mainly due to ploughing effects at low uncut chip thickens and another side effect is also high burr formation.

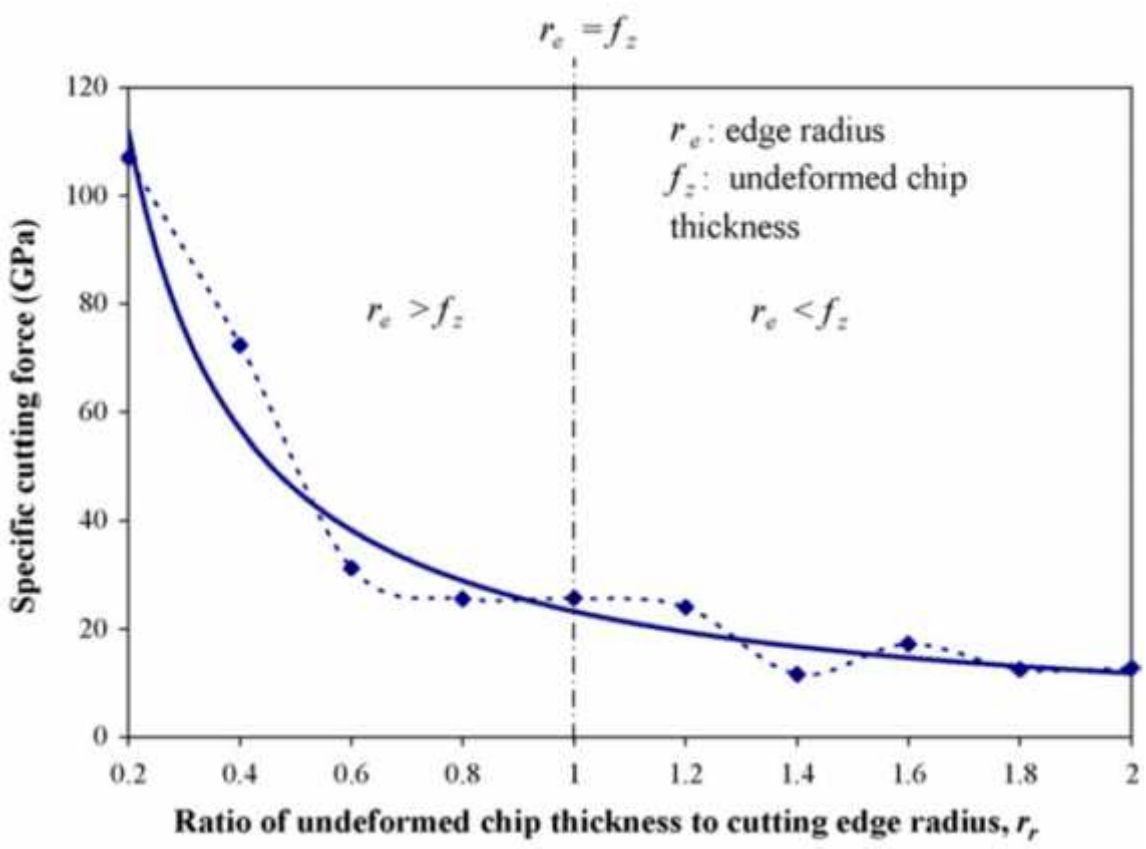

Figure 5 Specific cutting energy as a function of minimum chip thickness [3]

Thepsonthi and Ozel [11] were studying the influence of the most important cutting parameters on the micro-milling process while evaluating roughness and burr formation in their work. In the Fig. 6 are shown main effects plots while evaluating the importance of the tool coating, spindle speed, feed and axial depth of cut.

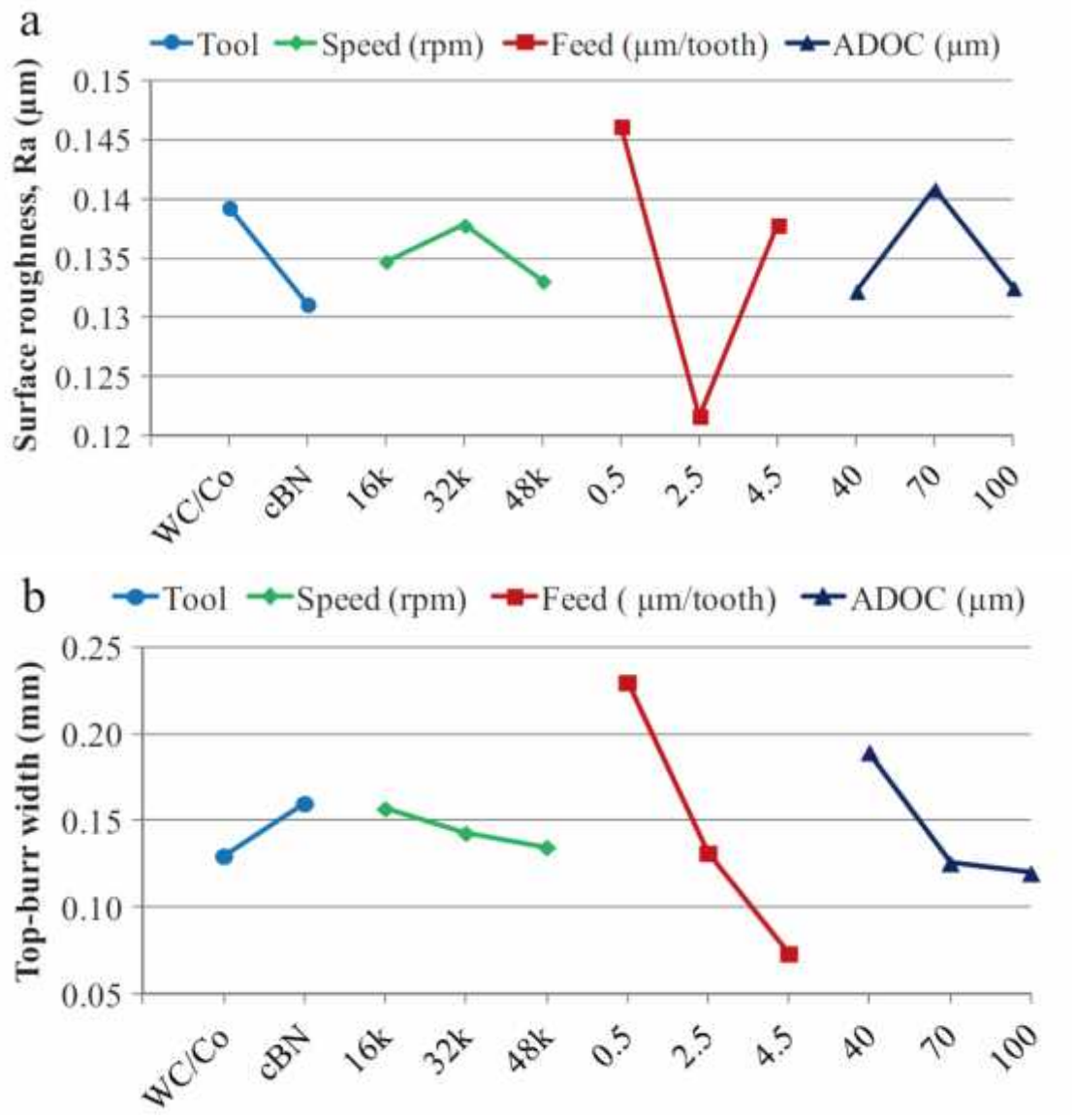

Figure 6 Main effect plots (a) for roughness and (b) burr size [11]

From the Fig. 6 is evident that the feed pert tooth is the most significant factor, which will influence roughness and burr size. In fact feed per tooth is related to the uncut chip thickness [11]. And as we have seen before the ration of the uncut chip thickens to cutting edge radius is the most critical parameter, thus feed per toot is the main parameter to be appropriately chosen during micro-milling.

Thepsonthi and Ozel determine that the minimum chip thickness in the cutting of titanium alloy Ti-6Al-4V is about 10• 20% of the cutting edge radius [11].

Liu et al., [22] have been studied the phenomenon of minimum chip thickness, their work is reputed for one of the most significant in the domain of the minimum chip thickness phenomenon. They have set the normalized minimum chip thickness which is determined by its own thermomechanical properties such as yield strength, ductility and is sensitive to the temperature, strain, and strain rate.

They study scratching process with its transition between plastic deformation and micro-cutting to better predict the normalized minimum chip thickness. In fact the similarity between micro-cutting and scratching is in normal pressures and relative lateral motion exerted in both cases [22].

They are using the Johnson-Cook model to describe the effective flow stress as a function of strain, strain rate and temperature. The equation is combination of three effects: strain hardening effect, strain rate effect, and thermal softening effect [22].

They found that in micro-machining is another heat source. Its origin comes from ploughing effect close to the dead metal cap due to the finite tool edge radius. This heat source influence strongly the final amount of generated heat and cutting temperatures [22].

For their further modelling they are using slip line model. As we can see in the Fig. 7 the zone denoted by letters ACD shows a dead-metal cap, due to the tool edge radius. A is the material separation point. Primary shearing zone with slip line BNMK, ploughing zone with slip line KJIHC and frictional interface AC and AD, and also frictional interface between tool and chip DF [22].

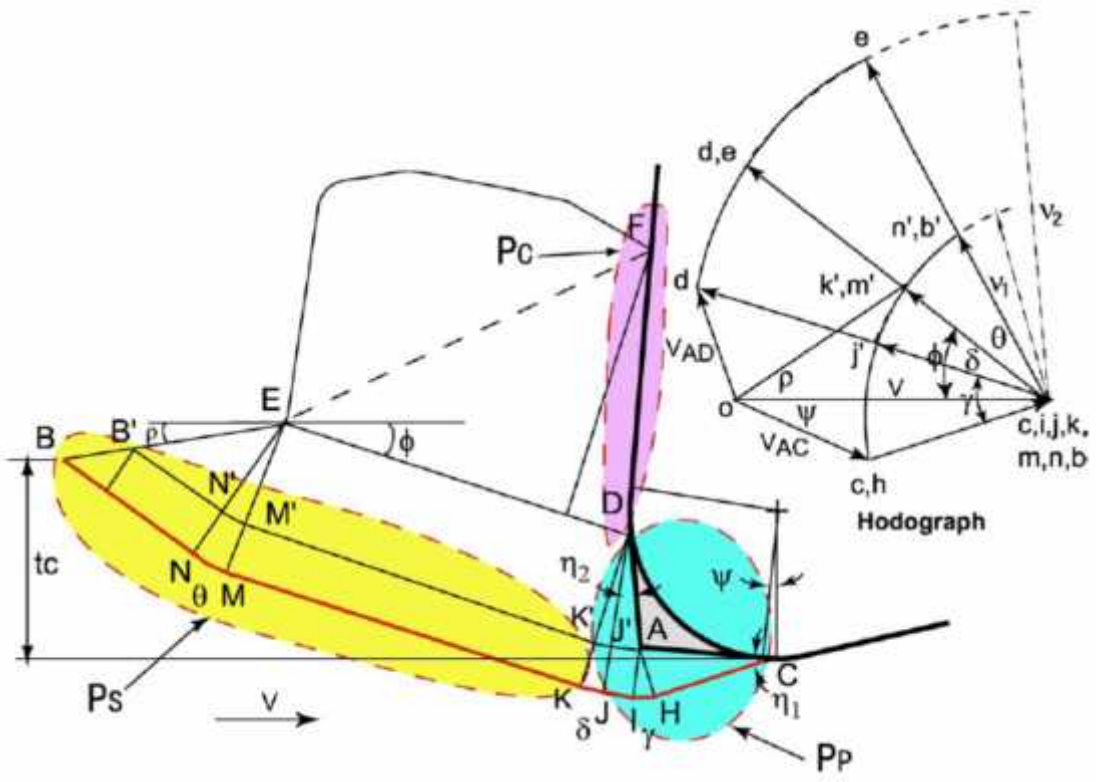

Figure 7 Slip-line model by [22]

In the Fig. 8 is shown sidewall surface generation taking into account minimum chip thickness effect by Liu et al., [22]. Let€s suppose that ABC is the machined surface from previous operation, now during the next pass the cutting edge starts to enter into the material at point A, starting with instantaneous uncut chip thickness going from 0 to its maximal value, following the trajectory ADE. But as the uncut chip thickness is under the critical value, no chip is formed. Supposing that the critical value will be reached at the position E and chip starts to be created. The material in zone ABCED will be undergoing the ploughing with elastic recovery and thus will not be removed from the surface, once the tool has gone, it will spring back to the original position and a †step‡ designed as CE in created. So the height CE is supposed to correspond to the value of the minimum chip thickness necessary to create a chip [22].

Liu et al., have verified this expectation by observation of the side walls under SEM and the changes in machined surface height were clearly seen, while leaving a thickness correspond to minimum chip thickness on the machined surface profile as shown in the Fig. 9 [22].

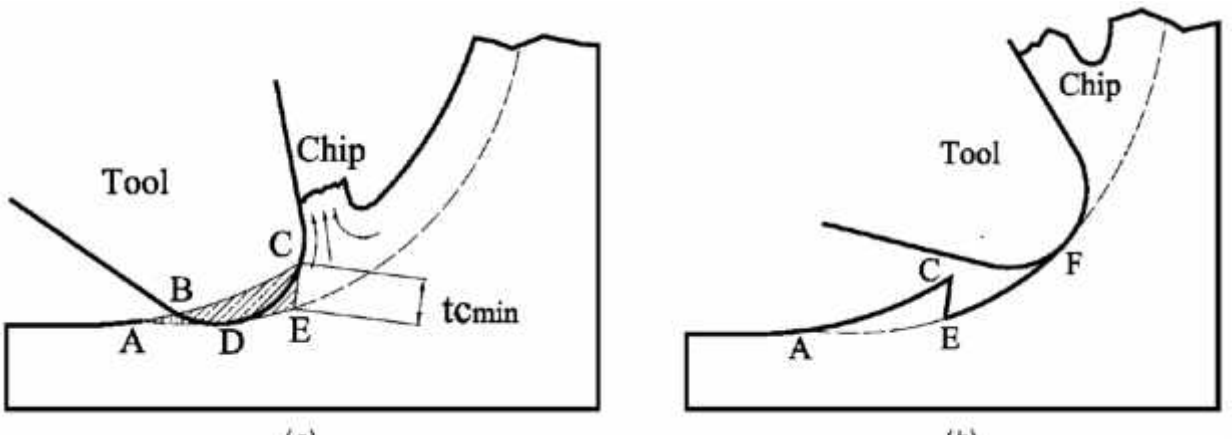

Figure 8 Sidewall surface generation [22]

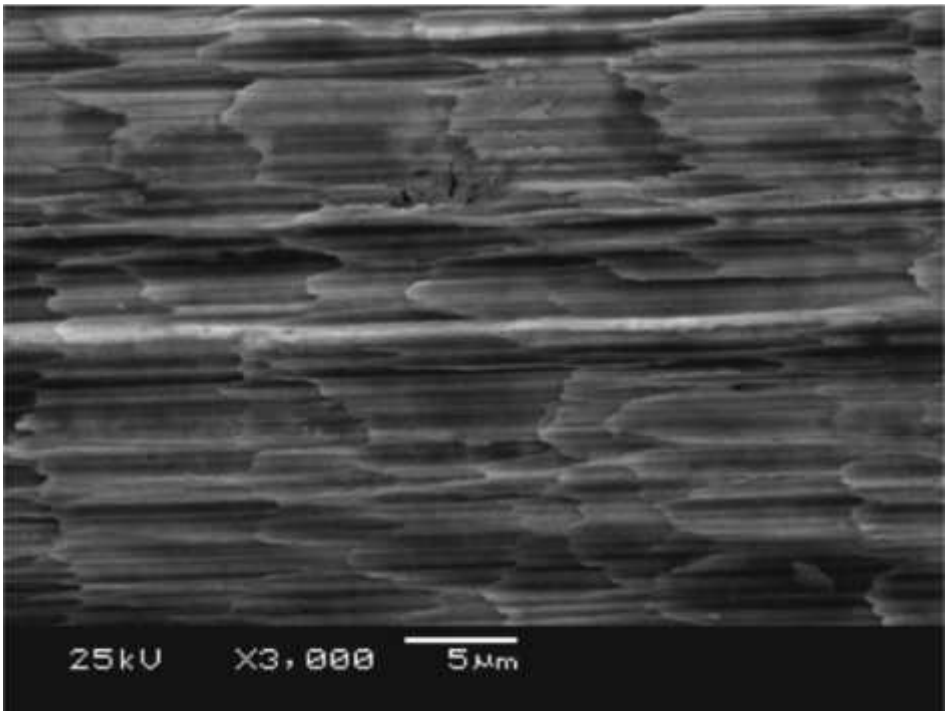

Figure 9 SEM image of sidewall surface with left t_{min} [22]

Liu et al., measure the height of this minimum chip thickness and then they determine the normalized minimum chip thickness as the ration of this minimum chip thickness to the cutting edge radius [22].

In the Fig. 10 can be seen the extracted and measured minimum chip thickness by Liu et al.

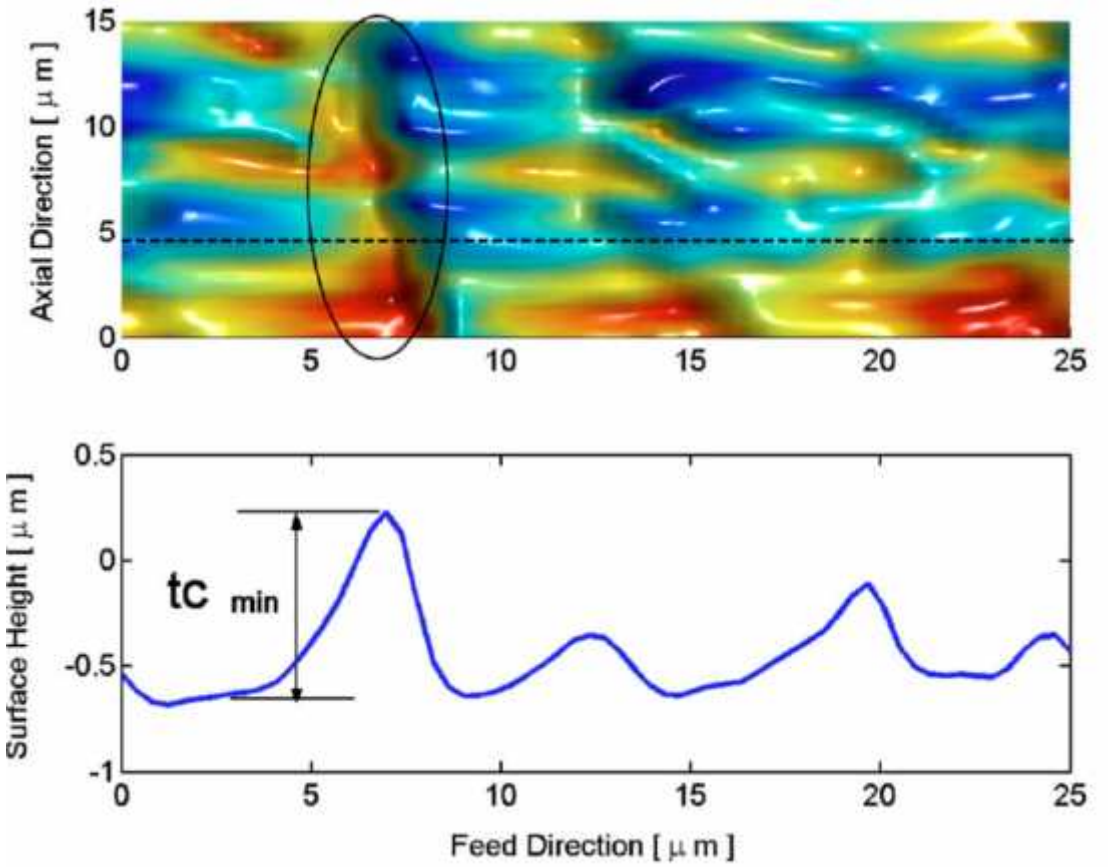

Figure 10 Extracted minimum chip thickness [22]

Liu at al., have found that in the case of carbon steel, normalised minimum chip thickness will increase with the increase of cutting speed, due to predominance of the thermal softening effect over the strain hardening effect [22].

Regarding the cutting edge radius they have confirmed that with increasing the radius, ploughing becomes more dominant, thus causes higher cutting forces, higher energy dissipation and higher cutting temperatures. Higher temperatures will introduce higher ductility and so the normalized minimum chip thickness becomes higher [22].

They have also shown that for higher carbon content, it is larger normalized minimum chip thickness [22].

Woon and Rahman [25] were studying the influences of the minimum chip thickness and the cutting process in the range of the cutting condition close to the minimum chip thickness criteria.

In conventional cutting, when the uncut chip thickness is large and the cutting tool radius is fixed, the resulting force R will be applied towards the cutting direction, forming an angle θ between its vector and the

vector of cutting force as shown in the Fig. 11, in this case the angle θ is very small. While the ratio of uncut chip thickness to the cutting edge radius will decrease the angle Š will be increasing and shifting the direction of the vector towards the thrust force vector. So the process becomes more thrust dominating [25].

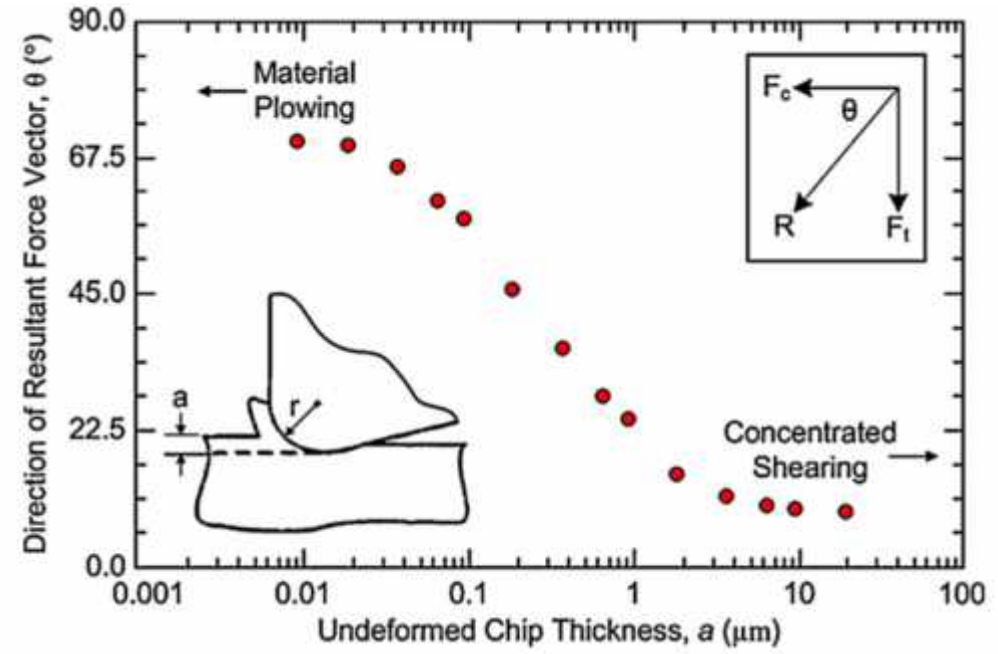

Figure 11 Transition of the resulting force vector direction for different uncut chip thickness [25]

Regarding the deformation zones, when the ratio of uncut chip thickness to cutting edge radius is bigger then 1, there is positive rake angle, primary deformation zone and secondary deformation zone on the rake face of the tool. But when the ratio is decreasing the negative rake angle is introducing, when the radio is reaching value of 1, the small negative rake angle is present and the secondary deformation zone is starting to be suppressed, while the ratio is decreasing under 1, the negative rake angle is more drastic and the secondary deformation zone disappears completely while the primary deformation zone is becoming highly localized and discontinuous chips are produced intermittently [25].

Woon and Rahman have found that at specific ratio of uncut chip thickness (a) to cutting edge radius (r) lower to 1, a continuous chip is extruded at negative rake angle and while the thrush force component is bigger than cutting force component [25].

They call this process as extrusion-like chip formation and they explain that the boundary of elastic• plastic deformation assumes the role of a die wall of an extrusion-forming process together with the tool edge radius as an ‹imaginary€ die set Thus in the micro-machining the extrusion occurs while producing extruded chip [25].

Woon and Rahman explain the process by Le-Chatelier€s principle which claims that if the system is subjected to some external impact which will push the system out of equilibrium, the system will apply processes to mitigate the results of this impact and come back to equilibrium. In this case of micro-machining the boundary of elastic• plastic deformation is redistributed while the external loading is increasing at each momentary states of equilibrium. As the chip size and deformation zone are increasing obviously the loading is increasing too. But the system is trying to keep the equilibrium by compensating this external loading and thus micro-catastrophic event like void nucleation is reduced by the boundary inclination as is shown in Fig. 12 [25].

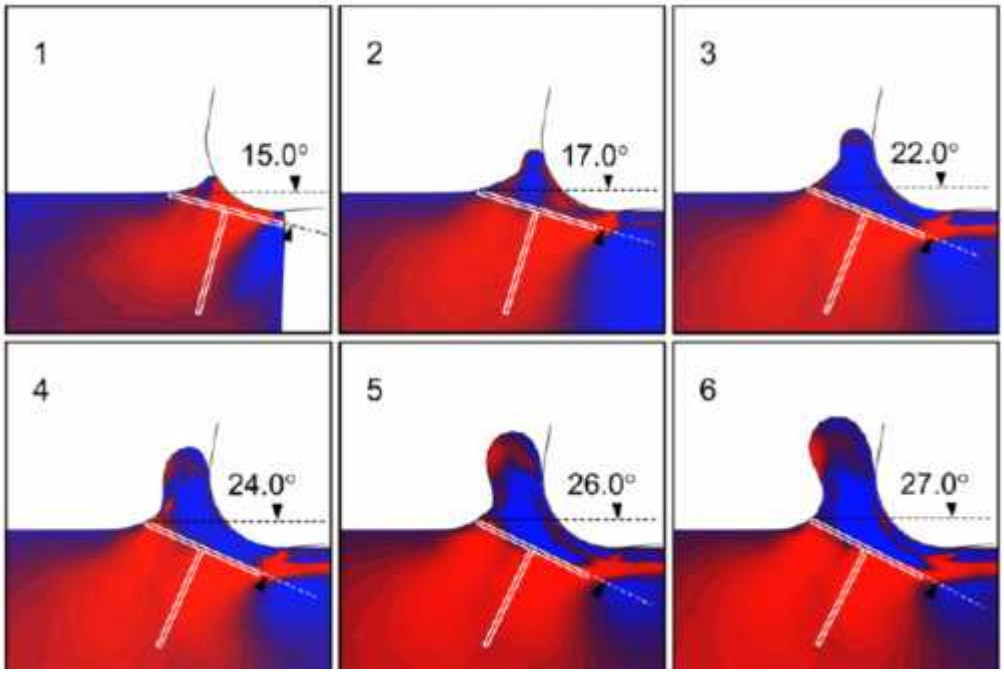

Figure 12 Redistribution of the elastic-plastic boundary during the extrusion-like chip cutting [25]

Not only boundary inclination is trying to oppose to the increased loading, but also active compressive stress and the reactive hydrostatic pressure from the bulk matrix react strongly prevent the

nucleation [25]. In the Fig. 13 are shown different stress states undergone by the material during extrusion-like chip cutting.

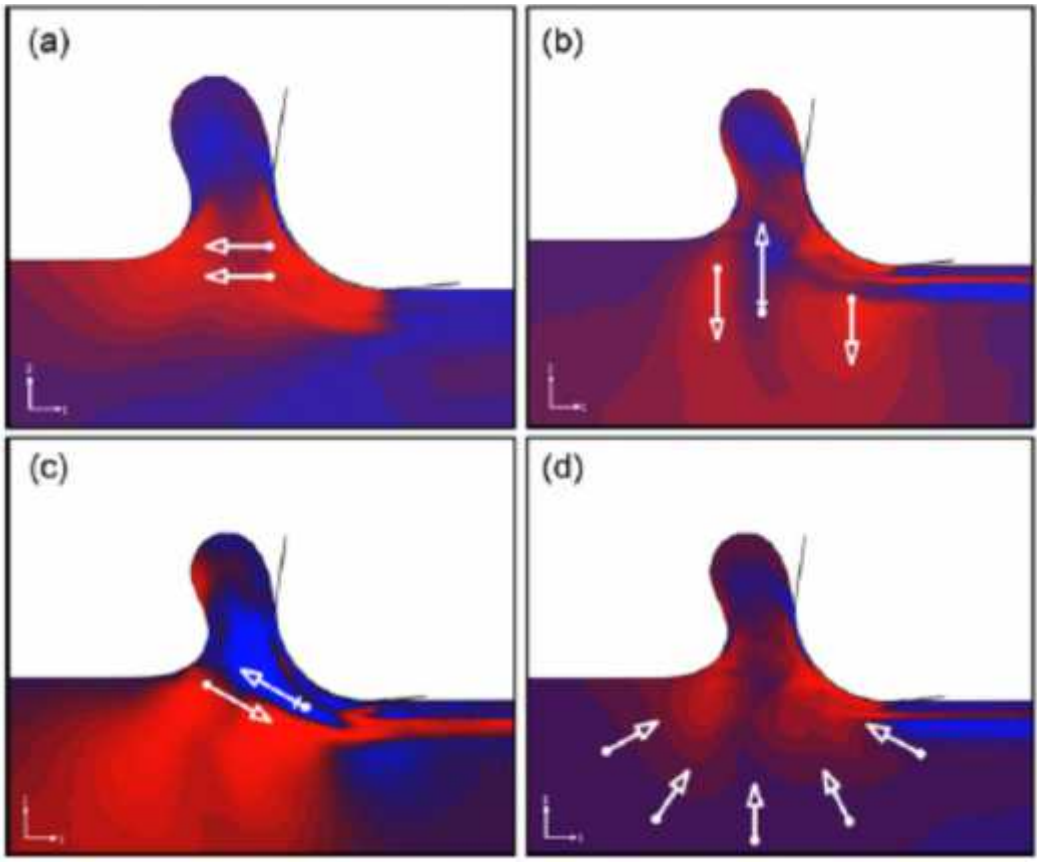

Figure 13 Stress states of extrusion-like chip cutting (a) principal horizontal stress, (b) principal vertical stress, (c) shear stress, (d) hydrostatic stress [25]

Woon and Rahman demonstrated that the surface quality improves with decreasing ratio of uncut chip thickness to the cutting edge radius, reaching exceptional surface finish approaching the quality of grinded surfaces while cutting under condition of the extrusion-like chip formation mechanism. In Fig. 14 are shown pictures of chips cut for different ratios of uncut chip thickness to cutting edge radius [25].

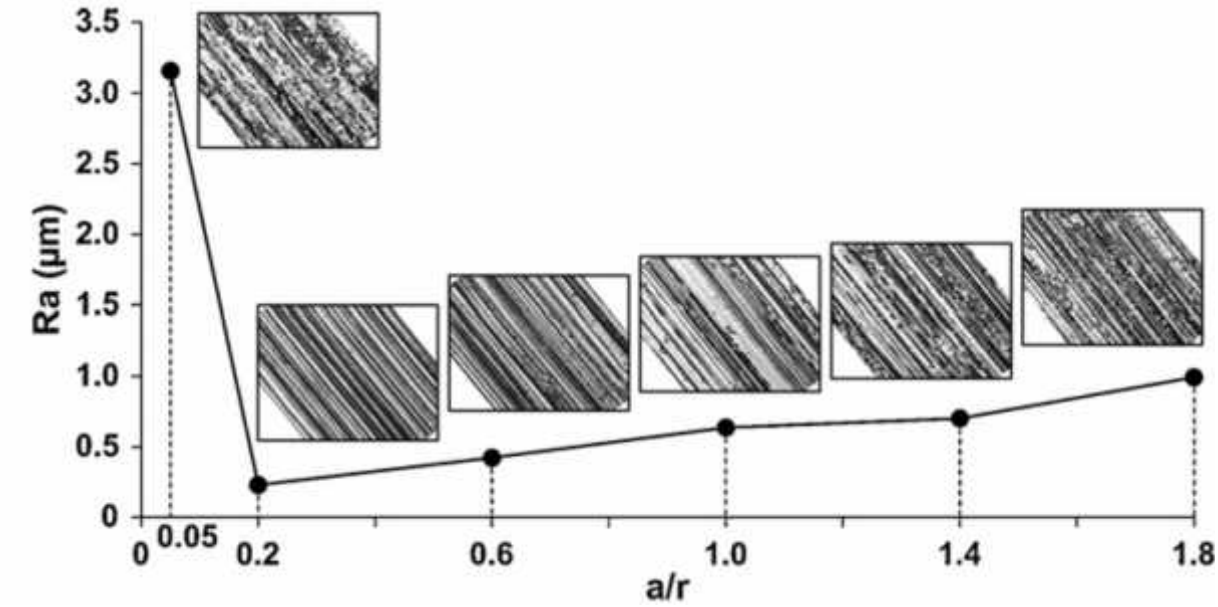

Figure 14 Surface roughness for different values of ratio of uncut chip thickness to cutting edge radius [25]

It is visible that the best surface finish is achieved at some specific critical value of the ratio, further decreasing will not improve the surface quality [25].

Thus the extrusion-like chip formation is activated at a critical value of the ratio, due to the tool edge radius, creating negative rake angle. This mechanism involves severe localized stress, void nucleation is prevented through the redistribution of plastic-elastic deformation boundary [25].

Also Camara et al mention the mechanism of quasi-shear-extrusion of the softer grain (ferrite) in the case of steel micro-cutting. When the uncut chip thickness becomes smaller than the average grain size [4].

1.2.3 Microstructural influences

The material microstructure has a significant impact on micro-machining. At micro scale, when the tool or the features to be machined are in the same order as the grain size, the material properties become non-homogeneous and non-isotropic [2], [12], [26].

Micro-machining of multi phases or multi grains materials exhibits changes in various parameters, such as cutting force, chip formation, and surface roughness [2].

Material properties as microstructure, hardness and phases influence the minimum chip thickness. In fact when micromachining inhomogeneous, multi-phase material with different hardness, ductility, different ratios of cutting radius to grain size will be reached and thus the cutting process, mechanism might change between different phases [3].

The minimum chip thickness value in multiphase materials is lower for a harder phase than for a softer phase. Obviously this variation in minimum chip thickness can cause switching between different cutting mechanisms for different phases and consequently affecting surface quality [8].

As the cutting process might vary between different grains also the surface roughness varies between the grains of material. Beside the parameters influencing the roughness as discussed in previous chapter (tool edge radius, minimum chip thickness effects, elastic recovery), material properties will influence strongly roughness too especially microstructure phases, crystallographic orientation, material and phase dependent elastic-plastic anisotropy [8].

Concerning the grain size, smaller is preferable. Because the chip formation will take place at scale similar to the individual grains, the ratio of grain size to uncut chip thickness is close to one and tool is forced to fracture a single grain [4], [8], it is thus preferable to use ultra-fine grain, hard and high homogeneous workpiece materials [8].

Also Camara et al., suggest to use homogenized grains with smaller average grain size and thus minimized the spring back effect [4]. In fact the different elastic recovery between phases causes higher surface roughness compared to single phase material cutting [8].

The elastic recovery of the grains depends on crystallographic orientation and material phase, thus the surface roughness varies between the grains of the material [21].

In the case of single crystal face centred cubic (FCC.) materials, intrinsic plastic behaviour of individual crystals seems to be more significant parameter on surface roughness than crystallographic cutting direction [8].

In the Fig. 15 and 16 is clearly visible the difference between the grains and its different elastic recovery / spring back. Some grains look like be placed lower and another higher, creating 3D effect instead of desired flat surface. In the Fig. 15 (b) is shown that the difference in the height between perlite and ferrite phase can be about 0.7 μm.

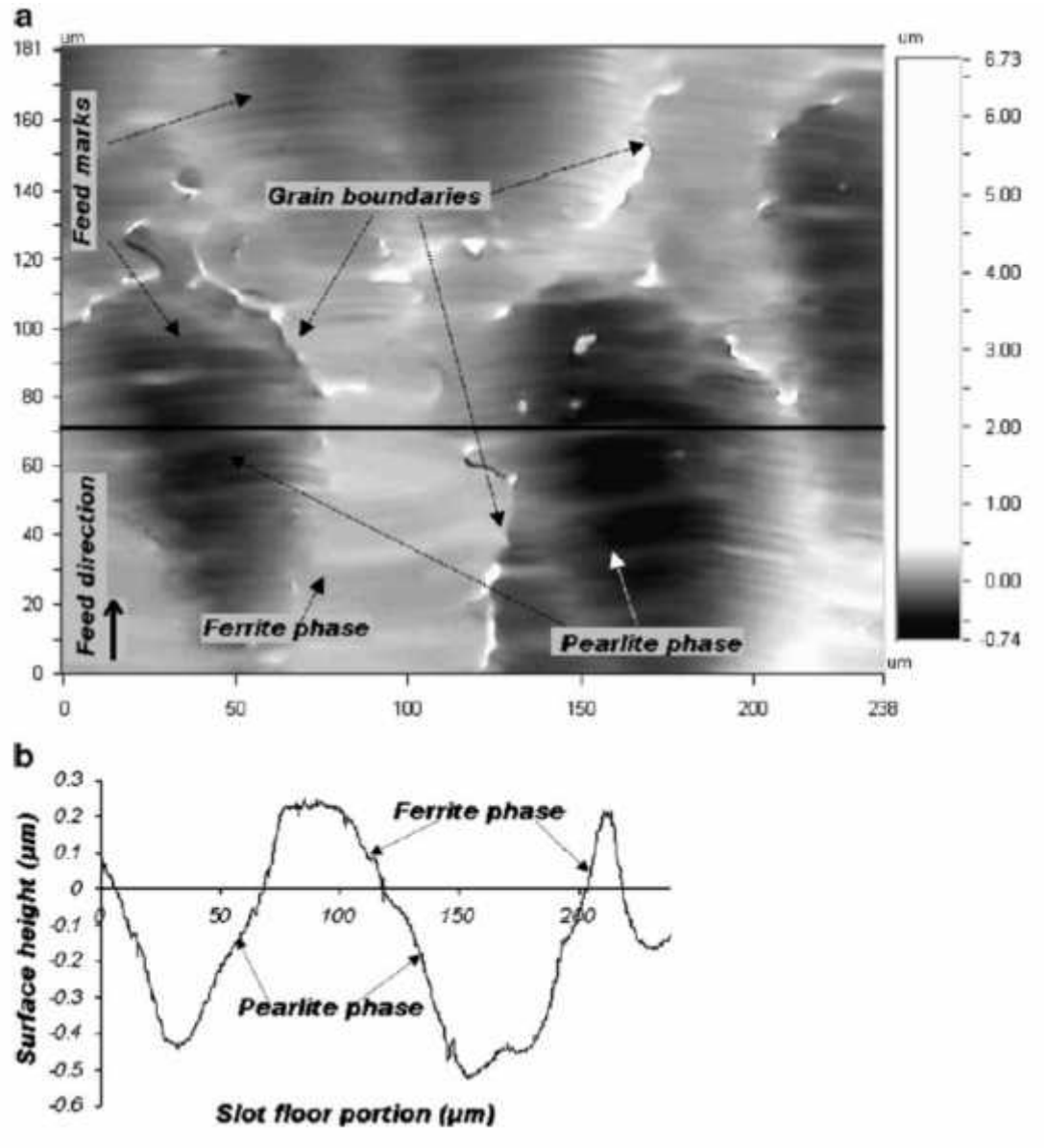

Figure 15 Phase influence on surface quality [8]

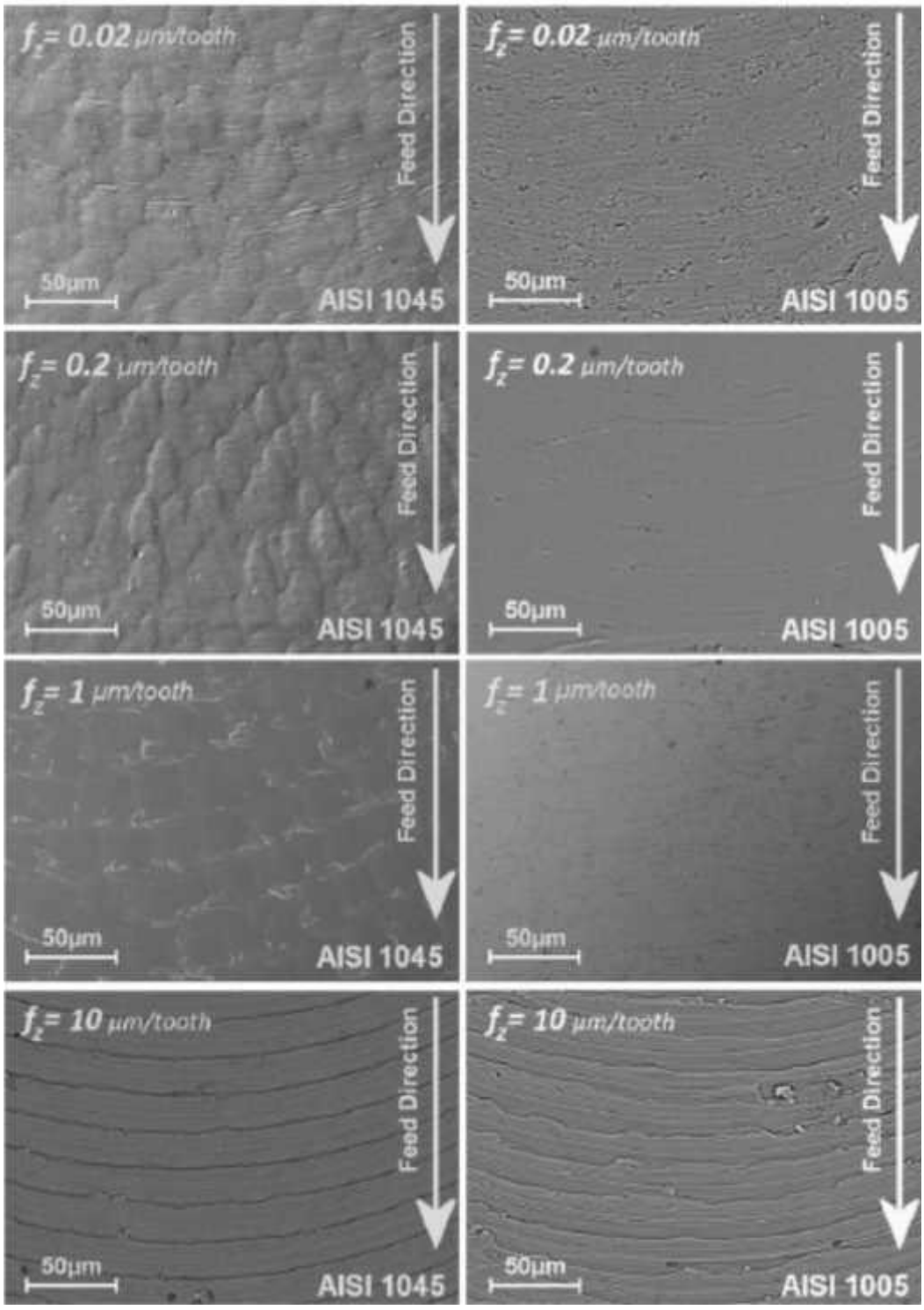

Figure 16 Spring back of material phases for different cutting conditions [8]

During the micro-machining tool passing through the material will activate different crystallographic slip systems [5].

The crystallographic orientation will have a great impact on many parameters as for example surface and force variation, roughness [2], regarding the burrs the crystallographic orientation seems to be more important than cutting speed and feed rate [4], [5].

Filiz et al., [21] describe some miniature burrs found on the surface at the phase boundaries, because of interruption-like cutting caused by the different material phases.

Also Dornfeld et al., [2] reported poor surface finish due to interrupted chip formation while the tool passed through different phases.

Min et al., found that the critical depth of the cut will vary as a function of crystallographic orientation. [5].

Mian et al. suggest to use chip loads ten time larger than the grain size to minimise the effect of crystallographic orientation on surface roughness [8].

Another troublesome parameter is the hardness of adjacent grains, which is also influencing micro-milling process [4].

The variation in the hardness will promote cutting tool vibrations leading to deteriorated surfaces, especially at low feed and cutting speed [2].

Mian et al., [8] state the challenge regarding surface finish because of cutting discontinuities and formation of grain boundary burrs. They found that the best surface finish was obtained for feed rates close to the tool edge radius for different tested materials and thus they conclude that best surface finish is more sensitive to tool edge radius than material grain size.

They have also found the influence of the milling mode, down milling is increasing the nano-hardness of the workpiece material [8].

Simoneau et al., [26] discuss the importance of the materials defects at micro scale. In fact these defects can be of the same order as features being produced during micromachining. They have observed defects such as dimples, prows, micro-voids, and micro-cracks on a machined surface regardless cutting speeds or feeds (prows disappear at higher cutting speeds). There was found that there is a link between material microstructure and surface finish

The surface dimple size can minimized by reduction in grain size and influencing the orientation of grain boundaries in such a way that they won€t beparallel to the shear plane during micro-cutting. [26].

1.2.4 Forces and temperatures in micro-milling

In any machining process forces are determinative aspects and this is also valid for micro-manufacturing. Machining forces could influence not only accuracy of the workpiece but also limit the applicable size due to the possible spring back of the tool and workpiece itself [1].

In general the forces and temperatures found in micro-milling are low, even that the specific cutting forces reach very elevated values due to the ploughing effects [4].

The analysis of cutting forces is key factor because through the forces we can characterize the cutting process, they bring us important information about mechanics and dynamics of machining processes and thus machining can be optimized while estimating some important parameters as for example tool life, dynamic stability, position accuracy, roughness, form errors etc. [15], [21].

Despite it all, the forces are not only important for the design of the process itself but also for the design of tooling and machine tools, as well as determination of power consumption and productivity [21].

The forces in micro-machining show different characteristics, it is due to the micro-machining process itself which is followed by specific phenomena as the minimum chip thickness effect, elastic recovery, ploughing, and tool-tip runout [21].

In Fig. 17 are shown the forces accompanying micro-end milling process, where is the feed force Fy, Fx normal (to the feed) force and in-plane resultant force R [21].

In micro-milling, the forces are characterized by variations due to the minimum chip thickness effect, which is considered to be the main reason of this erratic representation [21], minimum chip thickness is typical by intermittent chip formation - chip is not generated at small feed rates - small uncut chip thickness, till enough big uncut chip thickness is accumulated by multiple tooth passes, moreover large amount of elastic recovery of the workpiece material causes the normal and frictional stresses at the flank face [19], [21]. Cutting forces are similar to those seen when indenting the workpiece material by an indenter with the same geometry as that of the cutting edge [21].

We can talk thus about steep fluctuation which is characteristic for forces in micro-milling due to the switching between shearing and ploughings regimes [4], [17], [19], [24].

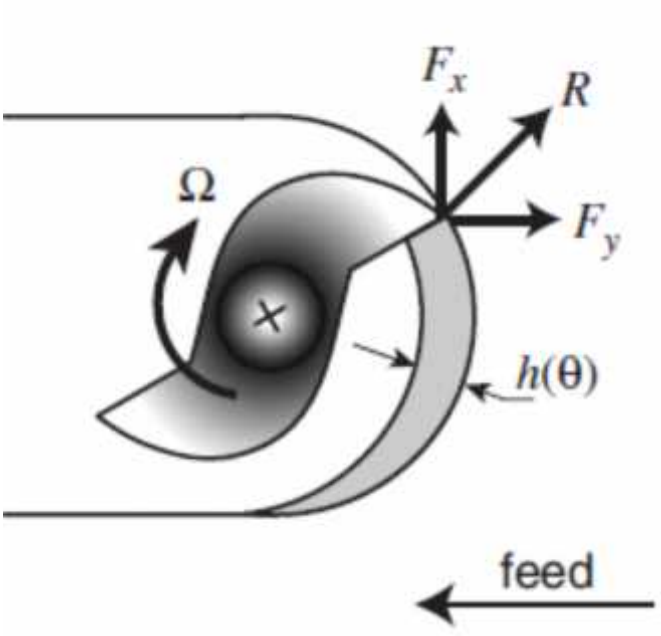

Figure 17 Forces in micro-end-milling [21]

For feed larger than the cutting edge radius (higher than minim chip thickness) cutting forces are similar to those seen in conventional machining [4], [21].

Even though micro-milling forces are low, due to small shear area, however specific cutting force increases dramatically, non-linearly, for small feed rates, because the uncut chip thickness is becoming too small and the minimum chip thickness criterion is not respected and thus the ploughing effect is predominant. This observation correspond to the well-known size effect [3], [4], [21].

The specific cutting force in fact determinates the force necessary to remove the specific volume of material [3]. It can be calculated by dividing the machining forces by the chip area. As in milling, the instantaneous chip area and forces vary during tool rotation, average specific energies can be calculated from the ratio of average forces to the average chip area (which is the product of the feed and the axial depth of cut) [21].

Filiz et al. in their work state that in general lower specific energies are seen in lower speeds, possibly due to the strong effect of strain rate in the absence of significant thermal softening of the workpiece material [21].

Dhanorker et al. as well as Ozel et al. estimate that the specific cutting forces can be almost twice higher than in conventional cutting. It is probably due to highly localized shearing [24] [17].

When increasing the uncut chip thickness, the feed and tangential forces increase slightly too but the specific cutting force decreases drastically [4].

Aramcharoen and Mativenga [3] state that effect of feed per tooth on cutting force is similar to conventional milling thus cutting force increase with feed.

Ozel et al., state that predicting of cutting force is more difficult and can introduce errors as the ratio of feed per tooth to cutting edge radius is much greater in micro-milling than conventional milling [17].

Cutting edge radius is thus the mostly influencing parameter on the cutting forces in micro-milling [11].

Obviously the cutting forces increase together with increasing the edge radius as the cutting edge radius will introduce minimum chip thickness and ploughing effects as stated by Afazov et al. [12]. They have been testing two different rake angles 0° and 8°, smaller rake angle results in higher forces and lower stability limits. The increase of the cutting forces and decrease of the stability limits is more significant for small edge radii and high uncut chip thicknesses.

Kuram and Ozcelik [7] have studied the influences of different parameters on cutting forces, they have found that Fx and Fy increase with an increment of spindle speed and feed per tooth. Increment of depth of cut leads to decrease of Fx and initially increases Fy; but with further increasing Fy decreased.

Conversely Dhanorker et al., [24] noticed that cutting forces is much more sensitive to the increase in the axial depth of cut than the feed per tooth. Thus they suggest to use combination of low axial depth of cut and high feed rate to keep high material removal rate while limiting the cutting forces.

Beside the parameters controlling forces in micro milling as the effects of minimum chip thickness, ploughing, indentation, and elastic recovery [21], others parameters influencing the force variation are crystallographic orientation [5], both static and dynamic tool-tip runout and as in conventional milling process, they are vibrations, and repeated entry and exit of the cutting flutes [21].

It was also observed that stable built-up-edge formed on the cutting edge increases significantly the ploughing force when the feed rate is smaller than the cutting edge radius [2].

Regarding the temperatures in comparison with conventional milling, they are considerably lower as small uncut chip thickness is used, very small chip loads. However, its determination is not easy, requiring equipment with high sampling rates [4], [24].

Increasing feed per tooth increases in the temperatures [24]. Also the temperature gradient in the workpiece will increase in front of the cutting edge due to the material flow relative to the cutting tool [2].

Dhanorker and Ozel [19] in their work were studying and modelling the temperatures during micro-milling. They have found maximum temperatures in the cutting zone around 60„C for AL2024-T6 aluminium and around 150„C for AISI 4340 steel. These temperatures are very low compared to meso-milling. They explain it be very small chip loads. Similar results were found also by Ozel et al. in [17].

Thepsonthi and Ozel [11] state that average tool temperature increases as cutting speed and feed per tooth increase (material removal rate increases). On the other hand, there is almost no difference in cutting forces while changing cutting speeds.

Same authors in [11] stated the same conclusion in the case of micro-end milling of Ti-6Al-4V titanium alloy, increased feed and cutting speed generally increases tool temperatures. They also declare that conversely in the case of forces the cutting edge radius is not influencing significantly temperatures.

1.2.5 Burrs in micro-milling

The burrs represent an important issue, because it is unwanted projection, plastic formation of material during the machining process and represent the deviation from required properties. As in general in the drawing the ideal or designed edge is †burrs fŧee‡ surface[27].

Moreover in micromachining burr formation is a critical and the principal limiting factor, as it affect the capability to meet desirable tolerance and geometry definitions [4], [8], [21]. In addition the burrs in micromachining are usually larger than those in conventional machining [21].

There can be found 3 main reasons why burrs are undesired and should be removed or minimized. Firstly because they represent the deviation from designed geometry. Second reason is the risk for the functionality (problems during assembly, gap between parts, possible breaking and loss of burrs which can go into the devices and damage them) and third reason is the security risk for operators when then can be injured, especially on fingers while handling the sharp edges with burrs [27].

In addition the de-burring process is time consuming, costly and doesn€t bring any add value operation. Aurich et al. estimated that deburring represent 9% or more of costs and in Germany it would reach about 500 millions of Euro per year, thus the deburring has a large economic impact on whole machining process and its costs [27].

Aurich et al. [27] also define the main aspects which will influence burr creation are:

- Tool and its geometry
- Use of the cutting fluids
- Geometry of the workpiece, features to be machined
- Material of the workpiece
- Sequences of machining operations
- Tool path strategy
- Cutting condition

From the literature main parameters influencing burr formation are cutting speed, undeformed chip thickness, tool sharpness, tool feed and workpiece material [3], [10], [16], more ductile workpiece materials produce larger burr size [3], [8], [10], but on the other hand harder materials will promote wear and thus also burr formation [3], [9], [10].

The mechanism of burr formation in micromachining is dominated by the interaction between cutting edge radius and feed per tooth and thus with increasing the negative effective rake, material ahead the tool will be pushed/compressed, flows away, bent and a portion moved

in the axial direction of the tool and deformed plastically into a burr [3]. Therefor burr size will decrease while ploughing will be minimalized [3], [4], [8], [21].

The lowest burr formation occurs at low speeds and high feed rates [9], [21], increasing cutting speed also increases burr formation, increase of feed is limited by chip load on the tool [9].

Min et al., found a significant variation of burr height with crystallographic orientation compared to micro-milling [8].

Camara et al. state that burr height and thickness are significantly affected by tool diameter, number of flutes and depth of cut, increasing of these parameters will decrease burr height [4].

Thepsonthi and Ozel have found axial depth of the cut and feed per tooth the main factors influencing both top burr formation and surface roughness [10], [11].

Many authors study the importance of chosen milling strategy, they have found that down milling generates larger burr size as compared to that of up milling. In down milling larger wavy burrs are obtained while up milling produces smaller ragged type burrs [3], [4], [8], [21].

Piquard et al. [28] would also add the importance of the chosen strategy in micro-end milling as down and up milling , beside the importance of cutting conditions. Where the height and width of burrs are strongly affected by feed per tooth, width of cut and chosen strategy (up-milling represents wider and curly shape burrs). The cutting strategy is also the most influent parameter for the burr thickness (thinner in up-milling).

Moreover in the domain of micro-milling the removing of burrs is even more difficult and make of them the main issue and limitation for micro-milling use [29]. Deburring of micro-features is expensive and eventually technical not feasible as it can result in microstructural damage [3], [4], [9], [10], [21]. Because the removal by traditional way (brushing, etching, electrolyte or ultrasound) is very complex and may lead to size errors, residual stresses and also damages of the surface [30].

Another important parameter to be mentioned is that in micro-milling the relation between microstructure and uncut chip thickness [29] as well as the ration of uncut chip thickness to cutting edge radius is in the rages when ploughing for certain cutting conditions could be predominated and thus might influence the burrs formation, which might differ from macro-milling cases [30], [31].

Moreover Kiswanto et al. [32] state that in micro-milling process, burr formation has an important impact on the work piece quality, because the size of burr could be approaching the size of cutting tool diameter.

Lee and Dornfeld [33] found in the case of micro-milling that he burr in hole formation larger than in conventional milling, because the radius of the cutting edge is larger compared to the feed per tooth. Burr height is linearly proportional to feed per tooth and related to tool wear. For ft/R<1, tool life increases as cutting speed is increased.

As the burr formation is important issue in machining world, different theories and burr classifications can be found in the literature. We can split them in mainly two groups of classification: by burr formation mechanism and by burr formation mechanism, location and shape.

1. **Classification based on burr formation mechanism**

Gillespie as cited in [27], [33] is classifying the burrs by the formation mechanism. There are four types of machining burr: Poisson burr, rollover burr, tear burr and cut-off burr.

The **Poisson burr** is a result of the material€s tendency to bulge to the sides when it is compressed until permanent plastic deformation occurs. It is the lateral deformation that occurs whenever any solid is compressed [27], [31], [33], [34].

The **roll-over burr** occurs when it is easier to bend the chip than to cut it. Roll-over burr is resulting in a comparatively large burr. This type of burr is also known as an exit burr because it is usually formed at the end of a cut [27], [31], [33], [34].

The **tear burr** is the result of material tearing loose from the workpiece rather than shearing clearly. Tear burr formation is due to crushing of the chip particles [27], [31], [33], [34].

The **cut-off burr** is the result of workpiece separation from the raw material before the separation cut is finished. [27], [33], [34]

2. **Classification based on burr formation mechanism, burr location and burr shape**

Another approach is to classify the burr by taking in consideration moreover the burr formation mechanism also the burr location and burr shape.

According to Hashimura [35] as mentioned in the Tab. 1 three kinds of burrs were considered according to the location of the cutting edge and workpiece surface: exit, side and top burr. Additionally two kinds of shape for exit burrs, three kinds for side burrs and three kinds for top burrs were defined.

The **exit burr** is attached to the surface machined by the minor edge of the tool [35].

The **side burr** is attached to the transition surface machined by the major edge [35].

The **top burr** is attached to the top surface of the workpiece [35].

Table 1 Classification on milling burrs by Hashimura [35]

<table>
<tr><td colspan="2">Location</td><td colspan="2">Type</td></tr>
<tr><td>Surface</td><td>Name</td><td>Shape (Macro view)</td><td>Mechanism (Micro view)</td></tr>
<tr><td rowspan="4">Machined surface
Surface cut by minor edge</td><td rowspan="4">Exit burr
Remains attaching to machined surface</td><td rowspan="3">Discontinuous</td><td>Ductile plus fracture (DF)</td></tr>
<tr><td>Fracture plus ductile (FD)</td></tr>
<tr><td>Fracture (F)</td></tr>
<tr><td>Continuous</td><td>Completely ductile (CD)</td></tr>
<tr><td rowspan="3">Transition surface
Surface cut by major edge</td><td rowspan="3">Side burr</td><td>Discontinuous (DC)</td><td rowspan="3"></td></tr>
<tr><td>Spiral (S)</td></tr>
<tr><td>Continuous (C)</td></tr>
<tr><td rowspan="3">Top surface
Surface cut by major cut</td><td rowspan="3">Top burr</td><td>Discontinuous</td><td rowspan="3"></td></tr>
<tr><td>Ragged</td></tr>
<tr><td>Longitudinal</td></tr>
</table>

In the case of micro-milling we can found mainly the classification of burrs based on Hashimura classification and depending on authors some additional locations are added.

For example Piquard et al. [28] define 12 different locations for burrs (Fig. 18). In addition of exit, side and top burr, they specify separately

burrs for down and up-milling and they add tip, entrance and side burrs

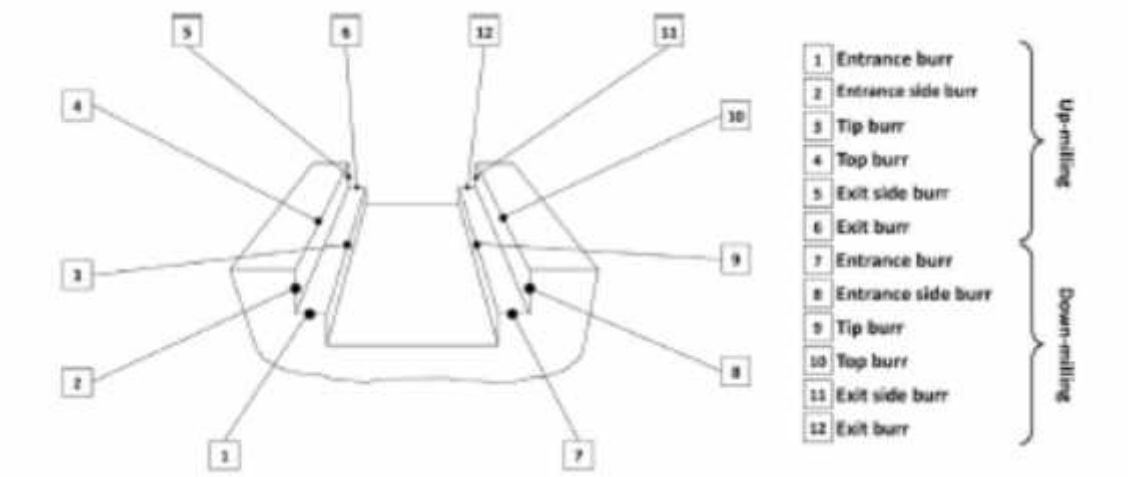

Figure 18 Burrs location in micro-milling by Piquard et al. [28]

The **tip burrs** are considered as exit burrs, they are created by the end-mill tip on the lowest edge of the square shoulder [28].

Also Lekkala et al. [31] studied burrs in the case of micro end milling. They are combining together the classification made by Gillespie and by Hashimura stating that the mechanism of burr formation in micro-end milling of aluminium and stainless steel consist mainly of six different mechanisms: Poisson burr, roll-over burr, tear burr, entry burr, exit burr and top burr.

The **entry burr** formation occurs when the cutter enters the work surface [31].

The **exit burr** is created when the tool exits from the work surface [31].

The **top burr** formation involves wavy burrs on entry as well as exit sides [31].

Similarly also Kiswnto et al. [32] state that they have found four types of burr in their micro-milling experiments, which were top burr, entrance burr, side burr, bottom burr, and exit burr.

Top burrs occurrence on the micro-channels surface and are mostly formed on down-milling side of the slot [32].

Entrance burr formation is related to the tool wear [32].

Bottom burr could occur on both sides of the micro-channel, burr would rapidly increase in function of increasing tool wear, in this case

the machining process would be dominated by rubbing instead of cutting [32].

Based on the literature can be concluded that in the case of micro-milling, there are mainly presented **top, entrance, exit** and **bottom** burrs [3], [10], [28], [31], [32].

Mian et al., mention that there is not any common approach in terms of measuring curled 3D burr shape, especially in the micro domain. But they state that burr can be quantitatively measured in terms of burr width and burr height [8].

Aurich et al., in [27] classify the burr measurement methods as:

- one-, two- or three-dimensional,
- destructive or non-destructive,
- with or without contact
- in-process and out of process

In the Tab. 2 are shown classifying of different methods of burr detection and burr measurement.

Table 2 Methods of burr detection and burr measurement [27]

<table>
<tr><th colspan="5">METHODS OF BURR DETECTION AND BURR MEASUREMENT</th></tr>
<tr><th colspan="4">OUT of PROCESS</th><th rowspan="3">IN-PROCESS</th></tr>
<tr><th rowspan="2">With contact</th><th colspan="3">Contactless</th></tr>
<tr><th colspan="2">Optical</th><th>Electro-mechanical</th></tr>
<tr><td>Stylus methods</td><td>Optical microscope</td><td>Light-slit methods</td><td>Eddy-current sensor</td><td>Process monitoring</td></tr>
<tr><td rowspan="4">Metallographical profiles</td><td>Borescope / endoscope</td><td>Laser triangulation</td><td>Inductive sensor</td><td>Force, moment</td></tr>
<tr><td rowspan="3">Scanning electron microscope</td><td>Fring pattern projection</td><td rowspan="3">Computer tomography</td><td rowspan="3">Sound emission analysis</td></tr>
<tr><td>Autofocus methods</td></tr>
<tr><td>Confocal microscopy</td></tr>
</table>

Stylus methods are suitable to measure burr heights. But the real profile can€t be measured as the data can be influenced by conical shape of the tracer point. All contact measurement methods are limited by the workpiece stiffness, as the burrs can be destroyed or pushed down because of the contact forces [27].

Destructive method is for example a metallographic cross-section of the burr. This method allows measure burr values from the cross-sections but also burr hardness and structural changes in the material after the machining. It is the only method to measure burr thickness and also burr length especially in the case of rolled and spiral burrs On the other hand the preparation of metallographic samples is very time-consuming and allows only to measure at one specific workpiece position [27].

1.2.6 Additional comments about chip formation and tool wear in micro-milling

Wang et al., [36] state that conventional and precision machining of metals can produce three basic types of chip: discontinuous, continuous and continuous chips with built-up edge.

In the micro-cutting, Wand et al,. [37], demonstrate strong evidence between fluctuation in the cutting force and the variation of chip thickness and of shear plane angle.

High strain rate, which causes strain inhomogeneity, like in high-speed machining and impact and torsion experiments, will promote the formation of shear bands. In the vicinity of shear bands, material experiences relatively little plastic deformation but the bands themselves experience very large plastic strains and propagates at very high rates. And the local heat generation rate is much larger than the rate of heat conduction to the surrounding material, this will lead to adiabatic softening [37].

Shear bands will initiate at the free edge of the chip and propagate towards tool tip [36], [37]. This propagation process is in fact the repetition of elastic• plastic deformation. As the tool advances the elastic stressed chip above the formed shear band will be pushed upward and forward with the elastic stress concentration facilitating repeated production of serrated chips. Accumulation of elastic energy increases shortly the cutting force before shear band is formed. Later the plastic deformation will release the stored energy leading to a load drop on the cutting tool [37].

Wang et al., found that in the case of micro-cutting with a constant strain rate, elastic strain concertation created by the free edge can introduce shear band in the serrated chips. And thus the shear bands will propagate from the free edge towards the tool tip [37].

Simoneau at al., [26] studied the transition between macro-, meso-, and micro-scale cutting and the influence of the microstructure. They have found that there is always transition in chip type while the scale is decreasing especially for smaller uncut chip thickness. They have also stated that while comparing the two microstructures, the impact of grain refinement on shifting the chip formation mechanism is evident.

In the Tab. 3 are shown different types of chip formation for different level of scaling in the cutting process demonstrated by Simoneau et al., [26], there is visible the influence of the initial microstructure and its refinement to the uncut chip thickness and thus chip formation type. For the microstructure with finer grain size, lower value of uncut chip thickness are possible without changing the chip formation type.

Table 3 Chip formation types for different sized microstructures [26]

Scale of cut	Uncut chip thickness in μm for microstructure type		Chip type
	Normalized	Refined	
Macro-sacle	> 100 μm	> 20 μm	Continous chip
Meso-scale	10 - 50 μm	8 • 20 μm	Transitional chip
Micro-scale	< 10 μm	< 8 μm	Quasi-shear extrusion chip

The tool wear is parameter which will strongly influence machining process and the quality of the final workpiece. Thus it is important to be able evaluate and predict the tool wear before breakage of cutting tool [7].

Increasing tool wear will increase cutting forces, surface roughness will be worsen as well as burrs formation [4], [21].

Moreover as we are in the range of micro-scale even a little change in cutting edge radius will implement also change in tool diameter. The decrease of only 1% of the tool diameter of 500 μm will mean a difference about 5 μm which will be enough significant to deteriorate geometrical accuracy in micro-milling were the tolerances are normally within a few micron ranges [11].

As the tool wear will increase, the cutting edge radius will increase too, but if the feed per tooth will be kept constant during machining, the value of normalized minimum chip thickness will change and thus the ploughing effects will start to dominate the cutting process and thus further tool wear rate will be significantly increased [11].

Kuram and Ozcelik have observed mainly adhesion and abrasion wear mechanisms during micro-milling of aluminium material [7].

There are many parameters affecting tool wear such as spindle speed, feed per tooth, axial depth of cut, radial depth of cut, tool diameter, workpiece material, etc. But the most decisive parameters are spindle speed, feed per tooth and depth of cut [7].

Kurman and Ozcelik [7] have found that that tool wear will increased with spindle speed and depth of cut, also at the beginning with increase of feed per tooth, but further increase of feed per tooth might eventually decrease tool wear.

This trend related to feed per tooth is also confirmed by Filiz et al., they have found that the highest wear is experienced at the lowest feed rate, whereas the lowest wear was seen at the highest feed rates [21].

In fact Filiz et al., state that the wear mechanism at low feed rates is a basic form of attrition, where the individual tungsten carbide particles are dislodged from the softer cobalt matrix. Due to more uniform stress distribution on the tool rake, and lower forces, the lowest wear occurs at high feed rates [21].

They also mention that these observations are contrary to those from conventional machining, in which higher feeds and speeds usually result in more rapid wear progression [21].

Equally Zaman et al., empathises the contradiction with conventional milling. In micro-milling tool life is increasing within the range of axial depths of cut. At very low depths of cut, premature tool failures appears frequently [15].

Thepsonthi and Ozel have been studied the influence of the cBN coating on the tool wear, they have found that tool wear rate of cBN coated tool is lower than tool wear rate of uncoated WC/Co tool [11].

As the temperatures in micro-milling are considered to be significantly lower than in conventional milling, the mechanism of tool failure which in conventional• milling is based on temperature-depended accelerated wear rates must differ in micro-milling. The possible mechanism of tool wear as well as sudden tool failure and breakage in micro-milling is dependent on highly fluctuating forces due to a continuous shifting between ploughing and shearing mechanism [17], [19].

2 MATERIALS

2.1 TITANIUM AS ENGINEERING MATERIAL

Titanium alloys are widely used in engineering. The most commonly use titanium alloy is Ti-6Al-4V, which represent more than 50% of all parts produced from titanium alloys [38]. This large interest into Ti-6Al-4V is mainly due to its outstanding properties as mentioned bellow [9], [11], [38]• [44].

Some of most interesting properties of Ti-6Al-4V:

- excellent strength/mechanical properties up to 400°C
- low density and thus high strength to density ratio
- fatigue endurance
- excellent corrosion resistance at elevated temperatures
- biocompatibility and biological inertness
- chemical inertness

However this alloy has lower machinability. Ti-6Al-4V makes part of material groups called difficult-to cut. As there are many problems associated to machining process [9]• [11], [39] as:

- burr formation
- severe tool wear due to high reactivity of titanium with tool materials over 500°C (chemical affinity with tool materials leads mainly to adhesion and chemical reaction) [39]
- low thermal conductivity
- tendency to work hardening
- high cutting temperatures
- high cutting pressure (serrated chips formed during machining create a small contact area and thus high stresses) [39]
- chatter

Due to the low thermal conductivity and high cutting temperatures the application of titanium alloys is limited to temperatures below 400„C. Because otherwise titanium can catch fire and may cause severe damages [39].

These problems make the machining process of Ti-6Al-4V very expensive and also have impacts on the product quality in terms of surface finish [39].

Another economic constraint related to titanium alloy is the costs associated to intrinsic raw material extraction which are very high [39], [44].

Regarding the applications of titanium alloys, the main usage can be found in following fields:

- aerospace and aeronautic applications [11], [38], [41], [43], [45] as:
    - aircraft structures, turbine blades, aero-engines [10], [39], [44],
    - gas turbine engines, compressor blades, disks, casings, bypass ducts, engine cowlings, exhaust shrouds, structural forgings, fasteners, hot-air ducts, heat shields, hot area skinnings in the airframe, load bearing components [39]

- biomedical applications [10], [11], [38], [39], [42], [43], [45]• [48] as:
    - replacement for diseased bone and cartilage [39],
    - dental surgery [38], [41], [44], [45] with crown, clasp [48],
    - orthopaedic surgery [41], [45] with hip prostheses (femoral stems), screw, knee prostheses [38], [44]

- other applications as:
    - marine applications [39], [43]
    - micro-products [9]
    - food industries [39], [41]
    - automotive [43]
    - chemical industries [43]
    - power generation [43]
    - oil and gas extraction [43]
    - sports [43]

Pure Titanium has melting point at 1670„C, density of 4.5 g/cm3 is the fourth most abundant structural metal in the earth€scrust. As unalloyed material is very soft and don€t reach high values of mechanical properties as high strength, hardness as we know them for titanium

alloys [39]. In Tab. 4 are compared mechanical properties of pure titanium and most common titanium alloy Ti-6Al-4V. There is visible the high increase of mechanical properties by alloying titanium with other elements.

Table 4 Mechanical properties of pure and alloyed Ti [39]

Property		Titanium	Ti-6Al-4V
Density	[g/cm^3]	4.5	4.43
Hardnes	[HRC]	10-12	30-36
Ultimate tensile strength	[MPa]	220	950
Yield strength	[MPa]	140	880
Modul of elasticity	[GPa]	116	113.8
Ductility	[%]	54	14
Fracture toughness	[MPa m$^{1/2}$]	70	75
Thermal conductivity	[W/mK]	17	6.7
Max operating temperature	[°C]	150	315

Titanium based alloys are known for excellent properties especially at high temperatures. They are resistant in wide range of challenging environments (natural and chemical), they have high resistance to pitting and stress-corrosion cracking even at temperatures around 100„C for most agents, including acetic acid, hydrochloric acid, brine, and molten sulphur [39].

In the case of biomedical applications Ti•6Al•4V is known for excellent corrosion resistance in body, it is due to the formation of a spontaneous oxide film after exposure to oxygen or water [40]. As described by Niinomi [48], this film acts as an electrochemically passive film and inhibits negative ions from invading the matrix of the alloys. Nevertheless the fracture of the passive film is possible, especially when the bending stress is applied to the part. The facture of the film will occur even if the part itself will not be fractured. Moreover the fracture by corrosion fatigue will be accelerated in some environments as the Ringer€s solution.

In Tab. 5 is shown the chemical composition of standard Ti-6Al-4V grade 5 and Ti-6Al-4V ELI used especially for biomedical applications. More detailed mechanical properties of Ti-6Al-4V are presented in the Table 6.

Table 5 Nominal chemical compositions [wt.%] [40]

Element	Ti-6Al-4V grade 5	Ti-6Al-4V ELI (extra low interstitial) grade 23
Ti	bal.	bal.
Al	6	5.5 - 6.5
V	4	3.5 • 4.5
Fe	<0.2	0.25 max
C	<0.25	0.08 max
O	<0.2	0.13 max
N	-	0.05 max
H	-	0.013 max

Table 6 Mechanical properties of Ti-6Al-4V (forged and annealed) [49]

Property		Value
Tensile strength, yield ($\sigma_{0.2}$)	[MPa]	880
Tensile strenght, ultimate (UTS)	[MPa]	950
Elongation (ε)	[%]	14
Reduction of area (R)	[%]	36
Hardness	[Hv]	349
Young€s modulus (E)	[GPa]	113.8
Poisson€s ratio (ν)	[-]	0.342
Fatigue strenght (at $1*10^7$ cycles and K = 3.3)	[MPa]	240
Fatigue strength (unnotched at $1*10^7$ cycles)	[MPa]	510
Fracture toughness	[$MPa.m^{1/2}$]	75

At room temperature, the microstructure of pure Ti consists of 100% alpha phase. Titanium undergoes allotropic transformation from , phase, characterized by a close packed hexagonal structure (hcp), to the body centred *ƒ* phase (bcc). In the case of Ti-6Al-4V alloy, it is a typical , + *ƒ* alloy, which can include , (hcp), *ƒ* (bcc) and ,€ (hcp) martensite phase [39], [41], [50].

Table 7 Fundamental physical properties of Ti-6Al-4V [49]

Physical property		
Density of solid (ρ)	[g/cm^3]	4.43
Density of liquid (ρ)	[g/cm^3]	3.89
Solidus temperature	[K] / [°C]	1877 / 1604
Liquidus temperature	[K] / [°C]	1933 / 1660
Temperature of (,+*ƒ*) -> *ƒ*	[K] / [°C]	1253 / 980
Temperature of , -> *ƒ*	[K] / [°C]	~1023 / 750
Thermal conductivity of solid (k_s)	[W/m/K]	6.7
Thermal conductivity of liquid (k_l)	[W/m/K]	32.5
Specific heat capacity of solid (Cp_s)	[J/g/K]	0.526
Specific heat capacity of liquid (Cp_l)	[J/g/K]	0.872
Coefficient of thermal expansion of solid (K^{-1})	[µm/m/K]	8.6
Temperature of martensite phase transformation (M_s)	[K] / [°C]	~1053 / 780 or ~883 / 610

Alloying elements are defined as , -stabilizers and ƒ-stabilizers. In the case of Ti-6Al-4V aluminium acts as , -stabilizer and vanadium is ƒ-stabilizer. It means that they are changing (increasing or decreasing) the , Œ ƒ transition temperature. Aluminium as alpha stabilizer is increasing the temperature of the transus between ƒ and ,+ƒ while vanadium as beta stabilizer is decreasing the temperature of the transus between the biphasic and the , fields [39], [44], [50]. In the case of pure Ti, the transition temperature is about 885°C, and for the Ti• 6Al• 4V alloy the transition temperature increases to approx. 995°C [50]. Facchini in [44] states that the composition of Ti-6Al-4V alloy fixes the transus from , to biphasic field at 970 „C and the entry in the whole ƒ field at about 1010 „C.

In the Tab. 7 are mentioned the fundamental physical properties of Ti-6Al-4V titanium alloy.

Ti-6Al-4V at room temperature, its microstructure is a function of thermal history. Solidification will occur when liquid is transformed to beta phase. Nucleation, grow characteristics and thermal conditions will influence the grain size and morphology. With continuing cooling the beta grains will grow depending on temperature, cooling rate, and the driving force for grain growth. Reaching the beta transus temperature, transforming partially into alpha (hexagonal close packed) phase. The alpha can grow in one of up to 12 specific orientations relative to prior beta. The amount of beta transformed to alpha (or beta remained), size, morphology depends on cooling rate from beta transus. Also further heat treatment could alter the distribution, size, morphology of the alpha phase, but don€t effect the prior beta grains [51].

Facchini in [44] explain the presence of the two phases as the function of thermodynamic factors as well as kinetic factors. Determined by strain rate and temperature, which influence dynamic recrystallization [41]. In fact the bcc structure of beta phase is more open than the hcp (alpha phase), this also means that its vibrational entropy is higher. Thus the free energy of the bcc lattice decreases more rapidly during heating (bcc structure is stable at high temperature). Beside the diffusive mechanisms during the formation of different phases, also martensitic transformation can appear and martensite will form while rapid cooling from ƒ or ,+ƒ fields is applied. Martensite consists of hcp structure as alpha phase, but with different lattice parameters [44].

As typical , + ƒ alloy, Ti-6Al-4V properties depend strongly on its microstructure [41], [44], [50]. In fact a proper heat treatment can modify the properties by controlling the form in which the ƒ phase is presented [44].

Thermomechanical treatments, which combines deformation and heating produces different microstructures. During these treatments,

recrystallization and aging take place. Al element will also promote the solution strengthening [44].

In function of the working temperature and cooling rate as discussed above the microstructure might change. In general we can found lamellar or globular microstructure which fine or coarse [44], [45].

Lamellar microstructure with large dimensions of , colonies, which is generated by slow cooling down from the *ƒ* field will improve the resistance to fatigue, crack propagation, fracture toughness, creep resistance and oxidation behaviour but will have a detrimental effect on tensile elongation [41], [44], [45].

On the other hand , -globular (equiaxed) microstructure, which is the consequence of a recrystallization process, is advantageous in the case of good strength, toughness, ductility and fatigue crack initiation [41], [44], [45].

In fact the wrought titanium undergoes some different cycles, stage during its production which will influence the final properties as: (1) alloying, (2) the melting process used in ingot processing, (3) mechanical working history, (4) heat treatment temperatures and cooling rates and (5) aging treatment [50].

For example in the case of forging part at 1040 „C which is above the beta transus, coarse plate-like (acicular) , with some inter granular *ƒ* will be produced as shown in the Fig. 19 (a). In the case of forging and solution treating for 1 h at 950 „C, air- cooling and then annealing for 2 h at 700 „C. This resultant microstructure is equiaxed, *ƒ* very different form the previous one (as shown at Fig. 19 (b) [40].

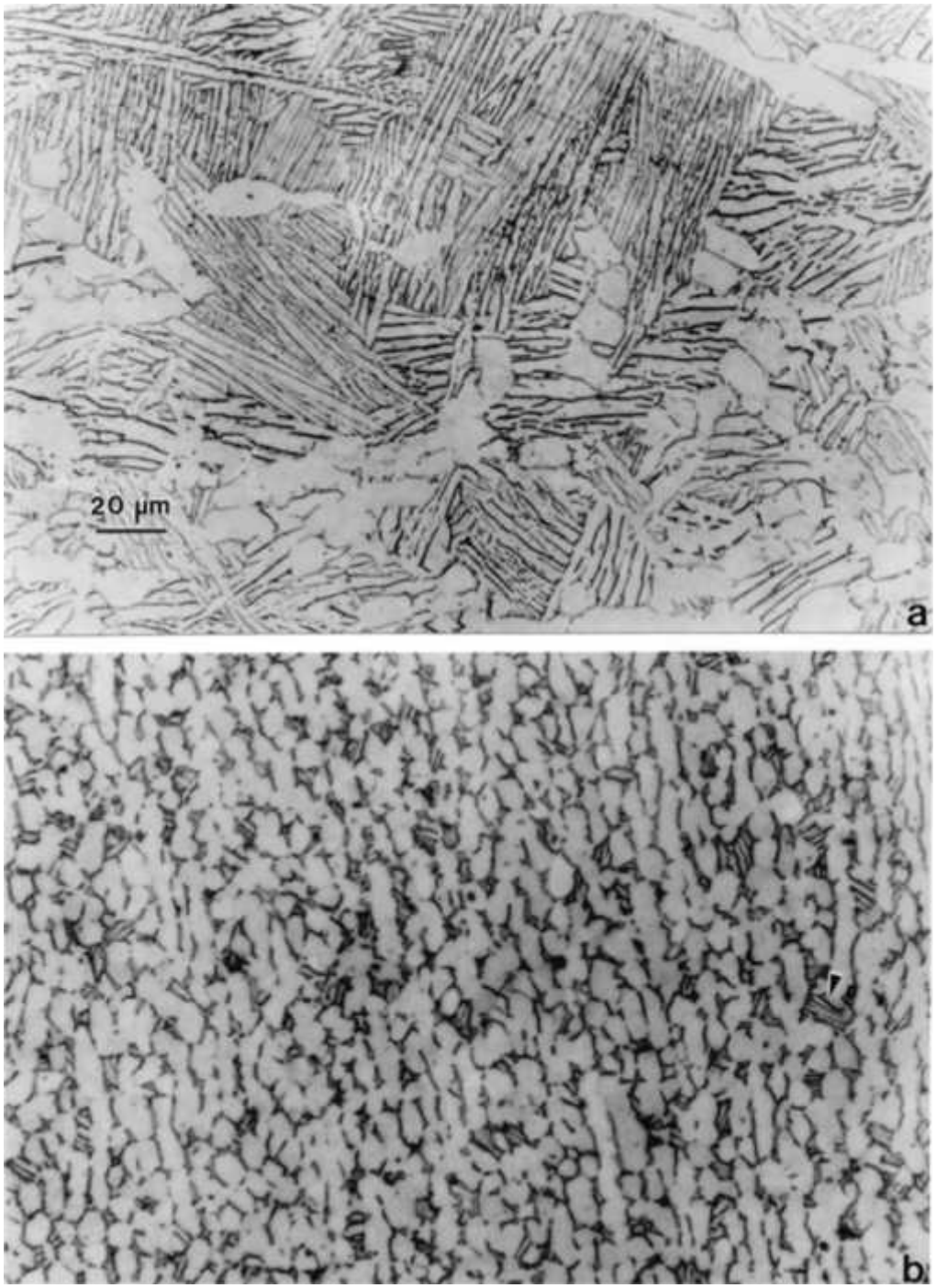

Figure 19 Two different Ti-6Al-4V microstructures: (a) coarse, plate-like (acicular) alpha with some intergranular beta • forging above the beta transus and (b) equiaxed alpha and beta phase mixture for forging and solution treating [50]

Murr et al. state that the advantage of wrought products compared to cast one, consists in the possibility of thermomechanical treatment

(cold/hot working plus heat treatment) into a final shape, which will promote tailoring of desired mechanical properties [50].

The cast parts themselves are produced with properties similar to or superior to wrought products (enhanced crack propagation, creep resistance). Possible post treatment consists of heat treatment and/or hot isostatic pressing (HIP) to eliminate porosity introduced during the casting process. The microstructure of cast Ti• 6Al• 4V consists of an , + ƒ platelet structure that is transformed from a dendritic ƒ structure during solid state cooling [50].

As Facchini describes ƒ-transus temperature (T), which separates the biphasic from the ƒ field is one of the most important parameters. Cooling from above T will result in a lamellar microstructure. In fact , phase nucleates at grain boundaries and then grows as lamellae into the prior ƒ grains. Original ƒ grain boundaries can be still well recognizable after cooling. The dimensions of the , lamellae can€t be larger than prior ƒ grain, they are related to the original dimension of the ƒ grains. Lamellar microstructure is formed when cooling rates are relatively slow [44]. An example of lamellar microstructure obtained by cooling from the beta field is shown in Fig. 20.

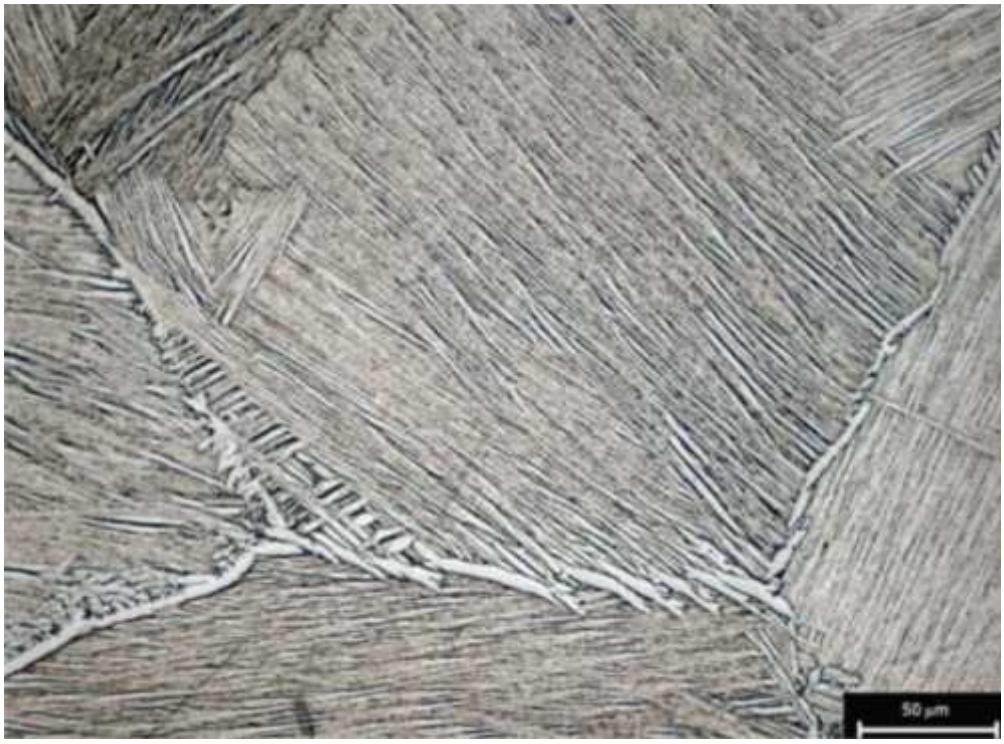

Figure 20 An example of lamellar microstructure obtained by cooling from the beta field [44]

Murr et al. state that the amount of *ƒ* phase in the final microstructure, increases with increasing process temperature in the , + *ƒ* phase, with 100% *ƒ* formation when processed in the *ƒ* phase, with or without deformation [50].

In fact the strain rate effect will influence the final microstructure as also mentioned by Murr et al. the geometry of the , platelets (equiaxed or acicular) will depend on the amount of deformation and cooling rate from the *ƒ* phase, and decrease in width with increase in cooling rate. With extensive deformation, the , platelets breakup into a spheroidized structure. Deformation of the *ƒ* phase can create martensite (‚€;hcp) [50].

When the strain rate is increasing can lead to change from an , - globular microstructure to a lamellar (Widmanst•tten) microstructure. In fact two temperature-strain rate regimes are described. For the lower temperature regime, deformation is non-uniform (intense localized shear makes the Widmanst•tten colonies break and spheroidize after a large amount of deformation). For the higher temperature regime, this non-uniform deformation does not exist and formation of a lamellar, rather than globular, microstructure is present [44].

Faccchini in [44] explain that when the alloy is cooled rapidly from the beta (bcc) field, *ƒ* will transform into acicular ,. Hcp phase can nucleate directly from bcc in the form of needles, creating a basket-weave morphology. The prior *ƒ* grain boundaries can be still recognized. , phase takes separates blocks of aligned needles. When the treatment temperature falls in the ,+*ƒ* field, , phase i s also present at equilibrium. With lower temperature in the biphasic field, smaller volume fraction of *ƒ* phase is created, but with higher stability due to high concentration of vanadium. In presence of a deformation, which furnishes a driving force for recrystallization, the microstructure of alloys treated in the biphasic field becomes equiaxed, globular primary , grains are di stributed in a lamellar matrix. Depending on the cooling rate, lamellae can be constituted by martensitic hcp phase (‚€) or by a biphasic ,+*ƒ* mixture [44]. An example of equiaxed microstructure is shown in Fig. 21.

Facchcini also explain the formation of martensite in Ti-6Al-4V and its different forms. Metastable martensitic structure can be achieved by a rapid quenching from above the ,/,+*ƒ* transus. If the cooling rat e is lower, , phase can nucleate and grow into the prior *ƒ* grains giving rise to a typical Widmanst•tten morphology, which is a consequence of a nucleation and growth mechanism. Martensite can have two structures: hcp (‚€) or orthorhombic (‚€€). Hcp is themost common for titanium martensite [44].

Deformation-induced ,€ is a common occurrence in Ti- alloys containing unstable ƒ phase [50].

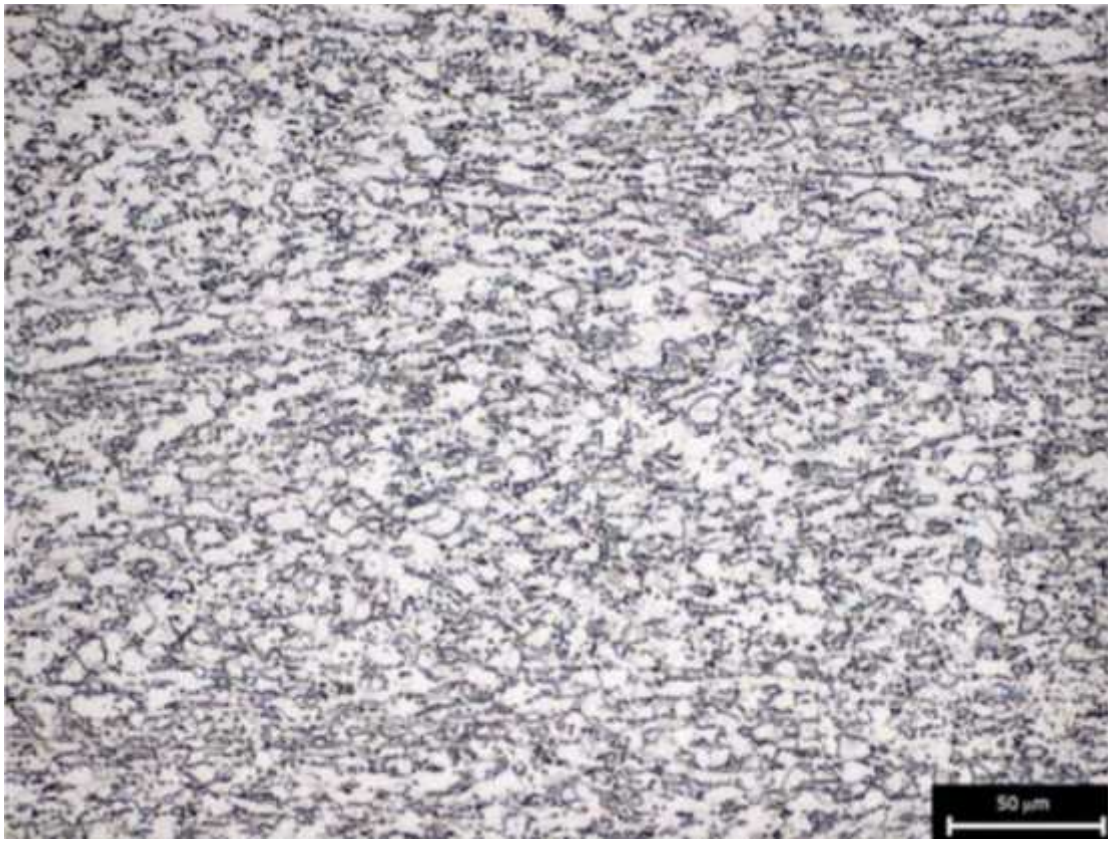

Figure 21 Example of alpha globular microstructure obtained by cooling form alpha + beta field in the presence of deformation [44]

Another aspect influencing the properties is the size of the grains, in fact grain refining allows a retardation of nucleation and growth for small cracks. In lamellar microstructure cracks nucleate at slip bands in the lamellae or in the , phase a t the prior ƒ grain boundaries. In equiaxed material, cracks generates along the slip planes of , grains . And in the case of duplex microstructures, where , -globular grains lie in a biphasic acicular matrix, cracks can start from the lamellar matrix, the equiaxed grains or from the interfaces [44].

2.2 PRINCIPLES OF AM TECHNIQUE

In the recent years use of Additive Manufacturing (AM) technique especially for production of metallic components is raising [38], [50].

Additive manufacturing is in fact comprising all different name and designations as layer manufacturing, solid freeform fabrication, rapid prototyping, digital manufacturing, or e-manufacturing, the principles are the same [52].

In the market there are several machines utilizing different building methods, such as 3-D printing, fused deposition modelling, laminated object manufacturing, selective laser sintering (SLS), selective laser melting (SLM) and 3-D laser cladding etc. [52].

Additive manufacturing is family of techniques where material is deposited and consolidated in successive layers using a focused heat source to build up a component from 2D slices [53].

The origin of the layer manufacturing techniques for metals will come up to 1971 when Ciraud patented an ancestor of 3-D laser cladding, later in 1977 Housholder came with concept of SLS and SLM techniques [52].

These techniques are able to fabricate layer-by-layer final complex or even customized 3-D solid object directly from CAD design through computer controlled process. In general by sintering or melting powder using a laser or an electron beam [38], [40], [41], [45], [50], [52], [54].

Thus this technique is typical by melting and rapid solidification of a powder layer; under specific process conditions, resulting in full dense body after solidification [44], [45].

As Hollander et al., in [54] describe, the structural information of the given 3D model is processed layer-by-layer. In fact the model is split into layers with a defined thickness. During the production process each layer is processed separately. Once the layer is finished the table is moved down and new layer starts to be produced. This is repeated till the whole part is produced. The schema of the AM process is shown in Fig. 22.

Moreover this production process is able to create components with graded materials compositions and/or properties which can change in function of requirements and they can propagate across scales. We can talk about tailored properties. While creating porous materials especially for biomedical applications with controlled porosity [40]• [42], [44].

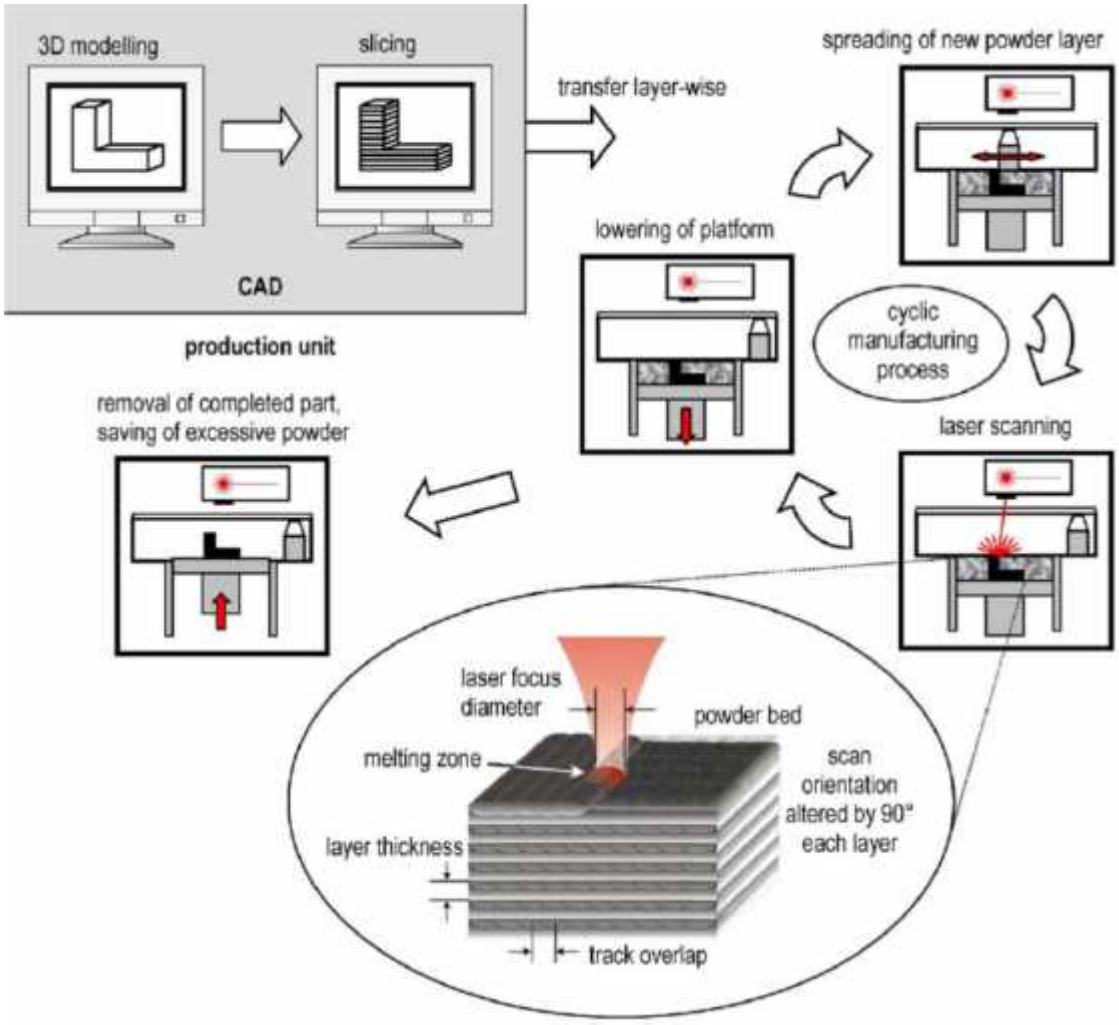

Figure 22 Schema of additive manufacturing process [54]

On the other hand for applications where the porosity is not desirable such as aerospace applications, AM technique can eliminate pores without need of any consequent process such as HIPing [53].

In fact AM techniques have a potential to control the metallurgical structure and texture due to the wide range of melting and casting conditions that are feasible [55].

In general advantages of AM process are creation of mass- efficient, mass-customized designs, optimised geometries, without extensive machining, shorter lead times, high material utilisation rates, reduced tooling costs, high component complexity [50], [52], [53], [56], reducing also costs of machining with significant waste material reduction as the unused powder can be recycled [50], [54].

The typical applications of AM will be any high-technology industries which has high aggregate value [40], [46], such as aerospace [38], [42], [46], [52], [53], [56], automotive [46], [52], [56], biomedical and prosthesis [38], [42], [46], [52], [53], [56] and also some power generation sectors, load absorption, heat exchangers [56], architectural parts and deign object [46].

On the other hand AM techniques present also some problems. Especially in the case of final microstructures, which is might not be from a conventional viewpoint, favourable for the production of engineering materials while dynamically loaded [56]. It is related to the solidification which is the introducing thermal stresses causing component distortion and cracking systems. On the other hand when the temperature is held high during the solidification a degree of annealing is possible causing coarsening of the as-solidified structures. [56]

In fact very large thermal gradients occurs. Due to the very rapid heating of the top layer, combined with a rather slow heat conduction. Then the expansion of the heated top layer is limited by the cool underlying material, resulting in compressive strain in the layer. If the yield stress is reached the compression will become plastic and during the cooling this are will shrink and become smaller. This process will be repeated every time a new layer is created and introducing the heat to already solidified layers in the vicinity. This shrinkages will also add some tensile stresses on top of the layers underneath. As the molten top layer has tendency to shrink during cooling, but it is limited by underlying bulk. As a result, the top layer undergoes a tensile stress, while the previously solidified material is subjected to compressive stress [44].

An understanding of structure and better control of solidification conditions are critical and would allow control over microstructural morphology and thus mechanical properties [51], [56].

The main issues or objectives to optimize as stated by Facchini et al., in [45] would be:

- production of a fully dense material,
- control of the residual stresses (causing distortion and cracks),
- control of the as-built microstructure.

Another limitation are still very high costs associated with this manufacture process, poor surface finish, relatively small building area [42], [46].

Electron beam melting (EBM)

Electron beam manufacturing is promising technology which is able to crate freeform metal products by direct manufacturing a powder precursor melted layer-by-layer with an electron beam in vacuum. The 3D model is sliced into individual layers which can be about tens of microns thick and they are progressively melted through the controlled EB scanning process to build the product model [40], [41], [53].

The first step of the technological process is the spreading of a powder bed on a working plate by mean of a mobile rake. The uniformity of the bed is very important for the proper melting of the layer and for the preservation of the rake, which can be damaged. After spreading, an electron beam (emitted by electron gun which uses a tungsten filament to produce an electron beam) provides the energy for the consolidation of the powder: passing on the bed at a constant speed, it locally melts the powder. Then the working plate is lowered by a distance equal to a layer thickness. Another powder bed is spread and the melting process goes on. The deflection of the beam is accomplished by electromagnetic lenses, resulting in high scanning speed and spotting accuracy [41], [42], [44], [47].

In the Fig. 23 is shown schematically Arcam A2 EBM system. Powder is placed in powder cassettes (4), which by gravity feed it to the part to be produced (6) on a build table (7), where it is raked (5) into layers. The electron beam is generated in electron gun (1) passing through a lens system (2) and scanned across the powder layer (3) by a CAD system. The beam initially preheats the powder. Then beam current selectivity melts the raked layer. As layers are completed, the build table (7) moves down. Then the process will be repeated [40], [42], [47], [56], [57].

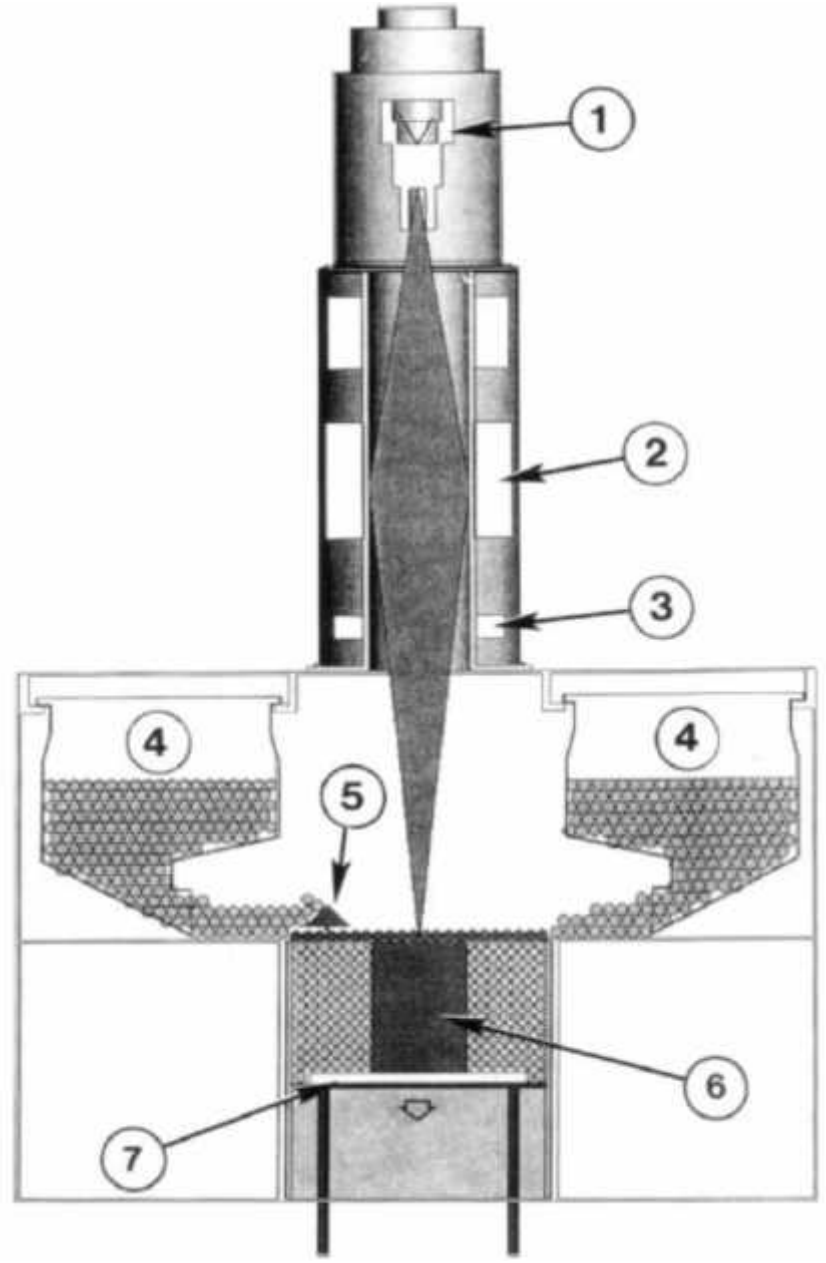

Figure 23 Schema of Arcam A2 EBM system [57]

The non-melted powder is recycled by using powder recovery system. All powder used during the process passes through power recovery system [44], [56].

The advantage of EBM system is a greater energy density which leads to reduced build times and thus manufacturing costs. The high energy also helps to fully melt the metal powder resulting in dense parts with better control of the mechanical properties [42], [44].

The most important parameters to control the process are melt current, focus offset, speed function, beam focus, and beam velocity [56].

Al-Bermani et al., state that lower temperatures result in poor sintering of powder, charging of powder particles, repulsion and higher temperatures result in thermal expansion, powder delivery problems and component distortion. [56]

Titanium Ti6Al4V (Grade 5) powder has a particle size between 45 and 100 microns [43].

In the case of biomedical application, the biggest advantage of EBM process is possibility of tailored properties, adjust strength, fatigue resistance, and elastic modulus of the part to ensure greater bone compatibility. This is possible due to correct choice of process parameters as well as using lower particle sizes [40].

Another advantage is in easily controlled beam focus and energy as well as electrically controlled scan. This of course helps in controlling the building process and allows switching between sintering and complete particle melting or layer melting [40], [50].

EBM process reduces the amount of machining operations to be carried out after the building process, in general semi-finishing or finishing operations are sufficient to ensure required surface quality [38].

EBM compared to other techniques as SLM (selective laser melting) work with preheated powder. It is due to scanning at relatively low beam current and a relatively high scan speed. The preheating of powder leads to the reduction of the thermal gradient between the just-melted layer and the already built up body. This will lead to minimizing the residual stresses in the workpiece [44], [45], [53], [58]. Preheating together with vacuum will also ameliorate the melting itself and its energy efficacy as the particles will be partially sintered and remained at the position during melting [44], [58]. Another advantage of high vacuum is the possibility to build material with densities of greater than 99.8% by reducing the porosity level [53].

The surface finish of parts produced by EBM is worst that those produced by SLM, it is due to the dimension of the melting pool and the accuracy of the beam [44].

The original powder used for EBM has a bit different composition than the final build-up part because the content of the aluminium and oxygen might drop. It is due to high pressure and temperature under vacuum [56]. Moreover as the powder is pre-alloyed and doesn€t contain any additive consequent heat treatment isn€t necessary to remove them [44].

Direct metal laser sintering / melting (DMLS /DMLM)

Laser additive manufacturer, laser sintering or laser melting offer advantage to build a solid freeform part [51], [54] from wide range of materials as metals, ceramics or polymers [54].

Obviously this method is highly interesting for titanium aerospace components because it can greatly reduce the buy-to-fly ratio and lead time for production [51].

The main distribution of the laser method can be divided into methods with non-melting and melting processes. As shown in Fig. 24 [52].

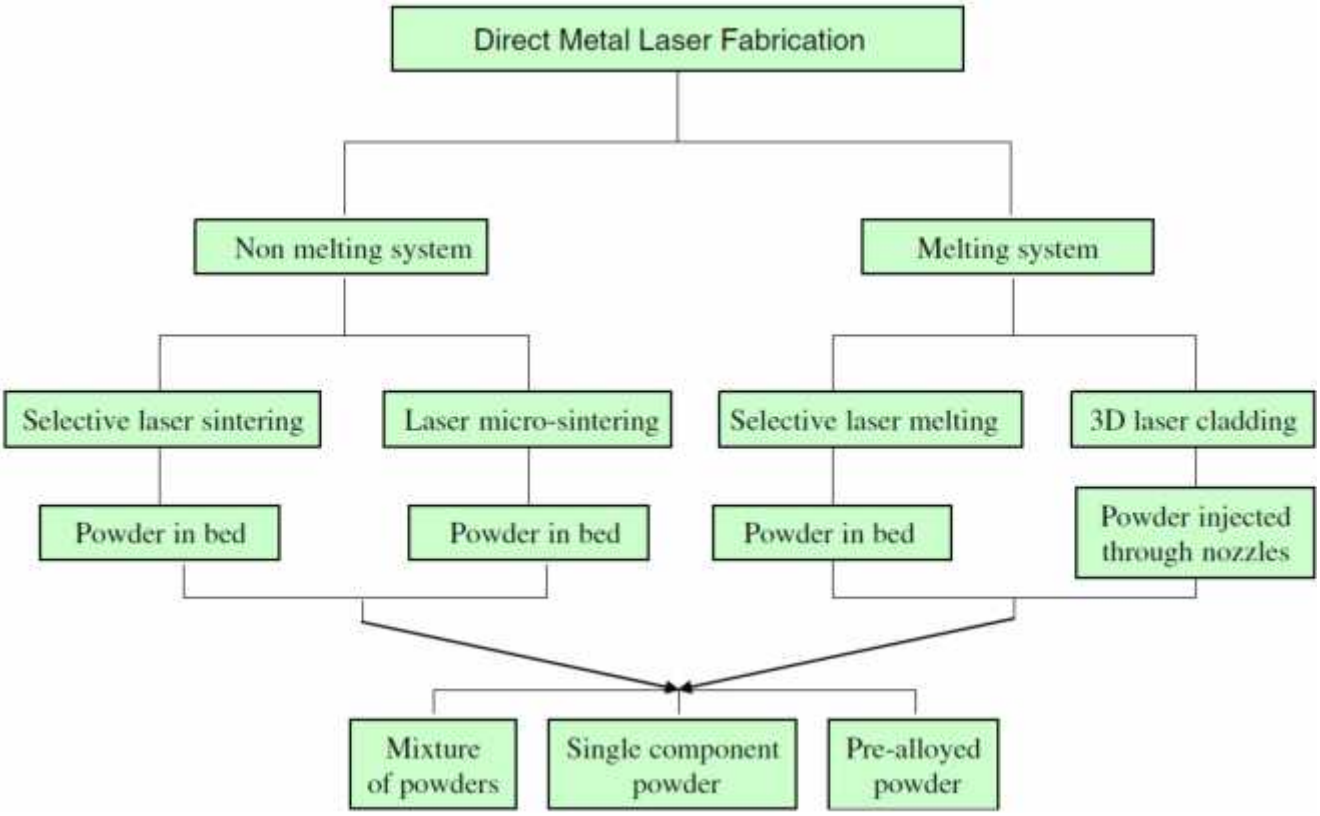

Figure 24 Classification of direct laser fabrication methods [52]

In fact selective laser melting and sintering are very similar methods in terms of equipment. The difference is in the use of much higher energy density, which enables full melting of the powders in the case of SLM, this will ensure very high density of the material [47], [52].

As the laser process can provide functional and mechanical optimization, and weight reduction [46], it is used to build-up titanium parts to produce both permanent and temporary implants [47].

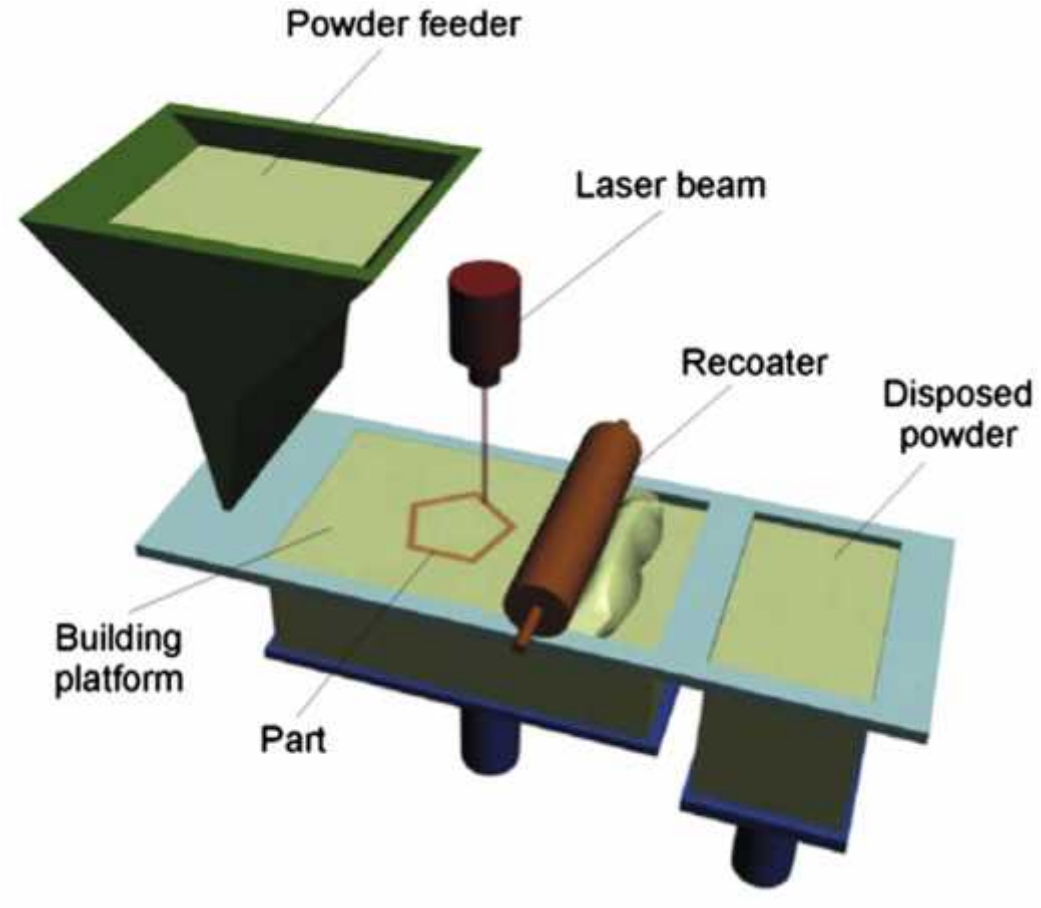

Figure 25 Principles of laser sintering method [46]

In the Fig. 25 are shown schematically the laser sintering process. During the sintering process (or melting process) metal powder is fused into a solid part by melting it locally and by using a laser beam directed by a computer which scans the powder surface. The process is governed layer by layer. Firstly a thin layer of powder is deposited from the powder feeder to the part-build area. Then the laser beam guided by an optical fibre beam expander, scanner mirrors, and a focusing objective is scanned onto the powder bed to form sintered layer. Once the layer is finished the table is moved down about one layer thickness. The creation of new layers is prepared by the powder feeder and recoater, then the process is repeated to create a new layer until the whole part is built-up. The chamber is closed and the process is performed in an inert atmosphere (nitrogen or argon) to avoid oxidation [46], [50]• [52].

In the case of selective laser melting as the metal powder fully melts. The fully dense material will be created, this is resulting in better mechanical properties, but at the same time the process control becomes much more difficult [44], [54].

Contrarily to the EBM process no preheating is applied. It means that the temperature of the chamber is similar to the room temperature and thus the part undergoes a severe thermal gradient and a large undercooling. The solidification occurs rapidly resulting in very fine microstructure [44], [51].

The second effect of sever thermal gradient and quick solidification consist in large residual stresses, which can affect the resistance of the material (by delamination or cracking) and cause geometrical deformations [44].

The variables that influence the final product (its mechanical properties, microstructure, porosity, residual stresses, micro-cracks, texture surface finish) as cited by Kobryn and Semiatin are laser type, laser power and power distribution, laser spot size and shape, laser traverse speed, line spacing, layer thickness, deposition pattern, powder shape, size, and size distribution, powder feed rate, powder velocity, substrate temperature, substrate surface finish, substrate thickness, substrate microstructure and texture, and the size and shape of the deposit [51].

Facchini et al. state that the energy involved in the melting of the metal powder is directly proportional to the power of the beam and inversely to the scan speed, the hatch distance and the layer thickness [45].

In the Tab. 8 are discussed main advantages and disadvantages of SLM process.

Table 8 Main advantages and disadvantages of SLM process [47]

	Advantages	Disadvantages
Material	No distinct binder and melt phases	Not suitable for well controlled composite materials (e.g. WC-Co)
Cost and processing time	Elimination of time consuming and costly furnace post-treatments for debinding, infiltration or post-sintering	High laser power and good beam quality (expensive lasers); smaller scanning velocities (longer build times)
Part quality	Suitable for producing fully dense parts in a direct way	Melt pool instabilities and higher residual stresses

If we should compare EBM and SLS the fundamental difference is in the use of an electron beam to melt the powder in EBM process, while SLS and SLM uses laser to melt the powder. It means that EBM process is faster while creating fully dense parts. Also the availability of high energy electron beams ensures complete melting of the powder particles. Moreover as the EBM process is held under vacuum, impurity free titanium parts are build, unaffected by oxygen and other chemical species available in the atmosphere. The residual stresses are also minimized [42].

In the Tab. 9 main differences between EBM and SLM process are stated.

Table 9 Comparison between EBM and SLM [47]

	EBM	SLM
Thermal source	electron beam	laser
Atmosphere	vacuum	inert gas
Scanning	deflection coils	galvanometers
Energy absorption	conductivity limited	absorptivity limited
Power preheating	use electron beam	use infrared heaters
Scan speed	very fast, magnetically driven	limited by galvanometer inertia
Energy costs	moderate	high
Surface finish	moderate to poor	excellent to moderate
Feature resolution	moderate	excellent
Materials	metals (conductors)	metals, ceramics and polymers

2.3 AM TI6AL4V CHARACTERISTICS

Advantage of AM technique either EBM or SLM is ability to create a wide range of pore sizes and shapes, by variation of process parameters. This is particularly interesting for production of biomedical implants where porosity improve the ingrowth of bone [50].

As demonstrated by Facchini et al., in [41], the mechanical properties of parts produce by AM fulfil the ISO requirements for biomedical implants, on the other hand the microstructure is not recommended by ISO standard for biomedical implants.

The powder particle size influences the final surface roughness of the parts. When the particles are smaller, thinner layers can be achieved and thus higher surface quality can be ensured [42], [52].

As the powder is melted and solidified rapidly during AM process the resulting microstructure is strictly depending on the process characteristics [44].

Al-Bermani et al., describe that prior β grains form epitaxially and extend through many layers. The columnar structure is a typical feature of most AM techniques. The columnar nature of prior β grains is a direct consequence of the thermal gradient that exists in the z direction. [56].

AM process is characteristic by thermal cycling. It is due to the process itself. Melting of new layer will also increases the temperature of under- lying material. In the case of Ti-6Al-4V it means that the beta transus temperature is cycled during the process. Every time when the material is undergoing a phase transformation while some little stress is present, the weaker phase will undergoes irreversible plastic deformation, in the case of Ti-6Al-4V it would be beta phase. Thus in AM because of the thermal cycling and the thermal gradient which introduces the stress into material, some plastic deformation of beta phase will be found [56].

EBM

During the EBM process the process parameters have high impact on final characteristics, for example the build temperature will influence microstructure and mechanical properties. The adjustment of preheating can also increase or decreases necessary energy for consecutive heating, sintering of the layers before melting [56].

Al-Bermani et al. have found that variations in the build temperature between 899 K and 973 K (626°C and 700°C) have significant effect on microstructure and mechanical properties. While the temperature is increased above 951 K (678°C), mechanical properties will decrease and microstructural is coarser in the as-built condition [56].

The resulting microstructure is in fact a combination of solidification conditions, thermal environment, thermal cycling, kinetics, and phase transformations [56].

The difference in AM microstructure compared to the hot worked parts is due to the large undercooling during the process which will naturally promotes the formation of an acicular/lamellar hcp phase. Obviously this microstructure is less ductile than the globular microstructure formed during hot working. The as built EBM Ti-6Al-4V microstructure consists of acicular , and ƒ • phase which can€t be modified by heat treatment [45].

The microstructure is finer than the obtained by metal casting and coarser than that obtained from laser processing, it is an intrinsic characteristic of the EBM technology, where very high solidification rates are achieved. The microstructure is ,+ƒ very fine lamellar morphology, with some , phase at the ƒ grain boundaries [41], [43], where both colony and Widmanstatten morphology can be found [56].

We can talk also about uniform very fine acicular , -phase lamellae organized in a basket weave morphology, Widmanst•tten -like microstructure (with ƒ along the phase boundaries) [38], [40], [44], [56].

The microstructure is fully dense [40]. This microstructure is the result of the rapid solidification and the subsequent annealing, aging due the chamber is kept at elevated temperatures during the process [38], [43], [44].

As Facchini describe it is believed that at first, a martensitic hcp phase forms, due to the large undercooling as mentioned before and then due to the permanent temperature above 600„C the stabilization of the microstructure is possible, the formerly produced martensite is then transformed in an ,+ƒ mixture [41], [44], [56].

Al-Bermani et al., add that full decomposition of ‚€ (martensite) can be achieved at a temperature of 973 K(700°C), while at 873 K (600°C), only partial decomposition will happen [56].

Another result of the preheating, is the fact that the material obtained by EBM undergoes a less severe thermal gradient. Thus the amount of residual stress is lower. This residual stress can be also partially recovered due to permanence at quite high temperatures. Furthermore, preheating is responsible for the formation of *ƒ* phase. [44], [58].

This microstructure has good mechanical properties and is well stable and it will not transform to globular one after heat treatment. It is due to the fact that to create globular microstructure not only heat treatment is sufficient but also material has been pre-strained or dynamically strained, and even in this case the kinetics is quite slow. This not the case during the EBM process [41], [44].

In the case of biomedical applications, usually, a post-process hipping is used to improve implants (reducing of the residual porosity). Fcchini studied the influence of hipping on material produced by EBM. He found that the acicular microstructure undergoes a slight coarsening, but not any modification. Due to the coarsening, a slight increase in elongation and a slight decrease in yield stress and Ultimate Tensile Strength were found [41], [44].

Al-Bermani at al., in their work where Ti-6Al-4V alloy was produced through EBM process, determinate the temperature of solidus and liquidus as 1938 K (1665°C) and 1988 K (1715°C), respectively. [56].

They also state that the original (parent) beta grains will determine the orientation of newly growing alfa grains, there are 12 possible orientations [56].

In following figures (Fig. 26 - 29) are show some case of typical microstructures of Ti-6A6-4V built through EBM process, in all case we can see acicular microstructure, the slight differences are due to different specific process conditions.

In the Fig. 30 is show the microstructure after hipping treatment of as built Ti-6Al-4V EBM alloy, as described by Facchini in [44], not any modification of microstructure is visible, only its coarsening while compared to the Fig. 29 for example.

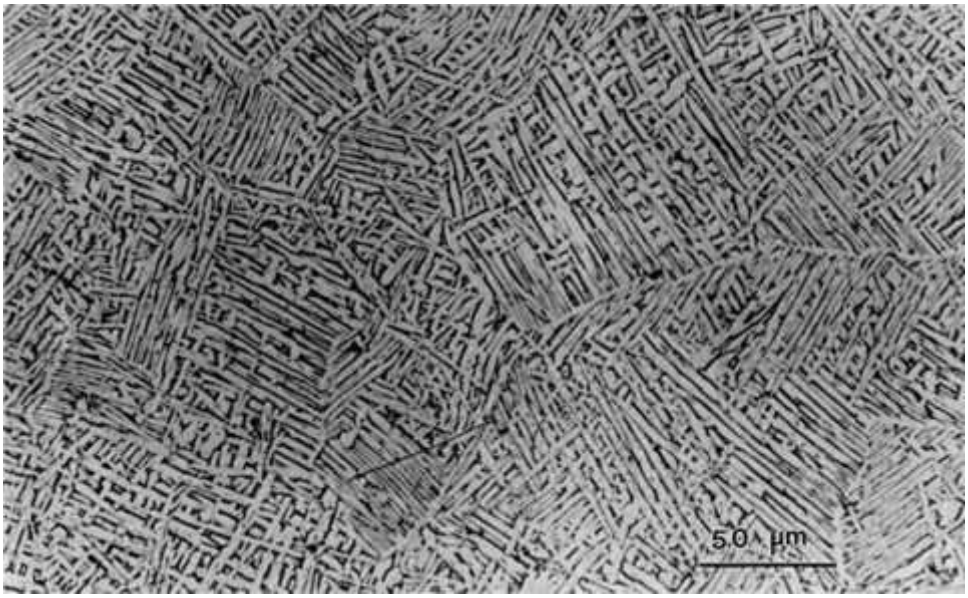

Figure 26 Typical acicular , -plate (Widmanstatten) microstructure of Ti-6Al-4V EBM sample [40]

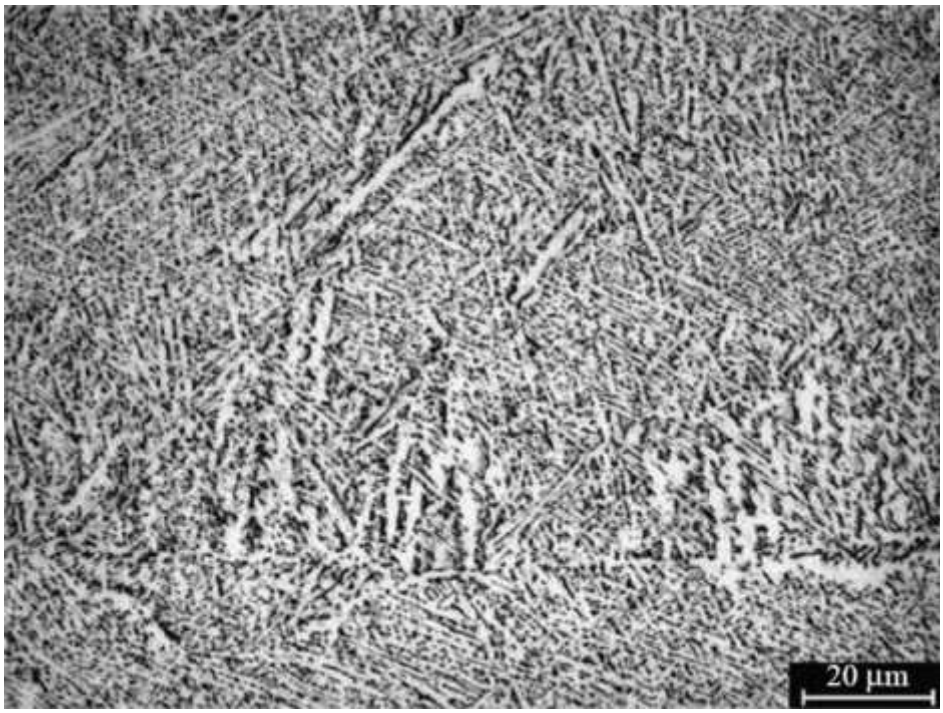

Figure 27 As built Ti-6Al-4V microstructure after EBM process, it is lamellar and very fine, with some , phase at the β grain boundaries [41]

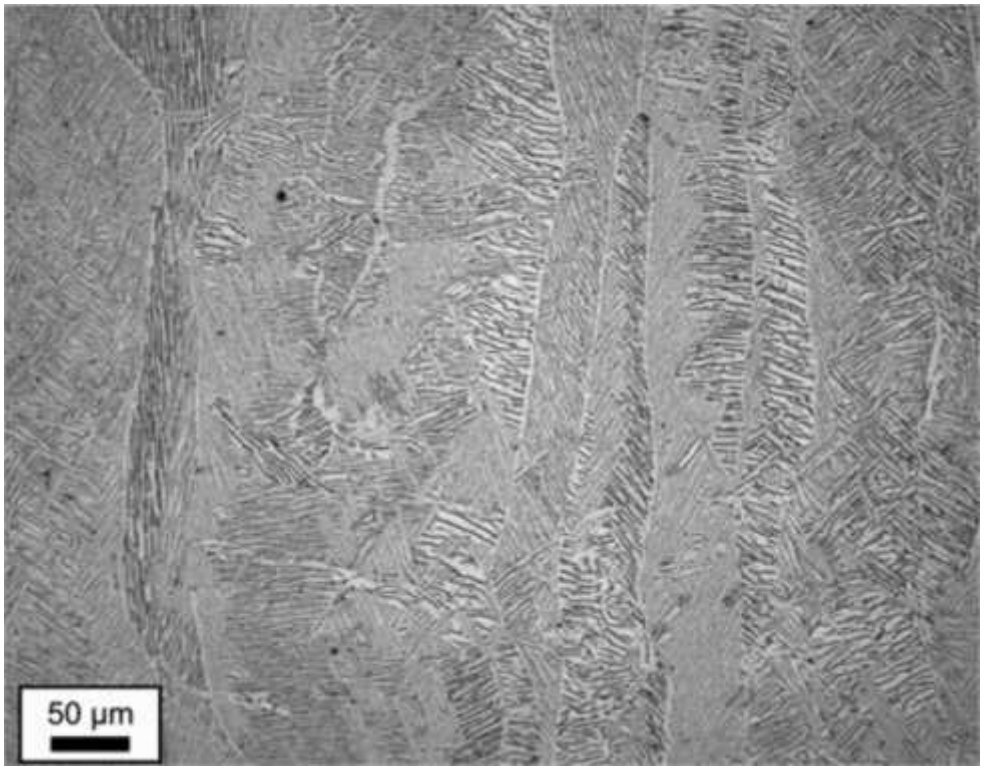

Figure 28 Typical bulk EBM Ti-6Al-4V microstructure [56]

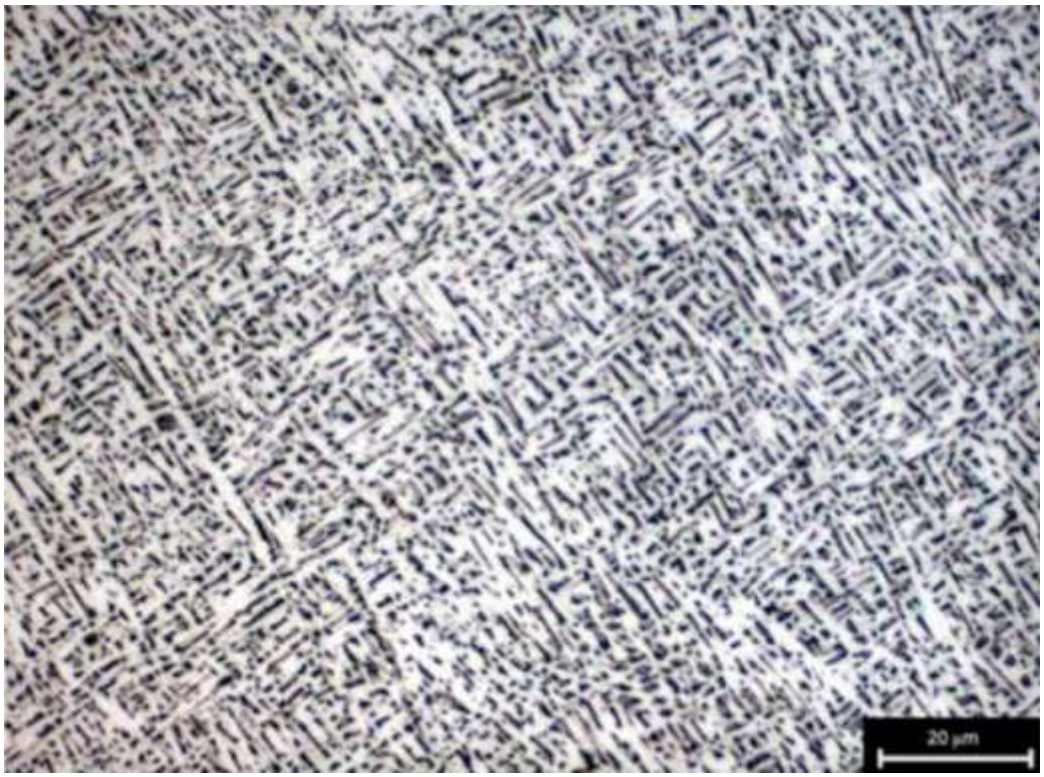

Figure 29 Microstructure of Ti-6Al-4V produced by EBM [44]

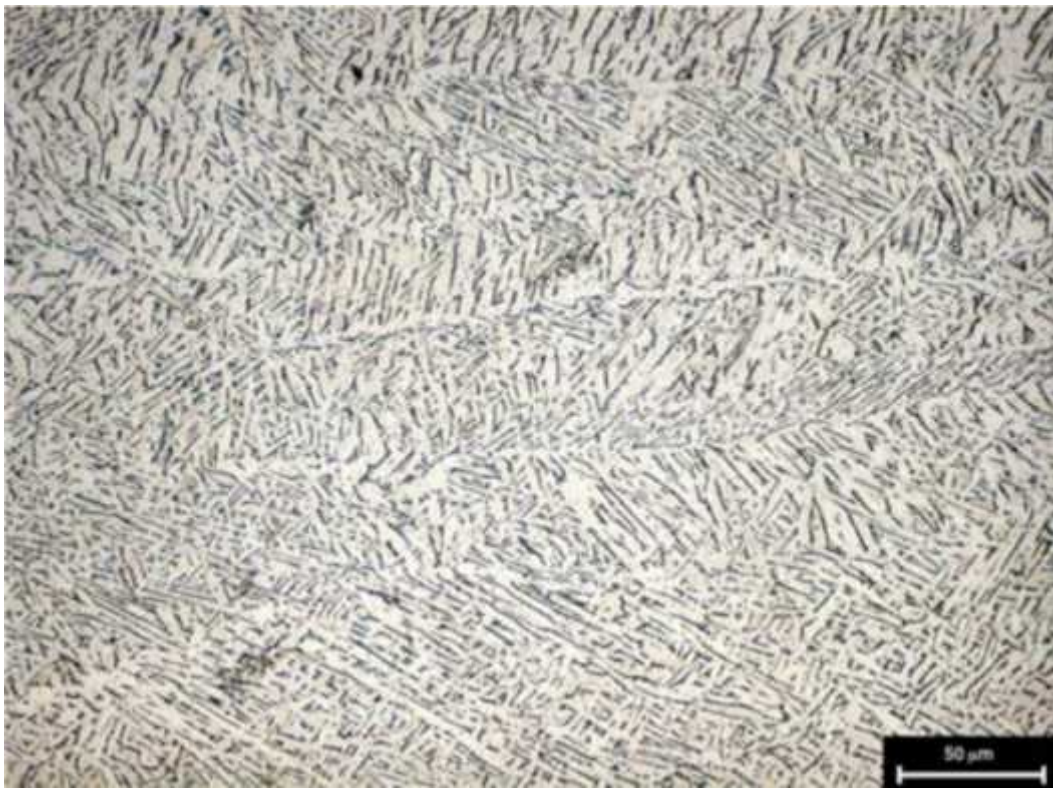

Figure 30 Microstructure of Ti-6Al-4V produced by EBM and hipped in the biphasic field [44].

Tab. 10 shows comparison of chemical composition for typical Arcam Ti-6Al-4V alloy produced through EBM process with Ti-6Al-4V wrought and casted alloy. It is visible that the chemical composition achieved by EBM process fully fulfils the requirements for alloys produced by traditional manufacturing processes as wrought or casted alloys.

In the Tab. 11 are compared the mechanical properties of typical Arcam Ti-6Al-4V EBM alloy with required mechanical properties of wrought and casted Ti-6Al-4V alloys. Once more it is visible that the mechanical properties of EBM alloys are comparable to wrought and annealed alloys or even better than the cast alloys.

Table 10 Comparison of required and EBM chemical composition of Ti-6Al-4V [43]

	Arcam Ti-6Al-4V typical	Ti-6Al-4V required*	Ti-6Al-4V required **
Aluminium Al	6%	5.5-6.75%	5.5-6.75%
Vanadium V	4%	3.5-4.5%	3.5-4.5%
Carbon C	0.03%	<0.1%	<0.08%
Iron Fe	0.1%	<0.3%	<0.3%
Oxygen O	0.15%	<0.2%	<0.2%
Nitrogen N	0.01%	<0.05%	<0.05%
Hydrogen H	0.003%	<0.015%	<0.015%
Titanium Ti	balance	balance	balance
*ASTM F1108 (cast material) **ASTM F1472 (wrought material)			

Table 11 Comparison of mechanical properties of Ti-6Al-4V EBM and traditional one [43]

	Arcam Ti-6Al-4V typical	Ti-6Al-4V required**	Ti-6Al-4V required ***
Yield Strength (Rp 0.2)	950 MPa	758 MPa	860 MPa
Ultimate Tensile Strength (Rm)	1020 MPa	860 MPa	930 MPa
Elongation	14%	>8%	>10%
Reduction of area	40%	>14%	>25%
Fatigue strength* at 600 MPa	>10 000 000 cycles		
Rockwell Hardness	33 HRC		
Modulus of Elasticity	120 GPa		
*after Hot Isostatic Pressing **ASTM F1108 (cast material) ***ASTM F1472 (wrought material) The mechanical properties of materials produced in the EBM process are comparable to wrought annealed materials and better than cast materials.			

Murr et al., in [40] have been studied two different alloys produced by EBM process with different process settings with two different wrought alloys. They have found that there is a correlation between the microstructure (average , -plate dimensions) and the hardness values (Vickers micro indentation hardness and the HRC values).

They have also demonstrated that the hardness is varying in the built material from HRC 37 to HRC 42 within a dimensional range of ~4cm without any systematic variations of the build parameters. Correspondingly elongation in parts built by EBM process is varying, ranging roughly from 23% to 92% greater than the average elongation for high-strength Ti• 6Al• 4V forgings. They suggest to use powder with smaller grain size to achieve thinner layers and thus refine these properties [40].

Murr et al., have compared the mechanical properties for different EBM settings with traditional Ti-6Al-4V alloys, the resulting mechanical properties are shown in Tab. 12. They conclude that the EBM properties are better than powder metallurgy Ti-6Al-4V for which even after HIPing, UTS and elongation do not exceed the ASTM Grade 5 values [40].

Table 12 Mechanical properties of Ti-6Al-4V EBM and wrought [40]

Material	Hv[a] (GPa)	HV (average) (GPa)	HRC	HRC (average)	YS[b] (GPa)	UTS[b] (GPa)	Elongation[b] (%)	Average dimple[c] diameter (μm)
Ti-6Al-4V grade 5 powder	-	5.0	-	-	-	-	-	-
EBM 1 (top) (coarse , -plates)	3.6	3.8	37	40	1.15	1.2	25	4.54
EBM 1 (bootom) (finer , -plates)	3.9	-	42	-	-	-	-	-
EBM 2 (top) (fine/coarse , -plates)	3.6	4.1	49	50	1.10	1.15	16	4.26
EBM 2 (bottom) (finer , -plates)	4.6	-	50	-	-	-	-	-
Wrought 1 (coarse , -plates)	-	3.8	-	48	1.17	1.23	12	5.24
Wrought 2 (equiaxed ,/ƒ)	-	4.3	-	52	1.22	1.29	14	8.07
Ti-6Al-4V ASTM Grade 5 nominal	-	-	-	37	0.90	1.00	15	-
[a] HV (Vickers hardness) for 25gf (0.25 N) lead at 10s dwell 1 HV = 0.01 GPa								
[b] YS (0.2% engineering offset yield stress), UTS and Elongation (%) were obtained from tensile testing at 20°C at a strain rate of $3 \times 10^{-3}\ s^{-1}$								
[c] Measurements using line intercept								

Regarding the fatigue resistance of the as-built Ti-6Al-4V alloy is lower than wrought and comparable with as-cast materials. HIP treatment can€t change the microstructures as stated before, but can increases fatigue resistance up to the level similar to wrought alloy [41]. In the Fig. 31 is shown High cycle fatigue test for typical Ti-6Al-4V Arcam EBM alloy.

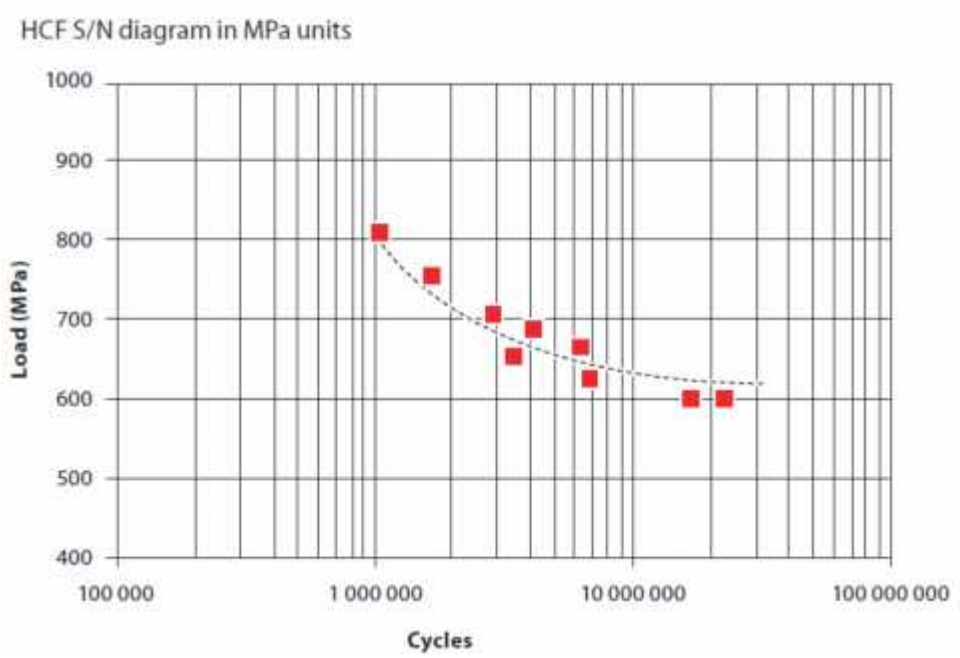

Figure 31 Ti-6Al-4V High cycle fatigue test [43]

SLS / SLM

Ti-6Al-4V microstructure varies based on thermal history. Grain morphology, grain size, and texture are result of solidification and can be controlled by the local thermal conditions during solidification, the transformed microstructure is controlled by cooling rate [51].

The as-built microstructure of the Ti-6Al-4V produced by SLM has a very fine, acicular morphology. Due to the very large undercooling which material undergoes during the process, the final microstructure is martensitic (hpc), with the typical needles. The matrix is composed of acicular , -phase, without β-phase. Contrarily to the EBM process, where the parent martensite is naturally due to elevated chamber temperature transformed into ,+β, in the case of SLM martensite remain the only phase at the room temperature [44], [45], [50].

The materials is fully dense as in the case of EBM [45]. The typical microstructure of the martensite characterized by the needles is shown in the Fig. 32.

To prove the presence of only martensite in the microstructure, Facchini in his work execute XRD analysis, which confirm the presence of hcp phase only [45]. In the Fig. 33 is shown XRD graph for Ti-6Al-4V as built sample after SLM process.

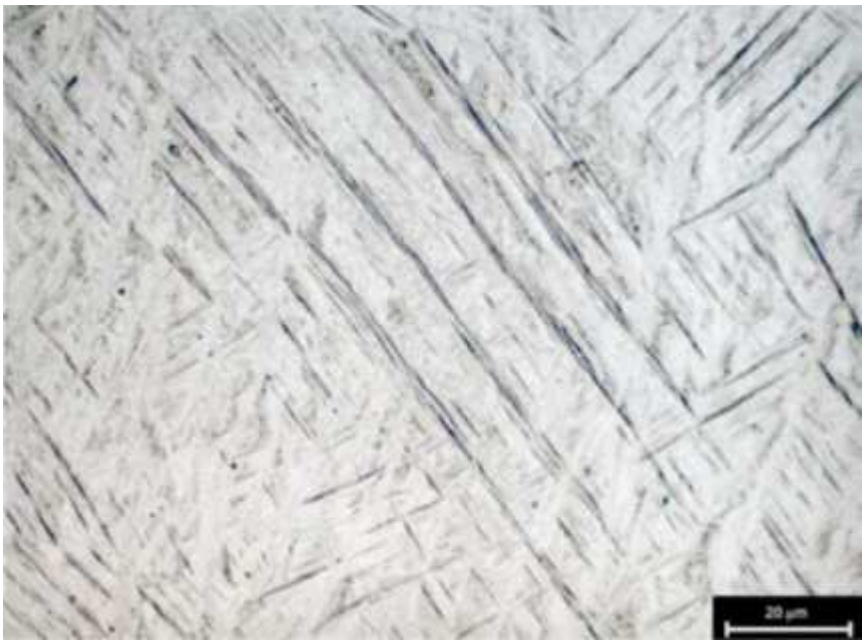

Figure 32 Microstructure of Ti-6Al-4V produced by SLM [44]

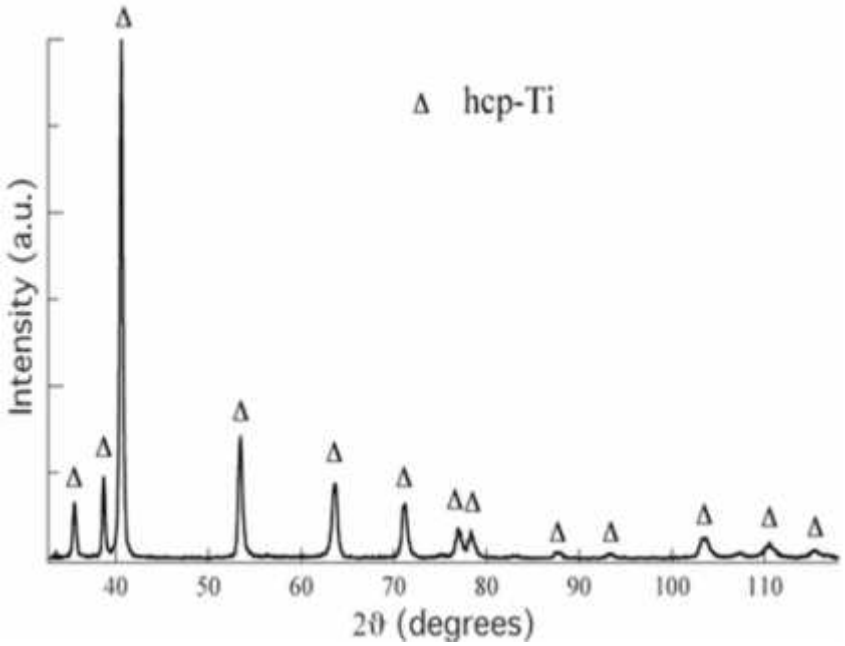

Figure 33 XRD pattern of Ti-6Al-4V produced by SLM [44]

As the hcp pattern is common for the , -phase and the ,€ martensite, they have the same crystalline structure and very similar lattice parameters, it is difficult to distinguish between them. But due to the large undercooling during the process it is reasonable expect that the microstructure consists only form martensite [44], [45].

Kobryn and Semiatin found that the variations in power and traverse speed did not affect the prior f- grain morphology, but on the other hand the effect on prior f-grain width was significant. The grain width will increase with incident energy, this is consistent with the fact that grain size tends to decrease with increasing cooling rate. High energy is resulting from high power together with low speed, yielding a low cooling rate. On the other hand low energy is due to low power, high speed, yielding a high cooling rate [51].

In the Fig. 34 is shown solidification map of Ti-6Al-4V, demonstrating different possible resulting microstructure in function of laser glazes and process settings.

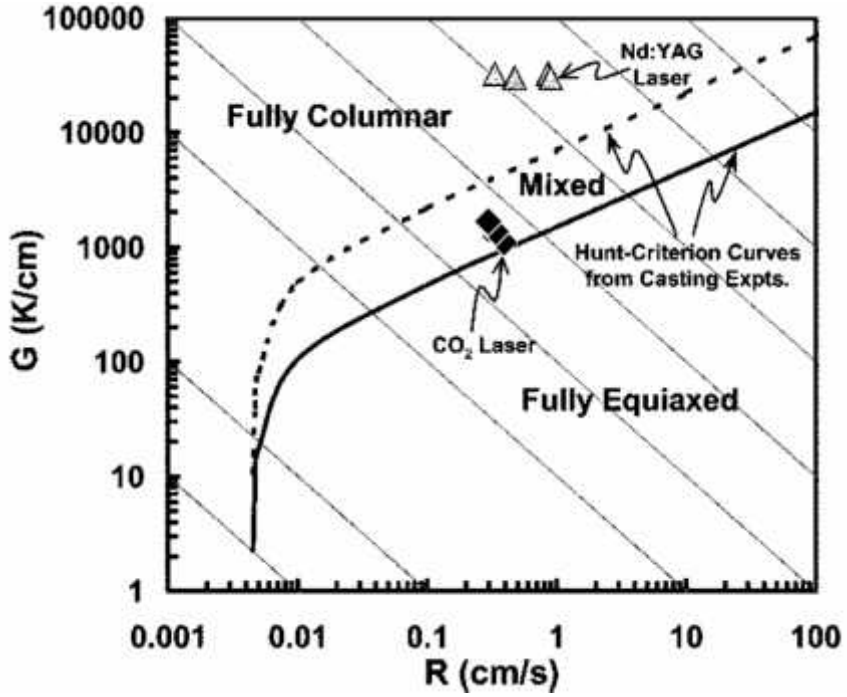

Figure 34 Ti-6Al-4V solidification map with simulated laser-glaze data points [51]

Regarding the mechanical properties of laser sintered/melted Ti-64-4V compared to wrought and cast alloys, the tensile strength variations is ranging to 50% greater than wrought products with corresponding changes in elongation as ranging from ~4.4% to 25% [50].

The alloy produced by SLM reaches higher strength values [44].

Due to the process characteristics, higher level of residuals stress is found [49], [50]. This residual stresses can cause premature failure especially during dynamic testing such as fatigue. To overcome this issue, some heat treatment should be performed [49].

The presence of residual stress in combination with the presence of martensite leads to lower ductility. As the martensite is more brittle than , and β phases [44].

The advantage of the residual stress can be found in anticipating the limit for plastic fracture and thus provide significant advantages in wear applications [44], [50].

Regarding the fatigue endurance of Ti-6Al-4V alloy it depends on the microstructure, better fatigue limit is found for wrought and annealed alloys [44].

In the following figures (Fig. 35 • 37) are shown mechanical properties of as-built Ti-6Al-4V for different AM techniques. We can see that

especially in the case of elongation SLM and SLS techniques exhibit poor results. Thus some consecutive heat treatment is necessary.

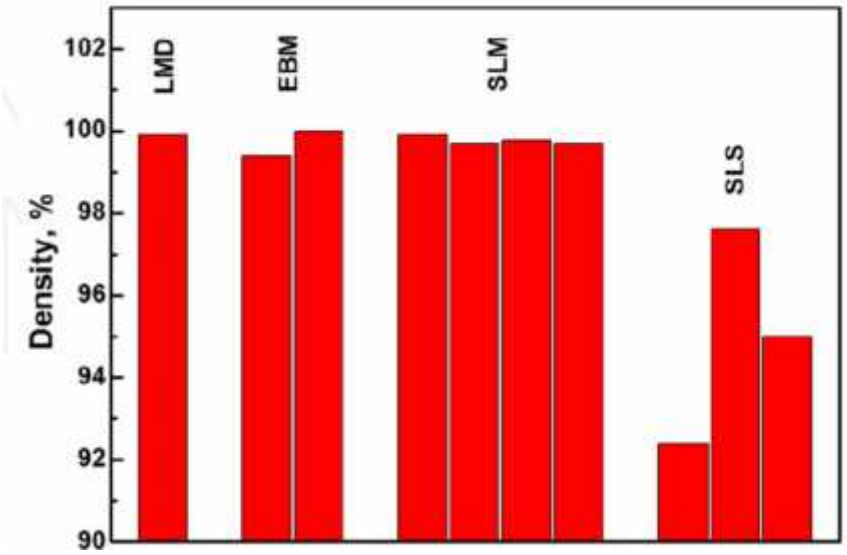

Figure 35 Material density for different AM techniques [49]

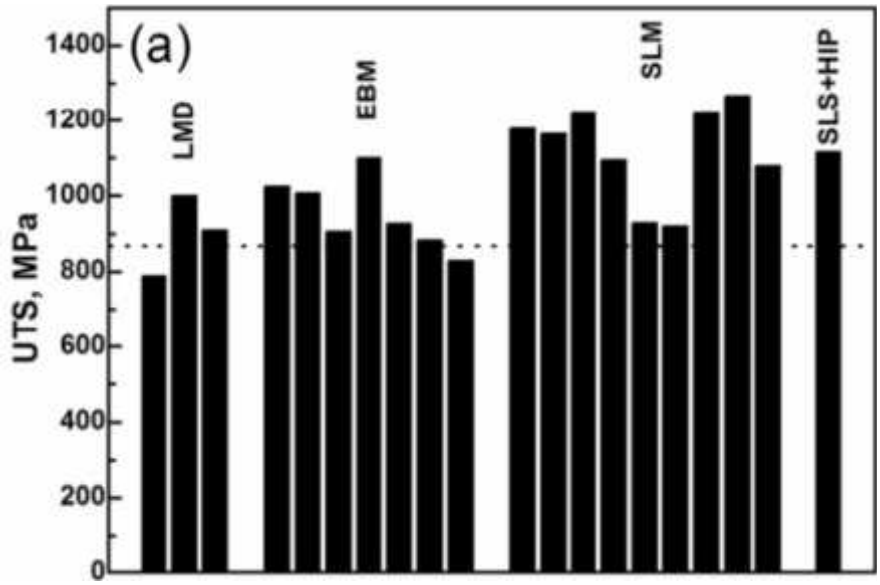

Figure 36 UTS of as-built Ti-6Al-4V for different AM techniques, dotted line represents corresponding ASTM specifications [49]

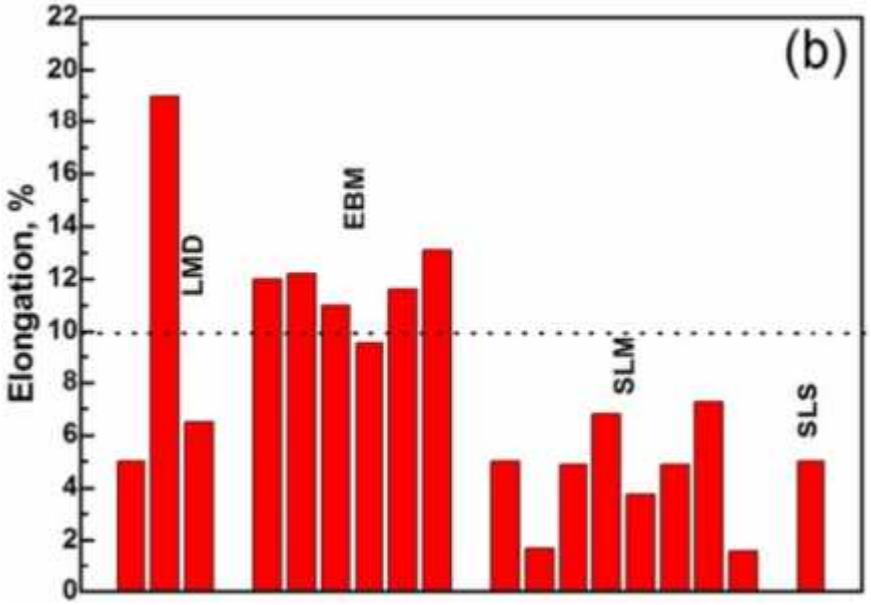

Figure 37 Elongation of as-built Ti-6Al-4V for different AM techniques, dotted line represents corresponding ASTM specifications [49]

In the Tab. 13 mechanical properties of Ti-6Al-4V alloy produced by EBM, SLM and wrought, annealed process are compared. The values are compared with requirement from ISO 5832-3 standard for biomedical implants. It is visible that the values of UTS and yield strength fully fulfil the ISO standard and overcome the wrought, annealed alloy properties. On the other hand the value of elongation especially in the case of SLM built alloy is not satisfying the ISO standard and some heat treatment to improve the elongation should be applied.

Table 13 Comparison of mechanical properties for EBM, SLM, wrought and annealed Ti-6Al-4V [44]

		EBM	SLM	wrought and annealed	ISO 5832-3
Elastic Modulus	[GPa]	118	112	104	-
Yield stress	[MPa]	830	1005	790	>780
Ultimate Tensile Strength	[MPa]	914	1166	872	>860
Elongation	[%]	13.1	8.9	18.1	>10
Limit at 50% of resistance probability	[MPa]	391	381	445	-

Modification of process parameter can improve the wetting during the melting of the powder and thus reduce residual stresses, but ductility will not improve significantly, as the microstructure remains martensitic. Thus only post-building heat treatment can cause the transformation of the metastable martensite into a biphasic ,+ƒ matrix, with a morphology depending on the heat treatment [44], [45].

Facchini in his thesis was studying the heat treatment of Ti-6Al-4V SLM alloy. In fact as microstructure produced by SLM is out of equilibrium, consisting of martensite, which is a metastable phase, thus the necessary driving force is stored into the microstructure and when it will be activate by heat treatment, martensite can transform into stable ,+ƒ microstructure [44].

Facchini suggests to use common aging at temperature range between 480 „C and 595 „C, because as he states the as built SLM alloy might be in condition of solution treated and quenched material and thus aging in this temperature range might be sufficient to stabilize the martensitic microstructure. He tested three different treatments at 550„C: 4 h, 12 h and 24 h. But not any change in microstructure was evident, even not coarsering of the microstructure. Measured values of micro hardens remained similar to those of as-built material. He found that the real microstructural change will occur only in the case when the heat treatment is carried out at a temperature above the ,/,+ƒ transus. He applied a treatment of 30 min at 950 „C. The resulting microstructure after the treatment in biphasic fields is basket-weave type with lamellae of , phase representing the majority of the microstructure, but also some portion of ƒ phase is present (approx. 6%). The new microstructure is thus biphasic, with columnar , -phase crystals formed at the boundaries of the original martensitic plates and an ,+ƒ mixture. But still this microstructure is different form globul ar one of wrought alloy [44].

Facchini also explains that the transformation of the martensite will slightly reduce the strength, but on the other hand will improve significantly elongation. The microstructure is also the main factor which influence fatigue endurance. While comparing wrought and annealed alloy, which commonly has an , -globular microstructure with Ti-6Al-4V produced by EBM and SLM which has in general very fine acicular microstructure a lower fatigue limit is found. In fact, the acicular microstructure is better for the resistance to crack nucleation, but is worse for the propagation of the nucleated cracks. The morphology can be modified by heat treating, the , globular microstructure can€t be never achieved. Such microstructure results from hot working processes, in which dynamic recrystallization is promoted by deformation [44], [45].

In the Fig. 38 is shown Ti-6Al-4V as built SLM microstructure after the heat treatment at 950°C for 30 min. The change of martensite is clearly visible, but it still remains lamellar / acicular one.

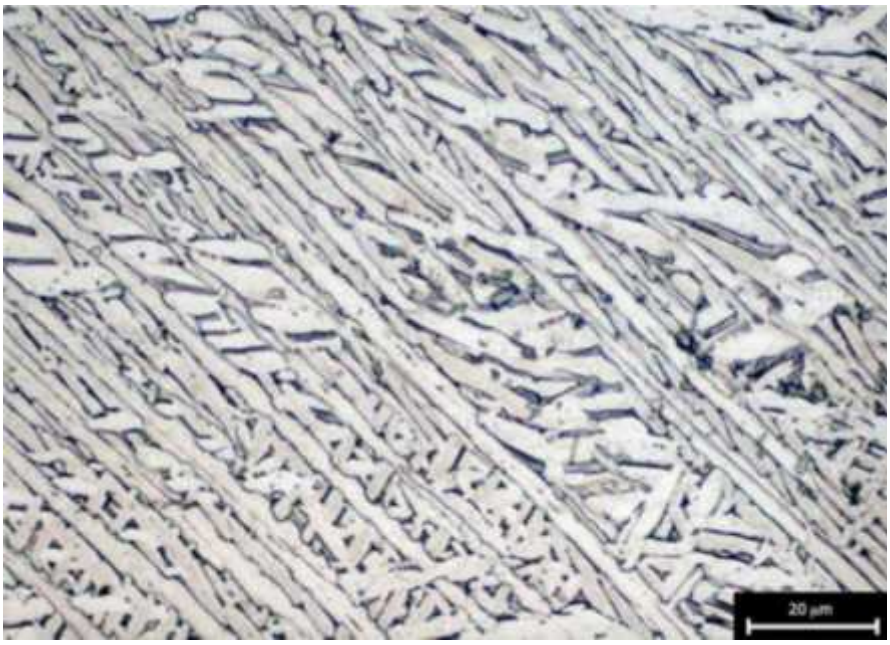

Figure 38 Microstructure of Ti-6Al-4V alloy produced by SLM and heat treated at 950„C for 30 min [44]

Regarding the defects in AM techniques concretely EBM or SLM, due to the not proper control of the process parameters, in particular, the incomplete homologous wetting phenomenon is responsible for the formation of cracks with dimensions in hundreds of microns. This problem may be overcome by proper control of process parameter resulting in fully dense and homogenous material [44].

In Fig 39 is shown one of the micro-crack in the Ti-6Al-4Vproduced by SLM technique.

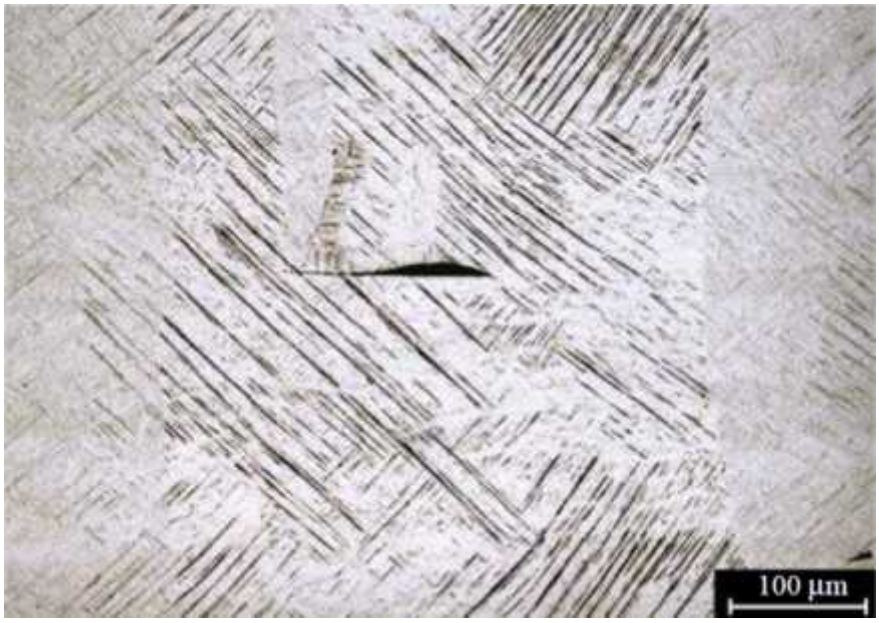

Figure 39 Micro-crack in Ti-6Al-4V SLM [45]

We can conclude that both the EBM and SLM processes can produce a wide range of characteristic crystallographic phases ‰ , (hcp), ƒ (bcc), ,€ (hcp martensite). Resulting microstructure is very fine, biphasic for EBM and monophasic (martensitic) for SLM. Moreover EBM and SLM are able to build any geometries having mechanical properties similar or superior to wrought or cast Ti• 6Al• 4V alloys, which makes from them very interesting technology suitable for producing biomedical implants [44], [50].

3 EXPERIMENTS

3.1 AM IN BIOMEDICAL APPLICATIONS - CASE STUDY

Medicine is as old as the humankind itself. Bartolo et al., in their work [47] mention that evidences of head surgery are dating from 8000 BC and in archaeological museums can be easily found many evidences of using metals and other material as implants as bone, for dental restoration and cranioplasty. Harrysson in [58] is adding that the first successful use of hip implants is dating 18th century and continue till nowadays.

Murr et al. in [50] have estimated that the number of join replacements only in US excesses more than 300 000 surgeries per year and in worldwide scale the metal orthopaedic joint replacements (hip or knee joints) and bone plate surgeries are in millions per year.

As the ageing of the population is progressing every year, a demand on the production of implants is increased too. Requirement is not only the number of implants but also the quality of the products. The implants should serve to the patient for longer time without any possible failure and improve its functionally by fitting in better way to specific patient€s needs[47].

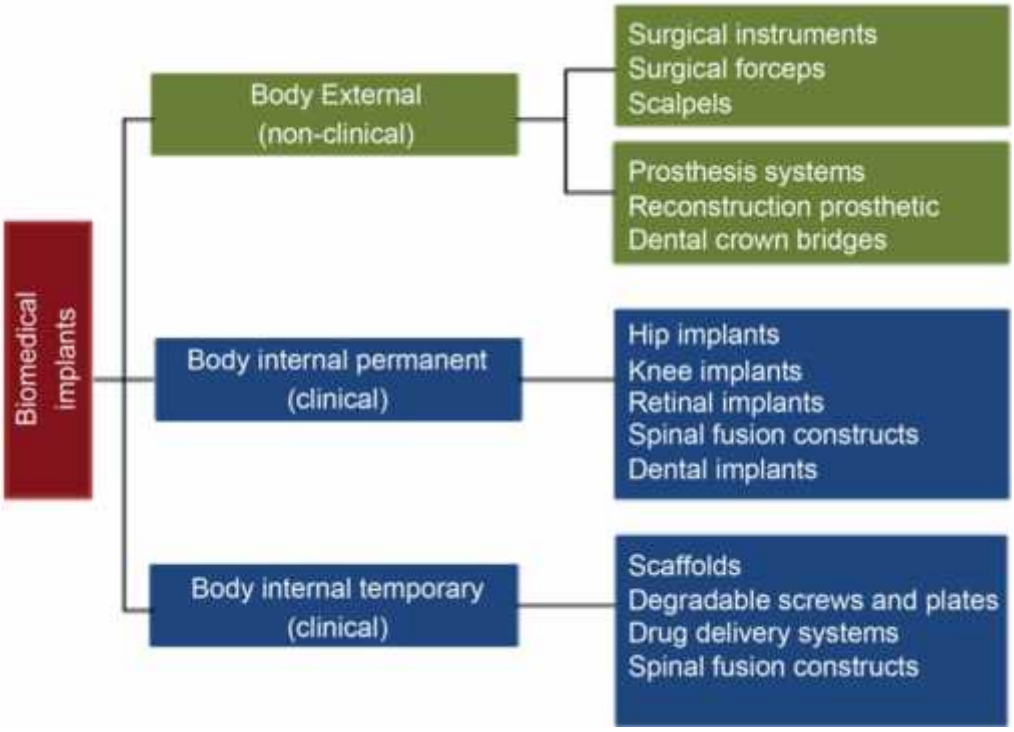

Figure 40 Classification of biomedical implants [47]

Bartolo et al., define biomedical implants as devices which are implanted to the body (inside or on the surface) with some particular function as replacing, assisting or enhancing some functionality of the biological structure. In general we can find implants which are replacing some missing parts as knee, hip replacement, dental pins etc. [47].

Fig. 40 shows the classification of the biomedical implants. The first division can be done between internal and external implants. Internal can be later divided into permanent as mentioned knee, hip implants or temporary as some degradable screws etc. The permanent implant as the name is suggesting, it is device which intended to be implanted into the body and remain there to replace the function of some organ or system. On the other hand, the temporary ones are just supporting some function for limited time as during healing process and in the future will be no more necessary [47].

Because implants are during significantly long time period in contact with body they have to be biocompatible. Bartolo et al., specify that the biocompatibility is time dependent and application related. Because some material can be biocompatible for shorter period but later can be become dangerous, or depending on the location and the environment, tissue which might influences the biocompatibility too [47].

Another classification of the implants can be done based on the use, as functional or cosmetic. The typical functional implants are: hips, knees implants, dental pins, vascular prostheses, artificial ligaments, heart valves, cages, artificial hearts etc. The cosmetic implants as from the name, they will provide some aesthetic function such as breast, nose, ear implants [47].

Obviously another requirements beside biocompatibility on the implants it that their chemical composition and mechanical properties improving the acceptance by the body and its life time [42], [44].

Good implant€s material should be strong and ductile to fit the bone structure with high corrosion resistance and structural integrity [46].

Further maybe not so evident requirement is to use such implant€s material which should ensure the possibility of post- operative imaging methods such as MRI and CT scans by not interfering with these procedures [42].

Widely used are metals and their alloys thanks to their mechanical reliable properties as strength, stiffness, toughness, impact resistance. There are used mainly for load-bearing implants, as a hip, knee implants, fracture fixation wires, pins, screws and plates, Moreover there are also classified as inert, because there is minimal tissue response to them [47].

Between the mostly used metallic materials we can find: stainless steel, cobalt chromium alloys, pure titanium [40], [42], [46] and it is alloys, Au based materials as well as Ag-Sn alloys [47] and tantalum [42].

Medical Ti-6Al-4V is widely used in biomedical metallic implants it is due to its outstanding properties as: excellent biocompatibility, excellent mechanical properties, light weight - low specific weight but significant strength and fatigue endurance, corrosion resistance, human allergic response [40], [42], [44], [47], [48], [50] and osseointegration properties [42].

ISO 5832-3 standard define the requirements for Ti-6Al-4V alloy used in the manufacture of implants for surgery [44]. The basic requirements on the chemical composition tensile properties are mentioned in the Tab.14.

Table 14 Requirements on Ti-6Al-4V by ISO 5832-3 standard for implants as cited by [44]

Tensile properties	
Proof stress on non-proportional elongation	> 780 MPa
Tensile strength	> 680 MPa
Percentage elongation after fracture	> 10%
Chemical composition	
Element	[%]
Al	5.50 • 6.75
V	3.5 • 4.5
Fe	0.3 max
O	0.2 max
C	0.08 max
N	0.05 max
H	0.015 max
Ti	balance

Other mechanical properties of Ti and Ti-6Al-4V alloy used in biomedical implants applications are mentioned in Tab. 15 and 16.

Fig. 41.shows the relation between elongation and Yield strength for different biomedical titanium alloys.

Table 15 Ti-6Al-4V for dental application and its mechanical properties [48]

Property		Ti-6Al-4V casting	Ti-6Al-4V superplastic forming
Tensile strength	[MPa]	976	954
Yield strength	[MPa]	847	729
Elongation	[%]	5.1	10
Vickers hardness	[Hv]	-	346

Table 16 Mechanical properties of biomedical Titanium [48]

Alloy	Tensile strength [MPa]	Yield strength [MPa]	Modulus [GPa]	Elongation [%]	Type of alloy
Pure Ti grade 1	240	170	102.7	24	,
Pure Ti grade 2	345	275	102.7	20	,
Pure Ti grade 3	450	380	103.4	18	,
Pure Ti grade 4	550	485	104.1	15	,
Ti-6Al-4V ELI mill annealed	860-965	795-875	101-110	10-15	,+f
Ti-6Al-4V annealed	895-930	825-869	110-114	6-10	,+f

One of the main advantages of the titanium is in its low Elastic Modulus which helps distribute more equally the stress between the bones and implants and thus minimizing bone resorption and osteolysis [44].

Regarding the fatigue crack propagation rate of titanium alloys, as cited by Niinomi [48], it is affected by body environment. The fatigue crack propagation rate of pure titanium will be higher in NaCl solution than in dry air.

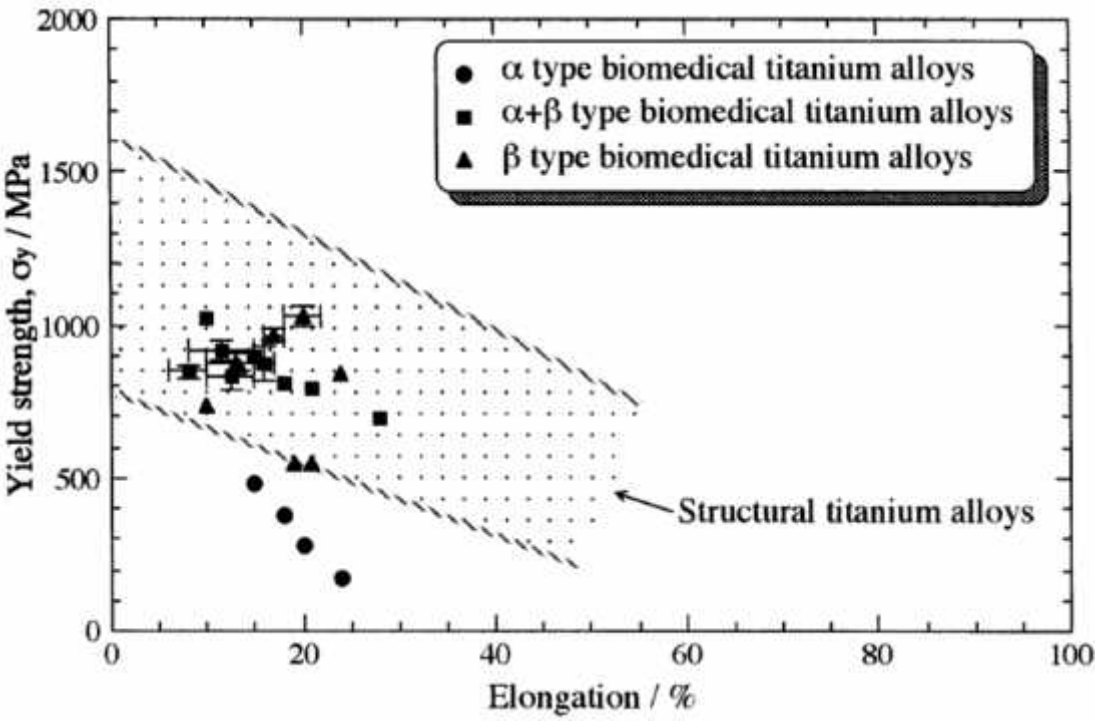

Figure 41 Elongation to Yield strength dependency for Ti alloys [48]

The traditional fabrication process of Ti-6Al-4V biomedical implants consists mainly of hot working and machining of wrought semi-products [44].

The implants are fabricated mainly from wrought or cast bar stock by CNC, precision CAD-driven machining [40], [50].

These operations have some critical factors which will influence the final properties. These factors are: alloying; the melting process used in ingot processing; mechanical working history; heat treatment temperatures and cooling rates and aging treatment [50].

One of the main issue of biomedical implants is very low success rate especially in the case of young patients as reported by Harrysson et

al.. They estimate that the average useful implant life is typically 10 to 15 years. This time range depends on more factors such as: patient, implant type, fixation method, material of the implant. The origins of implant€s failure is mainly implant wear, bone resorption and related osteolysis [58].

Bone as a part of live organism is adapting to the conditions in which is living. It means that the bone system will react to the mechanical conditions. In the case of dynamical loading the bone will have tendency to add some mass to compensate this loading and analogically in the areas which are unloaded or loaded statically the mass will be reduced. The bones need thus appropriate stress loading in order to be properly remodelled. The process when the bone is broken down by osteoclasts and the minerals are released is called bone resorption [42], [58].

Bone resorption is result of stress shielding which is the term describing the decrease in the stress applied to the bone and thus the reduction in bone density. Stress shielding and bone resorption may result in premature aseptic loosening of the implant [42], [58].

As reported by many authors [42], [47], [48], [50], [58], the mechanical properties of implants are much higher than those of bones. In fact materials with higher elastic moduli than of natural bone, will cause stress shielding characterised by bone resorption and thus possible loosing of the implant.

Niinomi states that the moduli of metallic biomaterials like stainless steel and Co type alloy are round 206 and 240 GPa. Compared to the bone modulus of elasticity which is generally between 17 and 28 GPa, they are much greater [48].

Also Parthasarathy et al. state that in the case of titanium which is approximatly twice as heavy as natural dense cortical bone equivalent. The elastic modulus of Titanium alloy is about 114 GPa while that of cancellous and cortical bone range from 0.5 GPa to a maximum of 20 GPa [42].

Therefore Murr et al., suggest that mechanical biocompatibilities (mechanical properties) of the implants should be adjusted to levels suitable for structural implants which are replacing tissue [50].

Harrysson et al. add that even the use of flexible materials will reduce stress shielding and bone resorption, but they will increase interface stresses between the implant and bone. Often they fail due to insufficient interface strength between bone and implant [58].

Consequently many authors recommend to create implants where not only their weight but also their effective stiffness will be comparable to that of healthy bones. They suggest to create a porous structure, which will improve ingrowth surface and also minimise the stress

shielding by balancing the mechanical properties between implant and bone [42], [50], [58].

Another causes of implants failure as described by Murr et al., are due fatigue or fatigue-related failure such as fretting fatigue and also wear or wear resistance [50].

Bartolo et al., specify the reasons of failures, there are obviously more possible reasons such as wrong design (not designed for a specific patient), material selection, application, manipulation, installation and misuse. They also split the causes into biologically related as infection and excessive tissue responses. And into mechanically related, such as stress concentration, micro-displacements, surface scratches affecting the passivation layer, wear generating particles and debris. They precise that fatigue and corrosion are mainly related to metal implants and conversely wear is typical for polymeric parts [47].

Also the revision surgeries to eliminate the issues with the first implants are often not preferable and sometimes even not possible due to potential bone loss. Moreover they are very costly [58]. Thus the use of maybe more expensive but in long-term more reliable implants would be preferable [46].

Above the problems related to the use of material with appropriated properties, the challenge is also in fabricating and machining implants of complex shapes. This would lead to long time cutting operations, with significant material removal, where up to 80% of bar stock material can be wasted as chips, this is typical for example for knee implants as specified by Murr [50].

Moreover the production of mass, generic components might not satisfy needs of specific patient as with abnormal anatomy. Also in the case of atypical surgeries and implants like in the case of craniolpasty where very specific and large part of bone is missing. In these cases a custom designed, tailored implants fabrication is required[50].

All these issues can be eliminated or at least minimized by using AM technologies to produce biomedical implants as specified below:

AM technologies are characteristic by ability to create customized, tailored products. The customization can be provided in the terms of mechanical properties, microstructural characteristics, material porosity, free forma and complex shapes, etc.

(1.) AM is able to build up parts with graded mechanical properties, adjusting hardness, strength and wear properties as necessary. This is particularly beneficial to reduce the implant's bending stiffness while maintaining its strength and thus limiting the that will reduce stress shielding [40]• [42], [45], [46], [58].

(2.) Another advantage is ability to create porous materials. As discussed above, porosity will improve the ingrowth of the cells, tissue to ensure better joining between implants and body and mainly will overcome or minimize the problem of stress shielding and bone resorption [40]• [42], [45], [46], [50], [58].

(3.) AM builds up a free-form parts with complex shapes from any 3D CAD. Which can be designed to better fit a specific patient needs based on CT scans. This is a big advantage especially in the case of surgeries when some anatomical anomalies are found or for example in the case of cranioplasty [41], [42], [45], [46], [50], [54], [58].

(4.) AM is costs reducing, as the AM technique is building the final produce layer by layer from powder and creating almost near-net-shape parts. The material waste are considerably reduced [46], [50]. Murr et al., also mention that AM in the case of producing knee implants is far more cost and time effective than CNC machining [50]. Harrysson et al., add that even in the case when the design of AM would be more time consuming and more expensive but thanks to its customized properties its longevity is significantly improved and thus the overall costs are improved too [58].

(5.) AM is able also to control the microstructure of the part, creating fully dense materials, and minimizing the residual stresses [45].

3.2 EXPERIMENTAL SET-UP

3.2.1 Micro-milling centre

All the experiments have been carried out on micro-milling 5 axes canter Kugler Micromaster 5X (Fig. 42). This machine is devoted to micro-milling operations. Machine is placed in air conditioned room to prevent any possible thermal distortion. The room temperature is kept to 20°C +- 0.1°C. Moreover the structure of the machine is made from granite to ensure high stiffness.

Machine is equipped with air bearing spindle which is able to reach up to 180 000 RPM. Issue related to air-bearing spindle is the thermal expansion in the spindle direction (in our case Z axis) which can reach from few to tens of microns. Our machine is equipped by eddy current sensor, which is online monitoring and compensating the thermal expansion of the spindle axes.

All-over positional error is of 0.3 …m and the maximum linear axis speed of 6€000 mm/min.

Figure 42 Micro-milling centre

To be sure about spindle expansion some procedure was set up to ensure repeatability and precision of the experiments.

The procedure consists of the stabilisation of the spindle expansion. Before each experiment the spindle was left to run at the desired spindle speed for at least 5 min while value of the spindle expansion was checked regularly. Once the expansion was stabilizes a G-function G182 was called, which enables the online spindle compensation, in this case it is in order of tens of microns or up to 1-2 microns.

Then the macro function of the machine was run, using Renishaw touch probe to acquire position of the workpiece and thus set the reference system. Then tool€s length of rotating tool (always at the same spindle speed) was measured by laser device.

Now the reference system is set, but to be completely sure about the real position of Z0, some †scratching tœsts‡ have been processed. In fact at low feed rate and constant Z step tool was approached to the workpiece and we have been looking for presence of any scratch to be sure at which Z coordinated the surface will be scratched and where physically the Z0 is situated. Then the difference between Z value seen on the screen while scratching surface and theoretical Z0 in the machine coordinate system was compensated by offsetting the original coordinating system in + or • Z direction.

3.2.2 Workpiece

The workpiece material used in our studies was titanium alloy Ti-6Al-4V provided by different means of production techniques. We tested Additive Manufactured (AM) materials and compared their performances with those of wrought one. Regarding additive manufactured techniques Electron Beam Melting (EBM) and Direct Metal Laser Sintering (DMLS) have been used. The received as-built cylinders of the material was cut by Wire Electrical Discharge Machining (WEDM) to obtain flat parallel surface.

Later one of the surfaces cut by WEDM, was grinded by sandpapers and polished by solution of silica in order to remove the layer which has been influenced by WEDM process and ensure the best possible flatness. As one of the studied parameters is the microstructural alteration after the micro-milling process. Thus we want to minimize possible effects of previous operations on the final microstructure.

The workpiece was fixed on the machine€s table by using two-component epoxy adhesive as shown on the Fig. 43.

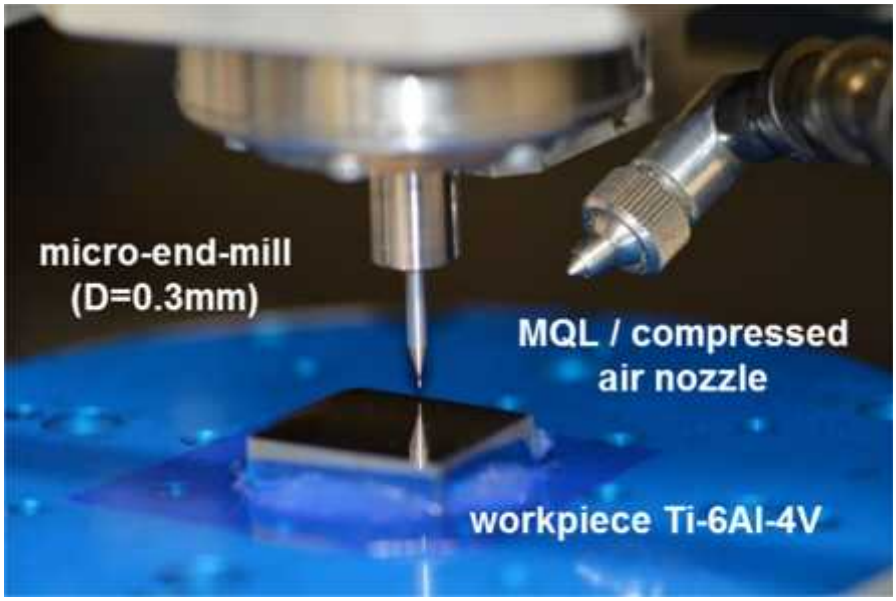

Figure 43 Experimental set-up

Alignment and the tilt of the workpiece were compensated manually, by acquiring some points with Renishaw touch probe. From their coordinates the angles to compensate the alignment of the workpiece€s edge along the machine€s Y axis and workpiece€s top plane towards machine€s XY plane were calculated. Then those values were used to compensate manually the alignment and tilt.

3.2.3 Tools

Tools used for micro-milling experiments were two-fluted uncoated tungsten carbide micro-end-mill with flat end-square geometry (Fig. 44). The tool€s manufacturer is Kyocera. Diameter of the tool is 0.3 mm.

Each tool was inspected before milling experiments with a FEIŽ Quanta 400 Scanning Electron Microscope (SEM) to verify the absence of any possible production defects, such as damages or micro-cracks on the cutting edge. For each experiment a new, fresh tool was used to not introduce the influence of tool wear into the studied parameters.

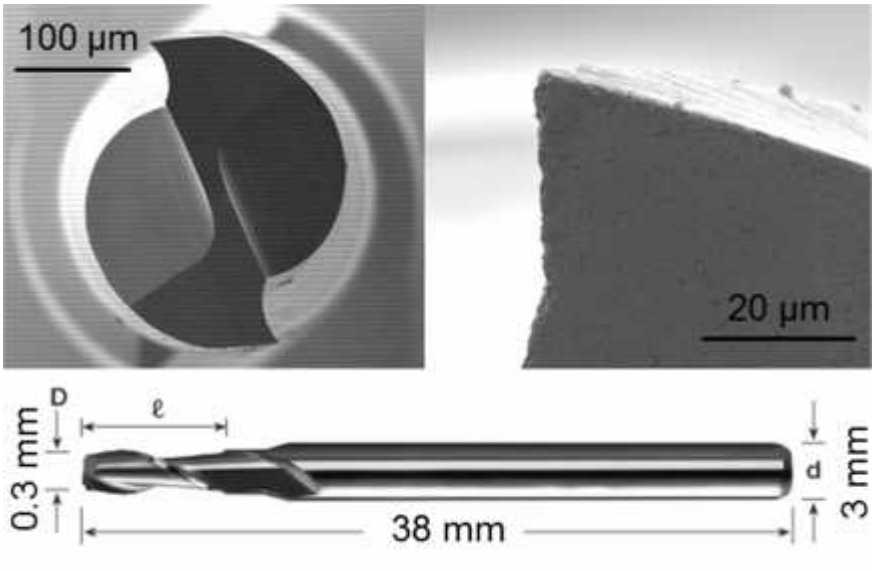

Figure 44 Micro-milling tool

3.2.4 Design of experiments

We are interested in the study of micro-machinability performances of additive manufactured materials devoted to biomedical sector. As the final products are biomedical implants, one of the most important parameter is the quality of the final surface and surface integrity. Thus we have been measuring surface roughness, checking the surface defects, microstructural alteration, tool state after the machining and the burrs formation, which one of the most limiting factors in micro-machining.

Chosen strategy was full immersion slotting where the width of the slot is equal to the tool diameter, in our case 300 µm. And the depth of the slot was equal to the depth of the cut a_p and was set constant for all experiments, equal to 30 µm. This value was chosen in regards of the final application. As the implants are produced by additive manufacturing, only finishing or semi-finishing is sufficient to finalize the implants. Thus the depth of the cut was set to 30 µm which is in correspondence to finishing of AM implants.

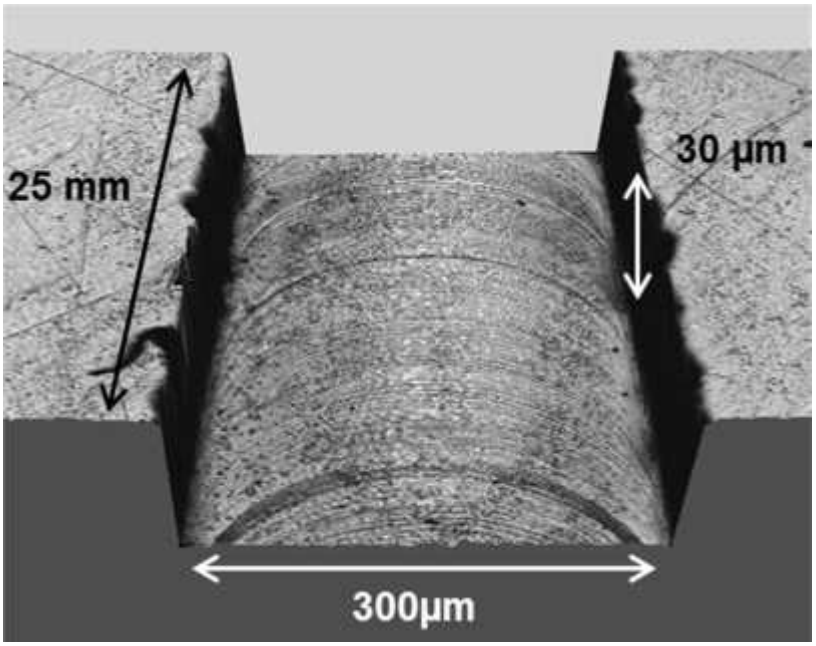

Figure 45 Geometry of the machined slots

Fig. 45 shows the geometry of the slots during the experiments.

The design of the experiments was chosen full factorial design with 2 factors cutting speed and feed per tooth with 3-4 levels and with 2-3 repetitions.

3.3 PRELIMINARY TESTS

As a first experimental campaign some preliminary tests were carried out to evaluate chosen cutting condition, strategy and design of the experiments.

The really first trials have been done on aluminium blocks, later once the feasibly of the procedure was verified EBM material has been used.

In the Fig. 46 is shown the microstructure of as delivered / as built EBM Ti-6Al-4V. We can see very fine acicular microstructure consisting of , -phase fine lamellae, organized in a basket wave morphology with 7% of bcc β-phase in a hcp matrix. The acicular microstructure of the EBM Ti6Al4V induces higher tensile strength and hardness, reduced elongation at fracture, and lower fatigue limit in comparison with the wrought alloy that generally shows a globular microstructure. As previously explained more in details in chapter 2.3.

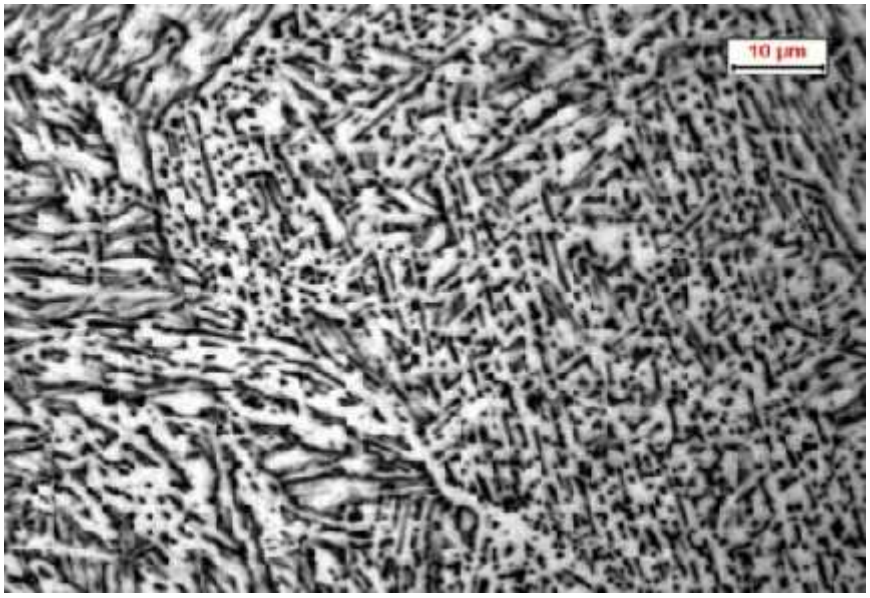

Figure 46 Microstructure of as built Ti6Al4V EBM

The micro-milling experiments have been carried out under nearly dry lubrication condition, MQL (minimum quantity lubrication) technique was used. The cutting fluid was mineral oil (isoparafin oil).

Three levels of cutting speed and three levels of feed per tooth were tested, the values are showed in the Tab. 17. Each combination was tested twice.

Table 17 Tested factors (preliminary tests)

		Levels		
Factors	v_c [m/min]	50	75	100
	f_z […m]	0.8	1.5	3.0

After the micro-machining experiments, the workpiece and the tools were gently cleaned in an ultrasonic bath in order to remove the cutting fluid residuals and the chips particles. Then, a qualitative estimation of the tool wear, chip morphology, microstructure alteration, as well as the measurement of the slots geometrical dimensions and of the surface roughness were performed. Also some samples of chips were collected for each experiment.

3.4 EBM TI6AL4V

3.4.1 EBM DRY experimental campaign

After the preliminary tests the experiments on EBM material machined firstly under dry lubrication condition were performed. As the target industry is the biomedical, the performances of dry cutting are very interesting to be tested as the cleanliness of the workpiece is extremely important and thus limitation of the cutting fluids would significantly improve it.

The tested cutting conditions are shown in the Tab. 18. All the combinations were repeated twice.

Table 18 Tested factors (EBM dry)

		Levels			
Factors	v_c [m/min]	63	92	145	-
	f_z […m]	0.1	0.5	1.5	3.0

The values of the cutting speed were chosen in the regards of the recommended cutting speed for titanium alloys which is in general around 80 m/min [59].

Concerning the feed per tooth, the value of the cutting edge radius of the tool was estimated to be around 1.1 μm. From a literature we know

that the radius of the cutting edge has influence on a cutting process, in fact ratio of the uncut chip thicknesses to the cutting edge radius is decisive parameter between sharing and ploughing mechanism and thus the choice of correct value of feed per tooth is primordial. The minimum chip thickness ensuring sharing process in the case of biphasic materials is about 0.3 • 0.4 times the cutting edge radius. [9] In our case it would be 0.33 • 0. 44 μm. For this reason value of 0.1 μm per tooth for feed was set to introduce into the machining ploughing effects and its consequence to the quality of the surface. Then values of feed per tooth 0.5μm and higher were used, in this case to be sure that ploughing is minimised and only sharing is contributing to the cutting process.

3.4.2 EBM MQL experimental campaign

After testing dry lubrication condition some tests of MQL lubrication on EBM material have been proceeded to compare the performances of the different lubrication methods.

The cutting conditions tested during MQL campaign are stated in the Tab. 19.

Values of the feed per tooth are same as in the case of DRY campaign, only the cutting speed of 92 m/min was excluded from the experiments as during the evaluation of dry campaign we have found that the results are perturbed by vibrations and thus we decided to eliminate this cutting speed from all next tests.

Table 19 Tested factors (EBM MQL)

		Levels			
Factors	v_c [m/min]	63	145	-	-
	f_z […m]	0.1	0.5	1.5	3.0

3.4.3 EBM CRYO experimental campaign

Once both DRY and MQL experimental campaign were proceeded, we decided to perform also micro-milling experiments under cryogenic condition, which would be another promising and interesting cooling option in the case of biomedical industry, while the cleanliness would be preserved.

As cryogenic fluid liquid nitrogen was used and the workpiece was placed inside a cryogenic chamber which was designed and built at the UNIPD. The cryogenic chamber was cooled down to approximately minus 160°C. The workpiece temperature was controlled through a J-type thermocouple, which was placed just under the top surface of the workpiece, inside a drilled hole.

In the Fig. 47 is shown designed cryogenic chamber. The chamber is well isolated to prevent cooling down of the micro milling machine and its environment. The workpiece is placed on the top surface and from the bottom the nozzle with liquid nitrogen is conducted to the workpiece to cool it down.

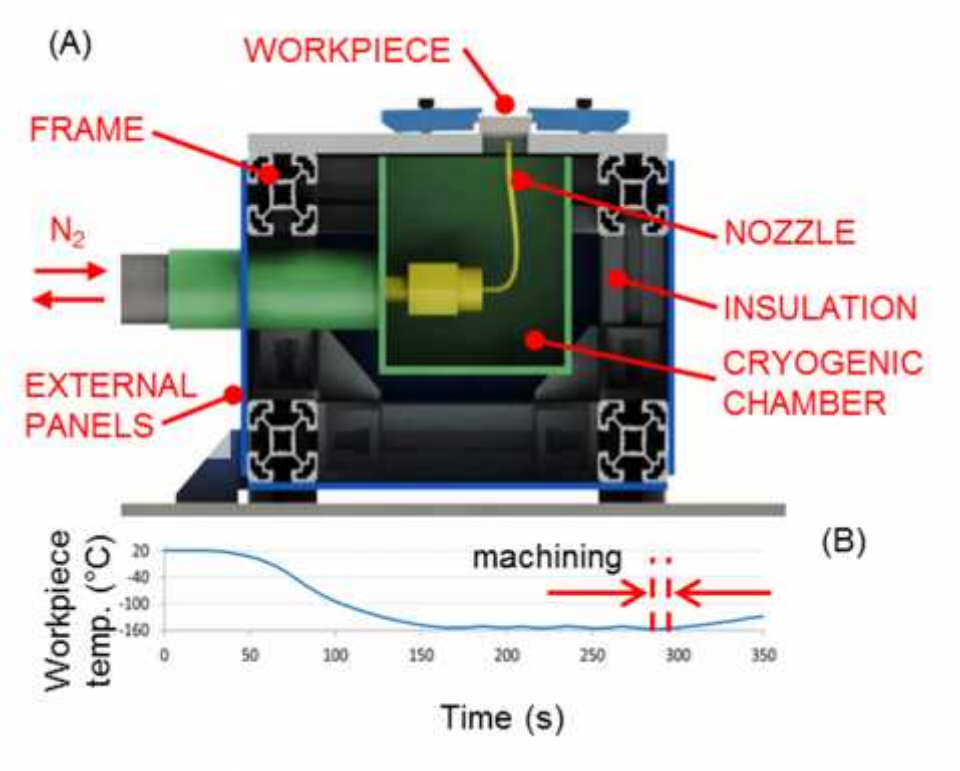

Figure 47 Schema of the cryogenic chamber

During this study mainly the feasibility of the cryogenic cutting in micro-milling condition was tested. For this reason only one cutting condition was chosen. Cutting speed of 63 m/min and feed per tooth equal to 1.5 μm. This combination of cutting condition was evaluated as the best trade-off of the studied parameters based on the results of †dry‡ and †MQL‡ campaign.

3.5 DMLS TI6AL4V

After the study of EBM material variation another additive manufactured Ti6Al4V have been tested. It was namely direct metal laser sintered (DMLS) as-built material. Which is for instance used in dental implantology. We have been studying the material variants in as-built form and also after heat treatment.

3.5.1 DMLS (not heat treated) experimental campaign

At first, the not heat treated DMLS material was studied. The material was in the condition as-built after the AM process. The microstructure in this case is shown in the Fig. 48.

Figure 48 As delivered microstructure of Ti6Al4V DMLS

DMLS microstructure is finer compared to EBM microstructure, but it is not in equilibrium, as it consists of martensite at room temperature. It is a consequence of the very high temperature gradient characterizing the process. The DMLS microstructure provokes higher strength but lower ductility.

All the experiments have been carried out under dry lubrication condition, only a jet of compressed air was used to facilitate the removal of the chips from the cutting zone.

As the study was carried out in the aim to compare the performances of DMLS material with EBM variation. The same cutting conditions have bene used. Full factorial design of experiments have been used

with two factors cutting speed and feed per tooth have been used. Each experiment was repeated twice. The values of factors€ levelsare shown in the Tab. 20.

Table 20 Tested factors (DMLS not heat treated)

		Levels			
Factors	v_c [m/min]	63	148	-	-
	f_z […m]	0.1	0.5	1.5	3.0

As in previous experimental campaigns, we have been studying the surface quality after the micro-milling process in terms of surface roughness, burrs formation, surface defects, microstructural alterations and tool state.

3.5.2 DMLS (heat treated) experimental campaign

Because as built microstructure after DMLS process is martensitic which is out of equilibrium. The heat treatment consisting of increasing the material temperature above the β-transus temperature, and then cooling down in order to obtain a final microstructure consisting of α and β coarse lamellas was performed and then the sample was tested following the same schema as in previous cases. The microstructure after the heat treatment is shown in the Fig. 49.

Experiment have been carried out under dry cutting condition and each experiment have been repeated twice.

In the Tab. 21 are shown the cutting conditions used during the experimental campaign.

Table 21 Tested factors (DMLS heat treated)

		Levels			
Factors	v_c [m/min]	63	149	-	-
	f_z […m]	0.1	0.5	1.5	3.0

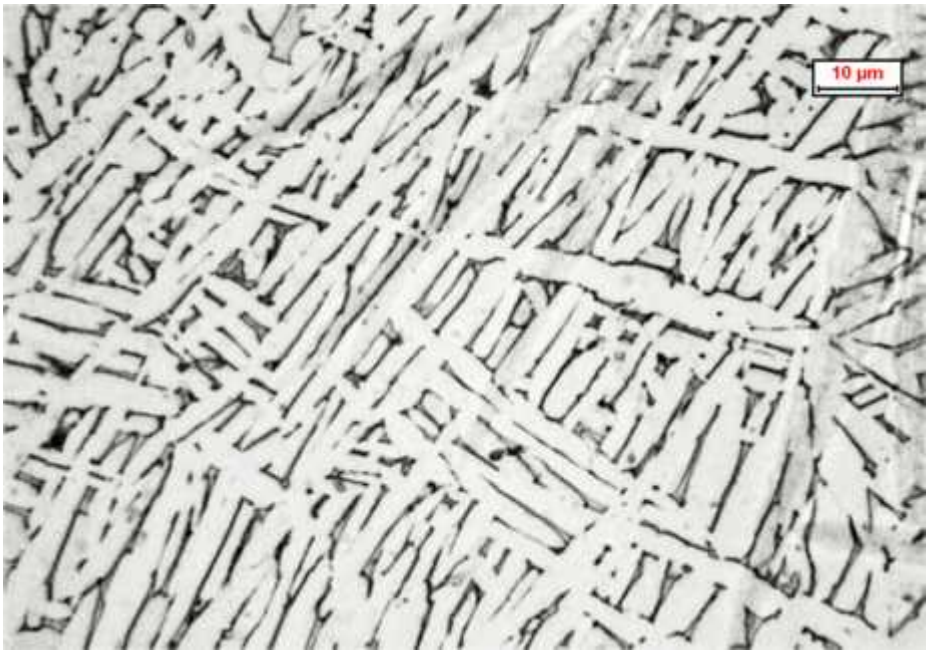

Figure 49 Microstructure of Ti6Al4V DMLS after heat treatement

3.6 WROUGHT TI6AL4V

In order to have a comparison of machining performances of AM Ti6Al4V, the micro-milling experiment have been carried out also on wrought Ti6Al4V. The same procedure was respected.

The microstructure of wrought Ti6Al4V at room temperature consists of alpha and beta grains which are almost globalized. In the Fig. 50 is shown the microstructure of the tested sample.

Experiments have been carried out under dry lubrication condition and each experiment has been repeated two times.

Regarding the cutting conditions, the same schema was respected as in previous campaign and the values are shown in the Tab 22.

Table 22 Tested factors (wrought Ti6Al4V)

		Levels			
Factors	v_c [m/min]	59	153	-	-
	f_z […m]	0.1	0.5	1.5	3.0

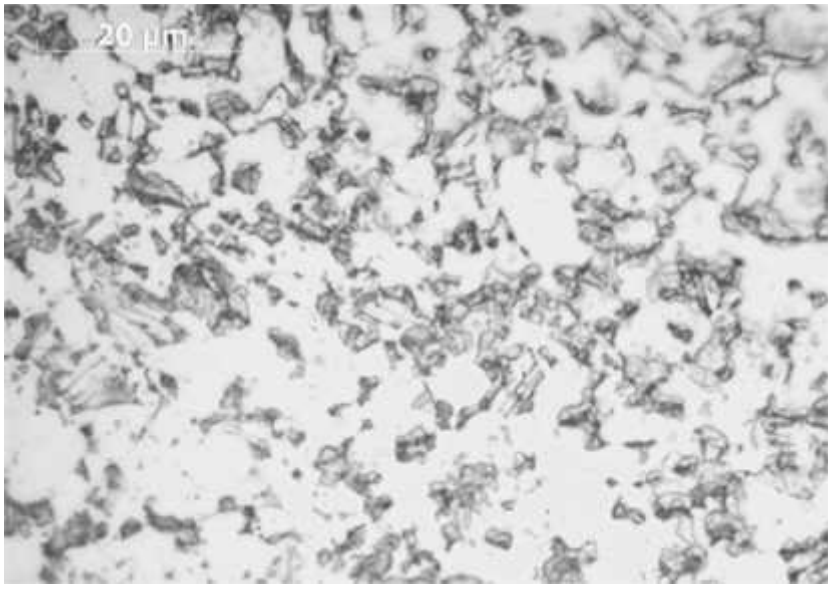

Figure 50 Microstructure of the wrought Ti6Al4V

3.7 DRILLING EXPERIMENTS

After the full immersion slotting experiments provided on different microstructural variances of Ti6Al4V, drilling experiments have been carried out. Our interest in drilling experiments is based on the case study which refers to the machining of high precision geometrical features on dental pins manufactured through the DMLS technology.

The dental pins are screwed directly into the jaw, their function is to ensure the connection between the jaw and the upper part of the implant (abutment and crown).

In the Fig. 51 is shown the CAD model of a dental pin (A) and as-built DMLS part (B).

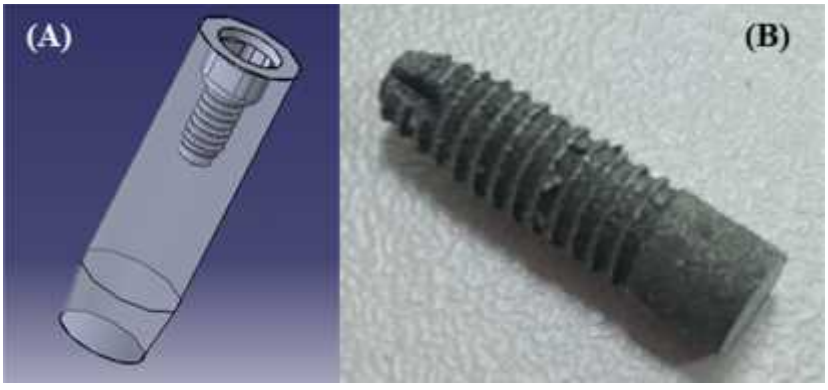

Figure 51 (A) CAD model of the dental pin before assembly, (B) as-built DMLS dental pin

The rough surface of the external thread is suitable to be implanted as it is, but both the pin top surface and internal features have to be machined, the latter employing first a drilling operation and then a threading one.

As the internal thread is M2x0.4 thus a uncoated tungsten carbide drill bit of 1.6 mm was used for drilling experiments. The total depth of the drilled hole was 5.8 mm. Again dry lubrication condition with jet of compressed air was used. The peck drilling strategy was chosen with constant One-Step-Feed-Length (OSFL) in order of tenth of the tool diameter as suggested by Kim et al. in [60] to improve the tool life and stability of micro-drilling. Peck drilling also facilitates the chip breaking and its removal from cutting zone.

In the Fig. 52 is shown the geometry of the tool. Each tool was inspected by means of FEIŽ Quanta 400 Scanning Electron Microscope (SEM) before machining, to avoid any possible manufacturing defect. For each experiment a new tool was used, to minimize the influence of wear on the results of interest.

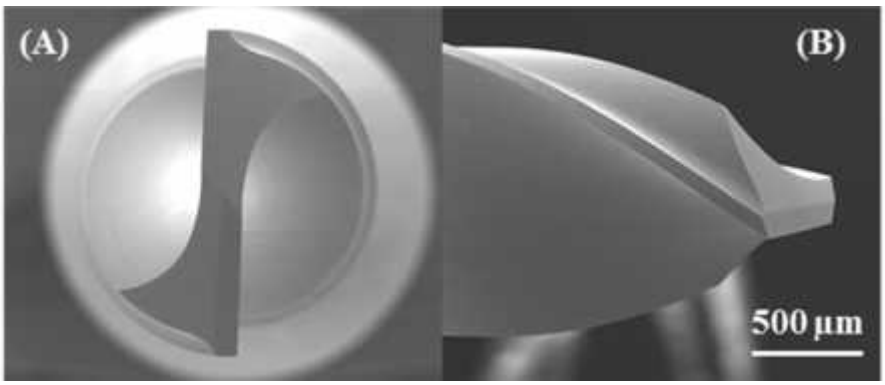

Figure 52 SEM detail of the drill bit (a) diameter and (b) helix angle

3.7.1 Drilling of DMLS (not heat treated)

Firstly the DMLS Ti6Al4V not heated was used for drilling experiments. Its microstructure was already described in previous sections, consisting only of , (hcp) grains, it is martensitic microstructure.

A full factorial design of the experiment was chosen, with two factors, the cutting speed and feed per tooth, with two and three levels, respectively (Table 23). Each experiment was repeated three times.

Table 23 Tested factors (DMLS drilling)

		Levels		
Factors	v_c [m/min]	60	110	-
	f_z […m]	10	15	20

The schema of the workpiece is shown in the Fig. 53, the lateral plane was used later for better alignment in CMM during the measurements of geometrical features.

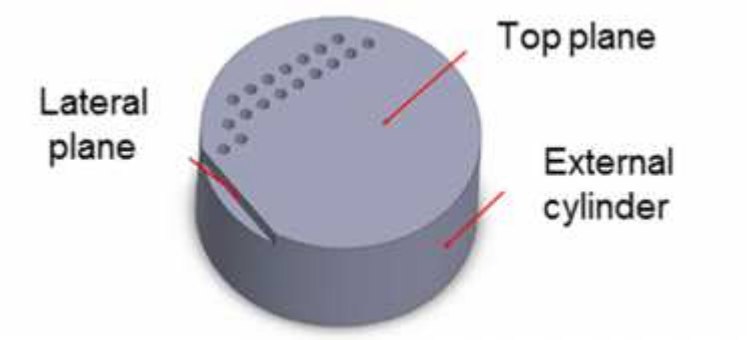

Figure 53 Workpiece for drilling experiments

As the function of drilled holes is the preparatory holes for consequent threading operation and later ensuring the connection between the dental pin and the abutment, the studied parameters were both the geometry of the generated holes (diameter of the hole, perpendicularity of the hole axis) and their surfaces as well as the burrs formation was evaluated. A microstructural analysis of the machined surface layer was carried out in order to evidence any microstructural refinement compared to the as-delivered structure.

Later also the feasibility of the threading operation was carried out. For this a solid micro single point thread mill was used with a diameter of 1.5 mm and 4 flutes. The cutting speed was set to 49 m/min and feed per tooth 2 μm. The two passes strategy was chosen to ensure better geometrical and surface quality under dry lubrication condition.

3.7.2 Drilling of wrought material

After experimental campaign carried out on DMLS material, the same campaign was repeated with wrought Ti6Al4V.

The tools, workpiece and design of the experiments with the cutting condition were same as in the case of DMLS material.

Thus a full factorial design of experiments was chosen. Each experiment was repeated three times. Dry cutting conditions were used. The factors with their levels are stated in the Tab. 24.

Table 24 Tested factors (wrought drilling)

		Levels		
Factors	v_c [m/min]	60	110	-
	f_z […m]	10	15	20

3.8 BURRS ANALYSIS

In collaboration with metrology group an experimental campaign dedicated to develop in-line burr measurement method was carried out.

During the experiments the wrought Ti6Al4V was used, under dry lubrication condition, using the same strategy (full immersion slotting), and the same tool as in previous experimental campaigns.

In the Tab. 25 are mentioned the cutting condition used to mill the slots that will be later used for burr analysis.

Table 25 Cutting parameters of the analysed slots

v_c [m/min]	60	60	150	150
f_z […m]	0.5	1.5	0.5	3.0

3.9 TOOL PERFORMACES

After comparing the performances during micro-milling of material variations of Ti6Al4V produced by AM process, different geometry of micro-end-mill was used to compare the performances of two commercially available micro-tools.

The workpiece material was the DMLS material which undergone consequent heat treatment, thus its final microstructure is consisting of , and f coarse lamellas as described in previous chapters.

The previously used two fluted tool (Fig. 54 A) was compared with flat-end square micro-mill (Fig. 54 B). Tool B is a four-fluted tool, also made of uncoated tungsten carbide. The diameter of both tools is the same and equal to 0.3 mm.

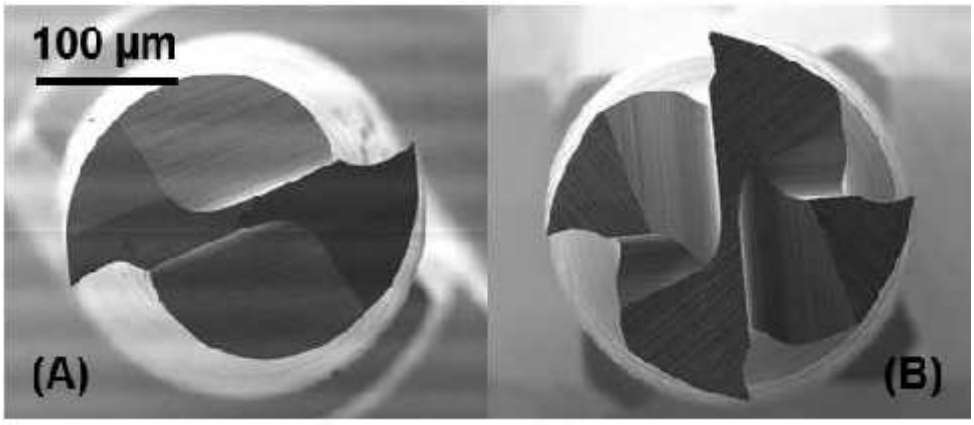

Figure 54 SEM images of the (A) two fluted and (B) four fluted flat-end-square micro-mills

As a milling strategy was again used full immersion slotting under dry lubrication condition with only a jet of compressed air to facilitate the removal of the chips from the cutting zone.

A full factorial design of experiments with two factors (cutting speed and feed per tooth) with two and four levels respectively was used. Each experiment was repeated twice. The factors with their levels are reported in Table 26.

Table 26 Cutting conditions used during the micro-milling experiments

Tool A (2 fluted)				
v_c (m/min)	63	149	-	-
f_z (…m)	0.1	0.5	1.5	3.0
Tool B (4 fluted)				
v_c (m/min)	58	154	-	-
f_z (…m)	0.1	0.5	1.5	3.0

3.10 FORCE ANALYSIS

In collaboration with the Technical University of Denmark (DTU) in Lyngby, during the researcher period spent at the Department of Mechanical Engineering the test of forces measurements feasibility in micro-milling was realized on EBM and wrought Ti6Al4V. Identical two fluted tool under full immersion slotting strategy were used as in previous experiments. Tested cutting conditions were identic for both studied materials and are shown in the Tab. 27.

Table 27 Tested factors during force measurements

		Levels			
Factors	v_c [m/min]	25	45	-	-
	f_z […m]	0.1	0.5	1.5	3.0

4 RESULTS

4.1 PRELIMINARTY TESTS

As described in previous sections, the mainly studied parameters were surface integrity in regards of surface topography, burrs formation, surface defects, tool state and microstructural alterations. In the Tab. 28 is shown experimental plan.

Table 28 Experimental plan (preliminary tests)

Process setting	a_p [€m]	v_c [m/min]	f_z [€m]
S1	30	50	0.8
S2	30	50	1.5
S3	30	50	3.0
S4	30	75	0.8
S5	30	75	1.5
S6	30	75	3.0
S7	30	100	0.8
S8	30	100	1.5
S9	30	100	3.0

4.1.1 Surface topography

The machined surface topographies were sampled by using a SensofarŽ PL… Neox confocal optical profiler at five locations along each of the slots, at regular distances from the border of the workpiece.

The instrument was equipped with a 100x lens characterized by a field of view of 127x97 …m2 and a vertical resolution of about 5 nm. A 2x2 images stitching with 25% overlap between the frames was performed for each measurement in order to increase the surface area to 223x167 …m2. The images were then trimmed to a 167x167 …m2 square format. The surface characteristics were finally evaluated by using the Image Metrology SPIPŽ software and the surface roughness Sa was considered as the surface roughness reference characteristic. Each digital surface sample was adjusted to filter out

voids or particles when present, and to correct any tilt of the surface that would affect the surface roughness measures.

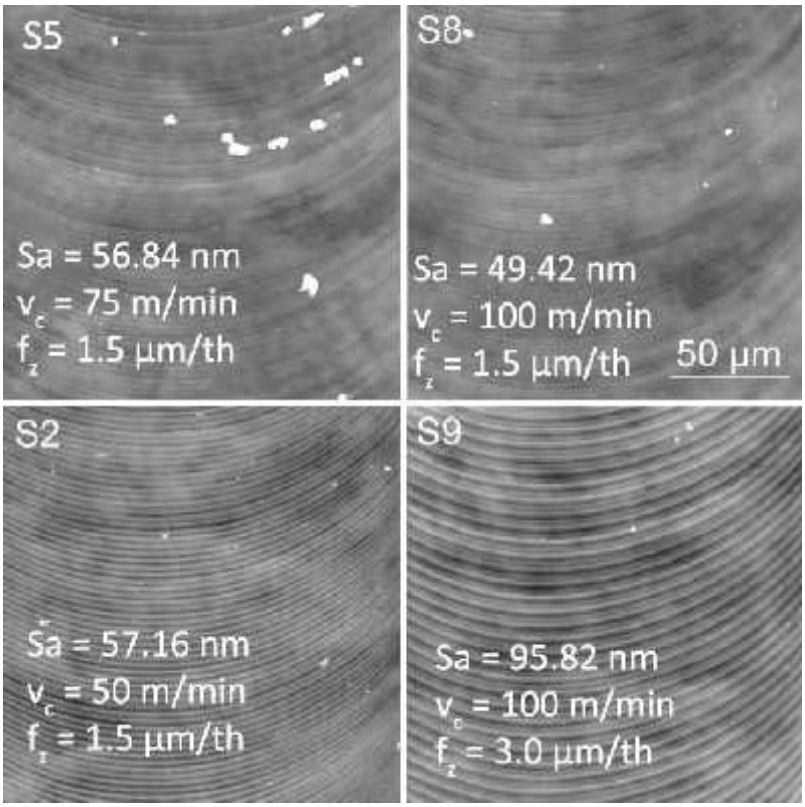

Figure 55 Surface topography (preliminary tests)

The obtained results show that the measured values of Sa are spread from 50 and 260 nm between experiments, but are rather consistent when the five different sampling locations along the slots machined with constant process parameter settings are considered.

In Fig. 55 are shown two of the best textures, namely S5 (middle cutting speed and feed per tooth) and S8 (highest cutting speed and middle feed per tooth), one average surface finish S2 (lowest cutting speed and middle feed per tooth), and a non- acceptable result S9 (highest cutting speed and feed per tooth) caused by tool vibrations.

Table 29 Qualitative overview of the experimental results (preliminary tests)

Process setting	Surface quality	Burr size	Vibrations
S1	4	1	2
S2	4	2	4
S3	1	1	1
S4	4	2	3
S5	4	3	3
S6	4	4	2
S7	5	2	3
S8	5	1	5
S9	4	5	2

4.1.2 Burr formation

To perform a quantitative dimensional analysis of the burrs formed during the micro-milling process is in general a difficult task due to the complex geometrical characteristics and small dimensions of the machined freeform parts. Due to that, a qualitative analysis by using SEM images is usually carried out, using for instance the burrs maximum or average length as a mean of comparison.

In our case, the burrs were qualified by SEM inspection, considering their dimensions and shape; ratings from extremely bad (1) to extremely good (5) were attributed to each process parameter setting used in experiments, the results are stated in Tab. 29.

During a slotting operation the micro tool removes material in both down milling (Fig. 56 S9a, S8a, S4a) and up milling (Fig. 56 S9b, S8b, S4b) conditions: in general, it was found that burrs were sensibly larger in down milling conditions S8 (highest cutting speed and middle feed per tooth), whereas in a few experiments burrs were comparable on both sides of the slot S9 (highest cutting speed and feed per tooth).

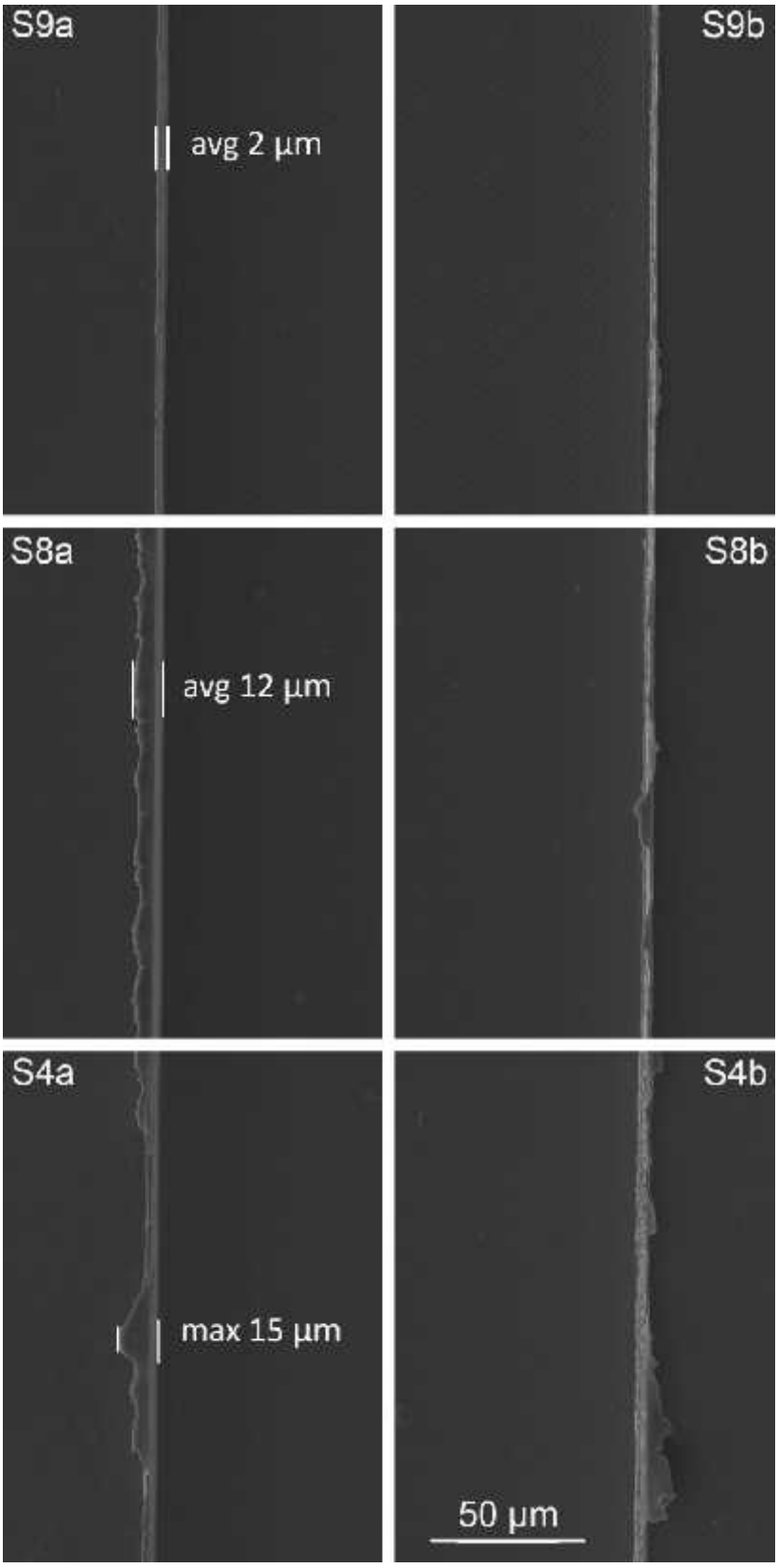

Figure 56 Burrs (preliminary tests)

4.1.3 Tool analysis

Tool wear in micro-milling can manifest mainly as a reduction of the tool tip diameter and as an increase of the cutting radius, thus affecting both the accuracy of the channel width and the surface quality of the channel floor.

The micro tools used during the experiments were inspected by means of SEM images before and after machining in order to obtain a qualitative estimation of the tool wear.

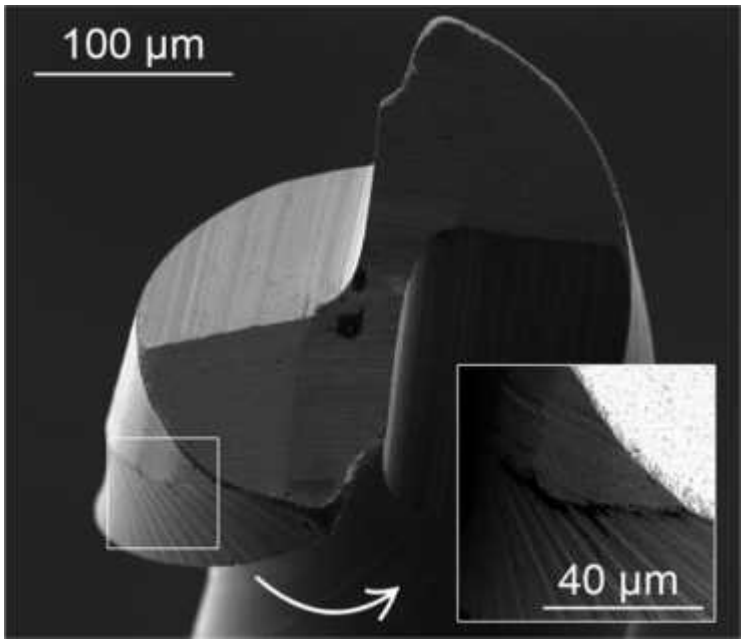

Figure 57 Tool state after machining (preliminary tests)

The analysis of the state of the tools after machining showed an appreciable difference in tool wear between different process parameter settings: in some cases the cutting edge of the micro tool was damaged (S9 • highest cutting speed and feed per tooth), in other cases the micro tool was not able to withstand the cutting forces and broke close to the end of the slotting operation (S3 • lowest cutting speed, but highest feed per tooth).

The most severe tool wear was observed in experiments S8 (highest cutting speed and middle feed per tooth, Fig. 57): the cutting edge is clearly rounded both from top and from lateral views. Furthermore, the flank of the tool shows evident effects of abrasion. The detail shown in Fig. 57 was captured with the SEM-BSED detector and the dark agglomerate suggests that material from the workpiece adhered on the tungsten carbide tool flank surface.

4.1.4 Chip morphology

The samples of chips that were collected during the micro-machining experiments were inspected through SEM analysis. Some examples of chips are shown in Fig. 58, where S7 and S8 correspond to the process parameters setting named S7 (highest cutting speed, lowest feed per tooth) and S8 (highest spindle speed, middle feed per tooth), respectively, while S1a and S1b represent two different samples both related to the experimental conditions named S1 (lowest cutting speed and feed per tooth).

The morphology of some collected chips shown in Fig. 58 is segmented, even if the level of segmentation is different: while the S7 chip morphology is similar to that of the S8 experimental conditions, there is a pronounced difference in the case of S1 conditions.

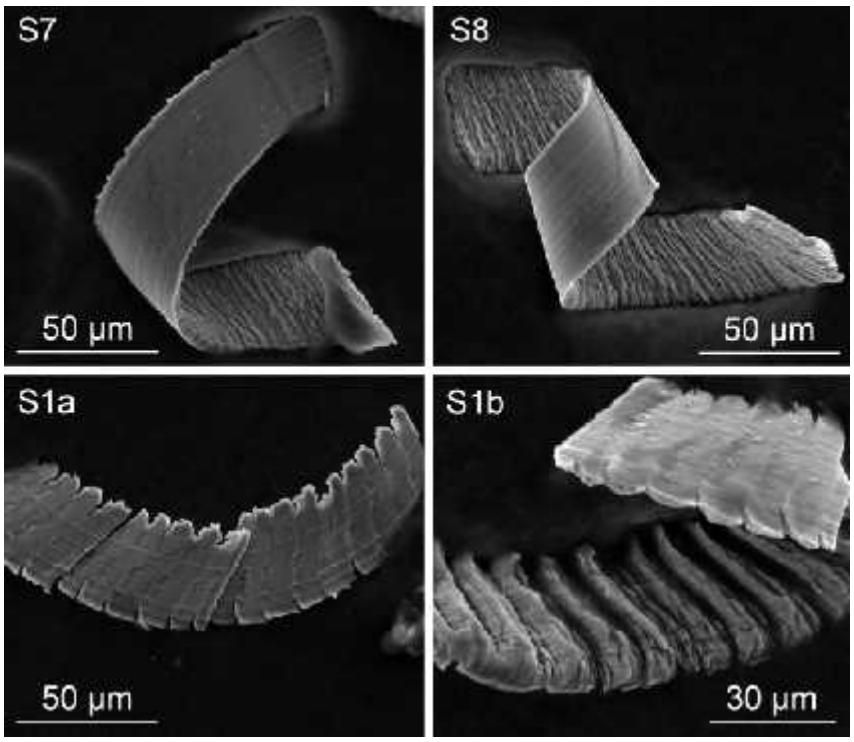

Figure 58 Chips samples collected during preliminary tests

The chip morphology is in general the combination of the chip formation mechanisms and the machining process dynamics. It is worth to note that the chips S7 and S8 in Fig. 58 are the results of the same cutting speed but with different feed per tooth, while the chips S1 and S7 were produced with the same feed per tooth with the S1 conditions characterized by a lower cutting speed. At lower cutting

speed (S1) the chips look more segmented than at the highest tested cutting speed (S7, S8). To be noted that the surface analysis relative to the process parameter settings S1 revealed the presence of tool vibrations during the micro-milling process.

4.1.5 Microstructural analysis

The machined workpiece was sectioned perpendicularly to the top surface and to the slots at about half of the slot length. The section was then prepared for metallurgical analysis. Once polished, the surface containing the sections of the slots was etched using the Kroll€s reagent and inspected by using an optical microscope.

Fig. 59 shows the microstructure after machining on the side wall and bottom surface, respectively (C is a detail of the bottom surface, roughly in the middle of the slot).

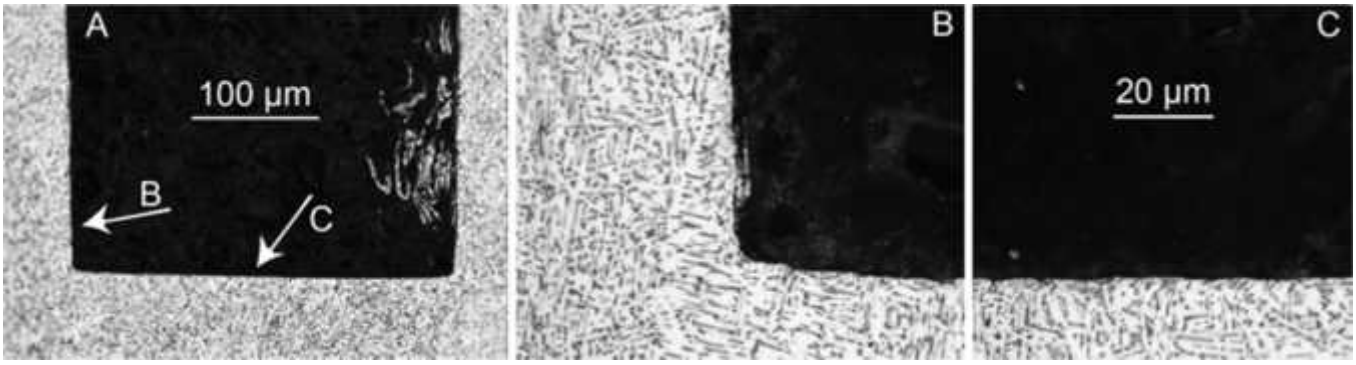

Figure 59 Microstructure analysis after the micro-milling experiments (preliminary tests)

These micrographs show that the slotting operation affected only a very thin substrate layer and that the alteration of the microstructure along the boundary surface is not homogeneous. In general, the acicular microstructure layer affected by the micro-milling process presents distorted and smaller grains as a consequence of the shear deformation.

4.2 EBM TI6AL4V

After the preliminary test, more detailed study of EBM Ti6Al4V was performed. The EBM material variance was tested under dry, MQL and cryogenic lubrication condition, stressing out the importance of the cleanliness in biomedical applications.

The integrity of the machined surfaces was evaluated in terms of topography characteristics, burr formation, surface defects, nano-hardness and tool analysis. In the case of use of MQL lubrication, the machined workpiece was gently cleaned in an ultrasonic bath in order to remove residual chips particles.

4.2.1 Surface roughness

The roughness plots of the slots bottom surfaces as a function of the cutting parameters under dry and MQL conditions are shown in Fig. 60, and related SEM images and profiler scans are in Fig. 61.

The images of the slots bottom were acquired by using a FEIŽ Quanta 400 SEM and a SensofarŽ PL… Neox confocal optical profiler.

The roughness values were measured with the confocal optical profiler, using a 100x lens characterized by a field of view of 127x97 …m^2 and vertical resolution of about 5 nm, at a distance of 12.5 mm from the edge, following the ISO 4288 standard. Stitching of images was acquired with 25% of overlapping, while the values of the cut-offs $\bullet_c$ were 0.08 mm, considering the arithmetic mean of 10 different profiles.

As expected, the lowest feed rate causes an evident surface damage, being the ploughing mechanism predominant over the shearing. As the feed rate increases, the surface quality becomes lower, as in macro-machining and not acceptable for finishing cutting at the highest investigated feed rate. From the analysis of Figs. 60 and 61 it is clear that for the intermediate feed rates a comparable surface quality can be achieved under dry and MQL cutting conditions. In case of MQL the influence of the cutting speed is negligible, whereas for dry cutting the best surface finish is obtained at the lowest investigated cutting speed.

The lower limit in the choice of feed rates for the best surface finish is given by the ploughing mechanism that affects the micro- machining process when the uncut chip thickness is smaller than the minimum chip thickness. The experimental results are in good agreement with the estimation of the critical feed per tooth, in particular the sharp change in slope of all the curves in Fig. 60 when the feed per tooth is between 0.1 and 0.5 μm.

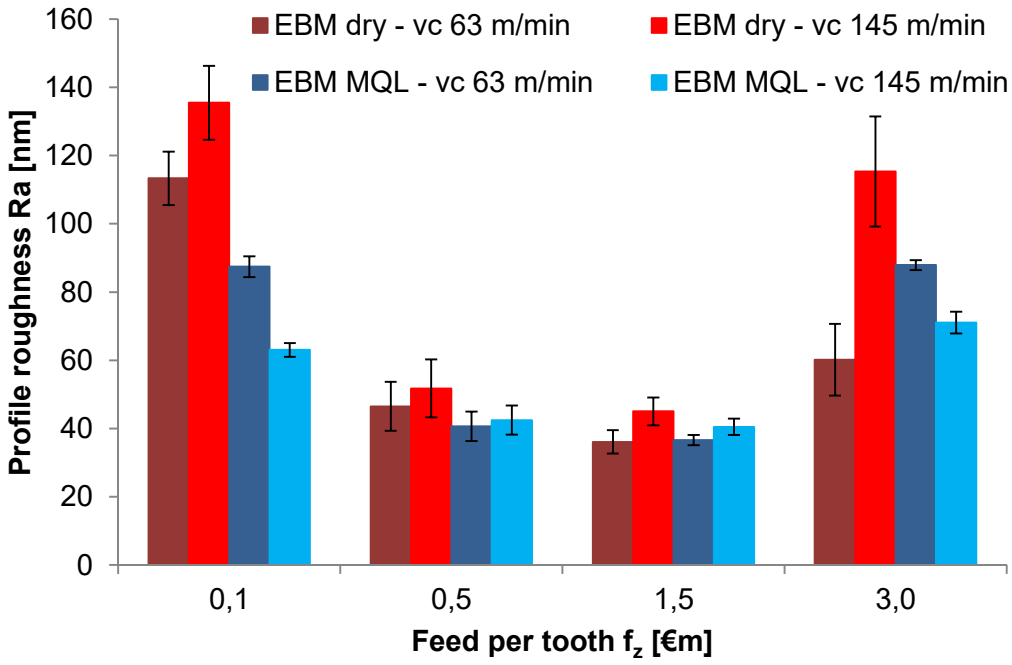

Figure 60 Profile roughness as a function ofthe cutting parameters under dry and MQL conditions

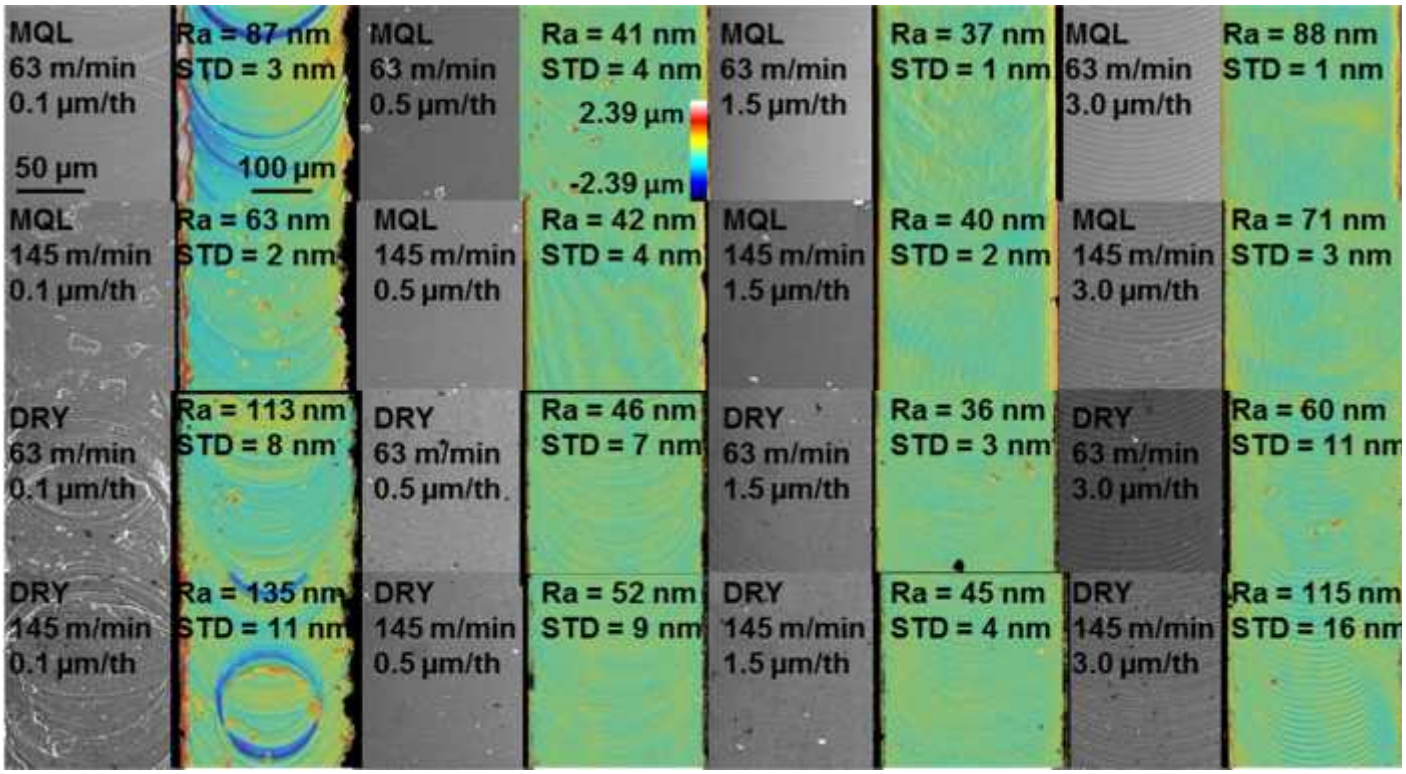

Figure 61 Topographies of the slots bottom surfaces at varying cutting parameters under dry and MQL conditions (SEM images and optical profiler scans)

4.2.2 Burr formation

Given the complex geometrical characteristics and small dimensions of the burrs, a qualitative analysis by using SEM images is usually carried out, using for instance the burrs maximum or average length as a mean of comparison.

Experimental results show that a minimum quantity of burrs is always present as shown in the Fig. 62.

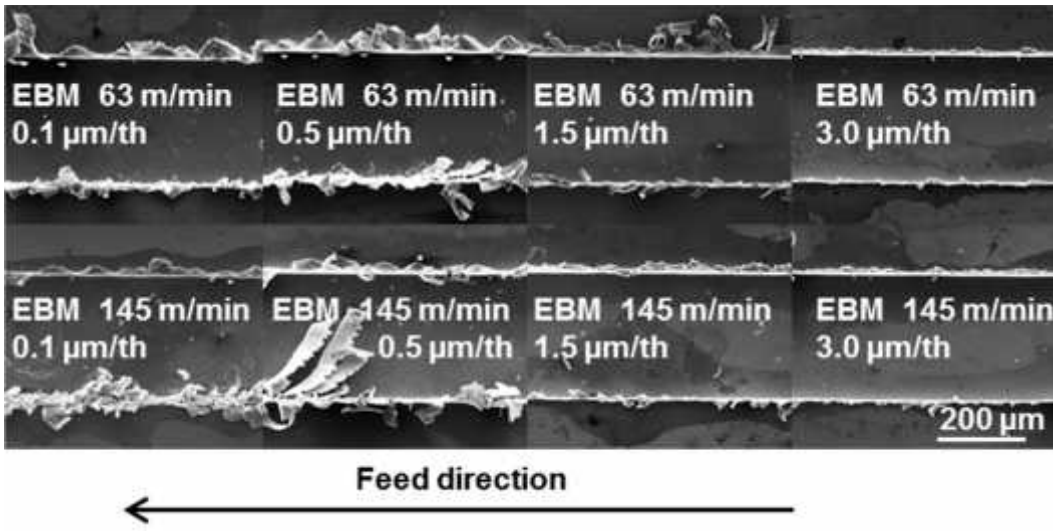

Figure 62 Burr in the case of EBM dry milling in function of the cutting conditions

Fig. 63 gives a view of the top burrs for intermediate feed rates and the lowest cutting speed under dry and MQL conditions. At the feed per tooth of 0.5 µm under both dry and MQL conditions, ploughing prevails on shearing and the consequent plastic deformation causes the burrs to be larger than at 1.5 µm. On the contrary, at the feed per tooth of 1.5 µm dry cutting provokes a slightly less amount of burrs, which are also more regularly developed, in comparison to MQL cutting. Similar phenomena were observed for the cutting speed of 145 m/min. We can also appreciate the different shape of the burrs as a function of the machining strategy, namely down-milling or up-milling.

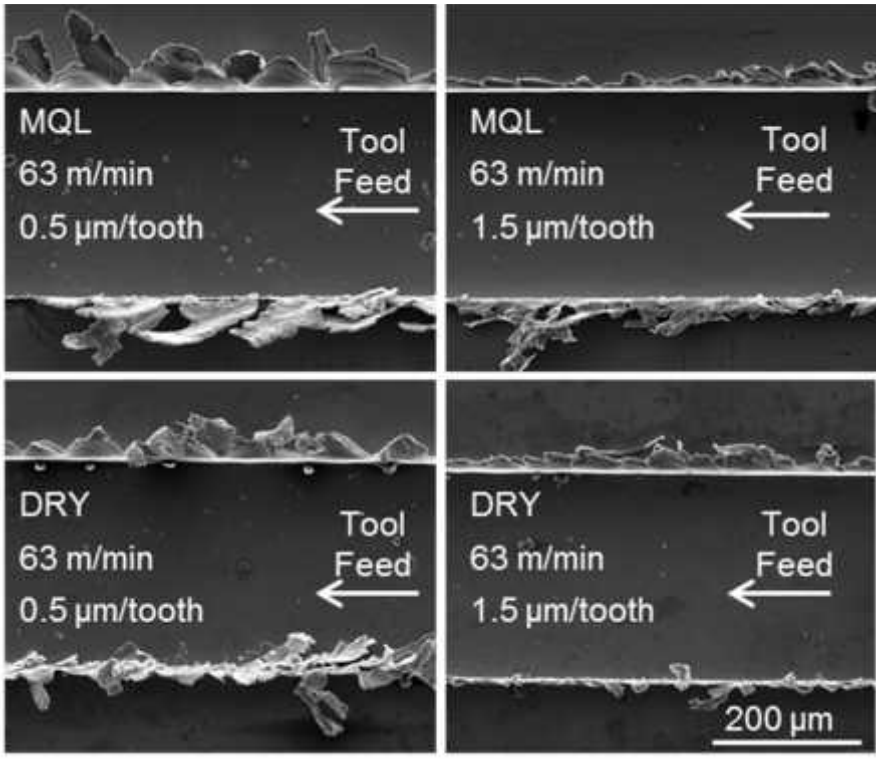

Figure 63 View of the top burrs (dry and MQL, v_c=63 m/min)

4.2.3 Surface defects

The SEM analysis of the machined surfaces permitted also to evaluate the presence and dimension of surface damages.

The surface defects found at the bottom of slots after machining experiments are similar regardless the lubrication condition, namely dry or MQL. For the lowest feed per tooth a high amount of surface defects is present, being the whole surface affected by their presence as a consequence of the ploughing mechanism that prevails at the lowest feed per tooth. On the contrary, a minimal amount of surface defects can be appreciated for the feeds per tooth of 0.5 and 1.5 …m, which are only characterized by the presence of some chip debris. When the feed per tooth is increased to 3.0 …m the defects are more evident, as the presence of smeared material is evident. The surface defects at varying cutting parameters are shown in Fig. 64 and Fig. 65 in case of dry and MQL conditions, respectively.

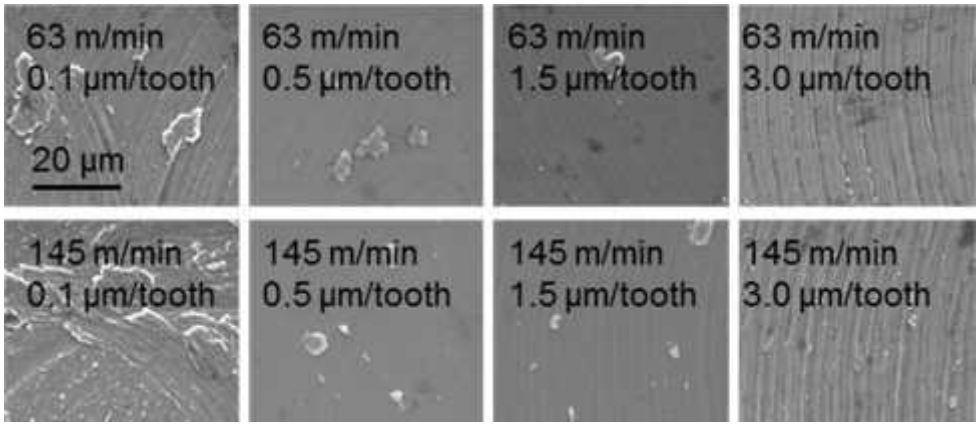

Figure 64 Surface defects in the case of dry cutting condition at varying cutting parameters

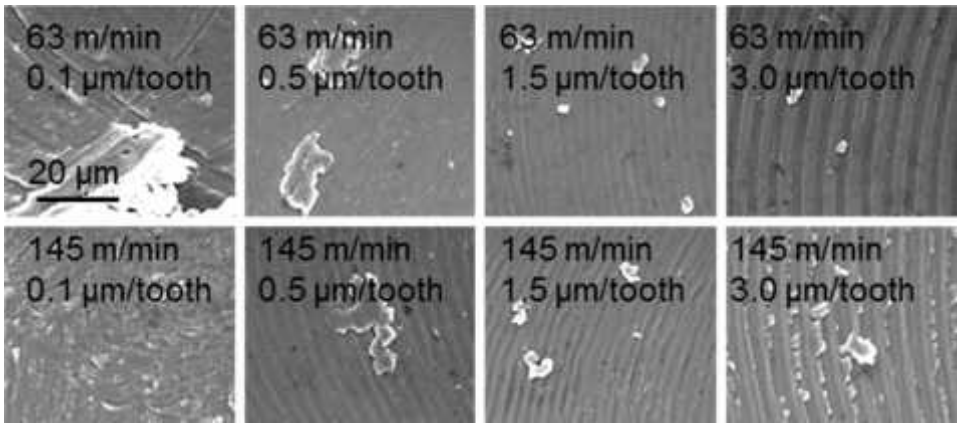

Figure 65 Surface defects in the case of MQL lubrication condition at varying cutting parameters

4.2.4 Tool analysis

Tool wear in micro-milling can manifest mainly as a reduction of the tool tip diameter and as an increase of the cutting edge radius, thus affecting both the dimensional accuracy and the surface quality of the machined micro-features. In this work, the estimation of the tool wear was carried out by inspecting the tool tip before and after the experiments by means of SEM analysis.

The tool inspection revealed an appreciable difference in tool conditions as a result of the different process parameter settings.

In the Fig. 66, it can be seen that, regardless the lubrication condition, there are some workpiece material adhered on the tool cutting edge. The EDS analysis proved the origin of the material presented on the

cutting edge: Fig.67 clearly demonstrates that the adhered material is titanium from the machined workpiece

Figure 66 SEM pictures the cutting edge state after machining at v_c = 63 m/min and fz = 1.5 µm

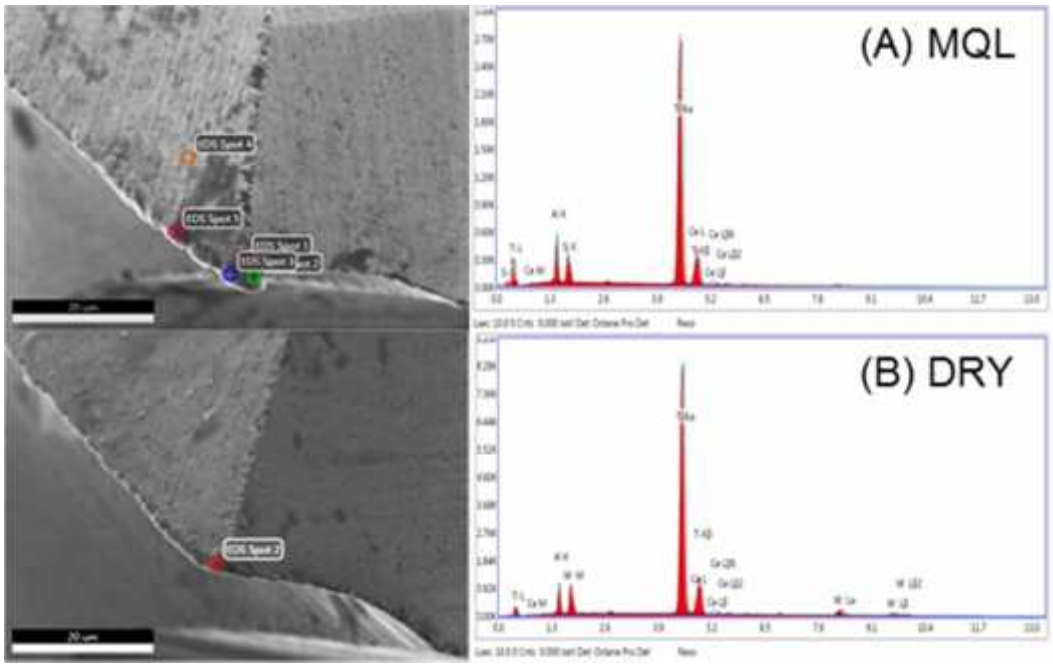

Figure 67 Example of the EDS analysis of tools after machining under MQL and DRY lubrication condition (v_c = 63 m/min and fz = 1.5 …m)

4.2.5 Nano-hardness

In the collaboration with the University of Calabria, the nano-hardness of micro-milled slots were evaluated. The mechanical properties of the micro-milled specimens were analyzed by nano-indentation tests using

a Berkovic tip. Preliminary tests were performed in order to choose the appropriate load and dwell time as suggested in [61]. In particular, the load and the dwell were respectively ranged from 5 to 150 mN and from 2 up to 100 s. The values that allow achieving stable nano-hardness results and avoiding creep effect were found to be 50 mN and 10 s. The indentations were performed from the top surface toward the bulk material. Five measurements were taken for each depth, with measurement locations well-spaced to avoid interference between indentations.

The hardness of the samples after EBM was 4.34 • 0.43 GPa. In the micro-milled samples, a 15 - 20 mm sub-surface layer of high hardness was observed, with a peak value of 6.5 GPa.

Fig. 68A shows the force-penetration depth curves for the samples processed through dry machining at different cutting speeds and fixed feed per tooth compared with the one of the as-received sample. The maximum penetration depth decreases when the cutting speed increases, and the slope of the unloading curve increases. This can be attributed to the presence of lamellae that are bent by plastic deformation.

In dry cutting (Fig. 68B), the hardness increases up to 6.5 GPa in the zone close to the machined surface for the highest cutting speed and feed per tooth, and decreases when the feed per tooth decreases. Similar results were observed for surfaces machined under MQL condition, but with slightly lower hardness values (Fig. 69). This difference between dry and MQL conditions is more evident at the highest cutting speed as shown in Fig. 69B.

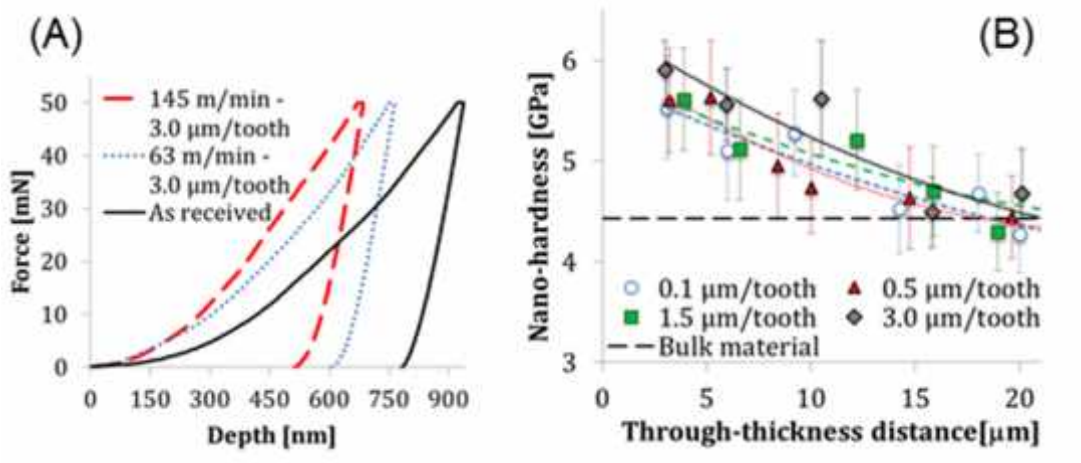

Figure 68 Force vs. penetration depth curves for Berkovich indentations (A); nano-hardness of samples dry micro-milled at 145 m/min (B)

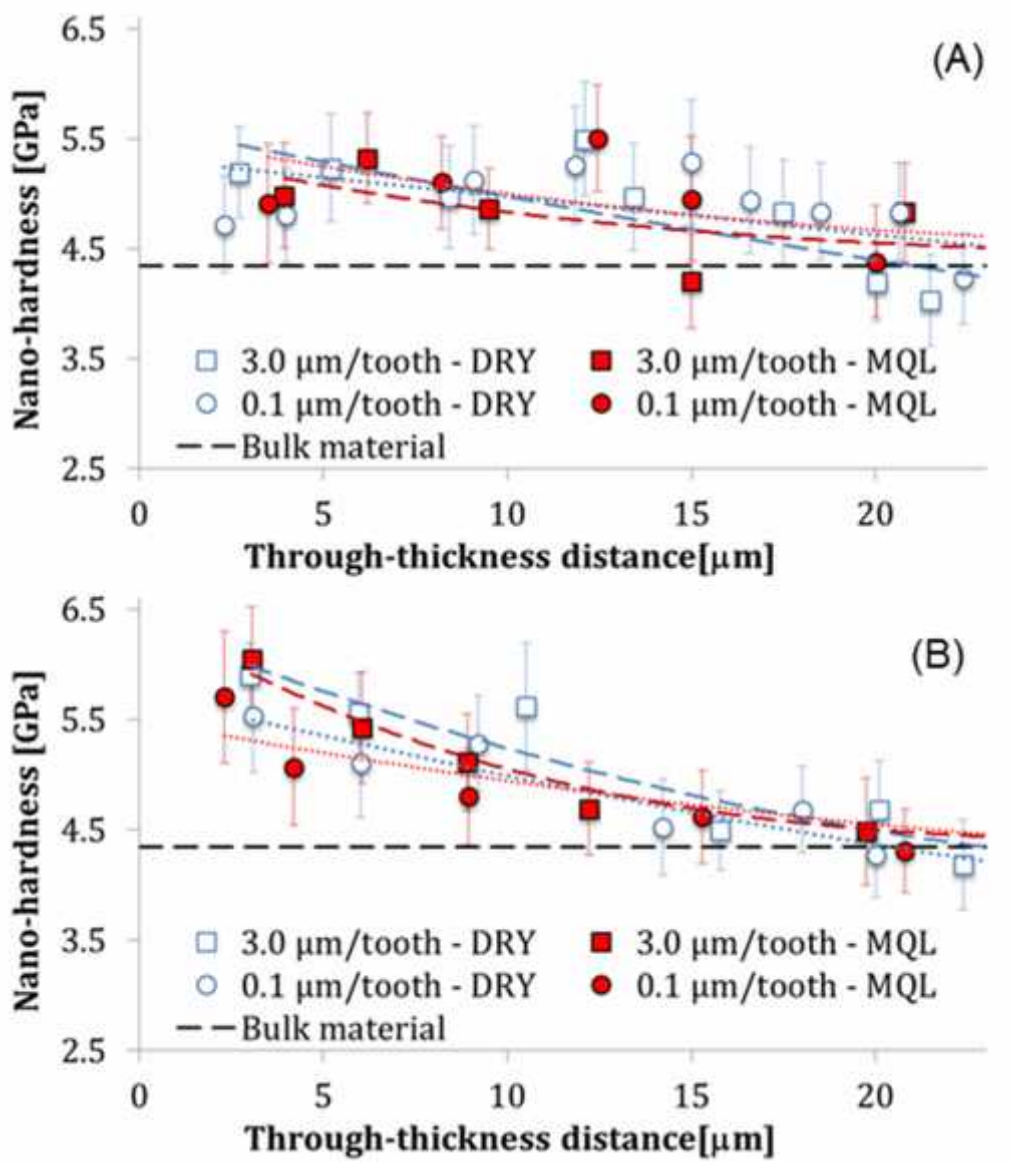

Figure 69 . Nano-hardness profiles through thickness distance for samples dry and MQL machined at (A) 63, and (B) 145 m/min

4.2.6 Microstructural analysis

The samples were metallographically prepared (grinded by different sand papers and polished by solution of silica) and etched with the Kroll€s reagent to analyze their metallurgical state by using both optical and scanning electron microscopy.

Fig. 70A shows the optical image (acquired through a Leica microscope at magnification of 200x) of the microstructure of the slot cross-section in case of dry condition, when using a cutting speed of 63 m/min and a feed per tooth of 1.5 μm. No microstructural alterations in terms of phase transformation and dynamic recrystallization can be appreciate, meaning that even without any cutting fluid the temperature rise due to cutting is not high enough to provoke a change in the material microstructural state. A closer examination of the slot sidewall microstructure by SEM analysis (Fig.70B) reveals the presence of bent lamellae to an average depth of 5 μm, but without any kind of damaging induced by the cutting process, whereas this kind of distortion is not present at the slot bottom surface.

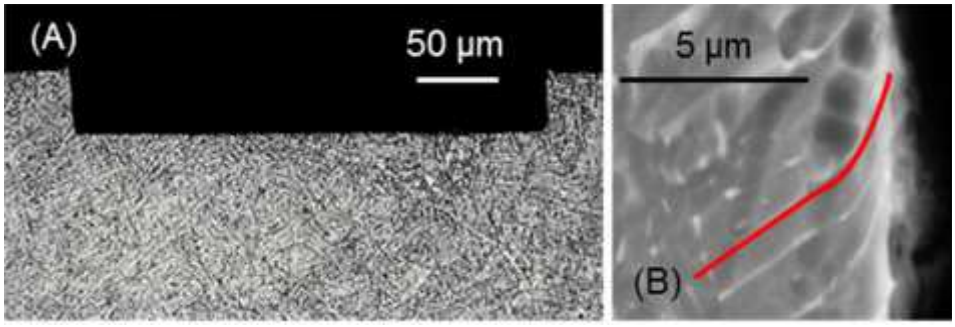

Figure 70 Microstructure of the slot cross-section (A), and SEM detail of the slot sidewall sub-surface (B) (v_c=63 m/min, f_z=1.5 μm)

4.2.7 Cryogenic cutting

The micro-milling tests under cryogenic cooling were carried out at those cutting parameters assuring the best performance in dry cutting, namely cutting speed of 63 m/min and feed per tooth of 1.5 μm. Fig. 71 shows the topography of the slot bottom surface machined under cryogenic cooling. In the same figure, the roughness profiles of the different cooling/lubrication conditions are compared.

The surface quality for cryogenic cooling is comparable to that obtained for dry cutting and MQL. However, a slight increase of the surface roughness is evident, with a more perturbed roughness profile of higher amplitude. This can be ascribable to a larger amount of smeared material on the machined surface of the cryogenic sample, as confirmed by the SEM observations (see Fig. 72A).

It is worth to note the fact that this phenomenon observed in micro-machining is not in agreement with what observed in cryogenic

conventional machining [38]. In Fig. 72B and 73 the SEM image of the tool after cryogenic cutting is shown: as for the other lubrication conditions, workpiece material adhesion is evident, without any sign of damaging.

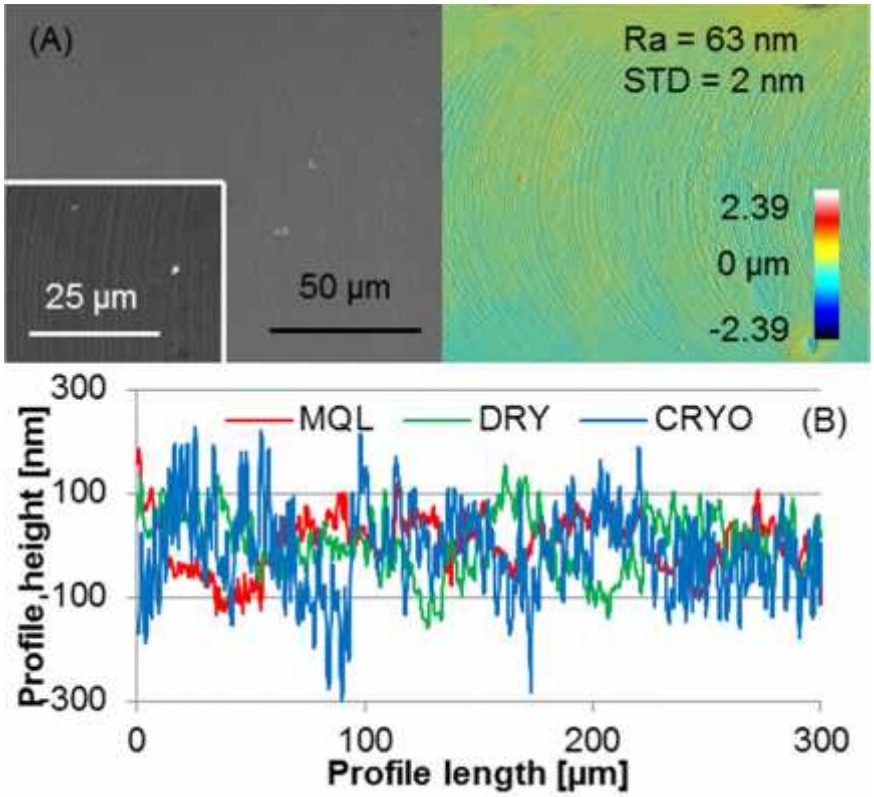

Figure 71 Bottom surface of the slot machined under cryogenic condition (v_c=63 m/min, f_z=1.5 µm) (A); roughness profiles at varying lubrication conditions (B)

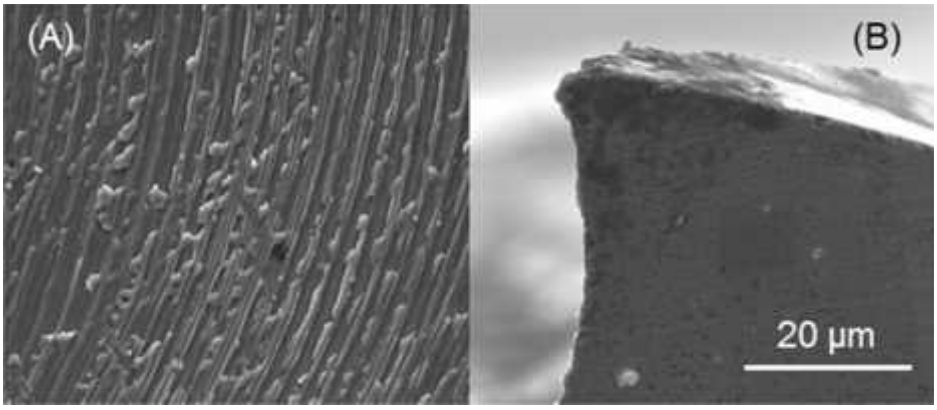

Figure 72 Bottom surface defects (A) and tool state (B) after machining at cryogenic condition (v_c=63 m/min, f_z=1.5 µm)

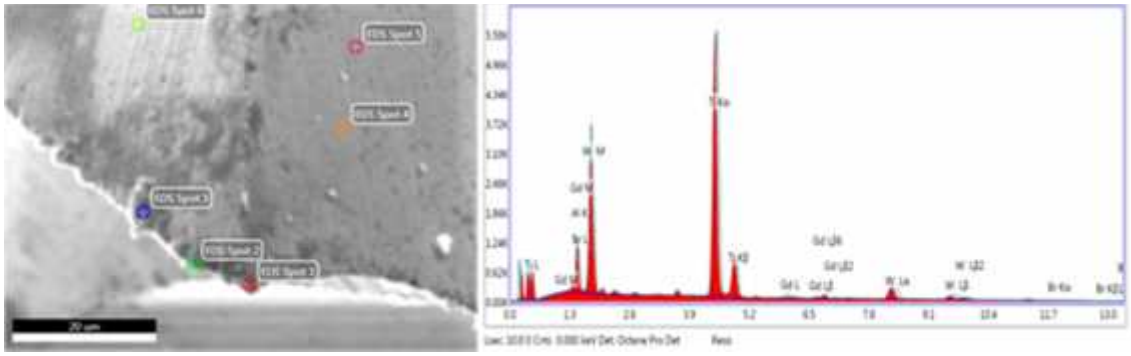

Figure 73 Example of the EDS analysis of tools after machining under cryogenic lubrication condition (v_c = 63 m/min and f_z = 1.5 …m)

The analysis of the burrs under cryogenic cooling (Fig. 74A) evidences an improvement compared to dry cutting, with the presence of more uniform and less jagged burrs on both sides of the slot. As shown in Fig. 74B, the nano-hardness measured in cryogenic cooling is very close to that for dry cutting, being the microstructure in both cases very similar.

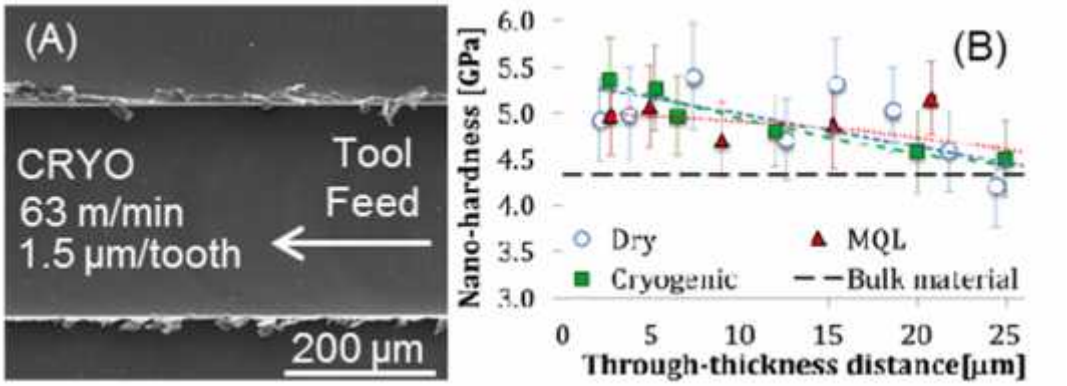

Figure 74 View of the top burrs under cryogenic cooling (A); nano-hardness profile through thickness distance at varying lubrication condition (B) (Vc=63 m/min, fz=1.5 µm)

4.3 DMLS TI6AL4V

Following the analysis of EBM additive manufactured Ti6Al4V another AM technique was studied. The two variances of DMLS material have been analysed following the same test procedure as in the case of EBM, thus surface roughness, burrs analysis, surface defects, tool state and microstructural analysis were evaluated.

4.3.1 Surface roughness

Surface topography and roughness were again acquired by using a FEIŽ Quanta 400 SEM and a SensofarŽ PL… Neox confocal optical profiler. Following the same procedure as in the case of EBM analysis, while using a 100x lens characterized by a field of view of 127x97 …m^2 and vertical resolution of about 5 nm, with 25% of overlapping of stitching and while using the values of the cut-offs $\bullet_c$ were 0.08 mm, following ISO 4288.Ten values of the profile roughness, at different random locations along the sampled length, were taken and their mean value calculated

Regardless of the cutting speed and material microstructure, we can appreciate the same trend in the surface topography as a function of the feed per tooth. For the lowest value of the feed per tooth, the surface quality is very poor, due to the ploughing mechanism that prevails over shearing, whereas, when increasing the feed per tooth, the feed marks become more regular. Fig. 75 shows the profile roughness as a function of the cutting parameters and initial material microstructure: the lowest feed per tooth always produces high roughness, because of the ploughing mechanism, whereas at increasing feed per tooth the roughness first decreases, then increases again at the highest feed per tooth, as it happens in the case of macro-machining. The influence of the cutting speed is negligible compared to the one of the feed per tooth.

Fig. 76 and 77 show the surface scans acquired by SEM and confocal optical profiler., the lowest feed per tooth regardless the cutting speed provokes a highly perturbed surface as discussed before, which is in agreement with the results shown in Fig 75.

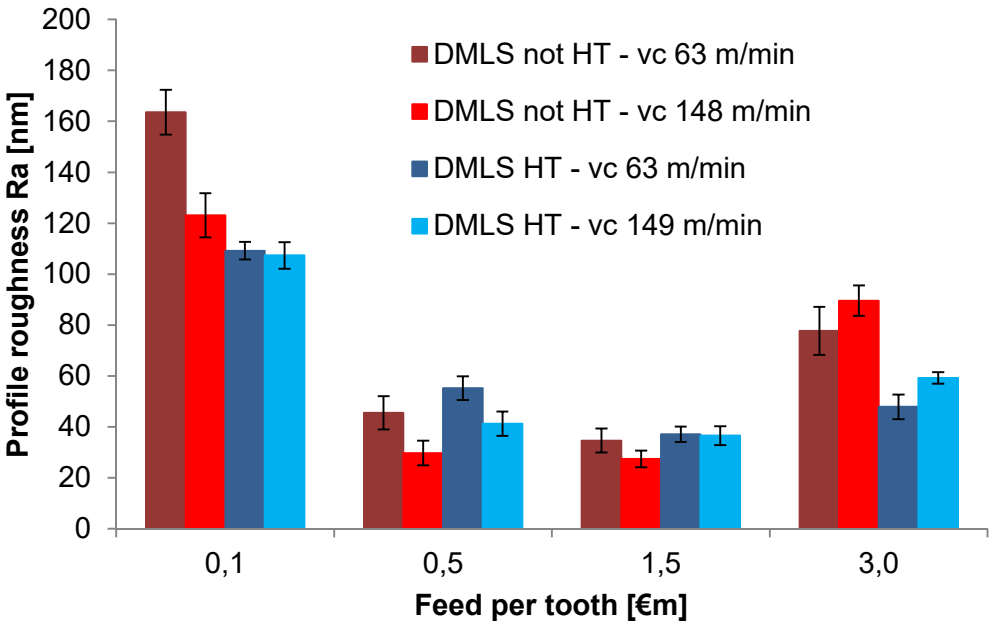

Figure 75 Profile roughness as a function of the feed per tooth for different cutting speeds and material microstructure

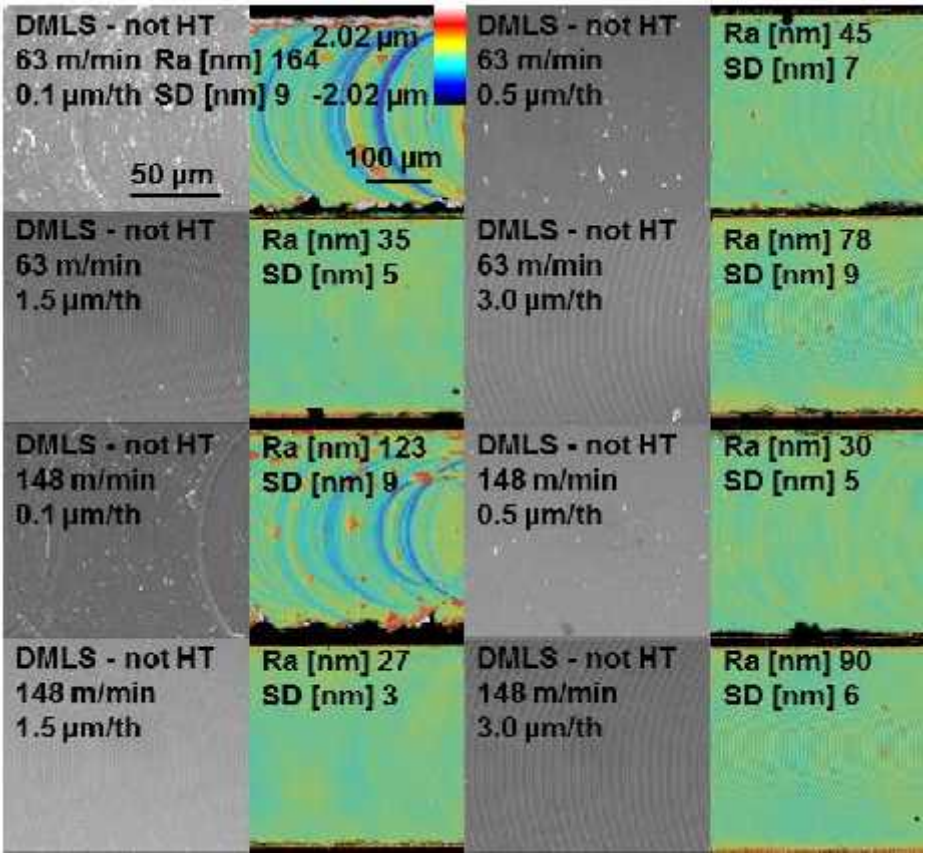

Figure 76 Images of the bottom of the slots acquired using SEM and optical confocal profiler (DMLS • not HT)

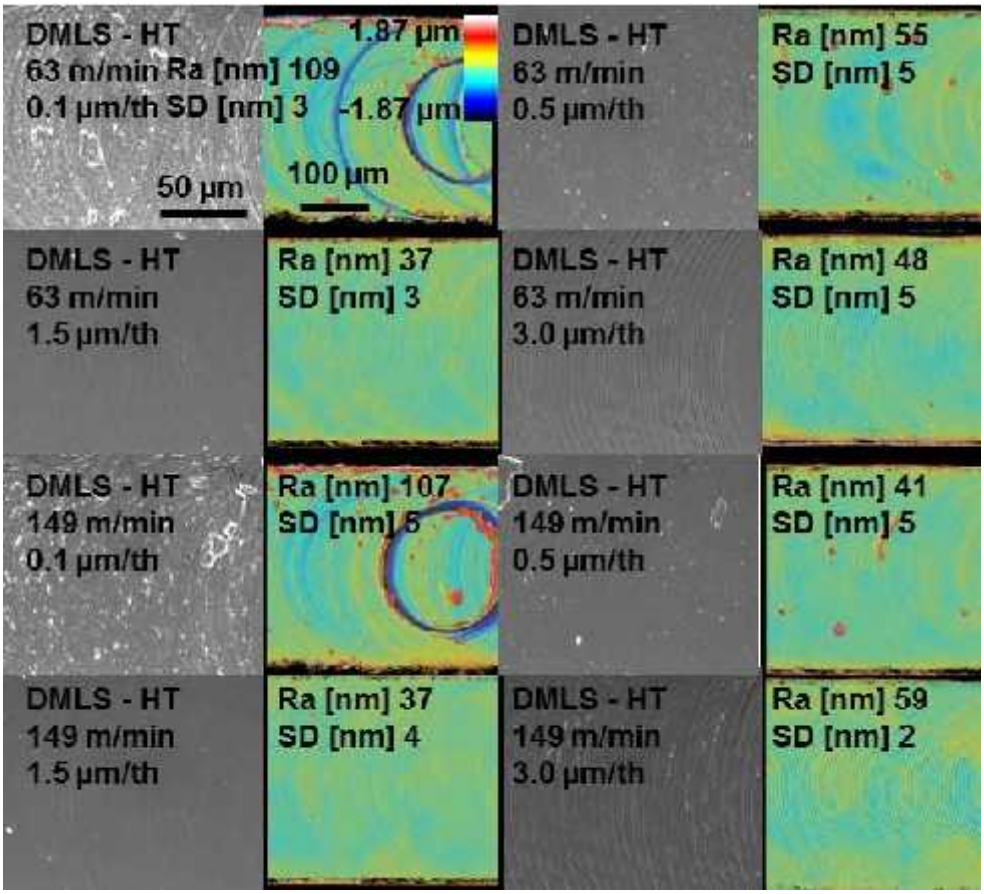

Figure 77 Images of the bottom of the slots acquired using SEM and optical confocal profiler (DMLS • HT)

4.3.2 Burr formation

A qualitative analysis of burr was based on SEM pictures. It is clearly visible that burrs can be found for all the combinations of the cutting parameters.

Fig. 78 shows the top burrs of the slots after micro-milling: again, it can be seen that the influence of the feed per tooth is predominant over the cutting speed. A minimum amount of burrs is evident at increasing feed per tooth regardless of the material initial microstructure.

The burr height was measured at the base of 1 mm long scans acquired by the optical confocal profiler. Then, ten random and independent cross sections were measured and their mean value was calculated. The associated burr height was comprised between 10 and 40 µm for all cutting conditions. With increasing feed per tooth the burr

high was decreasing. Also the values of burr height were higher for down milling condition.

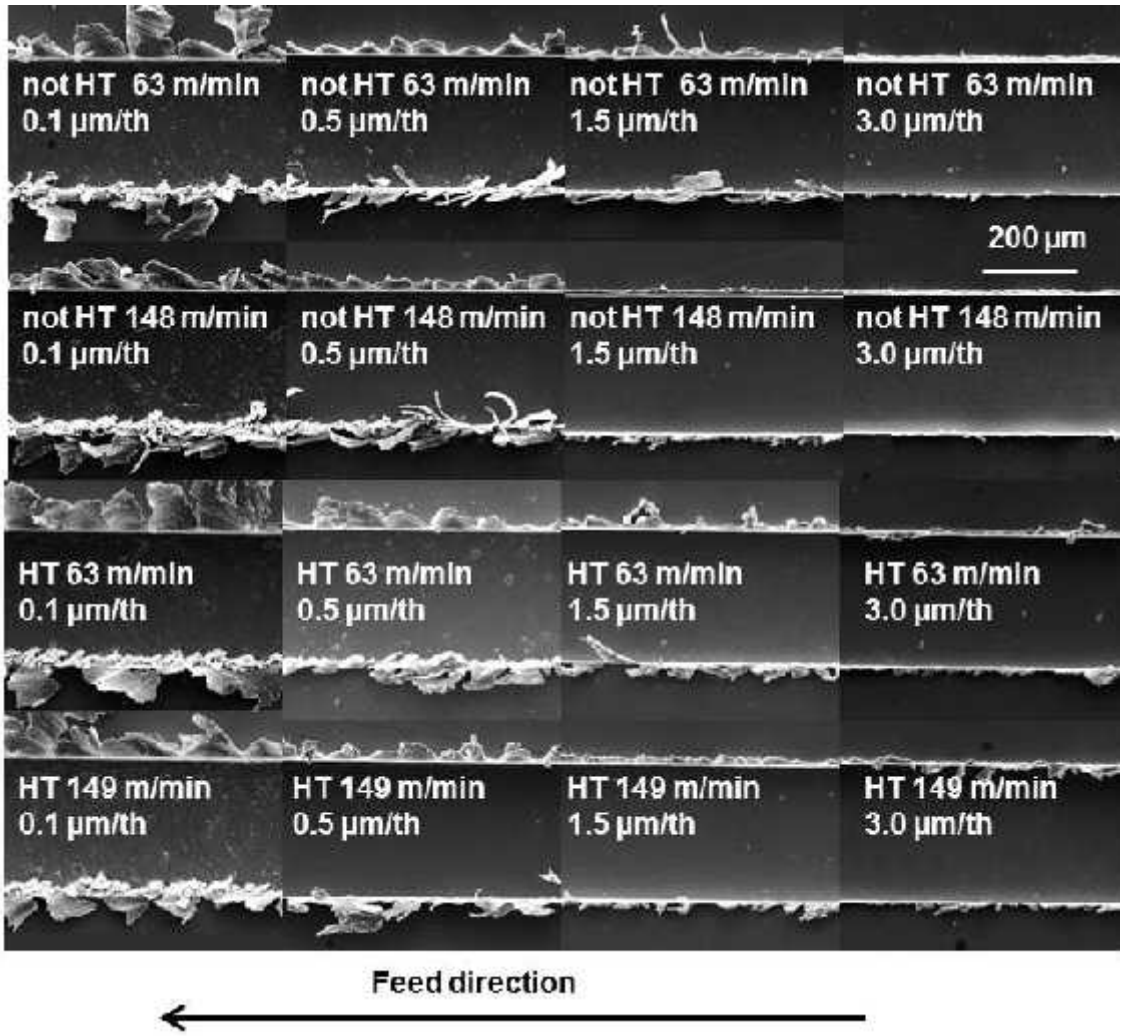

Figure 78 Burrs after micro-milling as a function of the cutting parameters

4.3.3 Surface defects

The analysis of the surface integrity cannot avoid the evaluation of the machined surface defects.

Fig. 79 shows the surface defects revealed at the bottom of the slots after micro-milling. In this study, mainly some chips debris were found for the lowest values of the feed per tooth (0.5 and 1.5 µm) and some smeared material for the highest feed per tooth (3.0 µm).

In the case of the lowest feed per tooth, being the ploughing predominant, the surface is highly perturbed, with a significant amount of defects.

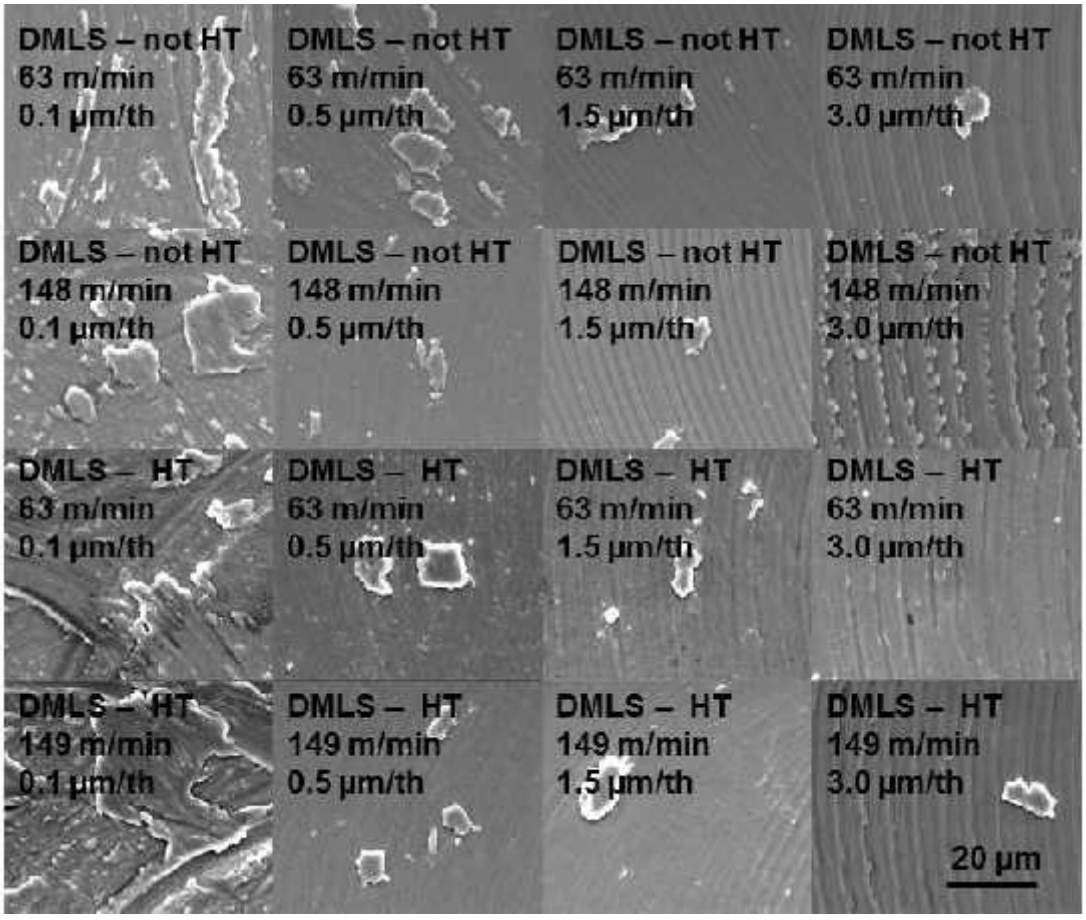

Figure 79 Surface defects as a function of the cutting parameters

4.3.4 Tool analysis

All the tools were inspected before and after the micro-milling experiments to evaluate their state. In all the cases, adhesion of the workpiece material to the tool can be found, to a different extent on the basis of the specific cutting conditions.

Fig. 80 shows an example of two tools that machined DMLS • not HT and DMLS • HT. The material adhesion on the cutting edge is evident, as witnessed by the EDS analysis.

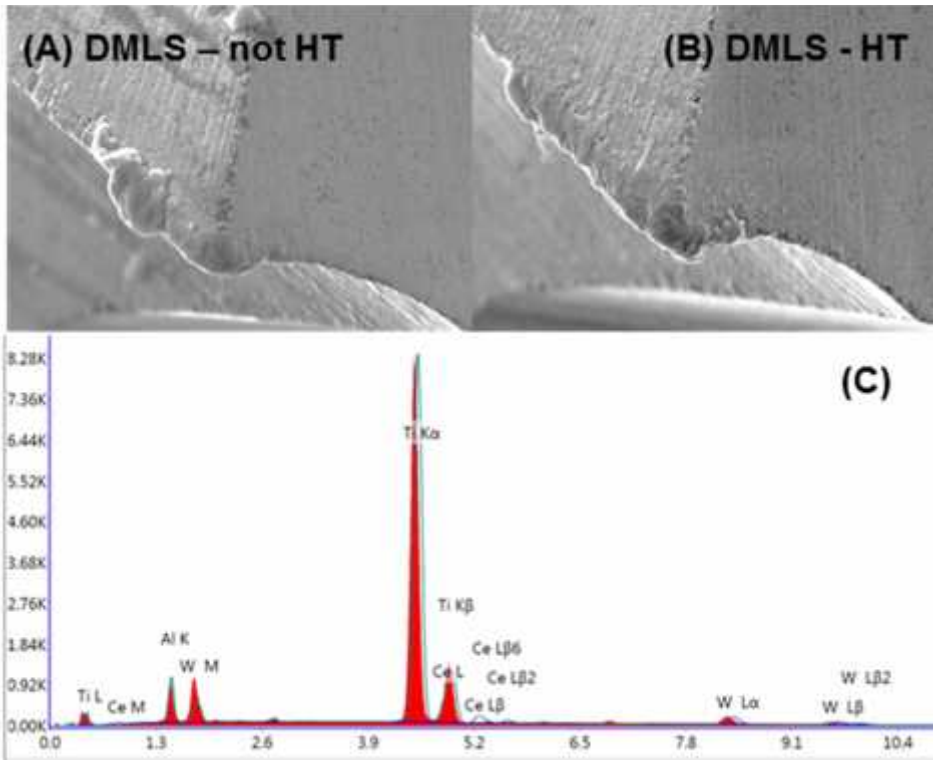

Figure 80 Tool state after machining and proof of the adhesion of the workpiece material on the cutting edge, (A) DMLS • not HT; (B) DMLS • HT and (C) EDS analysis of the material adhered on the cutting edge

4.3.5 Microstructural analysis

Metallographic samples after machining were prepared by polishing using different abrasive papers, grinding by using colloidal silica and chemical etching by using the Kroll€s reagent. The microstructural observations were carried out using both the optical microscope LeicaŽ and the FEIŽ Quanta 400 SEM. No changes in the microstructure or evidence of recrystallization were found.

The absence of microstructural alterations can be explained by the fact that both the temperatures and forces generated during micro-milling are lower than in macro-machining [62].

4.4 WROUGHT TI6AL4V

4.4.1 Surface roughness

Fig. 81 shows images of the slots bottom acquired by using a FEIŽ Quanta 400 SEM and a SensofarŽ PL… Neox confocal optical profiler. As in previous experimental campaigns we can see the same trend in the surface topography as a function of the feed per tooth. But it is necessary to mention, that contrary to previous results in the case of lowest feed per tooth the values of surface roughness are similar to other values of feed per tooth, which doesn€t correspond to the expectations of the ploughing regime.

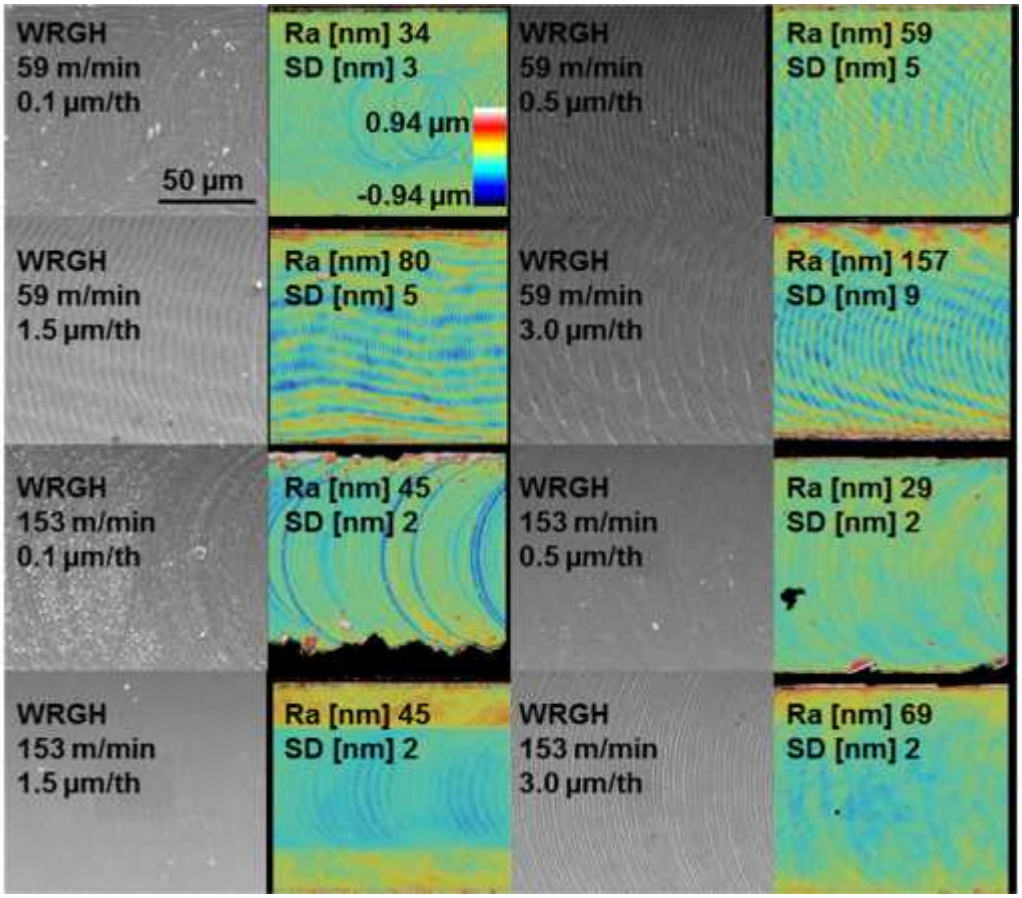

Figure 81 Images of the bottom of the slots acquired using SEM and optical confocal profiler (wrought)

On the other hand, by analysing the images from SEM, it is evident that in the case of lowest feed per tooth the surface is perturbed as in the case of the ploughing, but for higher values of the feed per tooth,

there are visible marks on the surface highly influenced by vibrations. Thus the values of the profile roughness are higher.

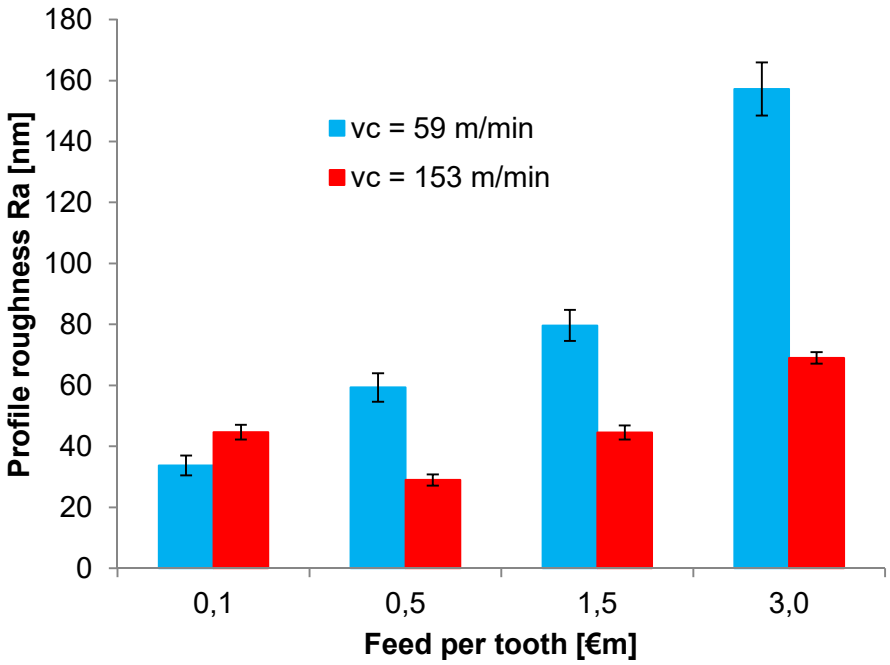

Figure 82 Profile roughness as a function of the feed per tooth

In the Fig. 82 we can see as written before that the value of surface roughness in quite low in the case of feed per tooth of 0.1 μm and Ra is increasing with the feed per tooth. This trend is more promoting in the case of lower cutting speed where the value of profile roughness for highest feed per tooth reach high value compared to previous experimental campaign. It is due to the vibrations. In the case of higher cutting speed (based on SEM pictures) the vibrations were also presented but with lower extent and thus the results are less influenced. The trend of the curve in this case is same as in previous chapters, Ra is firstly decreasing and then increasing in the function of the feed per tooth.

4.4.2 Burr formation

Also in the case of wrought Ti-6Al-4V, burrs can be found for all the combinations of the cutting parameters and should be minimised as much as possible by choosing the most appropriate cutting conditions. Fig. 83 shows the top burrs of the slots after micro-milling: again, it can be seen that the influence of the feed per tooth is predominant over

the cutting speed. The trend is once more same as in previous chapters, with increasing the feed per tooth, the burr€s size is decreasing.

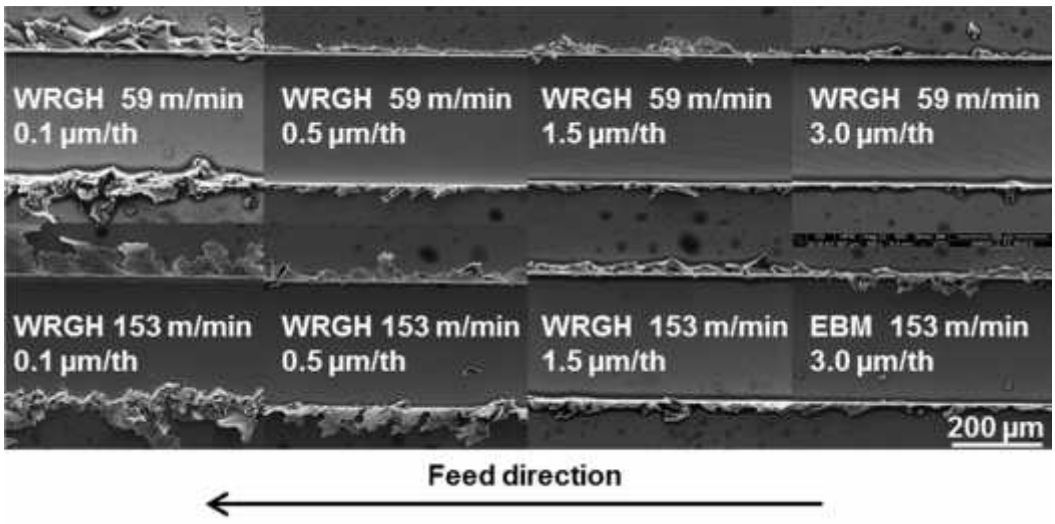

Figure 83 Burrs after micro-milling as a function of the cutting parameters

4.4.3 Surface defects

Fig. 84 shows the surface defects acquired at the bottom of the slots after micro- milling. As in all experimental campaigns we can see mainly smeared material and few of chips debris. Moreover for these experiments we can see also the influence of the vibrations presented by the interrupted feed marks.

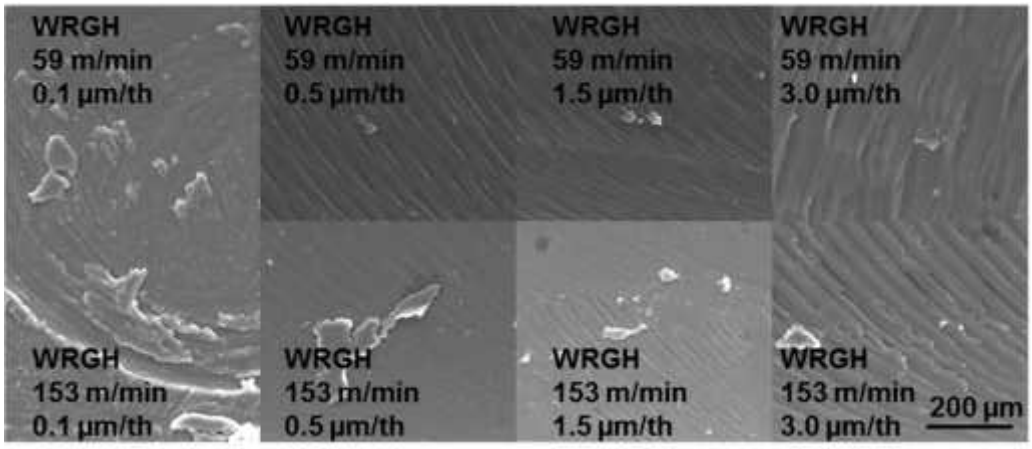

Figure 84 Surface defects as a function of the cutting parameters

4.4.4 Tool analysis

All the tools were inspected before and after the micro-milling experiments to evaluate their state. In all the cases, adhesion of the workpiece material to the tool can be found. Fig. 85 shows an example of two tools that machined at the feed per tooth of 1.5μm and cutting speed of 59 m/min (A, B, C) and 153 m/min (D, E, F). Pictures (C) and (F) are acquired by BSED detector to show the evidence of workpiece material adhered on the cutting edge.

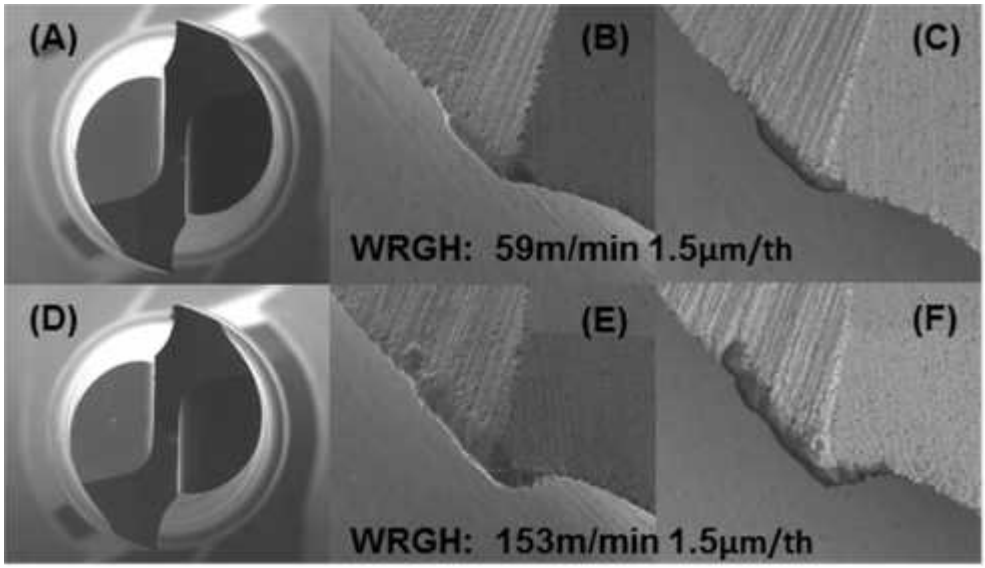

Figure 85 Tool state after machining and proof of the adhesion of the workpiece material on the cutting edge

4.4.5 Chip morphology

The samples of chips were collected during the micro-machining experiments and then were inspected through SEM analysis. Some of them are shown in the Fig. 86.

Except the case of lowest feed per tooth, the morphology of the chips seems to be same for all tested cutting conditions. In the case of lowest feed per tooth, where predominant ploughing regime is expected, the chips seem to be more segmented.

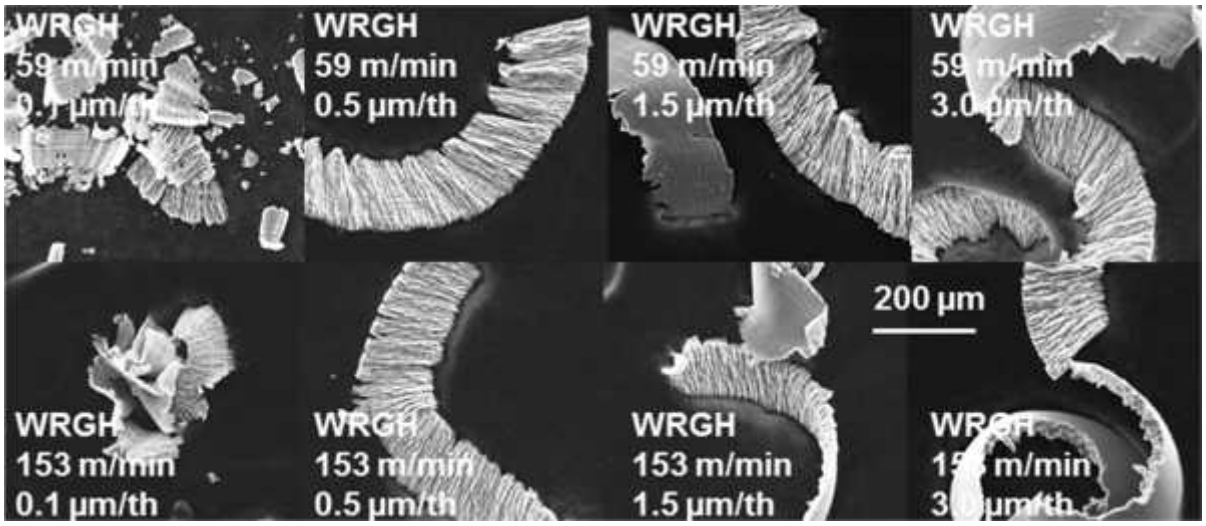

Figure 86 Chips morphology

4.5 DRILLING EXPERIMENTS

After the full immersion slotting, drilling experiment have been carried out. As a case study dental pins were used. With regards to the subsequent threading step and final functionality of the dental pin, the diameter and perpendicularity of the drilled holes are chosen as the most important geometrical parameters to be evaluated, because any deviation would affect the feasibility and final precision of the threading operation. For this reason, a preliminary drillability study was carried out on samples made of DMLS not HT and compared with wrought Ti6Al4V.

4.5.1 Geometrical features

In collaboration with metrology group the geometry of the drilled holes was checked using a coordinate measuring machine (Zeiss Prismo 7 VAST with a Maximum Permissible Error of 2.2+L/300 …m, L in mm). A single stylus with a 0.6 mm ruby tip was used. Thermal stability was ensured by laying the workpiece in the measuring room for a minimum of 12 hours before inspection. The temperature inside the measuring room was controlled and fixed at the standard reference temperature value of 20 „C to minimize measuring uncertainty. To check the geometrical quality of the holes the following characteristics were selected: the hole diameter (measured as cylinder, acquiring points in three circles at 1 mm, 2.5 mm and 4 mm from the top plane of the workpiece, see Fig. 87) and the perpendicularity between the cylinder axis and the top plane of the workpiece. On the basis of the ratio between the radius of the tip and the measured diameter, according with the relevant ISO standards, a UPR (Undulation Per Revolution) filter parameter of 50 was applied. The least squares method was used for the extraction of the fitting cylinder.

Part alignment was based on the lateral plane, top plane and external cylinder (see Fig.87). The mean values and standard deviations were calculated on the basis of 5 repetitions.

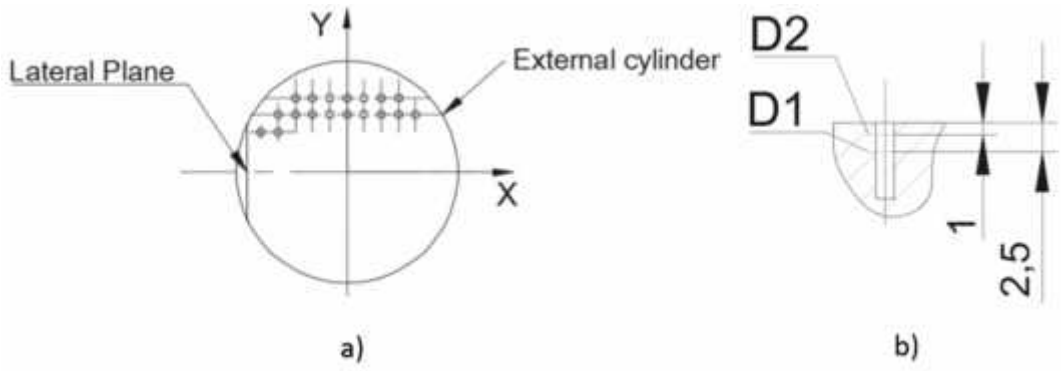

Figure 87 Sketch of the workpiece used for the tests and references used for the measurements

Fig. 88 shows the graph of the hole diameter as a function of the cutting conditions and Ti6Al4V as-delivered conditions. It is visible that for the lowest value of the feed per tooth the variation in between measured values is only in order of 0.002 mm for the different material samples and cutting speeds. The difference between nominal and measured values is between 4 and 6 …m. Once the feed per tooth increases, the difference between the nominal and measured hole diameters increases too in the case of the DMLS material at the lowest cutting speed, whereas at the highest cutting speed the difference remains almost constant. In the case of the wrought material, the difference decreases at increasing feed per tooth regardless the cutting speed.

Fig. 89 shows the perpendicularity of the drilled holes with respect to the top plane as a function of the cutting conditions and Ti6Al4V as-delivered conditions. The hole drilled on the wrought Ti6Al4V at a cutting speed of 60 m/min exhibits the highest deviation from perpendicularity compared to the other tested combinations. Except for the latter case, the influence of the feed per tooth appears negligible, being the cutting speed the most significant factor. The best combination of cutting conditions in the range of the tested values includes the lowest feed per tooth and highest cutting speed, regardless the Ti6Al4V as-delivered conditions.

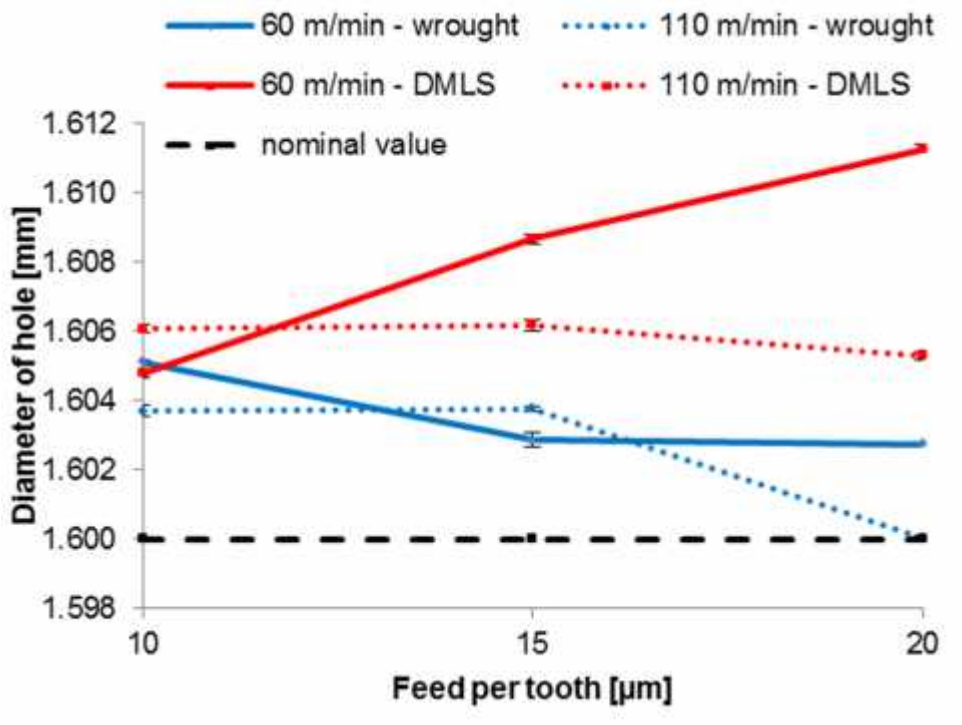

Figure 88 Diameter of the drilled holes as a function of the feed per tooth, cutting speed and Ti6Al4V as-delivered condition

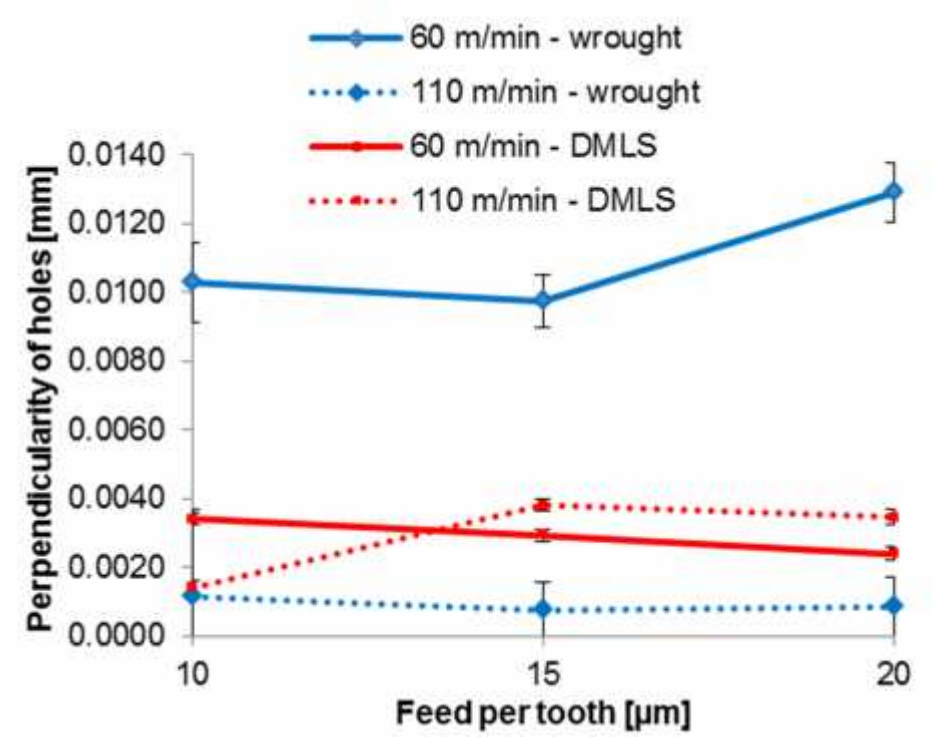

Figure 89 Perpendicularity of the drilled holes as a function of the feed per tooth, cutting speed and Ti6Al4V as-delivered condition

4.5.2 **Burr formation**

The burrs were qualitatively analyzed by means of the FEIŽ Quanta 400 Scanning Electron Microscope (SEM). Figs. 90 and 91 show the entrance burrs after drilling the holes for the DMLS and wrought Ti6Al4V, respectively. The reported images clearly show that there are no significant differences in the burrs shape and size for all the tested conditions.

Besides the qualitative analysis, the burrs height was acquired by means of the confocal optical profiler SensofarŽ PL… Neox. Ten independent cross sections were measured and the mean values calculated. The height of the burrs was found to be between 2.5 and 3.4 μm in the case of the DMLS material and between 1.2 - 2.0 μm in the case of the wrought one.

There is not any evident trend in the burrs height, shape or distribution as a function of the cutting parameters. This might be explained by the fact that the peck drilling approach was used in this study, which might remove most of the burrs.

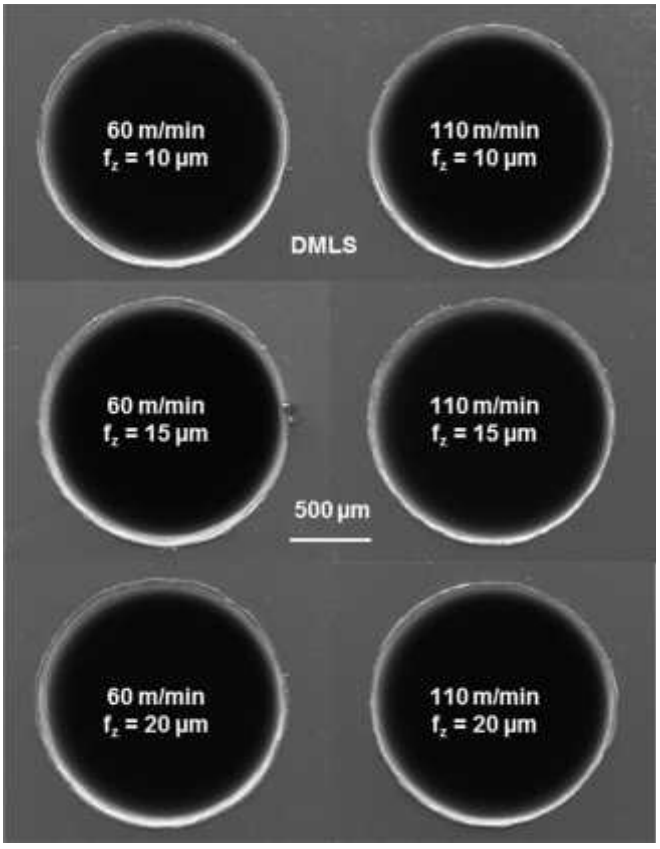

Figure 90 Entrance burrs after drilling the DMLS Ti6Al4V

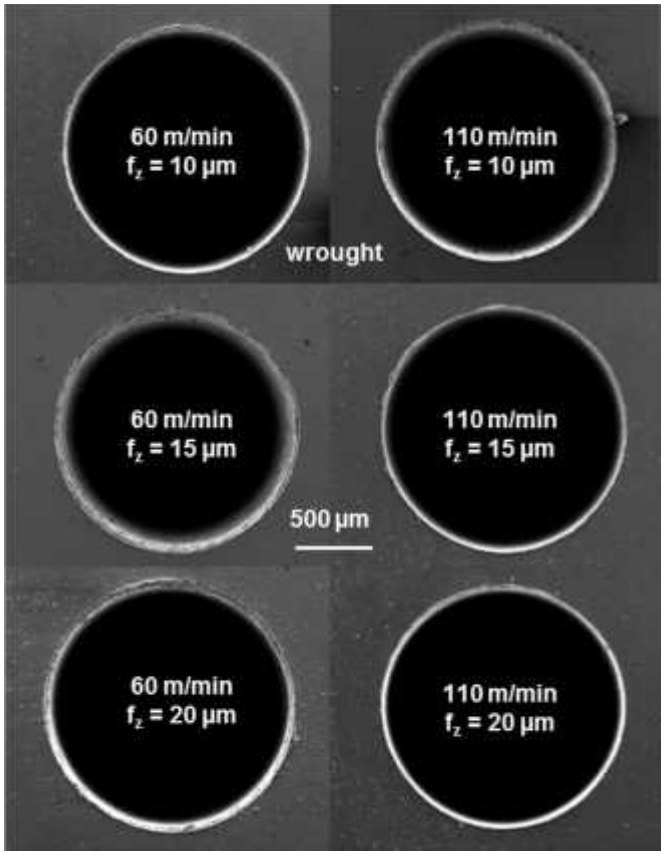

Figure 91 Entrance burrs after drilling the wrought Ti6Al4V

4.5.3 **Profile roughness**

For the evaluation of the surface finish the sample was machined again (the workpiece was cut to open the drilled holes for further roughness measurements) after the evaluation of the geometrical quality. The holes were sectioned parallel to their axis in order to check their surface roughness with the SensofarŽ PL… Neox. A confocal objective with a magnification of 20x and numerical aperture of 0.5 was used. In order to check most part of the hole surface, two topographies were acquired for each hole, one at 1 mm and the other at 3 mm from the top plane. The roughness parameters were extracted selecting 5 different profiles for each topography. The evaluation of the surface parameters was made with SPIPŽ software from Image Metrology and the choice of filter parameters was developed according to ISO standards.

Fig. 92 shows the roughness Ra for both the tested microstructure (wrought and DMLS) as a function of the cutting conditions. All the values are situated between 43 • 60 μm and no clear trend can be found as a function of the cutting conditions. The strategy of peck drilling with the choice of one-step feed-length could have impact on Ra through the feed rate and further investigations of OSFL€s importance should be carried out.

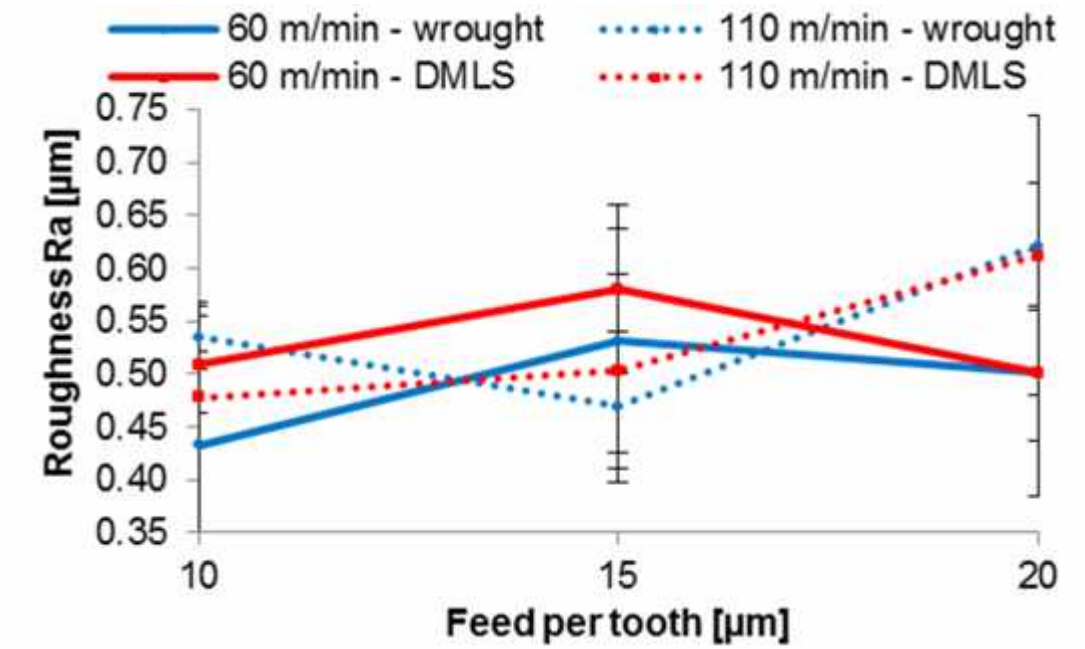

Figure 92 Roughness Ra as a function of the feed per tooth, cutting speed and Ti6Al4V as-delivered condition

4.5.4 Microstructural analysis

Finally, the samples were metallographically prepared, to observe the microstructure of the layer under the machined surface. The samples were ground using sandpapers, polished using solution of silica and finally etched using the Kroll€s reagent.

Fig. 93 shows the microstructures of the drilled hole wall. In the case of the wrought sample, some refining of the grains close to the edge can be seen, being the machined-affected layer in order of few tens of microns. On the other hand, in the case of the DMLS sample, there is

not any evident affected layer. The rough appearance of the wall edges is likely due to the grinding, which provoked the breaking and falling apart of the grains of martensitic DMLS microstructure.

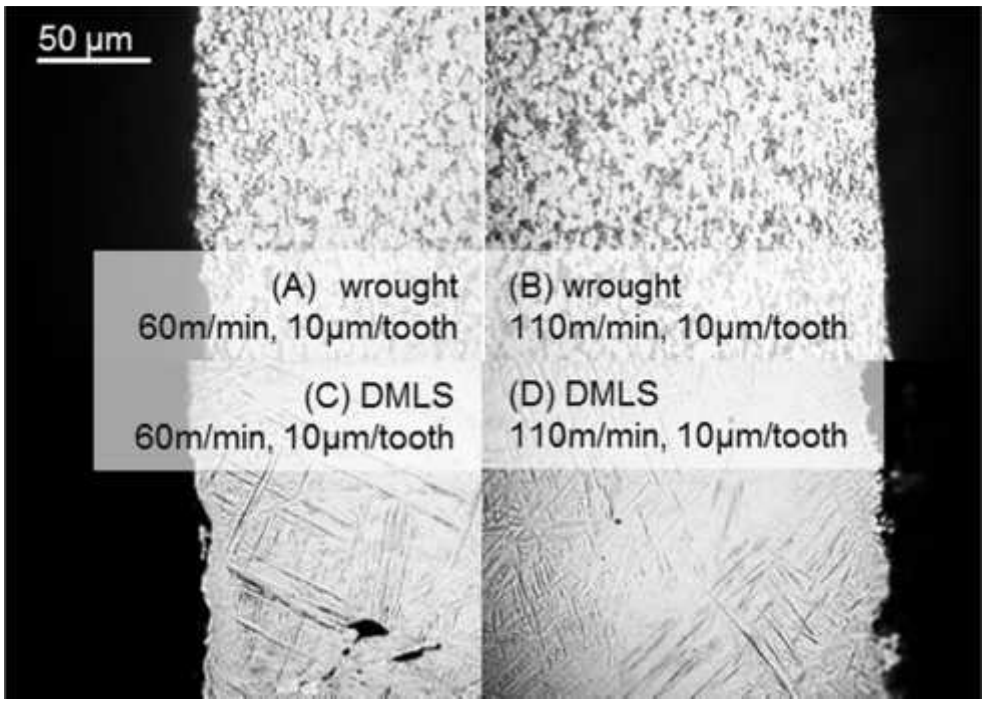

Figure 93 Microstructure after drilling, in the case of the lowest feed per tooth (10…m). (A) wrought material, v_c=60m/min, (B) wrought material, v_c=110m/min, (C) DMLS, v_c=60m/min, (D) DMLS, v_c=110m/min

4.5.5 **Threading experiments**

The threading operation is the last machining step. The thread is a functional feature as it ensures the connection between the dental pin and the implant. If the thread is not correct the functionality of the pin can be deteriorated.

To ensure the best possible conditions for the final threading operation, the best cutting conditions for the drilling (cutting speed and feed) were chosen on the basis of the previously described drillability tests. In this case, a cutting speed of 60 m/min and a feed per tooth equal to 10 µm were chosen, which were considered to be the best trade-off between precision of the drilled diameter and perpendicularity of the hole. Regarding the burrs, as no significant difference can be

appreciated for the different cutting conditions, they were not considered for the choice of the best drilling parameters.

Due to the small dimensions and internal features, the threaded holes studied in this work were not measurable with conventional measuring systems (e.g. CMMs). Therefore, an innovative measuring procedure in collaboration with metrology group was developed for this task, by exploiting the internal measurement capabilities of micro X-ray computed tomography (CT)]. Three selected specimens were scanned using a metrological CT system, Nikon MCT225, with micro-focus X-ray source (focal spot resolution down to 3 …m), and temperature controlled cabinet. The maximum permissible error (MPE) for length measurements, evaluated by tests in accordance to the guideline VDI/VDE 2630-13, was MPE = 9 + L/50 ‘m (where L is the length in mm). Further work is needed to determine the CT measurement uncertainty for the specific measurement task. The resolution related to the voxel size of the reconstructed volume (Fig. 94 (a)) is equal to (12 …m^3).

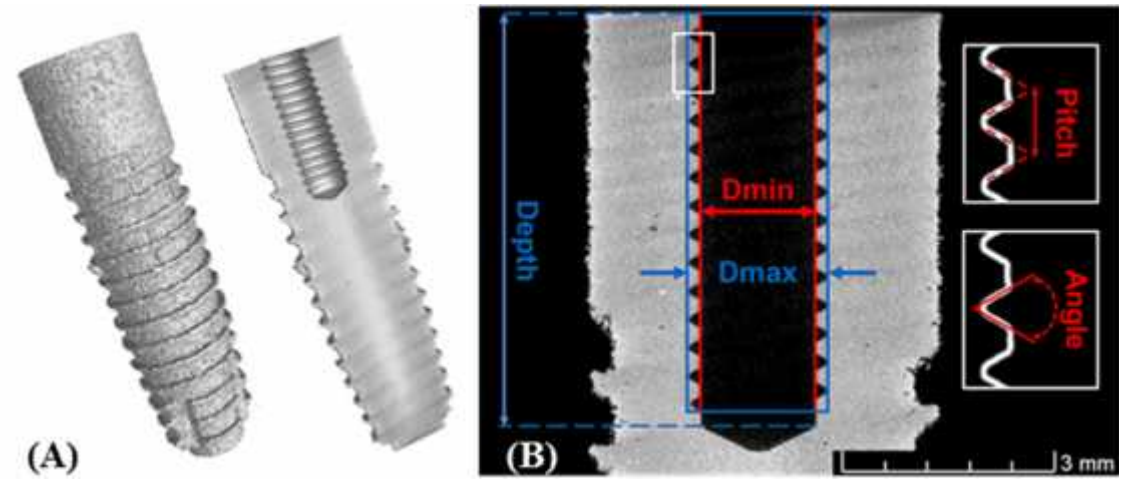

Figure 94 (a) Three-dimensional volume obtained by X-ray computed tomography (left). Internal thread is visible after virtual sectioning of the volume (right) and (b) Schematic representation of the dimensional measurements performed in the CT reconstructed volume

From the CT reconstructed volume, the quality assessment of internal thread€s machining was achieved by performing dimensional measurements of depth, minor and major diameters, pitch and angle as shown in Fig. 94 (b). For each specimen, the internal and external

cylinders were created by least-squares fitting and a total of 16 pitches and 16 angles were measured considering two different sections (0„ and 90„) of the CT volume. The alignment was done with respect to the internal cylinder axis. The obtained average measurement results are reported in Table 30.

Table 30 Average results obtained by CT measurements of three specimens machined using the same process parameters

Measurand	Average
Minor diameter [mm]	1,617
Int. cylinder form error [mm]	0,033
Major diameter [mm]	1,953
Ext. cylinder form error [mm]	0,018
Depth [mm]	5,839
Pitch [mm]	0,400
Angle [deg]	59,84

4.6 TOOL PERFORMANCES

Two different tools were compared to understand their influences during micro-milling. Flat-end-square uncoated tungsten carbide tool were compared. The main difference was in the number of the cutting edge. Two and four fluted tools were used during the tests.

4.6.1 Surface roughness

The machined surface topography was evaluated as in previous cases by using both a Quanta FeiŽ Scanning Electron Microscope (SEM) and a SensofarŽ PL‘ Neox confocal optical profiler. The 100x lens characterized by a field of view of 127x97 ‘m2 and a ve rtical resolution of about 5 nm was used for the acquisition of the samples. The profile roughness was evaluated on the basis of the ISO 4288 standard, while using a cut-off •c value of 0.08 mm to filter the profiles. Ten values of the profile roughness, at different random locations along the sampled length, were taken and their mean value was calculated.

Figure 95 shows the surface scans of the slot bottoms, comparing pictures acquired using the SEM and the profiler. Except for the cutting speed of 58 m/min while using the four-fluted tool, it is evident that the feed per tooth influences more the surface topography than the cutting speed. It is visible that for the lowest value of the feed per tooth the surface is highly perturbed while, at increasing the feed per tooth, the feed marks become more regular.

In the case of four-fluted tool and cutting speed of 58 m/min, especially the SEM pictures clearly evidences that the machined surface was strongly influenced by unexpected vibrations.

Figure 96 shows graph representing the profile roughness as function of the cutting conditions. Once again, if we exclude the lowest cutting speed with the four-fluted tool, the other results are in agreement with the available literature data [3]. When adopting the lowest feed per tooth, the profile roughness is quite high, as a consequence of the ploughing regime that prevails over shearing. It is due to the fact that the material is mainly plastically deformed rather than cut, as the criterion of the minimum uncut chip thickness is not respected [9,11].

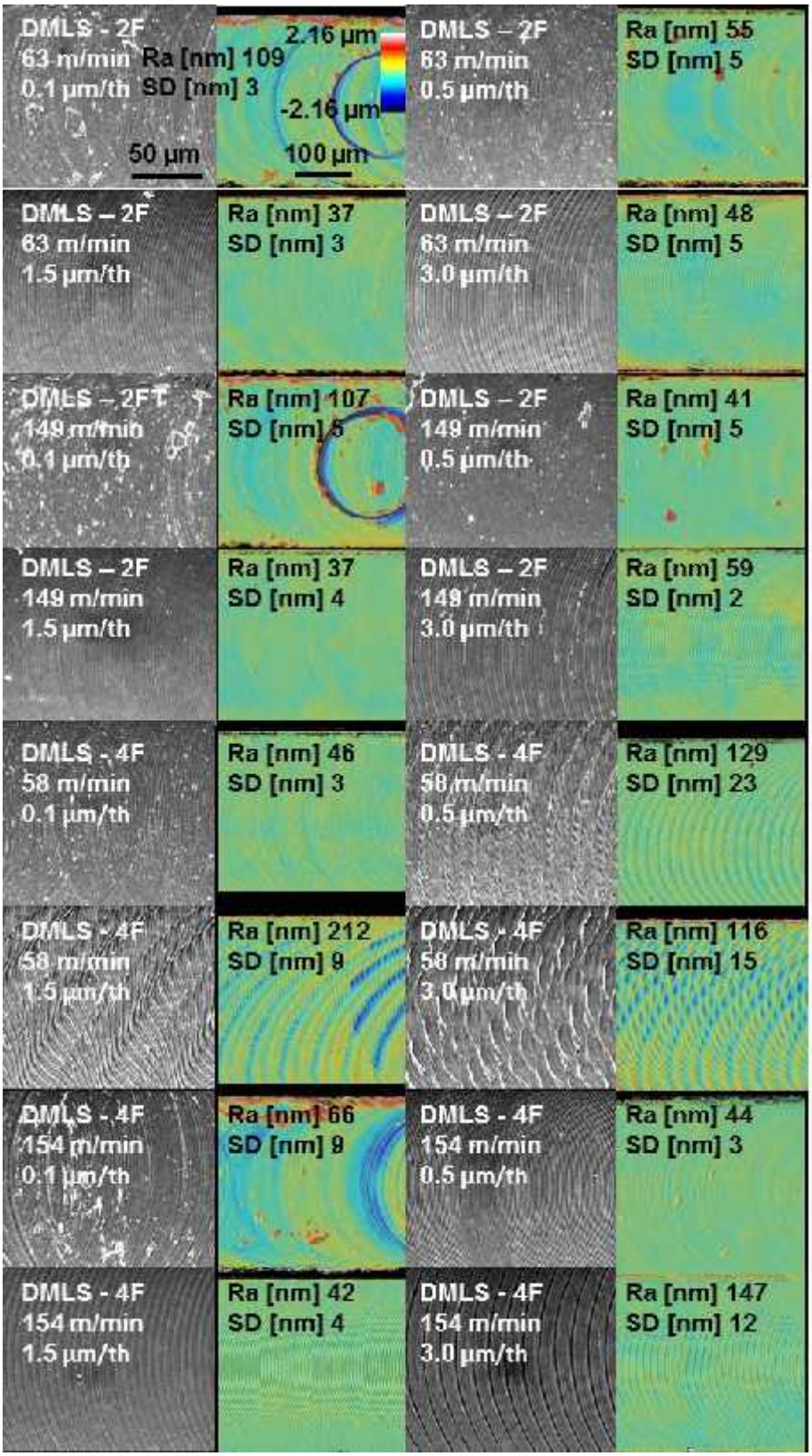

Figure 95 Surface topographies acquired using the SEM and the confocal optical profiler (2F: tow-fluted tool; 4F: four-fluted tool)

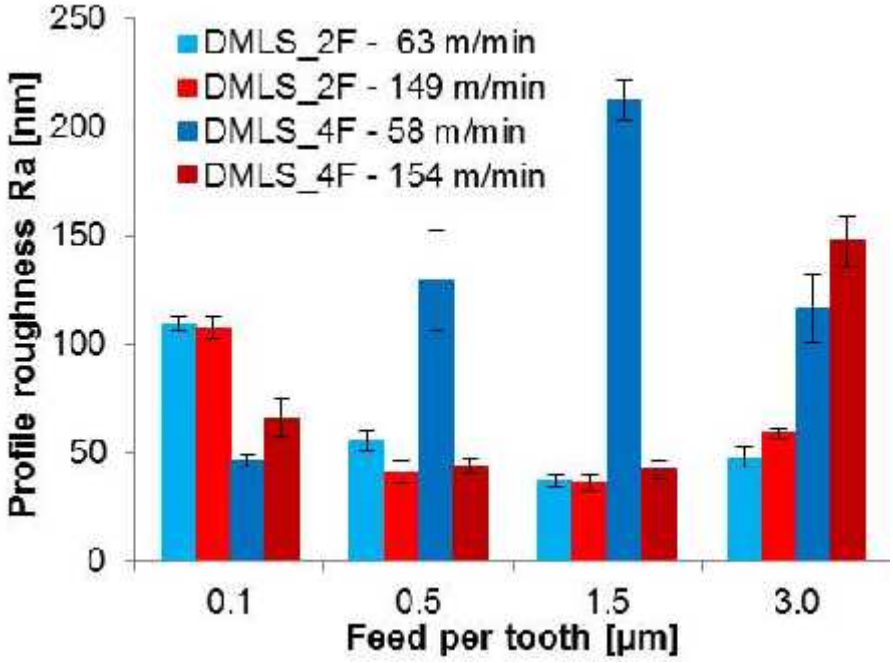

Figure 96 Profile roughness as function of the cutting conditions (2F: tow-fluted tool; 4F: four-fluted tool)

Regarding the four-fluted tool and the lowest cutting speed, as it is visible from the SEM images, the surfaces were perturbed by vibrations and, therefore, also the profile roughness value was much higher. Anyway, it is worth to notice that in case of the four-fluted tool, the roughness value for the lowest feed per tooth is very low, which is in opposition to the expected ploughing phenomenon and its consequences on the profile quality. More investigations are needed to understand this peculiar behaviour.

4.6.2 Burrs formation

Burrs were qualitatively analysed using the SEM. Figure 97 shows the burrs formed on the top surface of the micro-milled slots. The reported images clearly show that there are significant differences in the burrs shape and size as function of the tested cutting conditions. There is an evident influence of the feed per tooth, as at increasing the feed per tooth the burrs are minimised regardless the geometry of the tool. On the contrary, the influence of the cutting speed is minimal.

On the other hand, we can appreciate the difference of the burrs amount when using the two different tools. In the case of the four-fluted tool, the amount of burrs is lower also for the lowest values of the feed per tooth than when using the tow-fluted tool.

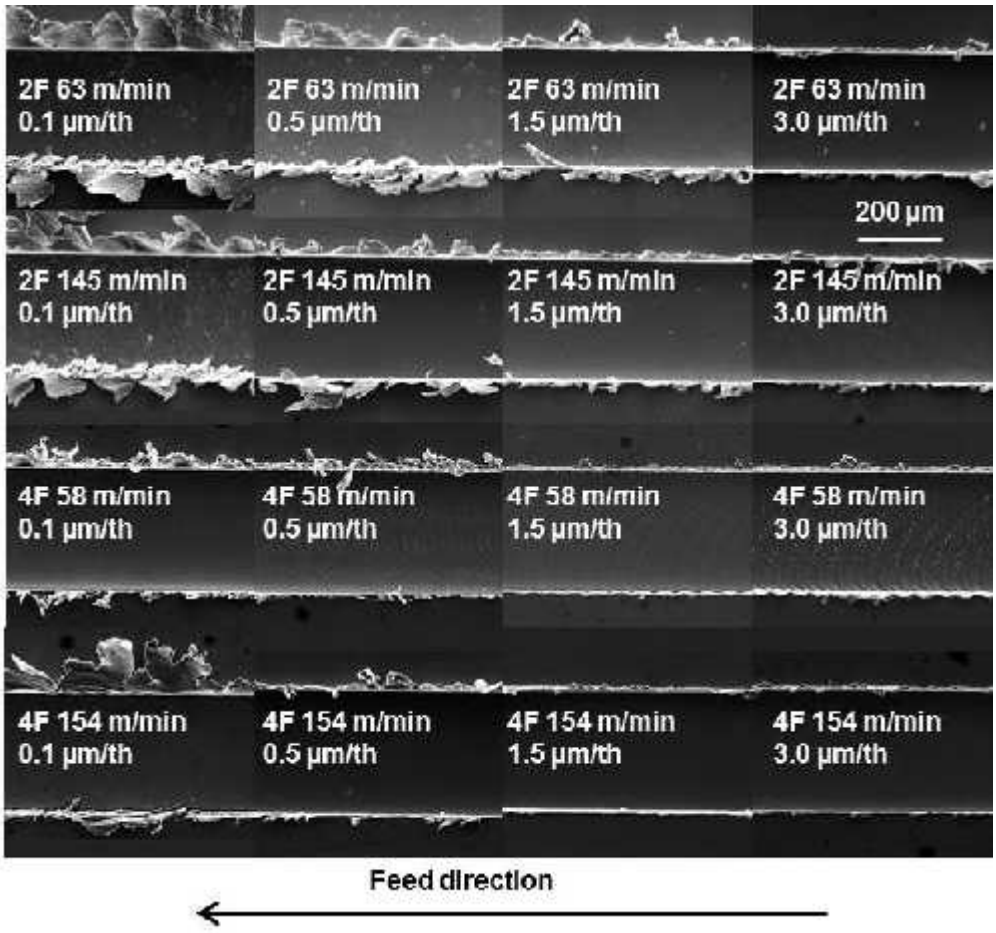

Figure 97 SEM analysis of burrs (2F: tow-fluted tool; 4F: four-fluted tool)

4.6.3 Surface defects

As illustrated in the Fig. 98 for the lowest value of the feed per tooth, due to the prevailing ploughing phenomenon, the surface is highly influenced and different types of defects are combined together. At increasing the feed per tooth, mainly chips debris and some smeared material can be found, especially for the highest value of the feed per tooth.

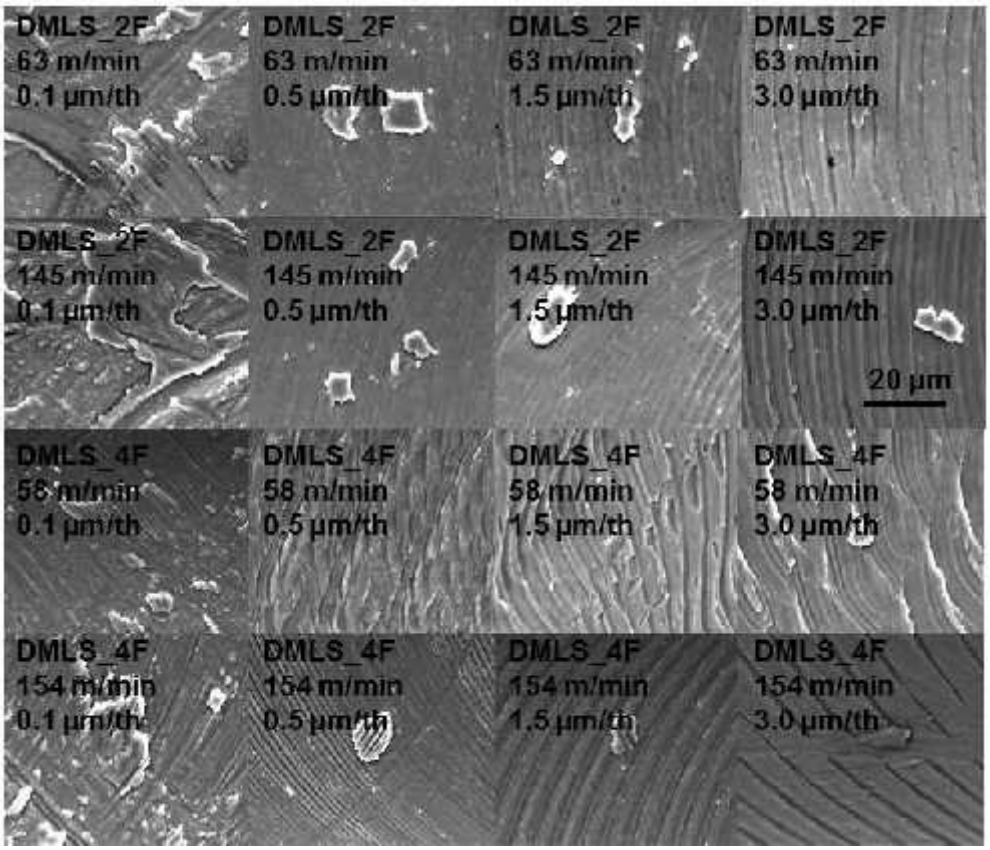

Figure 98 Surface defects at the slot's bottom (2F: tow-fluted tool; 4F: four-fluted tool)

4.6.4 Tool analysis

All the tools were inspected before and after the micro-milling experiments to evaluate their state. After testing, mainly the adhesion of the workpiece material to the tool was found, with also the cutting edge chipping present in some cases. Figure 99 shows a comparison of the two-fluted and four-fluted tools after machining at the lowest cutting speed and intermediate feed per tooth (1.5 …m): the material adhesion on the cutting edge is evident, as witnessed by the EDS analysis, regardless of the tool geometry.

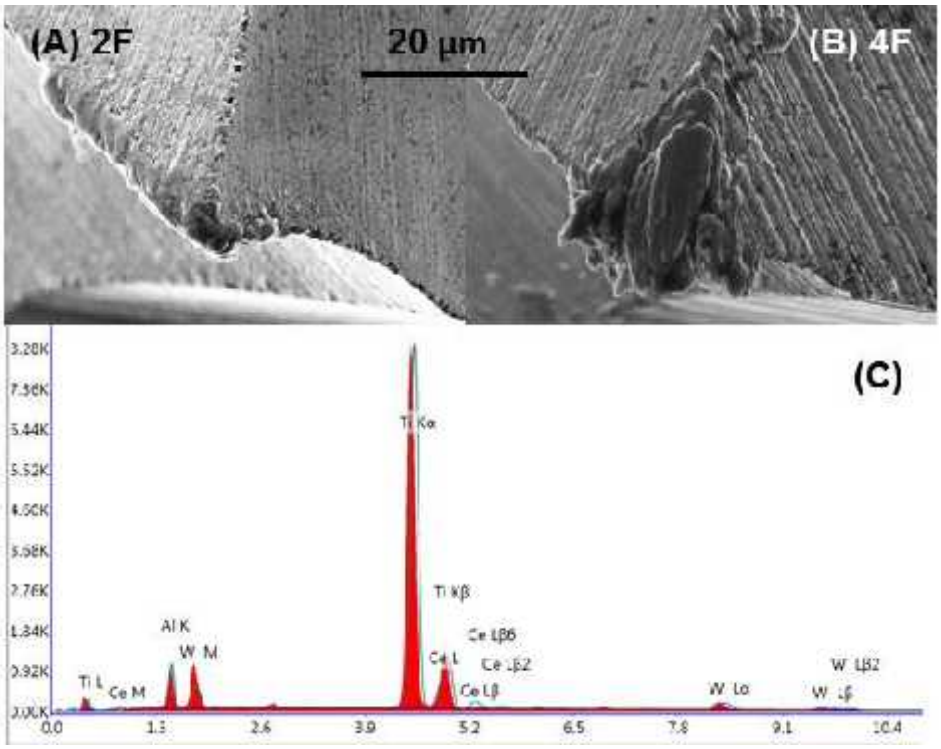

Figure 99 Adhesion of the workpiece material to the cutting edge (2F: tow-fluted tool; 4F: four-fluted tool)

4.7 FORCE ANALYSIS

During the research period spent at the Denmark Technical University (DTU) some tests of feasibility of forces measurements during micro-milling were realised.

Two different workpieces of Ti6AL4V titanium allow were used for the experiments: electron beam melted (EBM) and wrought one. Same Kyocera (D=0.3mm) tool was used during the experimental campaign.

The workpieces were grinded by an automatic machine (Fig. 100 (A)) to ensure the best possible flatness without introducing residual stress by machining operations.

Figure 100 Preparing of the experiments: (A) grinding machine; (B) dynamometer

For the measurement of the forces a Kistler dynamometer (Fig. 100 (B)), type 9347C was used. The dynamometer was connected to the charge amplifier, bench power supply and a PC with Labview software to measure forces in 3 directions Fx, Fy and Fz.

Fx force direction was corresponding to feed direction. Fy force is perpendicular to feed direction and Fz is coincidence with spindle axes direction.

In the Fig. 101 (A) is shown the grinded workpiece fixed to the dynamometer and ready for micro-milling experiments, while on 101 (B) is workpiece during the micro-slotting.

Figure 101 Workpiece fixing on the dynamometer (A), micro-milling of the workpiece fixed on the dynamometer (B)

4.7.1 Forces during micro-cutting

In the Fig. 102 and 103 are shown the values of effective forces (Fx • feed direction and Fy • direction perpendicular to feed) in the case of machining wrought and EBM Ti6Al4V.

In the case of wrought Ti6Al4V the difference between cutting conditions are balanced. For higher cutting speed the force are slightly higher but not with very strong difference. Also with increasing the feed per toot the cutting forces has tendency increasing too. If we compare the cutting force in feed direction for lower cutting speed at lowest and at highest and highest value of feed per tooth, it is visible that the cutting force has increased by factor of 1.5 but the value of feed per tooth increased 30 times. Therefore is evident the strong influence of the size effect and increased specific cutting forces in the case of very low values of feed per tooth.

In the case of EBM Ti6Al4V and lower cutting speed the values of forces and their trend is similar to wrought Ti6Al4V. But in the case of higher cutting speed the values reach much higher level especially in the case of direction perpendicular to feed. Both Fx and Fy have tendency to decrease with increasing the feed per tooth. This might be by very strong influence of size effect for this peculiar material and higher cutting speed. Further investigations and more robust experimental campaign dedicated to force measurements should be realised to understand this behaviour.

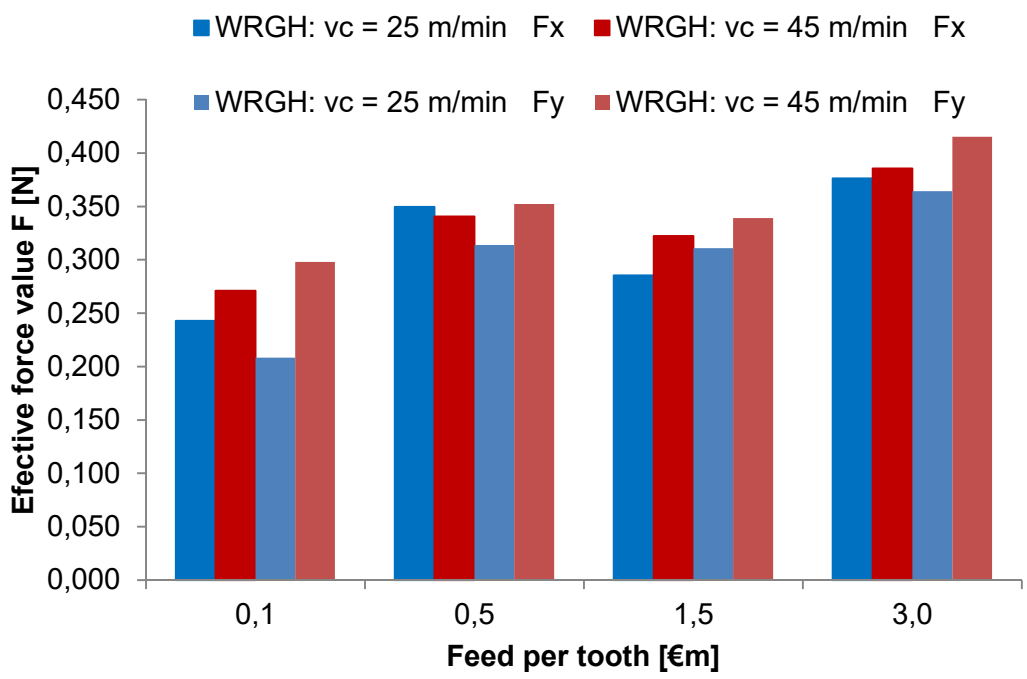

Figure 102 Effective forces during micro-milling of wrought Ti6Al4V

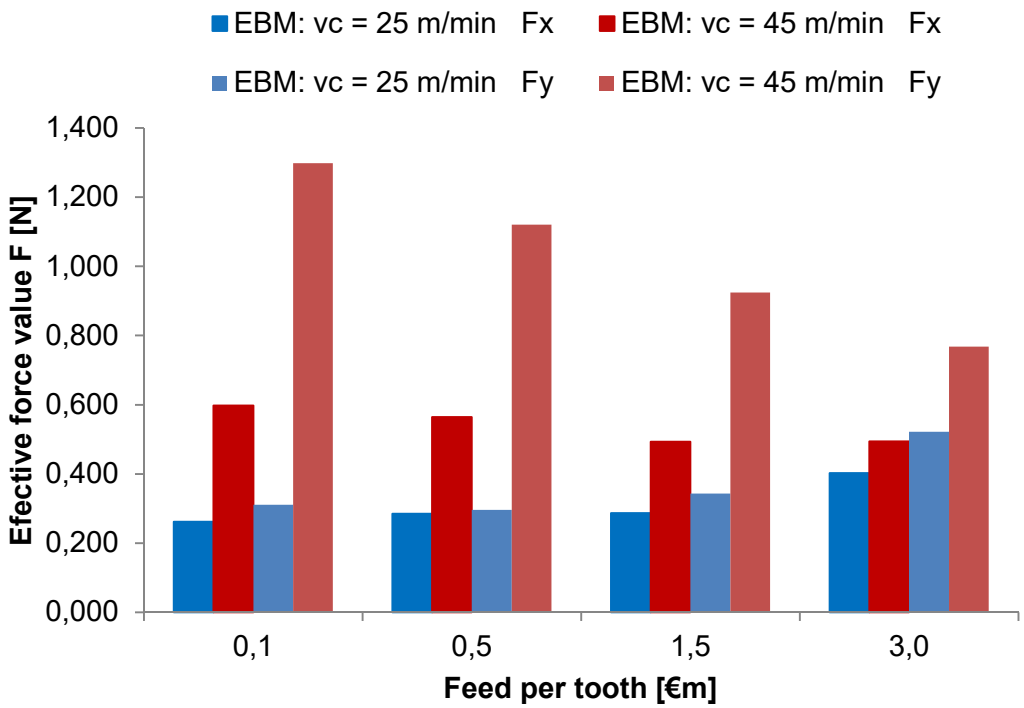

Figure 103 Effective forces during micro-milling of EBM Ti6Al4V

4.7.2 Surface roughness

After the machining the profile roughness of bottom slots was evaluated, following the same procedure as in previous experimental campaigns, using confocal optical profiler SensofarŽ PL‘ Neox 100x lens characterized by a field of view of 127x97 ‘m2 and a v ertical resolution of about 5 nm and scanning electron microscope Quanta FeiŽ. Ten independent profiles were measured and filtered using cut - off value •c equal to 0.08 mm following the ISO 4288 standard.

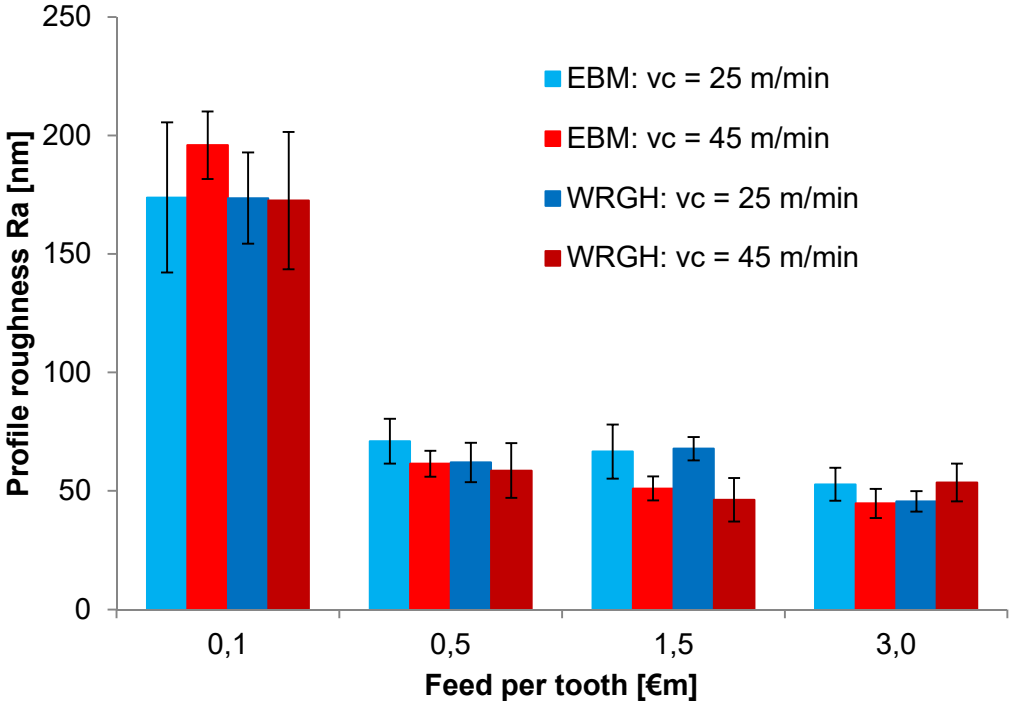

Figure 104 Profile roughness as function of the cutting conditions

In the Fig. 104 are shown the values profile roughness in function of the cutting conditions. There is not any strong difference between material variation and cutting speed, the trend is same and values are similar. For the loves value of the feed per tooth the values are very high as we have seen in previous experiments, it is due to the size effect and ploughing prevailing over sharing mechanism. It is evident that the most influencing parameter is the feed per tooth.

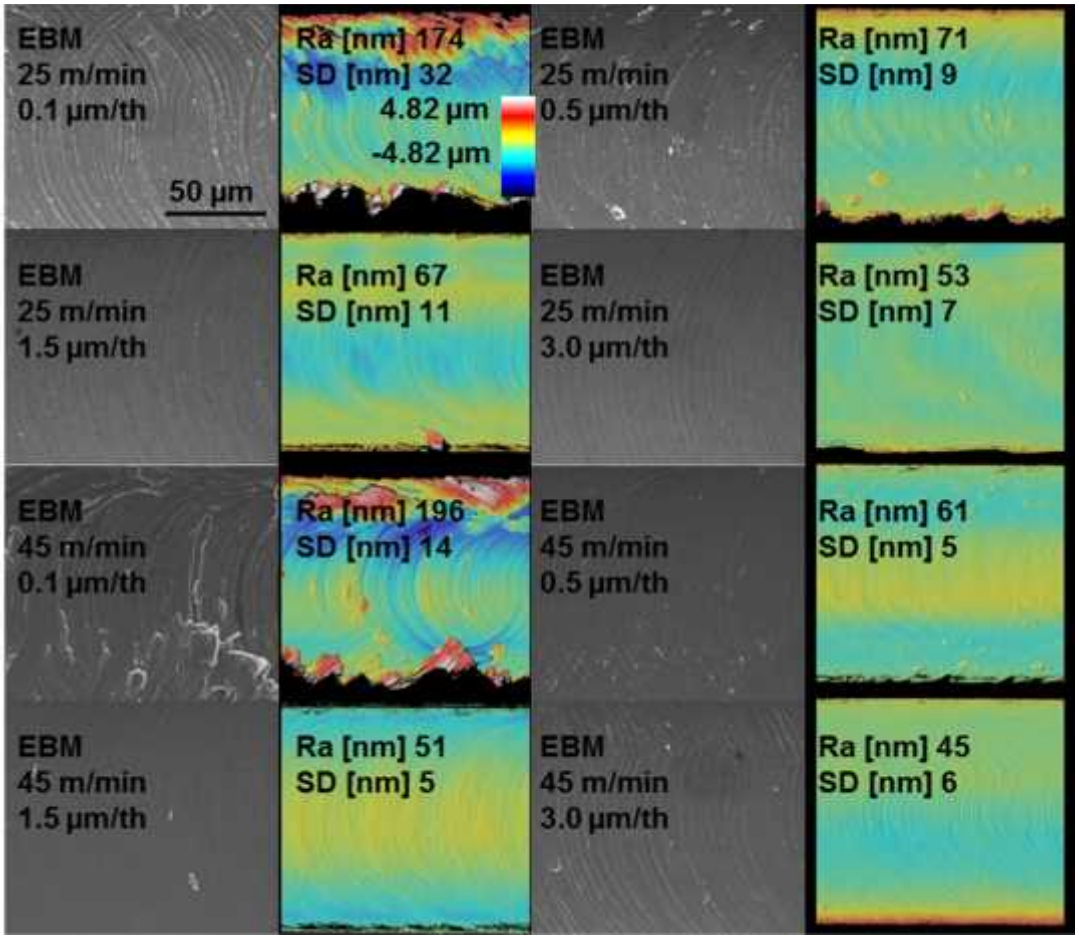

Figure 105 Surface topographies acquired using the SEM and the confocal optical profiler in the case of EBM Ti6Al4V

Figures 105 and 106 show the surface topographies of slots bottom acquired by SEM and confocal optical profiler in the case of EBM and wrought Ti6Al4V. Regardless the cutting speed and material variation, for the lowest feed per tooth the surfaces are more perturbed and with increasing feed per tooth, the feed marks are becoming more regular.

Comparing the results with previously performed campaigns in Italy, the surfaces in general seem slightly rougher, with more irregularities and also the values of Ra are slightly higher.

It is worth to mention that almost 40% of tools were broken during the machining and also the depth of the cut in some cases was deeper than desired. It seems that the control of the machine and its accuracy could have impact on the experiments.

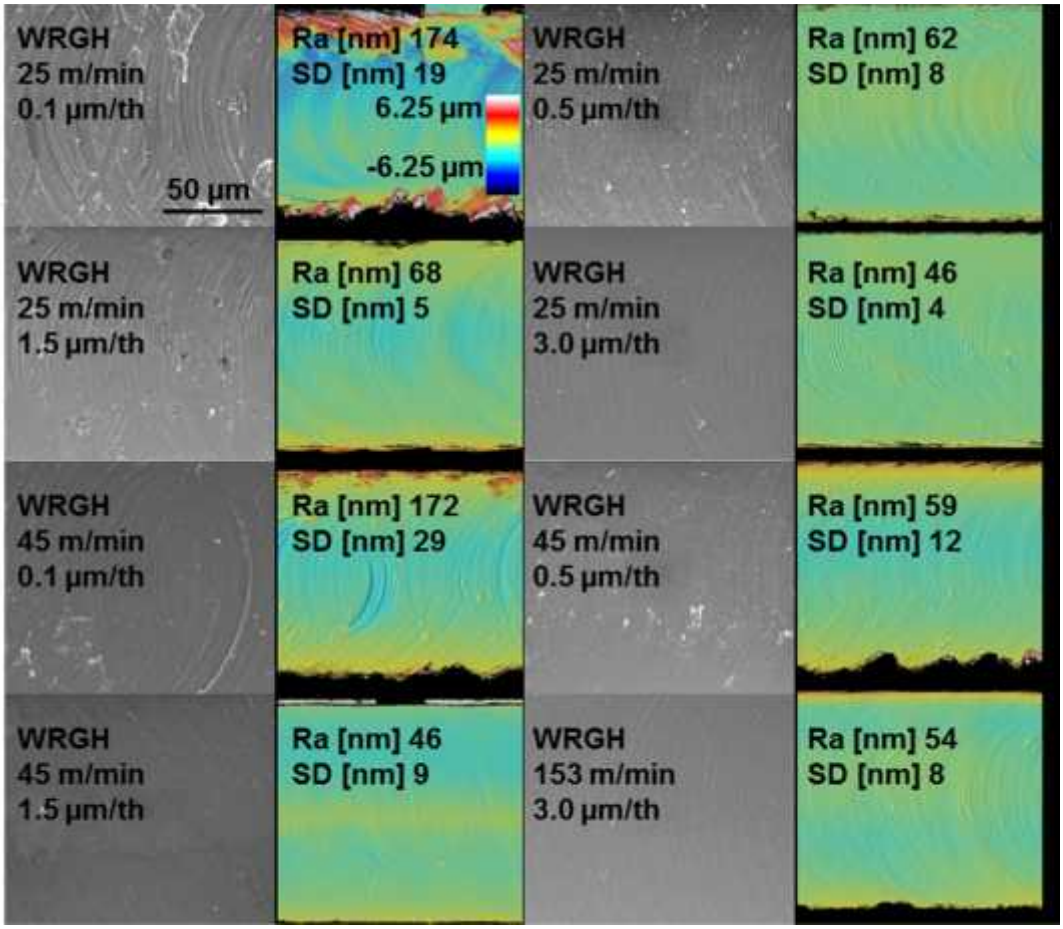

Figure 106 Surface topographies acquired using the SEM and the confocal optical profiler in the case of wrought Ti6Al4V

4.7.3 Surface defects

Fig. 107 shows the surface defects after the machining found on the slots€ bottom. There can be found lot of speared materials and chip debris. It seems that the extent of defects is a bit higher than in previous cases especially in the slots corners.

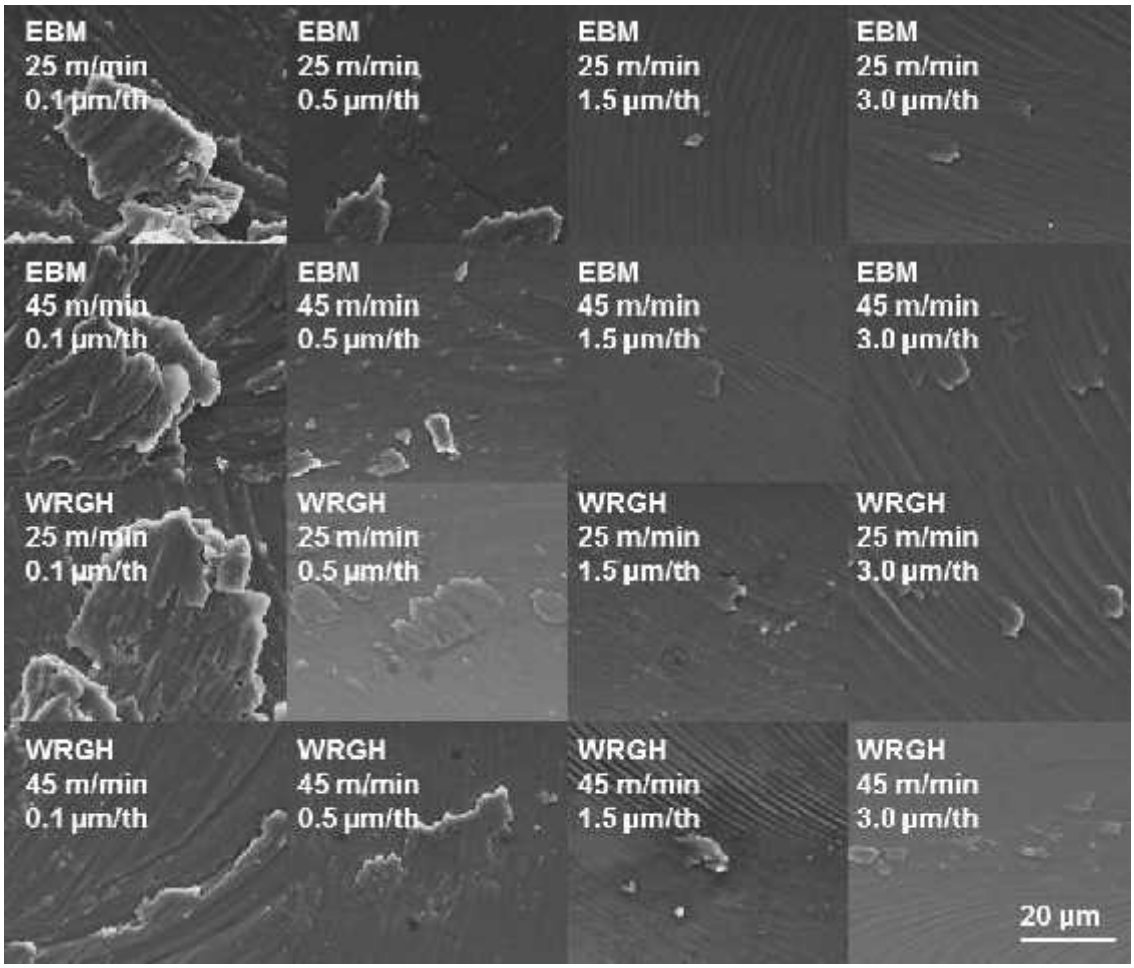

Figure 107 Surface defects for EBM and wrought Ti6Al4V

4.7.4 Tool analysis

The tool state after machining was studied as shown in the Fig. 108. As written above in the text, almost 40% of tools were broken during machining and the others exhibit strong tool wear, especially chipping of the cutting edge as shown in the Fig. 108 (B). Views (C) and (D) show the adhered material on the tool edge, view (D) is witnessing by BSED analysis the presence of the workpiece material adhered on the cutting edge.

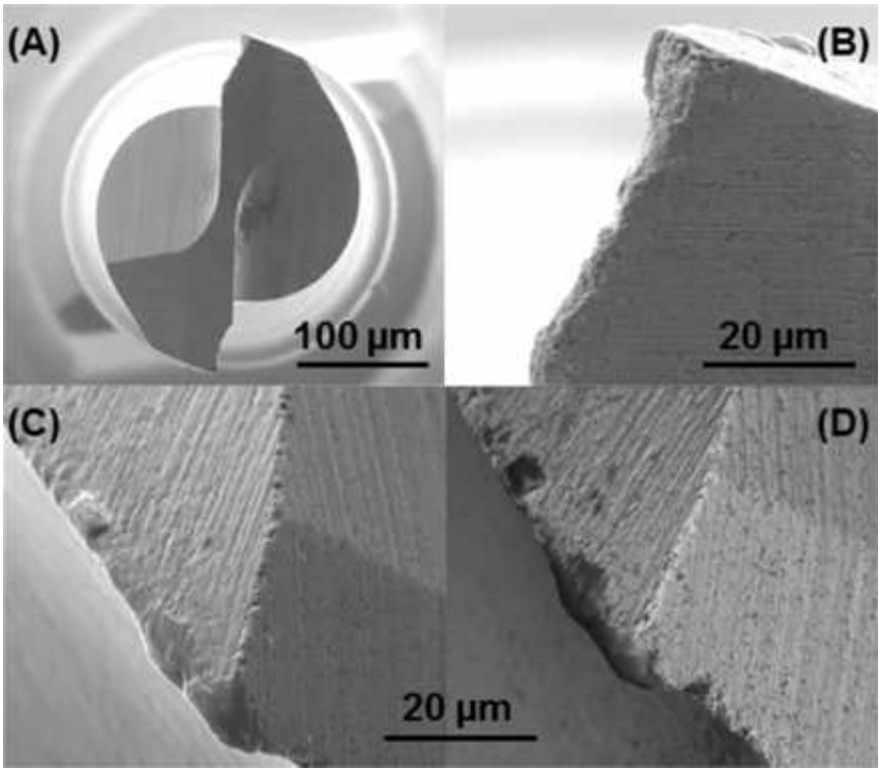

Figure 108 Tool state after the machining EBM v_c = 45 m/min, f_z = 1.5 µm (A) top view of the tool, (B, C) cutting edge details, (D) BSED image of cutting edge detail

5 CONCLUSIONS

In this thesis the study of micro-cutting of the Ti6Al4V titanium alloy produced by different Additive Manufacturing techniques namely Electron Beam Melting and Direct Meatal Laser Sintering, comparing with wrought material have been studied.

Titanium alloys fabricated by AM techniques exhibit different microstructures compared to the wrought material, which may affect the machined surface behaviour as a function of the cutting parameters.

The main aim of this work was the study of the micro-machinability by evaluating the influence of process parameters in terms of surface integrity • profile roughness, burrs formation, surface defects, tool damages and microstructural alterations.

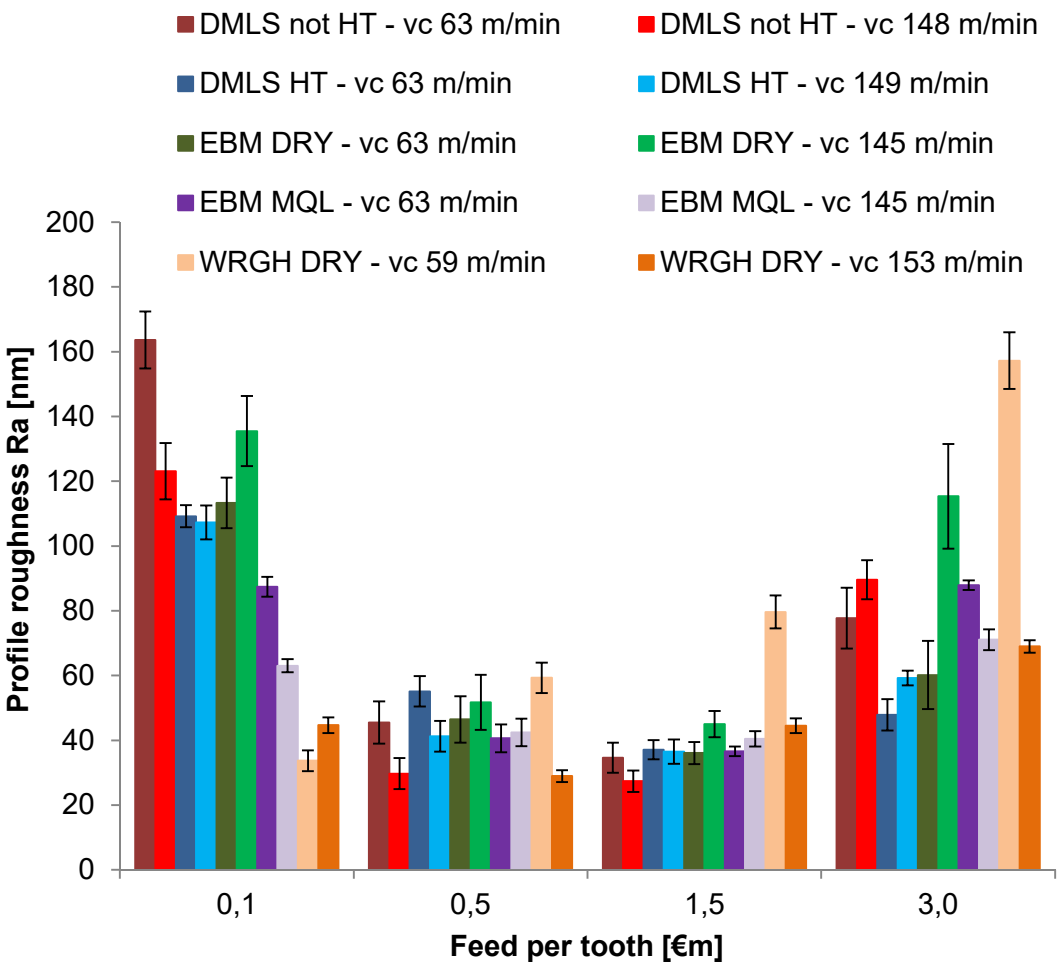

Figure 109 Profile roughness in function of feed per tooth

The study was realized mainly under dry lubrication condition by targeting the cleanliness of biomedical applications.

The effect of the lubricating/cooling conditions seems less significant in micro-milling compared to the machining operations carried out at macro-scale: this can be ascribed to the fact that both the forces and the temperatures arising during micro-machining are much lower compared to conventional machining, making the effect of the cutting fluid less relevant (Yang et al., 2010).

The presented results clearly show that dry cutting assures satisfactory surface quality. Moreover, dry cutting represents the most suitable option to decrease the environmental impact.

In the Fig. 109 are shown profile roughness for all tested material variations and cutting conditions.

There can be clearly seen the trend of profile roughness is same for all tested materials. Where firstly the values of Ra in function of feed per tooth are decreasing and once minimum chip thickness criterion is fulfilled the values or Ra increases again.

The main concluding remarks:

- the most important cutting parameter is the feed per tooth that directly influences the final surface roughness and burrs formation
- surface roughness is proportional to the chip thickness
- reduction of the chip thickness would cause a worse surface finish [16]
- surface quality can be improved by reducing the feed per tooth
- experimental results show that it is possible to achieve a profile roughness lower than 50 nm
- lowest feed per tooth is characterized by large and discontinuous burrs on both sides of the slots
- while the highest feed per tooth is almost burrs free
- for the higher values of the feed per tooth the burrs are minimal but the surface roughness starts to increase, trend suggests that a better surface finish can be achieved at the expense of more and larger burrs
- when the feed per tooth is smaller than the minimum chip thickness, both surface roughness and the amount of burrs increase rapidly

- mainly adhered material on the tool edges was observed, rather than abrasion wear
- considering proper coatings the wear resistance of the micro-tools can be greatly improved [11]
- occurrence of surface defects is mainly influenced by the feed per tooth and they are analogous for all tested microstructural cases, there have been found mainly smeared material and chip debris
- no microstructure alterations were observed, only some bended lamellas in order of few microns
- four-fluted tool produced a lower amount of burrs also at the lowest feed per tooth than the two-fluted tool on the other hand the surface quality is more influenced by vibrations

In case of micro-milling, it is proved that the feed per tooth is the cutting parameter that mostly affects surface integrity, being related to the minimum uncut chip thickness criterion. The feed increase leads to the burr size minimization, but, on the other hand, increases the surface roughness. Therefore, the best cutting conditions must be a trade-off between the surface topography and the burrs characteristics as a function of the final application: in our case the best trade-off between minimal burr size and minimal profile roughness is achieved when using a feed per tooth equal to 1.5 μm, regardless of the material initial microstructure.

To give a more comprehensive study of micro-cutting a more detailed evaluation of the tool wear in future work would be necessary. While setting a robust procedure to define, evaluate and measure tool wear in micro-cutting which is now delicate to measure and not a common consensus exists.

6 REFERENCES

[1] T. Masuzawa, †State of the Art of Micromachining,‡ *CIRP Ann. - Manuf. Technol.*, vol. 49, no. 2, pp. 473• 488, 2000.

[2] D. Dornfeld, S. Min, and Y. Takeuchi, †Recent advances in mechanical micromachining,‡ *CIRP Ann. - Manuf. Technol.*, vol. 55, no. 2, pp. 745• 768, Jan. 2006.

[3] a. Aramcharoen and P. T. Mativenga, †Size effect and tool geometry in micromilling of tool steel,‡ *Precis. Eng.*, vol. 33, no. 4, pp. 402• 407, Oct. 2009.

[4] M. A. Cˆmara, J. C. C. Rubio, A. M. Abr'o, and J. P. Davim, †State of the Art on Micromilling of Materials, a Review,‡ *J. Mater. Sci. Technol.*, vol. 28, no. 8, pp. 673• 685, Aug. 2012.

[5] S. Min, D. Dornfeld, I. Inasaki, H. Ohmori, D. Lee, M. Deichmueller, T. Yasuda, and K. Niwa, †Variation in machinability of single crystal materials in micromachining,‡ *CIRP Ann. - Manuf. Technol.*, vol. 55, no. 1, pp. 103• 106, Jan. 2006.

[6] X. Lai, H. Li, C. Li, Z. Lin, and J. Ni, †Modelling and analysis of micro scale milling considering size effect, micro cutter edge radius and minimum chip thickness,‡ *Int. J. Mach. Tools Manuf.*, vol. 48, no. 1, pp. 1• 14, Jan. 2008.

[7] E. Kuram and B. Ozcelik, †Multi-objective optimization using Taguchi based grey relational analysis for micro-milling of Al 7075 material with ball nose end mill,‡ *Meas. J. Int. Meas. Confed.*, vol. 46, no. 6, pp. 1849• 1864, Jul. 2013.

[8] A. J. Mian, N. Driver, and P. T. Mativenga, †A comparative study of material phase effects on micro-machinability of multiphase materials,‡ *Int. J. Adv. Manuf. Technol.*, vol. 50, no. 1• 4, pp. 163• 174, Jan. 2010.

[9] T. "zel, T. Thepsonthi, D. Ulutan, B. Kaftanolu, and B. Kaftano"lu, †Experiments and finite element simulations on micro-milling of Ti• 6Al• 4V alloy with uncoated and cBN coated micro-tools,‡ *CIRP Ann. - Manuf. Technol.*, vol. 60, no. 1, pp. 85• 88, Jan. 2011.

[10] T. Thepsonthi and T. "zel, †Multi -objective process optimization for micro-end milling of Ti-6Al-4V titanium alloy,‡ *Int. J. Adv. Manuf. Technol.*, vol. 63, no. 9• 12, pp. 903• 914, Mar. 2012.

[11] T. Thepsonthi and T. T. "zel, †Experimental and finite element simulation based investigations on micro-milling Ti-6Al-4V titanium alloy: Effects of cBN coating on tool wear,‡ *J. Mater.*

Process. Technol., vol. 213, no. 4, pp. 532• 542, Apr. 2013.

[12] S. M. Afazov, D. Zdebski, S. M. Ratchev, J. Segal, and S. Liu, †Effects of micro-milling conditions on the cutting forces and process stability,‡ *J. Mater. Process. Technol.*, vol. 213, no. 5, pp. 671• 684, May 2013.

[13] H. Ding, R. Ibrahim, K. Cheng, and S. J. Chen, †Experimental study on machinability improvement of hardened tool steel using two dimensional vibration-assisted micro-end-milling,‡ *Int. J. Mach. Tools Manuf.*, vol. 50, no. 12, pp. 1115• 1118, Dec. 2010.

[14] J. Fleischer, V. Schulze, and J. Kotschenreuther, †Extension of cutting force formulae for microcutting,‡ *CIRP J. Manuf. Sci. Technol.*, vol. 2, no. 1, pp. 75• 80, Jan. 2009.

[15] M. T. Zaman, a. S. Kumar, M. Rahman, and S. Sreeram, †A three-dimensional analytical cutting force model for micro end milling operation,‡ *Int. J. Mach. Tools Manuf.*, vol. 46, no. 3• 4, pp. 353• 366, Mar. 2006.

[16] S. Jahanmir, †Surface integrity in ultrahigh speed micromachining,‡ in *Procedia Engineering*, 2011, vol. 19, pp. 156• 161.

[17] T. “zel, X. Liu, and A. Dhanorker, †Modelling and Simulation of Micro-Milling Process,‡ in *4th International Conference and Exhibition on Design and Production of Machines and Dies/Molds*, 2007, pp. 21• 23.

[18] F. Vollertsen, D. Biermann, H. N. Hansen, I. S. Jawahir, and K. Kuzman, †Size effects in manufacturing of metallic components,‡ *CIRP Ann. - Manuf. Technol.*, vol. 58, no. 2, pp. 566• 587, Jan. 2009.

[19] A. Dhanorker and T. Ozel, †Meso/micro scale milling for micro-manufacturing,‡ *Int. J. Mechatronics Manuf. Syst.*, vol. 1, no. 1, pp. 23• 42, 2008.

[20] D. Biermann and P. Kahnis, †Analysis and simulation of size effects in micromilling,‡ *Prod. Eng.*, vol. 4, no. 1, pp. 25• 34, 2010.

[21] S. Filiz, C. M. Conley, M. B. Wasserman, and O. B. Ozdoganlar, †An experimental investigation of micro-machinability of copper 101 using tungsten carbide micro-endmills,‡ *Int. J. Mach. Tools Manuf.*, vol. 47, no. 7• 8, pp. 1088• 1100, Jun. 2007.

[22] X. Liu, R. E. DeVor, and S. G. Kapoor, †An Analytical Model for the Prediction of Minimum Chip Thickness in Micromachining,‡ *J. Manuf. Sci. Eng.*, vol. 128, no. 2, p. 474, 2006.

[23] Z. Liu, Z. Shi, and Y. Wan, †Definition and determination of the

minimum uncut chip thickness of microcutting,‡ *Int. J. Adv. Manuf. Technol.*, vol. 69, no. 5• 8, pp. 1219• 1232, 2013.

[24] A. Dhanorker, X. Liu, and T. “zel, †Micromilling Process Planning and Modeling for Micromold Manufacturing,‡ *ASME 2007 Int. Manuf. Sci. Eng. Conf.*, pp. 759• 769, 2007.

[25] K. S. Woon and M. Rahman, †Extrusion-like chip formation mechanism and its role in suppressing void nucleation,‡ *CIRP Ann. - Manuf. Technol.*, vol. 59, no. 1, pp. 129• 132, 2010.

[26] A. Simoneau, E. Ng, and M. A. Elbestawi, †Grain size and orientation effects when microcutting AISI 1045 steel,‡ *CIRP Ann. - Manuf. Technol.*, vol. 56, no. 1, pp. 57• 60, Jan. 2007.

[27] J. C. Aurich, D. Dornfeld, P. J. Arrazola, V. Franke, L. Leitz, and S. Min, †Burrs‰Analysis, control and removal,‡ *CIRP Ann. - Manuf. Technol.*, vol. 58, no. 2, pp. 519• 542, Jan. 2009.

[28] R. Piquard, A. D€Acunto, P. Laheurte, and D. Dudzinski, †Micro-end milling of NiTi biomedical alloys, burr formation and phase transformation,‡*Precis. Eng.*, vol. 38, no. 2, pp. 356• 364, 2014.

[29] G. Bissacco, H. N. Hansen, and L. De Chiffre, †Micromilling of hardened tool steel for mould making applications,‡ *J. Mater. Process. Technol.*, vol. 167, pp. 201• 207, 2005.

[30] Z. Kou, Y. Wan, Y. Cai, X. Liang, and Z. Liu, †Burr Controlling in Micro Milling with Supporting Material Method,‡*Procedia Manuf.*, vol. 1, pp. 501• 511, 2015.

[31] R. Lekkala, V. Bajpai, R. K. Singh, and S. S. Joshi, †Characterization and modeling of burr formation in micro-end milling,‡*Precis. Eng.*, vol. 35, no. 4, pp. 625• 637, Oct. 2011.

[32] G. Kiswanto, D. L. L. Zariatin, and T. J. J. Ko, †The effect of spindle speed, feed-rate and machining time to the surface roughness and burr formation of Aluminum Alloy 1100 in micro-milling operation,‡ *J. Manuf. Process.*, vol. 16, no. 4, pp. 435• 450, Jun. 2014.

[33] K. Lee and D. a. Dornfeld, †Micro-burr formation and minimization through process control,‡ *Precis. Eng.*, vol. 29, no. 2, pp. 246• 252, 2005.

[34] L. K. Gillespie, B. J. Neal, and R. K. Albright, †Burrs produced by end milling,‡ 1976.

[35] M. Hashimura, J. Hassamontr, and D. A. Dornfeld, †Effect of In-Plane Exit Angle and Rake Angles on Burr Height and Thickness in Face Milling Operation,‡ *J. Manuf. Sci. Eng.*, vol. 121, no. 1, p. 13, 1999.

[36] H. Wang, S. To, C. Y. Chan, C. F. Cheung, and W. B. Lee, †A study of regularly spaced shear bands and morphology of serrated chip formation in microcutting process,‡ *Scr. Mater.*, vol. 63, no. 2, pp. 227• 230, Jul. 2010.

[37] H. Wang, S. To, C. Y. Chan, C. F. Cheung, and W. B. Lee, †Elastic strain induced shear bands in the microcutting process,‡ *Int. J. Mach. Tools Manuf.*, vol. 50, no. 1, pp. 9• 18, Jan. 2010.

[38] A. Bordin, S. Bruschi, A. Ghiotti, F. Bucciotti, and L. Facchini, †Comparison between wrought and EBM Ti6Al4V machinability characteristics,‡ *Key Eng. Mater.*, vol. 611• 612, pp. 1186• 1193, 2014.

[39] S. I. Jaffery and P. T. Mativenga, †Assessment of the machinability of Ti-6Al-4V alloy using the wear map approach,‡ *Int. J. Adv. Manuf. Technol.*, vol. 40, no. 7• 8, pp. 687• 696, Feb. 2009.

[40] L. E. E. Murr, E. V. V. Esquivel, S. a. A. Quinones, S. M. M. Gaytan, M. I. I. Lopez, E. Y. Y. Martinez, F. Medina, D. H. H. Hernandez, E. Y. Y. Martinez, J. L. L. Martinez, S. W. W. Stafford, D. K. K. Brown, T. Hoppe, W. Meyers, U. Lindhe, and R. B. B. Wicker, †Microstructures and mechanical properties of electron beam-rapid manufactured Ti• 6Al• 4V biomedical prototypes compared to wrought Ti• 6Al• 4V,‡ *Mater. Charact.*, vol. 60, no. 2, pp. 96• 105, Feb. 2009.

[41] L. Facchini, E. Magalini, P. Robotti, and A. Molinari, †Microstructure and mechanical properties of Ti-6Al-4V produced by electron beam melting of pre-alloyed powders,‡ *Rapid Prototyp. J.*, vol. 15, no. 3, pp. 171• 178, 2009.

[42] J. Parthasarathy, B. Starly, S. Raman, and A. Christensen, †Mechanical evaluation of porous titanium (Ti6Al4V) structures with electron beam melting (EBM).,‡ *J. Mech. Behav. Biomed. Mater.*, vol. 3, no. 3, pp. 249• 59, Apr. 2010.

[43] Arcam, †Ti6Al4V Titanium Alloy,‡ 2014. [Online]. Available: http://www.arcam.com/technology/electron-beam-melting/materials/. [Accessed: 07-May-2015].

[44] L. L. Facchini, †Microstructure and mechanical properties of biomedical alloys produced by Rapid Manufacturing techniques,‡ Univeristy of Trento, Italy, 2010.

[45] L. Facchini, E. Magalini, P. Robotti, A. Molinari, S. H•ges, and K. Wissenbach, †Ductility of a Ti-6Al-4V alloy produced by selective laser melting of prealloyed powders,‡ *Rapid Prototyp. J.*, vol. 16, no. 6, pp. 450• 459, 2010.

[46] L. S. Bertol, W. K. J–nior, F. P. Da Silva, and C. Aumund-Kopp,

†Medical design: Direct metal laser sintering of Ti• 6Al• 4V,‡ *Mater. Des.*, vol. 31, no. 8, pp. 3982• 3988, Sep. 2010.

[47] P. Bartolo, J.-P. P. Kruth, J. Silva, G. Levy, A. Malshe, K. Rajurkar, M. Mitsuishi, J. Ciurana, and M. Leu, †Biomedical production of implants by additive electro-chemical and physical processes,‡ *CIRP Ann. - Manuf. Technol.*, vol. 61, no. 2, pp. 635• 655, Jan. 2012.

[48] M. Niinomi, †Mechanical properties of biomedical titanium alloys,‡ *Mater. Sci. Eng. A*, vol. 243, no. 1• 2, pp. 231• 236, Mar. 1998.

[49] M. Yan and P. Yu, †An Overview of Densification, Microstructure and Mechanical Property of Additively Manufactured Ti-6Al-4V ‰ Comparison among Selective Laser Melting, Electron Beam Melting, Laser Metal Deposition and Selective Laser Sintering, and with Conventional Powder,‡ in *Sintering Techniques of Materials*, Arunachalam Lakshmanan, Ed. InTech, 2015, p. 198.

[50] L. E. Murr, S. A. Quinones, S. M. Gaytan, M. I. Lopez, A. Rodela, E. Y. Martinez, D. H. Hernandez, E. Y. Martinez, F. Medina, and R. B. Wicker, †Microstructure and mechanical behavior of Ti-6Al-4V produced by rapid-layer manufacturing, for biomedical applications.,‡ *J. Mech. Behav. Biomed. Mater.*, vol. 2, no. 1, pp. 20• 32, Jan. 2009.

[51] P. A. Kobryn and S. L. Semiatin, †The laser additive manufacture of Ti-6Al-4V,‡ *JOM*, vol. 53, no. 9, pp. 40• 42, 2001.

[52] E. C. Santos, M. Shiomi, K. Osakada, and T. Laoui, †Rapid manufacturing of metal components by laser forming,‡ *Int. J. Mach. Tools Manuf.*, vol. 46, no. 12• 13, pp. 1459• 1468, 2006.

[53] S. Tammas-Williams, H. Zhao, F. L—onard, F. Derguti, I. Todd, and P. B. B. Prangnell, †XCT analysis of the influence of melt strategies on defect population in Ti-6Al-4V components manufactured by Selective Electron Beam Melting,‡ *Mater. Charact.*, vol. 102, pp. 47• 61, 2015.

[54] D. a Hollander, M. von Walter, T. Wirtz, R. Sellei, B. Schmidt-Rohlfing, O. Paar, and H.-J. Erli, †Structural, mechanical and in vitro characterization of individually structured Ti-6Al-4V produced by direct laser forming.,‡ *Biomaterials*, vol. 27, no. 7, pp. 955• 63, Mar. 2006.

[55] A. N. Kalinyuk, N. P. Trigub, V. N. Zamkov, O. M. Ivasishin, P. E. Markovsky, R. V. Teliovich, and S. L. Semiatin, †Microstructure, texture, and mehanical properties of electron-beam melted Ti-6Al-4V,‡ *Mater. Sci. Eng. A*, vol. 346, no. 1• 2, pp. 178• 188, 2003.

[56] S. S. Al-Bermani, M. L. Blackmore, W. Zhang, and I. Todd, †The Origin of Microstructural Diversity, Texture, and Mechanical Properties in Electron Beam Melted Ti-6Al-4V,‡ *Metall. Mater. Trans. A*, vol. 41, no. 13, pp. 3422• 3434, Aug. 2010.

[57] L. E. Murr, S. M. Gaytan, A. Ceylan, E. Martinez, J. L. Martinez, D. H. Hernandez, B. I. Machado, D. a. Ramirez, F. Medina, S. Collins, and R. B. Wicker, †Characterization of titanium aluminide alloy components fabricated by additive manufacturing using electron beam melting,‡ *Acta Mater.*, vol. 58, no. 5, pp. 1887• 1894, Mar. 2010.

[58] O. L. a. Harrysson, O. Cansizoglu, D. J. Marcellin-Little, D. R. Cormier, and H. a. West, †Direct metal fabrication of titanium implants with tailored materials and mechanical properties using electron beam melting technology,‡ *Mater. Sci. Eng. C*, vol. 28, no. 3, pp. 366• 373, Apr. 2008.

[59] Kyocera, †Technical info.‡ [Online]. Available: http://kyoceraprecisiontools.com/micro/speeds-feeds/metric-carbide-micro-end-mills.html.

[60] D. W. Kim, Y. S. Lee, M. S. Park, and C. N. Chu, †Tool life improvement by peck drilling and thrust force monitoring during deep-micro-hole drilling of steel,‡ *Int. J. Mach. Tools Manuf.*, vol. 49, no. 3• 4, pp. 246• 255, 2009.

[61] D. a. Lucca, K. Herrmann, and M. J. Klopfstein, †Nanoindentation: Measuring methods and applications,‡ *CIRP Ann. - Manuf. Technol.*, vol. 59, no. 2, pp. 803• 819, 2010.

[62] K. Yang, Y. C. Liang, K. N. Zheng, Q. S. Bai, and W. Q. Chen, †Tool edge radius effect on cutting temperature in micro-end-milling process,‡ *Int. J. Adv. Manuf. Technol.*, vol. 52, no. 9• 12, pp. 905• 912, Jun. 2010.

7 ANNEXES

International journal publications:

Bruschi S, Tristo G, Rysava Z, Bariani P.F., Umbrello D, De Chiffre L (2016). Environmentally clean micromilling of electron beam melted Ti6Al4V. JOURNAL OF CLEANER PRODUCTION, vol. 133, p. 932-941, ISSN: 0959-6526, doi: 10.1016/j.jclepro.2016.06.035

International conferences publications:

Rysava Z, Tristo G, Bruschi S (2014). INVESTIGATION ON MICROMILLING OF EBM TI6AL4V TITANIUM ALLOY. In: Proceedings of the 11th International Conference on High Speed Machining . HSM2014-14033, PRAGUE:CVUT, ISBN: 978-80-904077-7-0, Prague, Czech republic, 11-12/09/2014

Rysava Z, Tristo G, Bruschi S (2015). Process parameters optimization for micro-milling of EBM Ti6Al4V titanium alloy. In: Proceedings of the 4M/ICOMM2015 Conference. p. 162-165, SINGAPORE:RESEARCH PUBLISHING, ISBN: 978-981-09-4609-8, Milan, Italy, doi: 10.3850/978-981-09-4609-8 042

Rysava Z, Bruschi S (2015). Comparison between EBM and DMLS Ti6Al4V machinability characteristics under dry micro-milling conditions. In: Materials Science Forum. vol. 836-837, p. 177-184, Trans Tech Publications, ISBN: 978-3-03859-450-5, Nanjing, China, 18-20/10/2015, doi: doi:10.4028/www.scientific.net/MSF.836-837.177

Rysava Z, Bruschi S (2016). Process parameters optimisation in micro-milling of DMLS Ti6Al4V. In: Proceedings of 11th International Conference on Micro Manufacturing /ICOMM2016. 123, Irvine, USA, 29/03/2016

Rysava Z, Bruschi S, Carmignato S, Medeossi F, Savio E, Zanini F (2016). Micro-drilling and threading of the Ti6Al4V titanium alloy produced through Additive Manufacturing. In: Procedia CIRP. vol. 46,

p. 583-586, Chemnitz, Germany, 31/05/2016 - 02/06/2016, doi: 10.1016/j.procir.2016.04.030

Rysava Z, Bruschi S, Medeossi F, Savio E. Performances of precision drilling carried out on wrought and Additive Manufactured Ti6Al4V. Proc. 13th Int. Conf. High Speed Mach., Metz: 2016.

Journal of Cleaner Production 133 (2016) 932–941

Contents lists available at ScienceDirect

Journal of Cleaner Production

journal homepage: www.elsevier.com/locate/jclepro

Environmentally clean micromilling of electron beam melted Ti6Al4V

S. Bruschi [a], G. Tristo [a], Z. Rysava [a, *], P.F. Bariani [a], D. Umbrello [b], L. De Chiffre [c]

[a] Department of Industrial Engineering, University of Padova, Via Venezia 1, 35131, Padova, Italy
[b] Department of Mechanical, Energy and Management Engineering, University of Calabria, Via P. Bucci Edificio Cubo 46 C, 87036, Arcavacata di Rende, CS, Italy
[c] Department of Mechanical Engineering, Technical University of Denmark, Nils Koppels Allé Building 404, DK-2800, Kgs. Lyngby, Denmark

ARTICLE INFO

Article history:
Received 14 May 2015
Received in revised form
21 April 2016
Accepted 5 June 2016
Available online 7 June 2016

Keywords:
Ti6Al4V
Micro-milling
MQL
Dry
Cryogenic
Surface integrity

ABSTRACT

The paper is aimed at evaluating the performances of Minimum Quantity Lubrication (MQL), dry cutting and cryogenic cooling when applied to the micro-milling of Ti6Al4V titanium alloy samples obtained by Additive Manufacturing (AM) using the Electron Beam Melting (EBM) technology. The micro-milling tests were carried out on a high precision 5-axis micro-milling center, at varying cutting speed and feed per tooth. The performances of the different lubrication/cooling strategies were analyzed in terms of surface integrity, namely surface topography, nano-hardness and sub-surface microstructural alterations, in order to prove the impact of clean cutting conditions when applied to micro-machining of a AM titanium alloy of biomedical interest. It is shown that dry cutting assures the same performances of MQL, representing then the most suitable option to decrease the environmental impact of the machining process.

1. Introduction

The increasing ageing of population affects different aspects of the healthcare, being the surgery related to first implantation and/or replacement of implants one of the most challenging. On a global scale, the number of operations is in the order of millions every year (Murr et al., 2009). In the recent years, Additive Manufacturing (AM) technologies are increasingly being adopted in the biomedical field for the production of parts made of titanium alloys (Bartolo et al., 2012) —especially the Ti6Al4V - thanks to the chance they offer to realize complex geometrical features — even internal cavities — in just few manufacturing steps, thus reducing the manufacturing process chain, compared to the traditional process chain that generally includes forging at elevated temperature, roughing, semi-finishing, finishing, polishing and heat treatment; whereas, in the case of using AM, only semi-finishing or finishing machining steps can be needed to achieve the required quality, therefore limiting the material waste. AM technologies can also give an answer to the increasing demand of micro-sized implants and surgical instruments or parts characterized by micro-sized features, as is the case of dental implants. If, on one hand, the surfaces of an AM product favor particularly bio-characteristics, such as the osseo-integration of implants, on the other hand, semi-finishing and/or finishing machining operations may still be needed on those surfaces that have to undergo subsequent assembly. The investigation of the surface integrity of AM titanium alloys subjected to machining operations is therefore mandatory to guarantee the parts functional performances (Jawahir et al., 2011; Kaynak et al., 2014; Ulutan and Ozel, 2011). However, despite the growing interest in AM parts, scarce records can be found in literature addressing this topic (Bordin et al., 2014), only related to conventional machining processes at macro-level, still leaving the field of micro-machining of AM parts completely unexplored, whereas micro-cutting of wrought Ti6Al4V parts has been recently addressed (Özel et al., 2011).

In addition, the biomedical sector targets cleanliness issues achievable only through numerous and time-consuming cleaning steps; the avoidance of cutting fluids during the part manufacturing would limit these steps, thus reducing the cleaning procedure impact. However, the basic function of cutting fluids is to dissipate the heat generated by plastic deformation as well as friction phenomena in the cutting zone (Lawal et al., 2013; Li and Chou, 2010; Marcon et al., 2010; Sarıkaya and Güllü, 2015; Vazquez et al., 2015), which, in turn, helps in increasing the tool life, besides removing the chips from the cutting zone, improving the dimensional

* Corresponding author.
E-mail addresses: stefania.bruschi@unipd.it (S. Bruschi), gianluca.tristo@dii.unipd.it (G. Tristo), zdenka.rysava@studenti.unipd.it (Z. Rysava), paolo.bariani@unipd.it (P.F. Bariani), domenico.umbrello@unical.it (D. Umbrello), ldch@mek.dtu.dk (L. De Chiffre).

http://dx.doi.org/10.1016/j.jclepro.2016.06.035
0959-6526/

accuracy and surface quality and also limiting the burrs formation (Lawal et al., 2013; Li and Chou, 2010; Marcon et al., 2010; Sarıkaya and Güllü, 2015; Vazquez et al., 2015). On the other hand, cutting fluids represent a significant cost issue in the whole machining process, up to 17% of the total process cost (Lawal et al., 2013; Li and Chou, 2010; Vazquez et al., 2015), in addition to the costs for their disposal (Sarıkaya and Güllü, 2015). Among all the different concerns, the cutting fluids are considered the most prominent environmental issue for machining processes. Nowadays, cutting fluids have changed dramatically due to recent regulations on environment, health and safety issues, which identify some of the ingredients in cutting fluids as hazardous. In fact, the detection of a variety of illnesses and environmental hazards these ingredients cause has forced their reduced use, or even their elimination. Characteristics as biodegradability, toxicity, renewability, bioaccountability, biomagnifications have to be taken into account more and more as a consequence of the stringent environmental regulations (Debnath et al., 2014). Several researchers have carried out investigations aimed at classifying the potential hazards of the cutting fluids and their effects on the human body (Munoz and Sheng, 1995) and the toxicity levels, especially as a consequence of dermal and inhalation exposures. As an example, 80% of the operators' infections is due to the skin contact with the fluids that are irritant, allergic and can be carcinogen (skin cancer lung cancer) (Debnath et al., 2014). In general, the delivered cutting fluids delivered are oil-based, which are more responsible for significant environmental pollution and whose storage and disposal are more hazardous than aqueous-based and gas-based cutting fluids. Just in the countries of the EU some hundreds of Mt of cutting fluids are used every year and about 2/3 of this amount has to be disposed, being 85% of all the used cutting fluids mineral oils (Debnath et al., 2014). Moreover, the costs associated to the disposal of cutting fluids based on mineral oils are remarkably high as they are not biodegradable and the related post-use treatments are complicated and expensive, ranging between 2 and 4 times of their purchase cost (Debnath et al., 2014; Shokrani et al., 2012). In case of micro-milling, Minimum Quantity Lubrication (MLQ) is usually applied, in form of a mist where the cutting fluid is provided in tiny quantities, in the order of about ten-thousandth of the amount of cutting fluid in conventional flood lubrication. MLQ is generally considered to be an emission-free process thanks to the drastic reduction of cutting fluid use compared to conventional flood lubrication, nevertheless, the oil present in the MQL mist may decompose and produce pyrolysis products as a consequence of the cutting temperatures, which may cause major health concerns.

For the above listed reasons, it is of primary importance to define suitable processing routes to manufacture products using more sustainable methods and processes, which could ideally avoid or, at least, minimize the use of cutting fluids during machining, thus providing a healthy and safe working environment, but still maintaining the required process and product performance levels. Furthermore, in doing so, the cleanliness issues of the biomedical sector would be fully addressed.

However, the avoidance of cutting fluids is particularly challenging when machining titanium alloys that are recognized to be difficult-to-cut materials being their surface integrity and tool life strongly influenced by the applied lubrication conditions (Vazquez et al., 2015), which may be drastically reduced. In this context, the paper aims at investigating the performances of dry cutting and cryogenic cooling in comparison with the conventionally applied Minimum Quantity Lubrication (MQL), in case of micro-milling applied to the Ti6Al4V titanium alloy fabricated by means of Electron Beam Melting (EBM), an AM technique recently introduced in the biomedical field to produce implants of different sizes. It is worth to underline that the feasibility of adopting cryogenic cooling by using liquid nitrogen was for the first time investigated in micro-milling, on the basis of the wide literature available about cryogenic cooling in conventional machining (Kaynak et al., 2014; Umbrello et al., 2012). The performances of the different cooling and lubrication strategies were assessed and critically discussed in terms of surface integrity of the machined workpieces, namely topography characteristics, surface defects, microstructural state and mechanical properties and its sensitivity to the different lubricating conditions assessed and critically discussed, together with their environmental impact.

2. Experimental procedure

2.1. Material

The micro-milling experiments were carried out on samples of Ti6Al4V obtained by Electron Beam Melting (EBM), an AM technique capable of producing full dense parts and widely applied in the biomedical field. The microstructure of an AM metal alloy depends on the initial powder size and morphology, compaction and post thermal processing treatments (Murr et al., 2009); in particular, the typical microstructures obtained by EBM are acicular-type, characterized by fine lamellae, as a consequence of a very fast solidification and subsequent annealing due to the high working zone temperature.

In the as-built condition, the EBM Ti6Al4V samples used in this work presents a microstructure consisting of <alpha>-phase fine lamellae, with an average length less than 5 μm, organized in a basket wave morphology with 7% of bcc <beta>-phase in an hcp matrix (see Fig. 1). The acicular microstructure of the EBM Ti6Al4V induces higher tensile strength and hardness, reduced elongation at fracture, and lower fatigue limit in comparison with the wrought alloy that generally shows a globular microstructure(Facchini, 2010; Facchini et al., 2009) (see Table 1); the differences in both the microstructural characteristics and mechanical properties give the EBM alloy a different machinability behavior compared to the wrought one under conventional as well as micro-cutting conditions.

2.2. Micro-milling experiments

30 × 25 × 8 mm^3 workpieces, cut through Wire Electrical Discharge Machining (WEDM) from a cylinder of Ti6Al4V titanium alloy fabricated by EBM process, were used in the micro-milling experiments. Before machining, the top surfaces of the rectangular blocks of EBM Ti6Al4V were flattened, mechanically polished

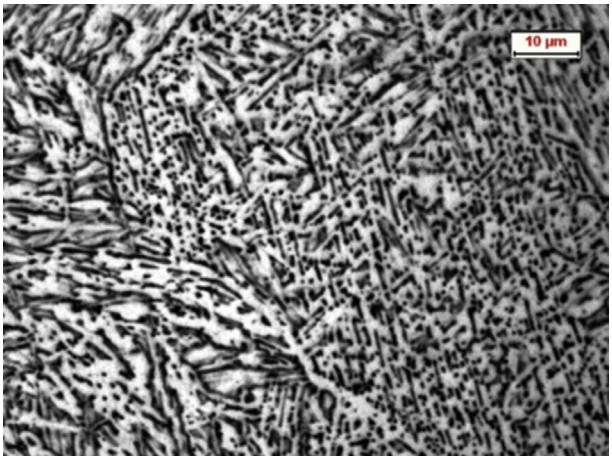

Fig. 1. Microstructure of Ti6Al4V EBM in as-built condition.

Table 1
Mechanical properties of the EBM and wrought Ti6Al4V (Arcam, n.d.).

	EBM	Wrought
Yield strength (R_p 0.2)	950 MPa	860 MPa
Ultimate tensile strength (R_m)	1020 MPa	930 MPa
Elongation	14%	>10%
Modulus of elasticity	120 GPa	114 GPa

(to remove any possibly affected material layer by the previous WEDM process) and clamped on the machine tool fixture in such a way to have the material layers growing direction parallel to the feed direction.

A Kugler™ Micromaster 5-axis ultra-precision micro-milling machine was used, equipped with an air bearing spindle suitable for micro-machining up to 180′000 rpm, and capable of an all-over positional error of 0.3 μm and a maximum linear axis speed of 6′000 mm/min. The possible thermal expansion of the machine spindle along the Z axis, which would have impact on the machining accuracy, was controlled in real time by a built-in eddy current sensor, and the related compensation was carried out using the dedicated machine software.

From the literature it is evident that the simple scaling of the machining process knowledge from the macro-to the micro-scale is not possible and is far from the real experiences (Dornfeld et al., 2006; Kuram and Ozcelik, 2013; Lai et al., 2008). Factors that at the macro-scale can be neglected may have a significant effect at the micro-scale, namely the tool edge geometry, microstructure (grain size and orientation), tool deflection, vibrations (Dornfeld et al., 2006; Kuram and Ozcelik, 2013; Lai et al., 2008; Thepsonthi and Özel, 2013, 2012). In micro-cutting, the ratio between the cutting tool edge (usually the cutting edge radius is between 1 and 5 μm (Dhanorker et al., 2007; Özel et al., 2011, 2007)) and the uncut chip thickness has to be considered in order to ensure that the shearing process prevails over the ploughing one, both characterizing the material removal in micro-cutting (Dhanorker et al., 2007; Dornfeld et al., 2006).

The scaling issue and the presence of both shearing and ploughing have indeed a great impact on the cutting forces, chip thickness and morphology, surface integrity, burr formations and tool wear (Dhanorker et al., 2007; Dornfeld et al., 2006; Thepsonthi and Özel, 2013). If only ploughing occurs, chips are not formed, leading only to material deformation and a very poor surface quality, as well as to specific cutting energy and tool wear increase (Özel et al., 2011, 2007). The switch from one cutting mechanism to the other is possible through a proper choice of the cutting conditions: when the uncut chip thickness is above the minimum chip thickness, shearing prevails over ploughing. The minimum chip thickness is mainly function of the cutting edge radius, with a secondary effect given by the workpiece material (in multiphase materials it varies as a function of the microstructural constituents (Câmara et al., 2012; Mian et al., 2010)). The ratio between the uncut chip thickness and the cutting edge radius is the critical parameter, being the uncut chip thickness proportional to the feed per tooth.

The full immersion slotting was chosen as machining strategy: in this case the instantaneous chip thickness is function of the rotation angle φ and it varies from zero at the beginning of the cutting to its maximum corresponding to the feed per tooth approximately in the middle of the slot and then decreases again to zero. When the uncut chip thickness is smaller than the minimum chip thickness, the chip is not formed, and the cutter must reach certain angle φ to create the chip (Dhanorker et al., 2007; Filiz et al., 2007; Özel et al., 2007; Thepsonthi and Özel, 2013). In each test a straight slot, 0.3 mm wide and 25 mm long, was machined. The experimental set-up is shown in the Fig. 2. The axial depth of cut was set equal to 30 μm and kept constant for the whole experimental campaign. The value of the axial depth of cut was chosen on the basis of the suggestion to use depths of the cut ten times larger than the grain size to minimize the crystallographic effect of the grains during machining (Dornfeld et al., 2006).

The cutting speed and feed per tooth were varied with two and four levels, respectively, according to a full factorial design, repeating three times each cutting condition. The values of the feeds per tooth were chosen to respect the criterion of the minimum chip thickness. The suitable range of the ratios between the uncut chip thickness and the cutting edge radius is from 0.09 to 0.4 depending on the material and cutting conditions (Afazov and Zdebski, 2013). For the multi-phase metal alloys this ratio is generally between 0.3 and 0.4, and for Ti− 6Al−4V was found to be about 0.1–0.2 (Thepsonthi and Özel, 2013). Furthermore, the combinations of cutting speed and feed per tooth were chosen in order to avoid tool vibrations that would have affected the tests outcomes. Based on the literature research and recommended cutting conditions for titanium alloys, different cutting speeds were tested, while acquiring the signal from accelerometers installed in the vertical and radial directions with respect to the spindle axis. These signals were then processed through FFT to verify the vibrations occurrence. The cutting parameters finally employed in the experimental campaign were chosen in such a way to avoid vibrations.

The experimental plan reported in Table 2 was carried out under both dry and lubricated conditions. A jet of compressed air without any cutting fluid was used during the dry experiments in order to cool down both the tool and the workpiece and clear the chips from the cutting area. Isoparafin oil in form of a mist was used as cutting fluid in a regime of Minimum Quantity Lubrication (MQL), with a consumption of 20 ml/h of oil. To prove the feasibility of the approach, the cryogenic cooling was later on applied only to those dry cutting conditions assuring the best performance in terms of surface integrity.

Liquid nitrogen LN_2 was employed to reduce the temperature of the workpiece from room temperature to cryogenic conditions at nearly −160 °C. In order to limit as much as possible the temperature variations of the tool machine components, while the specimen was reaching the cryogenic conditions, the customized fixture depicted in Fig. 3A was designed and set-up, where only the bottom surface of the workpiece is exposed to the LN_2, which is confined into a cryogenic chamber. A layer of polyurethane foam between the external panels and the cryogenic chamber provides the required insulation, limiting as much as possible temperature variations of the machine

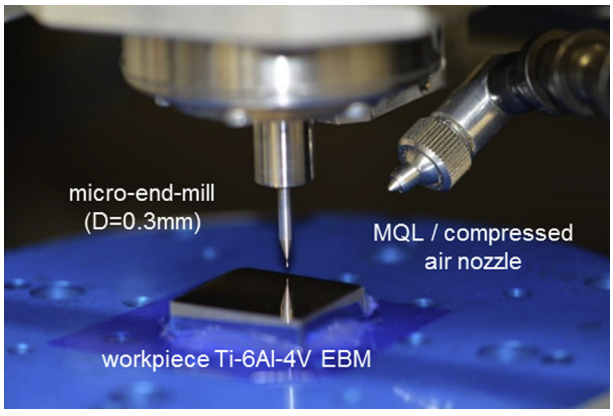

Fig. 2. Experimental set-up.

Table 2
Experimental plan.

N [rpm]	67,000				154,000			
V_c [m/min]	63				145			
f_z [μm/tooth]	0.1	0.5	1.5	3.0	0.1	0.5	1.5	3.0

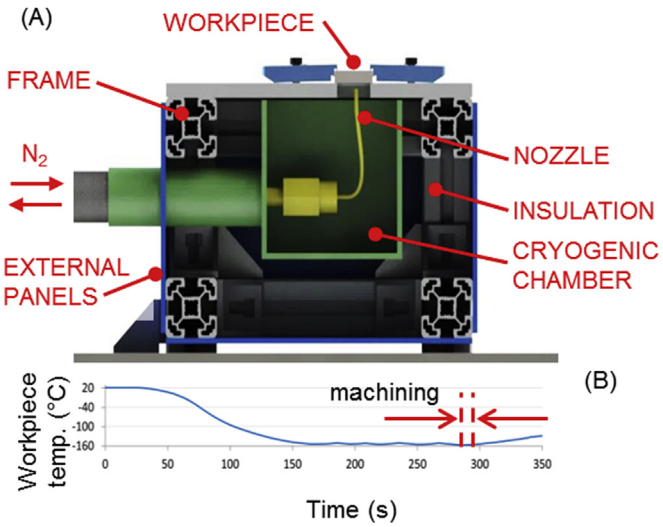

Fig. 3. Set-up of the cryogenic apparatus (A); evolution of the workpiece temperature (B).

tool components, during the time interval when the specimen is reaching the cryogenic conditions. The workpiece temperature was controlled through a J-type thermocouple, and a sample constant temperature of -155 ± 5 °C was assured during the machining phase by regulating the LN_2 flow (Fig. 3B).

Kyocera™ uncoated flat-end-square two-fluted micro-tools made of tungsten carbide with a diameter of 0.3 mm were used in the micro-milling experiments. A fresh tool was used for each cutting condition and repetition; before and after each test, the tools were inspected with a FEI™ Quanta 400 SEM to verify the cutting edges integrity and evaluate the tool state. Fig. 4 shows the cutting edge of a new tool, as received from the tool manufacturer: The edge radius of the fresh tool was measured to be about 1.1 μm, leading to a critical feed per tooth of 0.33–0.44 μm (Liu et al., 2006); therefore, for the investigated feed rate of 0.1 μm/tooth, the ploughing mechanism may prevail over shearing and its effect over surface integrity is worthwhile to be investigated.

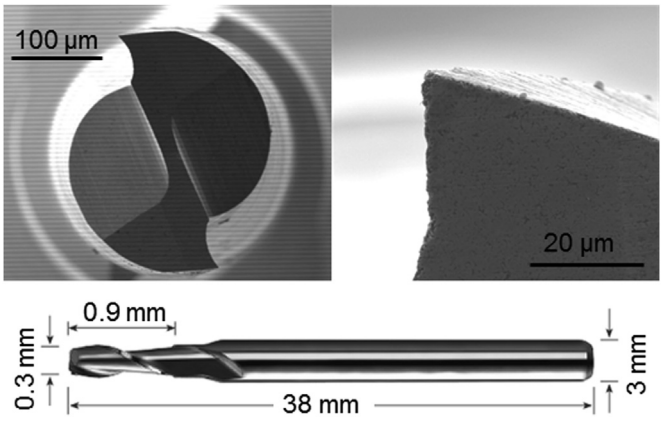

Fig. 4. SEM image of a fresh tool and its main dimensions.

2.3. Surface integrity analysis

The integrity of the machined surfaces was evaluated in terms of topography characteristics, surface defects, metallurgical state and mechanical properties. The machined workpieces were first prepared by gentle cleaning in an ultrasonic bath in order to remove residual chips particles.

The surface topography was first qualitatively assessed through SEM analysis and then sampled by using a Sensofar™ PLμ Neox confocal optical profiler at regular distances from the border of the workpiece, namely 12.5 mm. The instrument was equipped with a 100x lens characterized by a field of view of 127 × 97 μm^2 and a vertical resolution of about 5 nm. The roughness was evaluated following the ISO 25178 standard and the arithmetic mean value Ra was used to quantify the surface quality of the machined surfaces. The profile analysis was performed using cut-off values λ_c of 0.25 mm or 0.8 mm in a number of 5. To this end, respectively 21 × 1 and 51 × 1 stitched images with 25% of overlap were acquired along the bottom of the slots, close to the middle in order to avoid the entrance and exit areas. Average Ra values were calculated on the basis of 10 different profiles.

The SEM analysis of the machined surfaces permitted also to evaluate the presence and dimension of surface damages as well as the extension of the burrs.

The samples were then metallographically prepared and etched with the Kroll's reagent to analyze their metallurgical state by using both optical and scanning electron microscopy.

Finally, the mechanical properties of the micro-milled specimens were analyzed by nano-indentation tests using a Berkovic tip. Preliminary tests were performed in order to choose the appropriate load and dwell time as suggested in (Lucca et al., 2010). In particular, the load and the dwell were respectively ranged from 5 to 150 mN and from 2 up to 100 s. The values that allow achieving stable nano-hardness results and avoiding creep effect were found to be 50 mN and 10 s. The indentations were performed from the top surface toward the bulk material. Five measurements were taken for each depth, with measurement locations well-spaced to avoid interference between indentations.

3. Results and discussion

3.1. Surface topography and burrs

The roughness plots of the slots bottom surfaces as a function of the cutting parameters under dry and MQL conditions are shown in Fig. 5, and related SEM images and profiler scans are in Fig. 6. As expected, the lowest feed rate causes an evident surface damage, being the ploughing mechanism predominant over the shearing. As the feed rate increases, the surface quality becomes lower, and not acceptable for finishing cutting at the highest investigated feed rate. From the analysis of Figs. 5 and 6 it is clear that for the intermediate feed rates a comparable surface quality can be achieved under dry and MQL cutting conditions. In case of MQL the influence of the cutting speed is negligible, whereas for dry cutting the best surface finish is obtained at the lowest investigated cutting speed.

A qualitative analysis of the burrs formation was carried out through SEM inspection. Fig. 7 gives a view of the top burrs Poisson-type (da Silva et al., 2015) for intermediate feed rates and the lowest cutting speed under dry and MQL conditions. At the feed of 0.5 μm/tooth under both dry and MQL conditions, ploughing prevails on shearing and the consequent plastic deformation causes the burrs to be larger than at 1.5 μm/tooth. On the contrary, at the feed of 1.5 μm/

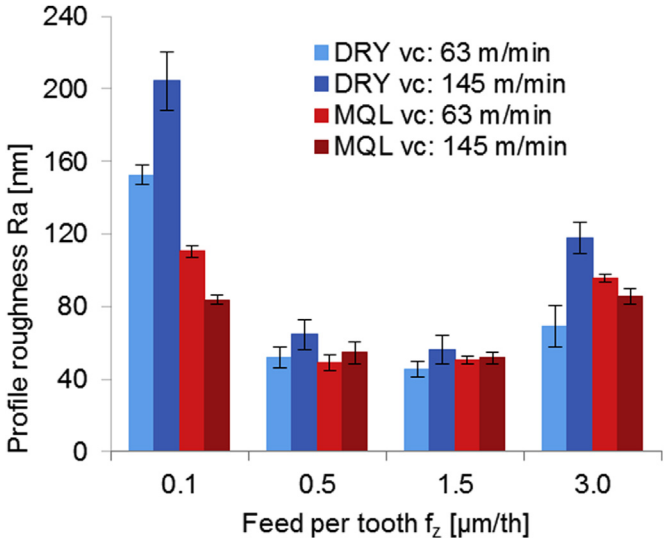

Fig. 5. Machined surface roughness as a function of the cutting parameters under dry and MQL conditions.

tooth, dry cutting provokes a slightly less amount of burrs, which are also more regularly developed, in comparison to MQL cutting. Similar phenomena were observed for the cutting speed of 145 m/min. We can also appreciate the different shape of the burrs as a function of the machining strategy, namely down-milling or up-milling. When down-milling is applied, the burrs result to be thinner, thus ensuring their easier removal after cutting (Piquard et al., 2014).

3.2. Microstructural alterations

Fig. 8A shows the optical image (acquired through a Leica microscope at magnification of 200x) of the microstructure of the slot cross-section in case of dry condition, when using a cutting speed of 63 m/min and a feed of 1.5 μm/tooth. No microstructural alterations in terms of phase transformation and dynamic recrystallization can be appreciated, meaning that even without any cutting fluid the temperature rise due to cutting is not high enough to provoke a change in the material microstructural state. A closer examination of the slot sidewall microstructure by SEM analysis (Fig. 8B) reveals the presence of bent lamellae to an average depth of 5 μm, but without any kind of damaging induced by the cutting process, whereas this kind of distortion is not present at the slot bottom surface.

3.3. Nano-hardness

The hardness of the samples after EBM was 4.34 ± 0.43 GPa. In the micro-milled samples, a 15–20 μm sub-surface layer of high hardness was observed, with a peak value of 6.5 GPa. Fig. 9A shows the force-penetration depth curves for the samples processed through dry machining at different cutting speeds and fixed feed per tooth compared with the one of the as-received sample. The maximum penetration depth decreases when the cutting speed increases, and the slope of the unloading curve increases. This can be attributed to the presence of lamellae that are bent by plastic deformation. In dry cutting (Fig. 9B), the hardness increases up to 6.5 GPa in the zone close to the machined surface for the highest cutting speed and feed per tooth, and decreases when the feed per tooth decreases. Similar results were observed for surfaces machined under MQL condition, but with slightly lower hardness values (Fig. 10). This difference between dry and MQL conditions is more evident at the highest cutting speed as shown in Fig. 10B.

3.4. Surface defects

The surface defects found at the bottom of slots after machining experiments are similar regardless the lubrication condition,

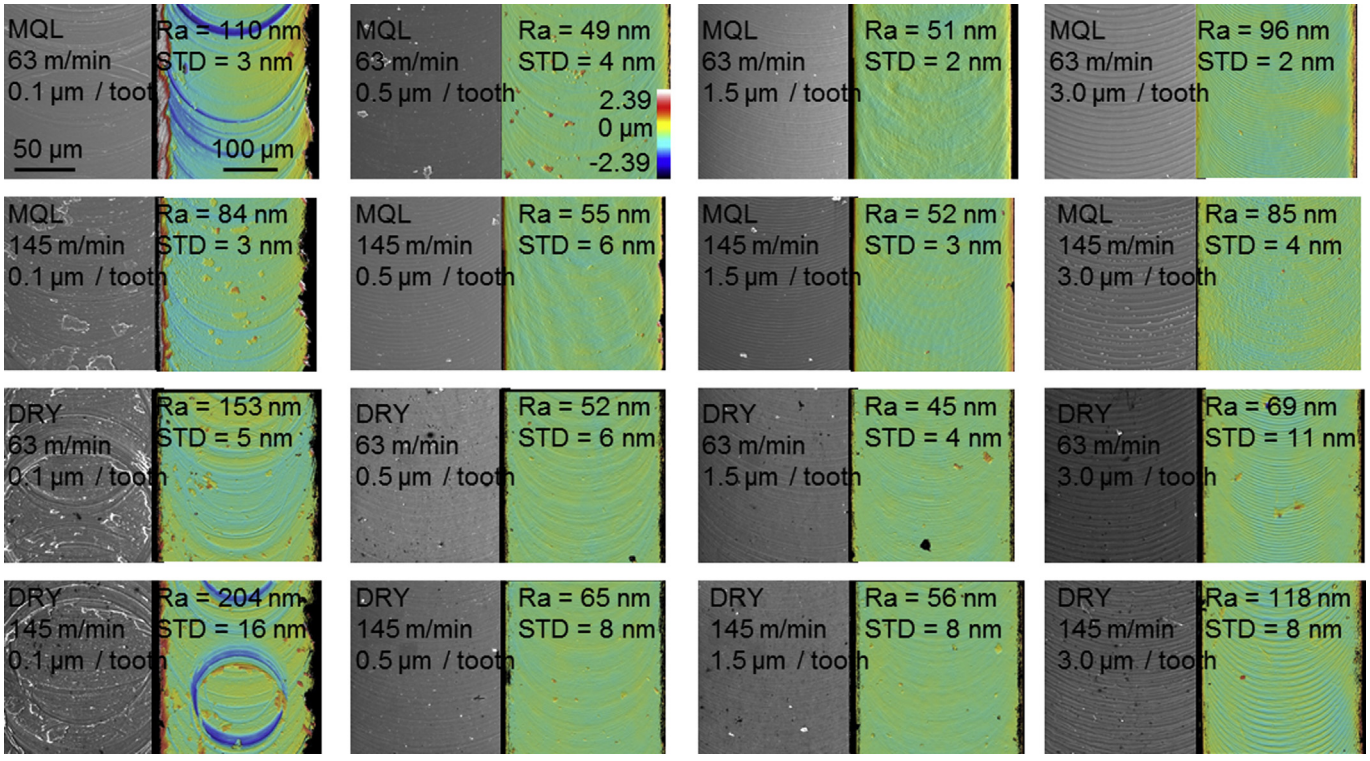

Fig. 6. Topographies of the slots bottom surfaces at varying cutting parameters under dry and MQL conditions (SEM images and optical profiler scans).

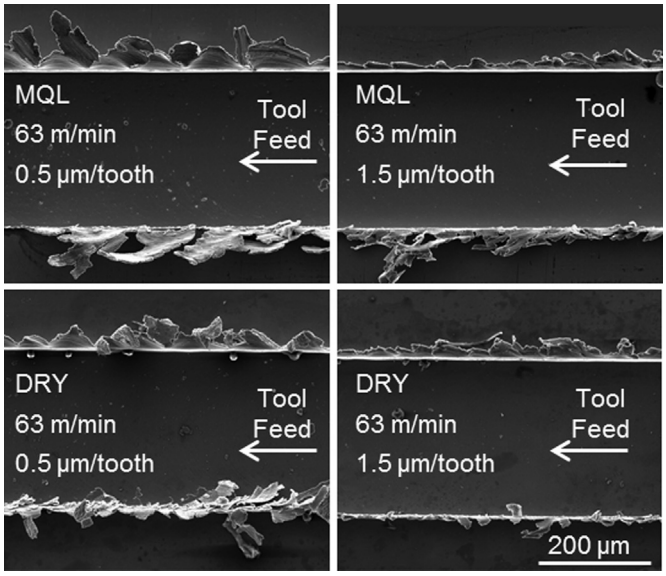

Fig. 7. View of the top burrs (dry and MQL, $V_c = 63$ m/min).

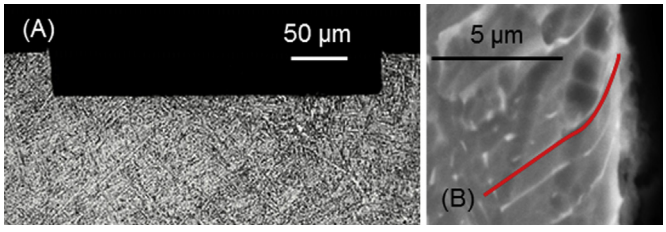

Fig. 8. Microstructure of the slot cross-section (A), and SEM detail of the slot sidewall sub-surface (B) (dry, $v_c = 63$ m/min, $f_z = 1.5$ μm/tooth).

namely dry or MQL. For the lowest feed per tooth a high amount of surface defects is present, being the whole surface affected by their presence as a consequence of the ploughing mechanism that prevails at the lowest feed per tooth. On the contrary, a minimal amount of surface defects can be appreciated for the feeds per tooth of 0.5 and 1.5 μm/tooth, which are only characterized by the presence of some chip debris. When the feed per tooth is increased to 3.0 μm the defects are more evident, as the presence of smeared material is evident. The surface defects at varying cutting parameters are shown in Fig. 11 and Fig. 12 in case of dry and MQL conditions, respectively.

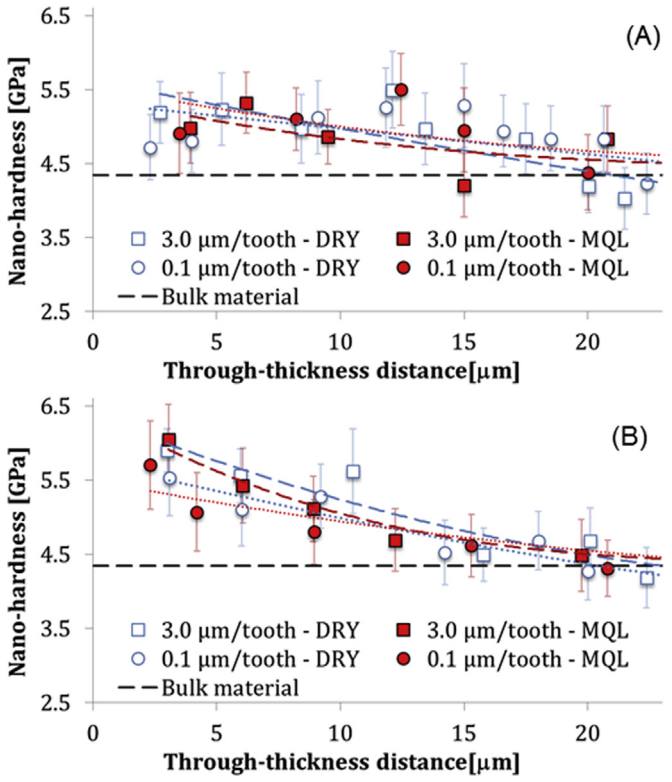

Fig. 10. Nano-hardness profiles through thickness distance for samples dry and MQL machined at (A) 63, and (B) 145 m/min.

3.5. Tool analysis

As previously underlined, each tool was inspected through SEM before as well as after the machining process, to evaluate the state of the tool as a consequence of the cutting process and lubrication conditions. In the Fig. 13, it can be seen that, regardless the lubrication condition, there are some workpiece material adhered on the tool cutting edge. The EDS analysis proved the origin of the material presented on the cutting edge: Fig. 14 clearly demonstrates that the adhered material is titanium from the machined workpiece.

3.6. Cryogenic cooling

The micro-milling tests under cryogenic cooling were carried out at those cutting parameters assuring the best performance in

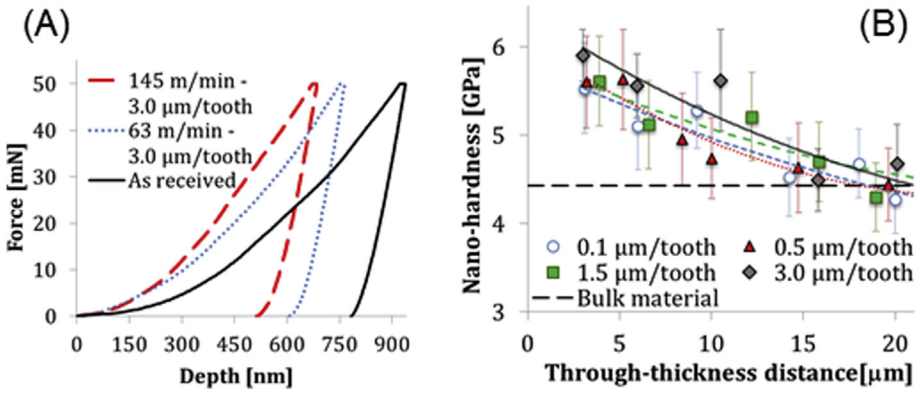

Fig. 9. Force vs. penetration depth curves for Berkovich indentations (A); nano-hardness of samples dry micro-milled at 145 m/min (B).

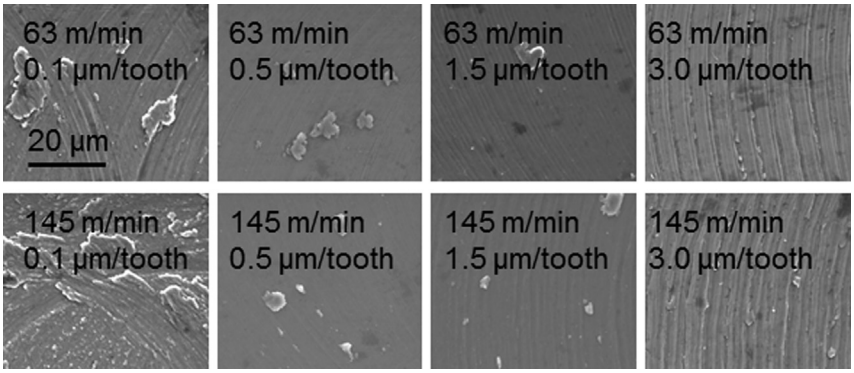

Fig. 11. Surface defects in the case of dry cutting condition at varying cutting parameters.

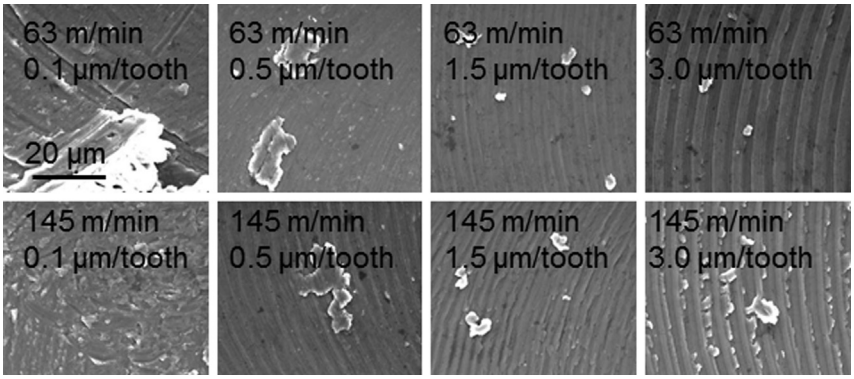

Fig. 12. Surface defects in the case of MQL lubrication condition at varying cutting parameters.

dry cutting, namely cutting speed of 63 m/min and feed rate of 1.5 μm/tooth. Fig. 15 shows the topography of the slot bottom surface machined under cryogenic cooling. In the same figure, the roughness profiles of the different cooling/lubrication conditions are compared. The surface quality for cryogenic cooling is comparable to that obtained for dry cutting and MQL. However, a slight increase of the surface roughness is evident, with a more perturbed roughness profile of higher amplitude. This can be ascribable to a larger amount of smeared material on the machined surface of the cryogenic sample, as confirmed by the SEM observations (see Fig. 16A). It is worth to note the fact that this phenomenon observed in micro-machining is not in agreement with what observed in cryogenic conventional machining (Bordin et al., 2014). In Figs. 16B and 17 the SEM image of the tool after cryogenic cutting is shown: as for the other lubrication conditions, workpiece material adhesion is evident, without any sign of damaging.

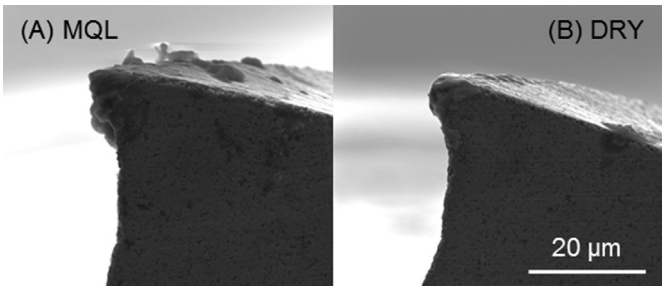

Fig. 13. SEM pictures the cutting edge state after machining at v_c = 63 m/min and f_z = 1.5 um/tooth.

The analysis of the burrs under cryogenic cooling (Fig. 18A) evidences an improvement compared to dry cutting, with the presence of more uniform and less jagged burrs on both sides of the slot. As shown in Fig. 18B, the nano-hardness measured in cryogenic cooling is very close to that for dry cutting, being the microstructure in both cases very similar.

4. Conclusions

The performances of Minimum Quantity Lubrication (MQL), dry cutting and cryogenic cooling were evaluated when micro-milling samples of Ti6Al4V obtained by the Additive Manufacturing Technology named Electron Beam Melting. The main findings can be summarized as follows:

- at intermediate feed rates the surface integrity characteristics of the machined samples are comparable under dry cutting and MQL;
- under cryogenic cooling conditions, the surface integrity improves, especially in terms of presence and quality of burrs, but with a slight worsening of the surface topography and increase of the surface defects;
- no alteration of the microstructure of the Ti6Al4V processed by EBM was observed for all the investigated cutting conditions.

The effect of the lubricating/cooling conditions seems less significant in micro-milling compared to the machining operations carried out at macro-scale: this can be ascribed to the fact that both the forces and the temperatures arising during micro-machining are much lower compared to conventional machining, making the effect of the cutting fluid less relevant (Yang et al., 2010).

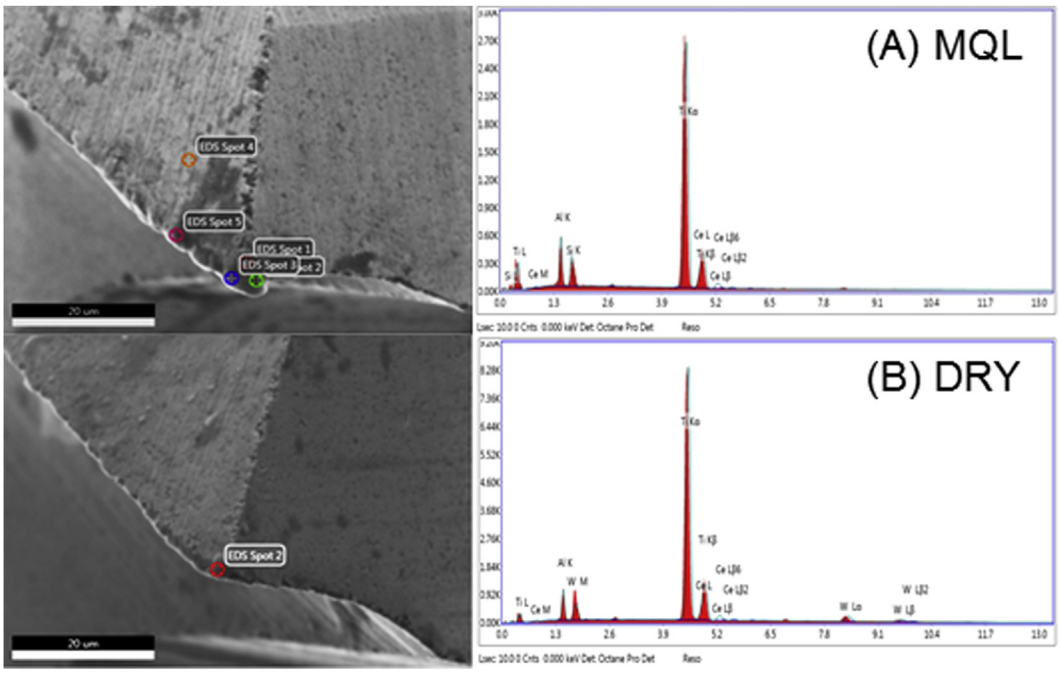

Fig. 14. Example of the EDS analysis of tools after machining under MQL and DRY lubrication condition (v_c = 63 m/min and fz = 1.5 µm/th).

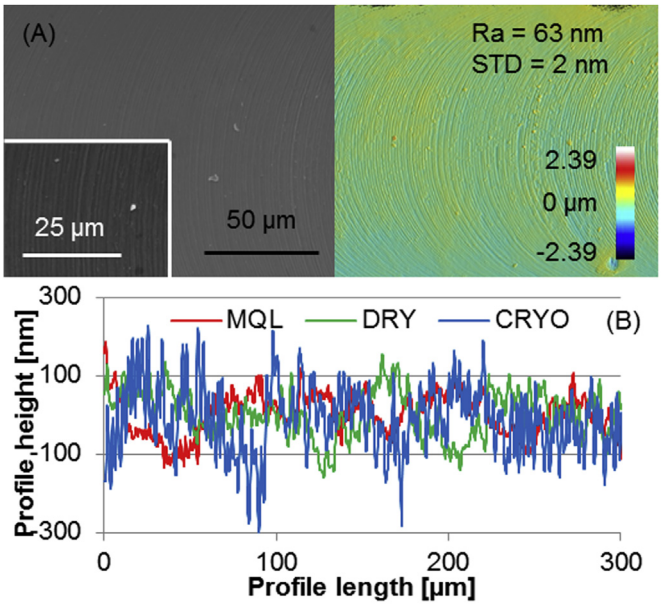

Fig. 15. Bottom surface of the slot machined under cryogenic condition (v_c = 63 m/min, f_z = 1.5 µm/tooth) (A); roughness profiles at varying lubrication conditions (B).

The presented results clearly show that dry cutting assures a surface quality comparable to that obtained when MQL is used in micro-milling Ti6Al4V samples produced by EBM. On the other hand, the use of the cryogenic cooling does not improve to a significant extent the performances of the machining operations, which can justify its use. Furthermore, cryogenic cooling requires high investment costs, transportation of the liquid nitrogen and, above all, the liquid nitrogen production is quite an energy-intensive process, which increase the overall carbon footprint of cryogenic cooling. In the case of MQL, the cutting fluid consumption in the micro-milling center devoted to the present experimental campaign is in the order of 20 ml/h, meaning an approximate

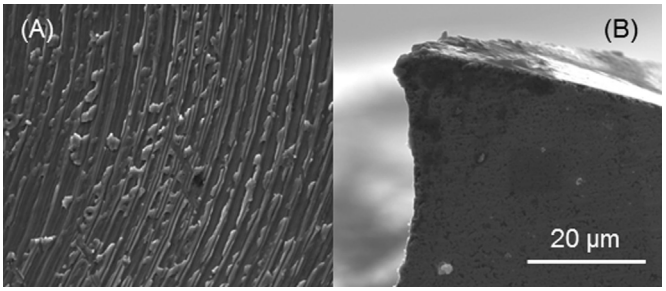

Fig. 16. Bottom surface defects (A) and tool state (B) after machining at cryogenic condition (v_c = 63 m/min, f_z = 1.5 µm/tooth).

consume of 40.3 l/year (considering 8 working hours/day, 21working days/month, 12 months), which can be fully saved in case of dry cutting, as well as its associated carbon foot print and energy necessary to produce, use and transport it. The employed MQL system uses paraffin oil as cutting fluid mixed with compressed air that is used also in dry cutting to cool down the interface between workpiece and tool and clear the chips from the cutting area. Therefore, being in the employed system the difference between MQL and dry cutting the sole use of the paraffin oil, the CO_2 and energy consumption related to its use must be considered more in detail.

Paraffin oil is a mineral oil that consists of saturated hydrocarbons - alkanes and is produced through a refining process of the crude oil carried out in industrial sites characterized by very significant consumptions of energy and water as well as production of wastes and emissions (Barthe et al., 2015).

The 2014 data report of the International Association of Oil & Gas Producers (IOGP) (International Association of Oil&Gas Producers, 2015) states that the quantities of emissions generated in the production (exploration, production and processing operations) of 1 kg of hydrocarbon include 134 g of carbon dioxide (CO_2), which means 5.4 kg of CO_2 emissions for producing the average quantity of paraffin oil needed to run the micro-milling process for 1 year. The

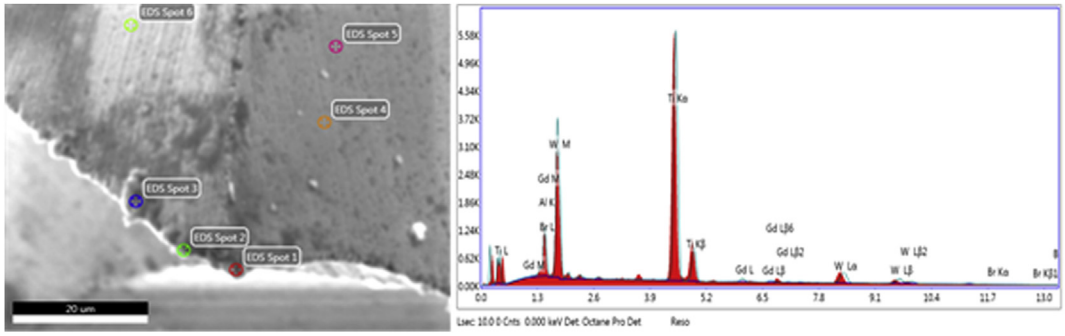

Fig. 17. Example of the EDS analysis of tools after machining under cryogenic lubrication condition (v_c = 63 m/min and fz = 1.5 μm/th).

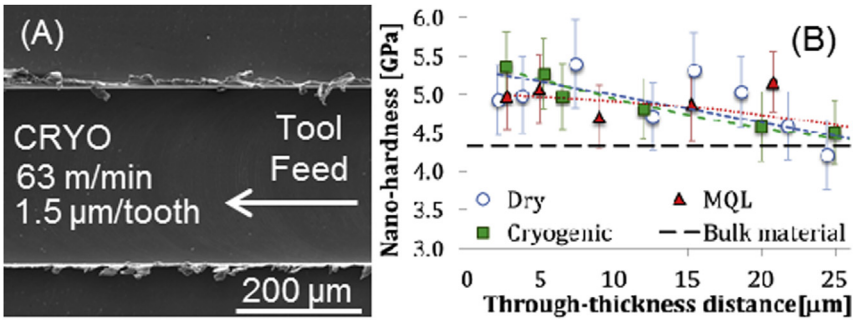

Fig. 18. View of the top burrs under cryogenic cooling (A); nano-hardness profile through thickness distance at varying lubrication condition (B) (V_c = 63 m/min, f_z = 1.5 μm/tooth).

same report (International Association of Oil&Gas Producers, 2015) states that 1.4 MJ are needed to produce 1 kg of hydrocarbon, which means approximately 56.5 MJ of energy consumption per year in the investigated case. Furthermore, additional CO_2 emissions and energy consumption derive from the paraffin oil transportation from the production site to the machining shop floor: from the 2011 data of an EU report (EEA, 2012), which states that approximately 80 g of CO_2 are emitted to the environment for the transport of 1 t of goods for 1 km distance,assuming an average distance of transportation of 60 km, approximately 194 g of CO_2 emissions per year due to the paraffin oil transportation will be avoided.

It is worth to underline that the use of dry cutting could increase the energy consumption, since the cutting forces may increase due an increase of the friction coefficient; nevertheless, additional cutting tests making use of a dynamometer for the forces measurements are necessary.

Safety data sheets (SIGMA-ALDRICH, 2014) indicates the paraffin oil as a not hazardous substance, thus not requiring any special means of transportation and handling. Regarding the carcinogenicity, the paraffin oil belongs to the Group 1 – IARC: Carcinogenic to humans, implying that its disposal must be accomplished by a licensed company. However, in MQL systems implemented in micro-machining centres, the cutting fluid is not recovered, and the produced aerosol goes directly into the environment. Even if the amount of oil is very low, some particles are spread in the air, which, being inhaled, can led to lipid pneumonia (SIGMA-ALDRICH, 2014).

From the above reported considerations, dry cutting represents the most suitable option to decrease the environmental impact of micro-machining applied to biomedical components, as no cutting fluids are used, with the consequent elimination of the related health hazards, as well as the components cleaning steps after machining can be significantly reduced, thus not only lowering the overall production costs but also the environmental impact of the whole process chain.

Future works will include the measurements of the cutting forces and temperatures in order to provide an analytical model of the process under the different lubricating/cooling conditions, as well as a comprehensive economic analysis of the process that will take into account the added costs that may eventually arise in case of a reduced tool life when dry cutting is applied.

References

International Association of Oil&Gas Producers, 2015. Environmental Performance Indicators – 2014 Data.

Afazov, S.M., Zdebski, D., 2013. Effects of micro-milling conditions on the cutting forces and process stability. J. Mater. Process. Technol. 213, 671–684. http://dx.doi.org/10.1016/j.jmatprotec.2012.12.001.

Arcam n.d. Ti6Al4V Titanium Alloy [WWW Document]. URL http://www.arcam.com/technology/electron-beam-melting/materials/(accessed 5.7.15).

Barthe, P., Chaugny, M., Roudier, S., Sancho, L.D., 2015. Best Available Techniques (BAT) Reference Document for the Refining of Mineral Oil and Gas. http://dx.doi.org/10.2791/010758.

Bartolo, P., Kruth, J.-P., Silva, J., Levy, G., Malshe, A., Rajurkar, K., Mitsuishi, M., Ciurana, J., Leu, M., 2012. Biomedical production of implants by additive electro-chemical and physical processes. CIRP Ann. Manuf. Technol. 61, 635–655. http://dx.doi.org/10.1016/j.cirp.2012.05.005.

Bordin, A., Bruschi, S., Ghiotti, A., Bucciotti, F., Facchini, L., 2014. Comparison between wrought and EBM Ti6Al4V machinability characteristics. Key Eng. Mater. 611–612, 1186–1193. http://dx.doi.org/10.4028/www.scientific.net/KEM.611-612.1186.

Câmara, M. a., Rubio, J., Abrão, A.M., Davim, J.P., 2012. State of the art on micro-milling of materials, a review. J. Mater. Sci. Technol. 28, 673–685. http://dx.doi.org/10.1016/S1005-0302(12)60115-7.

da Silva, L.C., da Mota, P.R., da Silva, M.B., Ezugwu, E.O., Machado, Á.R., 2015. Study of burr behavior in face milling of PH 13-8 Mo stainless steel. CIRP J. Manuf. Sci. Technol. 8, 34–42. http://dx.doi.org/10.1016/j.cirpj.2014.10.003.

Debnath, S., Reddy, M.M., Yi, Q.S., 2014. Environmental friendly cutting fluids and cooling techniques in machining: a review. J. Clean. Prod. 83, 33–47. http://dx.doi.org/10.1016/j.jclepro.2014.07.071.

Dhanorker, A., Liu, X., Özel, T., 2007. Micromilling process planning and modeling for micromold manufacturing. ASME 2007 Int. Manuf. Sci. Eng. Conf. 759–769. http://dx.doi.org/10.1115/MSEC2007-31070.

Dornfeld, D., Min, S., Takeuchi, Y., 2006. Recent advances in mechanical micro-machining. CIRP Ann. Manuf. Technol. 55, 745–768. http://dx.doi.org/10.1016/j.cirp.2006.10.006.

EEA, 2012. Specific CO2 emissions per tonne-km and per mode of transport in

Europe, 1995-2011 [WWW Document]. Eur. Environ. Agency Maps graphs. URL. http://www.eea.europa.eu/data-and-maps/figures/specific-co2-emissions-per-tonne-2.
Facchini, L., 2010. Microstructure and Mechanical Properties of Biomedical Alloys Produced by Rapid Manufacturing Techniques. Univeristy of Trento, Italy.
Facchini, L., Magalini, E., Robotti, P., Molinari, A., 2009. Microstructure and mechanical properties of Ti-6Al-4V produced by electron beam melting of pre-alloyed powders. Rapid Prototyp. J. 15, 171–178. http://dx.doi.org/10.1108/13552540910960262.
Filiz, S., Conley, C.M., Wasserman, M.B., Ozdoganlar, O.B., 2007. An experimental investigation of micro-machinability of copper 101 using tungsten carbide micro-endmills. Int. J. Mach. Tools Manuf. 47, 1088–1100. http://dx.doi.org/10.1016/j.ijmachtools.2006.09.024.
Jawahir, I.S., Brinksmeier, E., M'Saoubi, R., Aspinwall, D.K., Outeiro, J.C., Meyer, D., Umbrello, D., Jayal, a. D., 2011. Surface integrity in material removal processes: recent advances. CIRP Ann. Manuf. Technol. 60, 603–626. http://dx.doi.org/10.1016/j.cirp.2011.05.002.
Kaynak, Y., Lu, T., Jawahir, I.S., 2014. Cryogenic machining-induced surface integrity: a review and comparison with dry, MQL, and flood-cooled machining. Mach. Sci. Technol. 18, 149–198. http://dx.doi.org/10.1080/10910344.2014.897836.
Kuram, E., Ozcelik, B., 2013. Multi-objective optimization using Taguchi based grey relational analysis for micro-milling of Al 7075 material with ball nose end mill. Measurement 46, 1849–1864. http://dx.doi.org/10.1016/j.measurement.2013.02.002.
Lai, X., Li, H., Li, C., Lin, Z., Ni, J., 2008. Modelling and analysis of micro scale milling considering size effect, micro cutter edge radius and minimum chip thickness. Int. J. Mach. Tools Manuf. 48, 1–14. http://dx.doi.org/10.1016/j.ijmachtools.2007.08.011.
Lawal, S.A., Choudhury, I.A., Nukman, Y., 2013. A critical assessment of lubrication techniques in machining processes: a case for minimum quantity lubrication using vegetable oil-based lubricant. J. Clean. Prod. 41, 210–221. http://dx.doi.org/10.1016/j.jclepro.2012.10.016.
Li, K.M., Chou, S.Y., 2010. Experimental evaluation of minimum quantity lubrication in near micro-milling. J. Mater. Process. Technol. 210, 2163–2170. http://dx.doi.org/10.1016/j.jmatprotec.2010.07.031.
Liu, X., DeVor, R.E., Kapoor, S.G., 2006. An analytical model for the prediction of minimum chip thickness in micromachining. J. Manuf. Sci. Eng. 128, 474. http://dx.doi.org/10.1115/1.2162905.
Lucca, D. a., Herrmann, K., Klopfstein, M.J., 2010. Nanoindentation: measuring methods and applications. CIRP Ann. Manuf. Technol. 59, 803–819. http://dx.doi.org/10.1016/j.cirp.2010.05.009.
Marcon, a., Melkote, S., Kalaitzidou, K., Debra, D., 2010. An experimental evaluation of graphite nanoplatelet based lubricant in micro-milling. CIRP Ann. Manuf. Technol. 59, 141–144. http://dx.doi.org/10.1016/j.cirp.2010.03.083.
Mian, A.J., Driver, N., Mativenga, P.T., 2010. A comparative study of material phase effects on micro-machinability of multiphase materials. Int. J. Adv. Manuf. Technol. 50, 163–174. http://dx.doi.org/10.1007/s00170-009-2506-9.
Munoz, A., Sheng, P., 1995. Analytical approach for determining the environmental impact of machining processes. J. Mater. Process. Technol. 53, 736–758.
Murr, L.E., Esquivel, E.V., Quinones, S. a., Gaytan, S.M., Lopez, M.I., Martinez, E.Y., Medina, F., Hernandez, D.H., Martinez, E., Martinez, J.L., Stafford, S.W., Brown, D.K., Hoppe, T., Meyers, W., Lindhe, U., Wicker, R.B., 2009. Microstructures and mechanical properties of electron beam-rapid manufactured Ti–6Al–4V biomedical prototypes compared to wrought Ti–6Al–4V. Mater. Charact. 60, 96–105. http://dx.doi.org/10.1016/j.matchar.2008.07.006.
Özel, T., Liu, X., Dhanorker, A., 2007. Modelling and simulation of micro-milling process. In: 4th International Conference and Exhibition on Design and Production of Machines and Dies/Molds, pp. 21–23.
Özel, T., Thepsonthi, T., Ulutan, D., Kaftanoğlu, B., 2011. Experiments and finite element simulations on micro-milling of Ti–6Al–4V alloy with uncoated and cBN coated micro-tools. CIRP Ann. Manuf. Technol. 60, 85–88. http://dx.doi.org/10.1016/j.cirp.2011.03.087.
Piquard, R., D'Acunto, A., Dudzinski, D., 2014. Study of burr formation and phase transformation during micro-milling of NiTi alloys. In: Proceedings of the 11th Internation Conference on High Speed Machining (Prague).
Sarıkaya, M., Güllü, A., 2015. Multi-response optimization of minimum quantity lubrication parameters using Taguchi-based grey relational analysis in turning of difficult-to-cut alloy Haynes 25. J. Clean. Prod. 91, 347–357. http://dx.doi.org/10.1016/j.jclepro.2014.12.020.
Shokrani, a., Dhokia, V., Newman, S.T., 2012. Environmentally conscious machining of difficult-to-machine materials with regard to cutting fluids. Int. J. Mach. Tools Manuf. 57, 83–101. http://dx.doi.org/10.1016/j.ijmachtools.2012.02.002.
SIGMA-ALDRICH, 2014. Safety Data Sheet [WWW Document]. URL. http://www.sigmaaldrich.com/MSDS/MSDS/DisplayMSDSPage.do?country=GB&language=en&productNumber=18512&brand=SIAL&PageToGoToURL=/safety-center.html.
Thepsonthi, T., Özel, T., 2012. Multi-objective process optimization for micro-end milling of Ti-6Al-4V titanium alloy. Int. J. Adv. Manuf. Technol. 63, 903–914. http://dx.doi.org/10.1007/s00170-012-3980-z.
Thepsonthi, T., Özel, T., 2013. Experimental and finite element simulation based investigations on micro-milling Ti-6Al-4V titanium alloy: effects of cBN coating on tool wear. J. Mater. Process. Technol. 213, 532–542. http://dx.doi.org/10.1016/j.jmatprotec.2012.11.003.
Ulutan, D., Ozel, T., 2011. Machining induced surface integrity in titanium and nickel alloys: a review. Int. J. Mach. Tools Manuf. 51, 250–280. http://dx.doi.org/10.1016/j.ijmachtools.2010.11.003.
Umbrello, D., Micari, F., Jawahir, I.S., 2012. The effects of cryogenic cooling on surface integrity in hard machining: a comparison with dry machining. CIRP Ann. Manuf. Technol. 61, 103–106. http://dx.doi.org/10.1016/j.cirp.2012.03.052.
Vazquez, E., Gomar, J., Ciurana, J., Rodríguez, C.A., 2015. Analyzing effects of cooling and lubrication conditions in micromilling of Ti6Al4V. J. Clean. Prod. 87, 906–913. http://dx.doi.org/10.1016/j.jclepro.2014.10.016.
Yang, K., Liang, Y., Zheng, K., Bai, Q., Chen, W., 2010. Tool edge radius effect on cutting temperature in micro-end-milling process. Int. J. Adv. Manuf. Technol. 52, 905–912. http://dx.doi.org/10.1007/s00170-010-2795-z.

ISBN 978-80-904077-7-0
Proceedings of the 11th International Conference on High Speed Machining
September 11-12, 2014, Prague, Czech Republic

HSM2014-14033

INVESTIGATION ON MICROMILLING OF EBM TI6AL4V TITANIUM ALLOY

Z. Rysava[1], G. Tristo[1]*, S. Bruschi[1]
[1]University of Padua, department of Industrial Engineering, Padua, Italy
*Corresponding author; e-mail: gianluca.tristo@dii.unipd.it

Abstract
The paper deals with the micro-machinability of Ti6Al4V Titanium alloy parts fabricated by means of Electron Beam Melting (EBM) additive manufacturing process and devoted to the biomedical sector. A number of cutting experiments were conducted on an ultra-precise micromilling machine by varying the cutting speed and the feed rate. The experiments were carried out under minimum quantity lubrication (MQL) conditions by using uncoated tungsten carbide micro-end mills having a diameter of 0.3 mm. The surface topography of the milled surfaces was analysed as a function of the cutting parameters, as well as the burrs characteristics, tool wear, chip morphology, and microstructure were investigated.

Keywords:
Micromachining; titanium alloy; machinability; surface topography; burrs

1 INTRODUCTION

Titanium alloys, and in particular the Ti6Al4V alloy, are widely used in the biomedical sector because of their distinctive properties, such as excellent biocompatibility, high ratio between the strength and mass (density around 4.4 g/cm3), corrosion resistance, human allergic repose, osseo-integration, which make these alloys extremely suitable for manufacturing knees, hips and dental implants [Fachcini 2010, Murr 2009b, Parthasarathy 2010, Harrysson 2008]. As far as the conventional manufacturing route concerns, the implants are produced through a long process chain, which starts with the forming process, usually carried out at elevated temperature. Although the forming process allows producing near net-shape parts, other operations to finish the parts are still needed, namely machining steps, polishing, and finally cleaning. The machining steps in particular lead to material waste and require long production time. Moreover, the machining of titanium alloys is troublesome because of the high tool wear, the reactivity and low thermal conductivity of the material [Thepsonthi 2012, Thepsonthi 2013]. In addition, the raw material cost remains still high, which forces to limit the material waste as much as possible [Yan 2013].

Nevertheless, as the societal impact of the biomedical industry is rising due to the increase of the number of implants applications, (for instance in USA the number of knee joint replacements exceeds the 300'000 surgeries per year [Murr 2009a]), the need to apply innovative manufacturing routes capable to decrease the material waste is rising too.

One possible solution to decrease the material waste due to the machining steps [Yan 2013, Murr 2009a] is to use the emerging Additive Manufacturing (AM) technologies, which allow producing parts with geometrical features very close to the final ones, and also characterized by tailored mechanical properties, being the latter a strong request in biomedical applications [Harrysson 2008]. After being produced by AM, the parts need to be machined usually only on those surfaces that have to be later on assembled; furthermore, finishing or semi-finishing operations are generally sufficient to obtain the desired features, thus limiting the material waste.

The process chain including AM and machining operations is being applied also to micro-sized biomedical components, such as dental implants. Some literature records can be found dealing with micro-sized components or components showing micro-sized features produced either by AM technologies or micromachining. Whereas, micromachining of components produced by AM technologies still represents an unexplored research field. Therefore, the objective of this paper is to evaluate the machinability characteristics of the Ti6Al4V titanium alloy produced by the Electron Beam Melting (EBM) additive manufacturing process when worked under micromilling process conditions. The material machinability under micromilling conditions was evaluated focussing on the machined part surface characteristics, with particular regard to the surface topography and the presence of burrs, as a function of the process parameters. The tool wear, chip morphology and material microstructure alterations were also investigated.

2 EXPERIMENTAL SETUP

The experiments were carried out on a Kugler™ Micromaster 5 axis ultra-precision micromilling machine (Fig. 1), which provides an all-over positional error of 0.3 µm and a maximum linear axis speed of 6'000 mm/min.

The machine was equipped with an air bearing spindle suitable for micromachining that can reach 180'000 RPM.

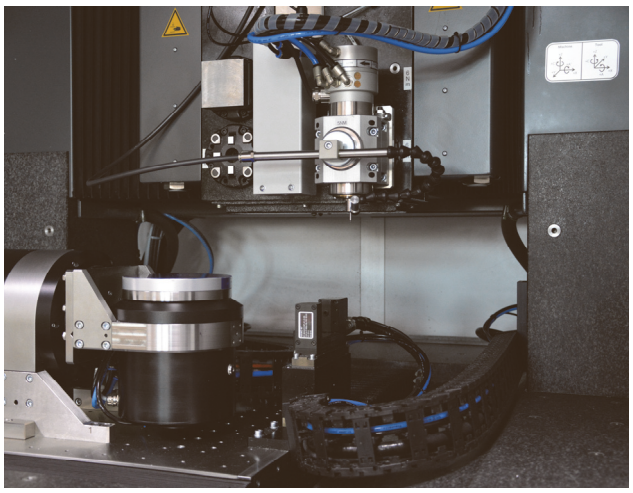

Fig. 1: Kugler™ Micromaster 5X used for the micromilling experiments

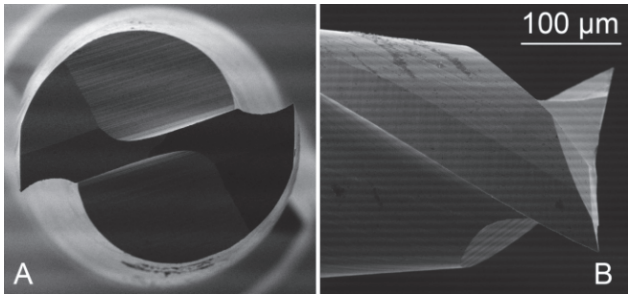

Fig. 2: SEM images of a fresh microtool

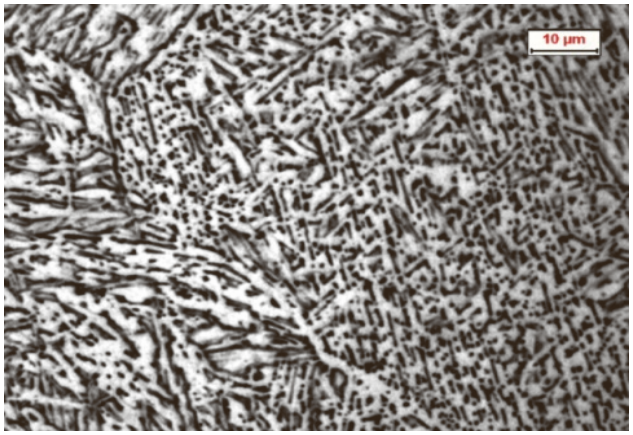

Fig. 3: EBM Ti6Al4V microstructure in the as-received condition

An uncoated flat-end-square two-fluted microtool made of tungsten carbide with a diameter of 0.3 mm (Fig. 2) was selected for the experiments. For each test, a fresh tool was used in order to avoid any influence of the tool wear on the experimental results. Each tool was inspected with a FEI™ Quanta 400 Scanning Electron Microscope (SEM) before machining to estimate the cutting edge geometry and to verify the absence of any possible production defects, such as damages or micro-cracks on the cutting edge. The microtools were again analysed by using SEM images after machining to evaluate the resulting tool wear.

50x50 mm^2 workpieces, obtained by Wire Electrical Discharge Machining (WEDM) from a cylinder of Ti6Al4V titanium alloy fabricated by EBM process, were used in the experiments. The chemical composition and the main mechanical properties of the EBM Ti6Al4V are reported in Table 1. The material microstructure in the as-received condition (Fig. 3) is a very fine acicular microstructure that mainly consists of α-phase fine lamellae, organized in a basket weave morphology.

Tab. 1: Chemical composition and mechanical properties of the EBM Ti6Al4V [ARCAM 2014]

Element	Weight [%]	Mechanical property	Value
Aluminium, Al	6	Yield strength (R_p 0.2)	950 MPa
Vanadium, V	4	Ultimate Tensile Strength (R_m)	1020 MPa
Carbon, C	0.03	Elongation	14%
Iron, Fe	0.1	Reduction of Area	40%
Oxygen, O	0.15	Fatigue strength at 600MPa (after hot isostatic pressing)	>10 000 000 cycles
Nitrogen, N	0.01		
Hydrogen, H	0.003	Rockwell hardness	33 HRC
Titanium, Ti	balance	Modulus of elasticity	120 GPa

Before performing the experiments, the top surface layer of the workpiece that was affected by the WEDM process was removed and flattened by using a 3 mm diameter tool and applying finishing process parameters in order to ensure the necessary surface quality for the inspection and measurements that were performed after the micromachining tests.

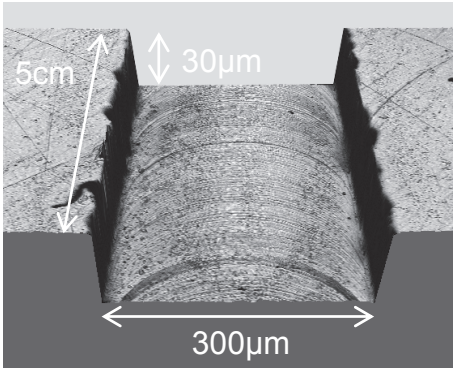

Fig. 4: Geometry of the machined slots

The machining strategy chosen for the experiments was the full immersion slotting: the geometry of the slot is shown in Fig. 4. Each micromilling experiment produced a slot long 50 mm. The machining operation was made to start far enough to ensure full acceleration at the moment of the tool engagement with the workpiece.

It is worth to underline that the micromilling process differs from conventional milling by the presence of both ploughing and shearing mechanisms [Dornfeld 2006, Dhanorker 2007].

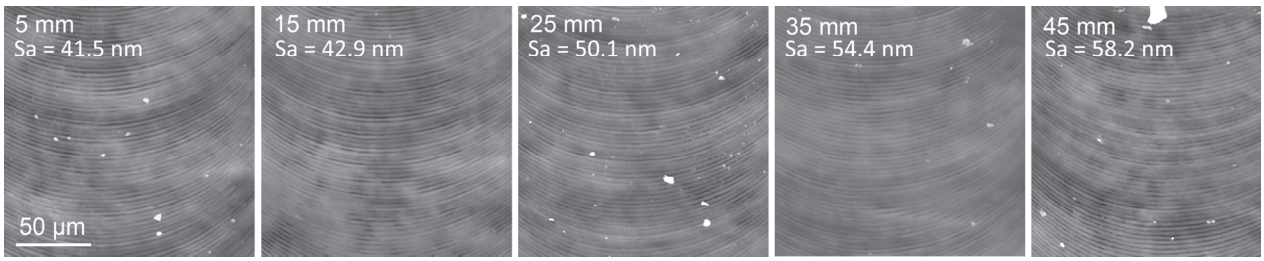

Fig. 5: Surface topography produced by process parameters S8 (v_c = 100 m/min, f_z = 1.5 µm/th) measured at different locations along the slot length

Machining in ploughing conditions should be avoided because it generally influences negatively the surface quality of the machined components [Aramcharoen 2009, Thepsonthi 2013, Milan 2010].

Tab. 2: Experimental plan

Process setting	a_p [µm]	v_c [m/min]	f_z [µm/th]
S1	30	50	0.8
S2	30	50	1.5
S3	30	50	3.0
S4	30	75	0.8
S5	30	75	1.5
S6	30	75	3.0
S7	30	100	0.8
S8	30	100	1.5
S9	30	100	3.0

Tab. 3: Qualitative overview of the experimental results

Process setting	Surface quality	Burr size	Vibrations
S1	4	1	2
S2	4	2	4
S3	1	1	1
S4	4	2	3
S5	4	3	3
S6	4	4	2
S7	5	2	3
S8	5	1	5
S9	4	5	2

It is possible to avoid the ploughing cutting mechanism and its effects on the workpiece surface finish by choosing a proper set of process parameters characterized by an uncut chip thickness greater than the minimum chip thickness [Dornfeld 2006, Özel 2007, Afazov 2013, Özel 2011, Liu 2006]. The uncut chip thickness is chosen on the basis of the feed per tooth [Dhanorker 2007], while the minimum chip thickness in case of machining of multi-phase metals can be estimated to be 0.3 ÷ 0.4 times of the cutting edge radius [Thepsonthi 2013]. The cutting edge radius of the microtools used in these experiments was measured to be about 1.3 µm, thus the critical feed per tooth was 0.39 ÷ 0.52 µm.

The experimental campaign followed the scheme of a full factorial design, consisting of two factors, three levels and two repetitions. The two factors were the cutting speed v_c and the feed per tooth f_z. Table 2 reports the experimental plan, with the identification of the process parameter settings for each cutting condition. When selecting the process parameter settings, a qualitative evaluation of the vibrations that could affect the machine-tool-spindle system at selected spindle speeds was carried out by using basic equipment based on piezoelectric sensors and visual indication of the vibration magnitude. Critical spindle speeds were thus avoided, though the vibrations affecting the system during the machining operations were not quantitatively measured. It is worth to underline that all the spindle speeds and related process parameters reported in this paper are nominal values, since the deviations between actual and nominal spindle speed values during the experiments were not measured. Furthermore, the run-out of the tool tip, which can also have an influence over the geometrical accuracy of the machined features and the associated surface quality, was not investigated in this preliminary study.

The axial depth of cut a_p was set equal to 30 µm and kept constant during all the experiments. The axial depth of cut can be affected by the tool and spindle thermal expansion during machining. To this end, the spindle expansion compensation of the machine, which is based on an eddy current sensor and on-line z-axis tool displacement correction, was activated.

Isoparafin oil was used as cutting fluid and provided on the workpiece by a minimum quantity lubrication system (MQL) in nearly dry conditions.

After each experiment, some samples of chips were collected and the leftovers carefully cleaned.

3 EXPERIMENTAL RESULTS

After the micromachining experiments, the workpiece and the microtools were gently cleaned in an ultrasonic bath in order to remove the cutting fluid residuals and the chips particles. Then, a qualitative estimation of the tool wear, chip morphology, microstructure alteration, as well as the measurement of the slots geometrical dimensions and of the surface roughness were performed. In the following paragraphs preliminary results are reported.

It is worth to note that the process parameter settings named S1 (lowest cutting speed and feed per tooth) and S9 (highest cutting speed and feed per tooth) in Table 2 led to a very rough surface finish, which could be explained with the presence of tool vibrations. Furthermore, the process parameter settings named S3 (lowest cutting speed and highest feed per tooth) revealed to be too demanding for the microtools used in these experiments since the slotting operation was not completed due to the microtool breakage after about 45 mm of machining in both the experimental repetitions.

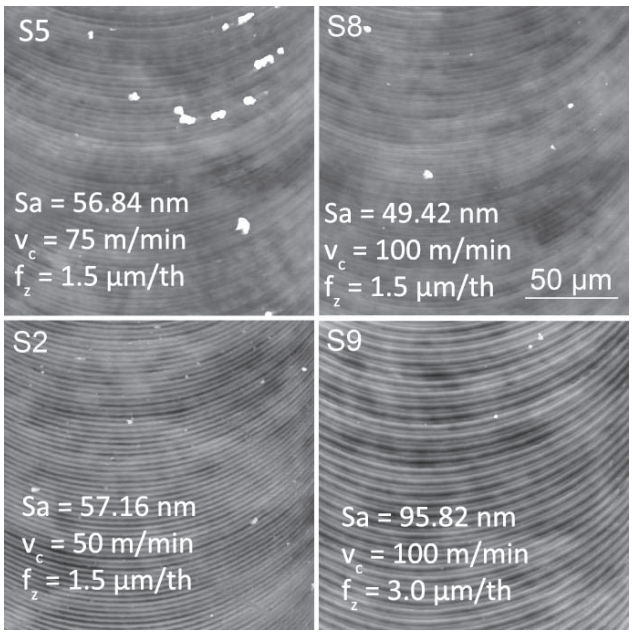

Fig. 6: Surface topography comparison between different cutting conditions

3.1 Surface topography

The machined surface topographies were sampled by using a Sensofar™ PLµ Neox confocal optical profilometer at five locations along each of the 50 mm long slots, at regular distances from the border of the workpiece, namely 5, 15, 25, 35 and 45 mm (Fig. 5).

The instrument was equipped with a 100x lens characterized by a field of view of 127x97 µm^2 and a vertical resolution of about 5 nm. A 2x2 images stitching with 25% overlap between the frames was performed for each measurement in order to increase the surface area to 223x167 µm^2. The images were then trimmed to a 167x167 µm^2 square format. The surface characteristics were finally evaluated by using the Image Metrology SPIP™ software and the surface roughness S_a was considered as the surface roughness reference characteristic. Each digital surface sample was adjusted to filter out voids or particles when present, and to correct any tilt of the surface that would affect the surface roughness measures.

The obtained results show that the measured values of S_a are spread from 50 and 260 nm between experiments, but are rather consistent when the five different sampling locations along the slots machined with constant process parameter settings are considered. Ratings from extremely bad (1) to extremely good (5) were attributed to each process parameter setting used in the experiments and are reported in Table 3, while in Fig. 6 are shown two of the best textures, namely S5 (middle cutting speed and feed per tooth) and S8 (highest cutting speed and middle feed per tooth), one average surface finish S2 (lowest cutting speed and middle feed per tooth), and a non-acceptable result S9 (highest cutting speed and feed per tooth) caused by tool vibrations.

3.2 Burrs

To perform a quantitative dimensional analysis of the burrs formed during the micromilling process is in general a difficult task due to the complex geometrical characteristics and small dimensions of the machined freeform parts. Due to that, a qualitative analysis by using SEM images is usually carried out, using for instance the burrs maximum or average length as a mean of comparison [Filiz 2007].

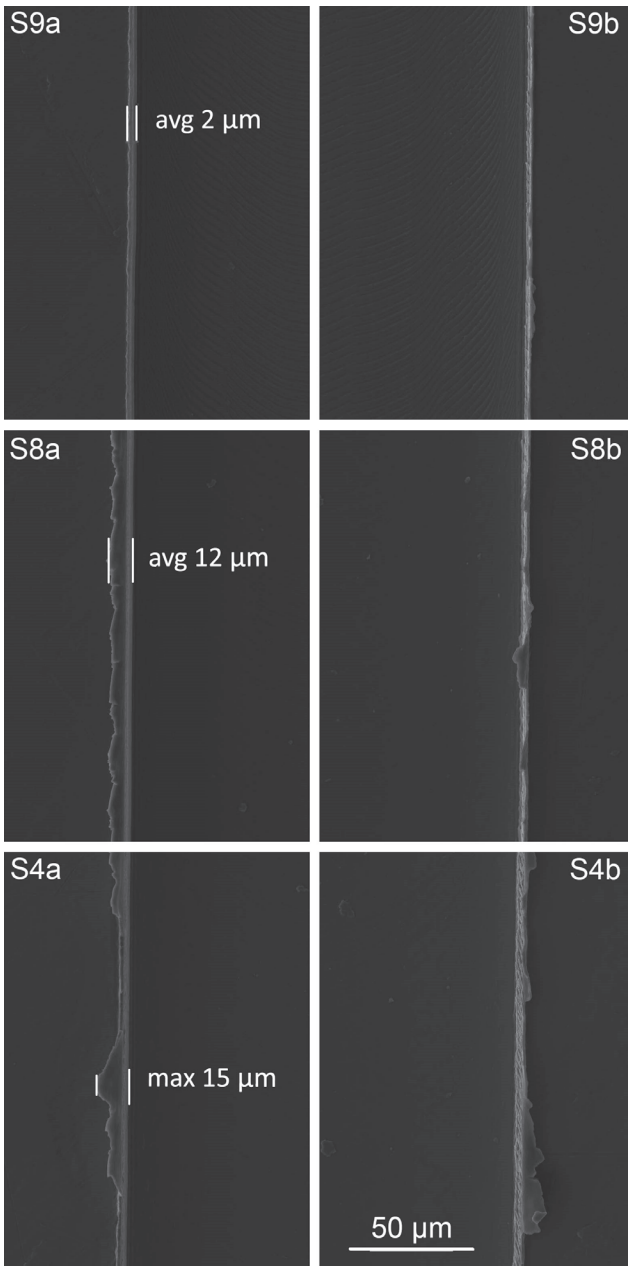

Fig. 7: SEM images of the burrs along the slots machined with different process parameters

However, the analysis of the samples in Fig. 7 proves that one single geometrical characteristic could lead to misinterpretation since it is not sufficient for an overall description of the quality of the burrs that characterise the machined samples. In this paper, the burrs were qualified by SEM inspection, considering their dimensions and shape; ratings from extremely bad (1) to extremely good (5) were attributed to each process parameter setting used in the experiments and are reported in Table 3. During a slotting operation the microtool removes material in both down milling (Fig.7 S9a, S8a, S4a) and up milling (Fig. 7 S9b, S8b, S4b) conditions: in general, it was found that burrs were sensibly larger in down milling conditions S8 (highest cutting speed and middle feed per tooth), whereas in a few experiments burrs were comparable on both sides of the slot S9 (highest cutting speed and feed per tooth).

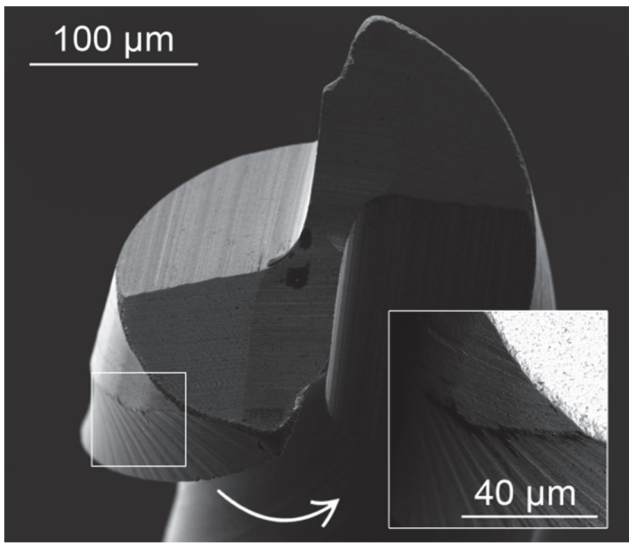

Fig. 8: SEM picture with BSED detailed view of the tool wear after the micromilling experiment (S8)

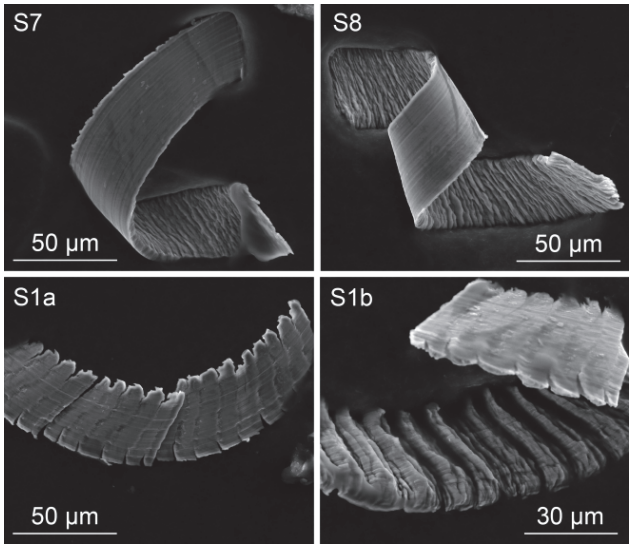

Fig. 9: SEM image of chips produced under different cutting conditions

3.3 Tool wear

Tool wear in micromilling can manifest mainly as a reduction of the tool tip diameter and as a increase of the cutting radius, thus affecting both the accuracy of the channel width and the surface quality of the channel floor.

The microtools used during the experiments were inspected by means of SEM images before (Fig. 2) and after machining (Fig. 8) in order to obtain a qualitative estimation of the tool wear. The estimation of the tool wear was carried out measuring the cutting edge radius and the tool tip diameter before and after the experiments.

The analysis of the state of the tools after machining showed an appreciable difference in tool wear between different process parameter settings: in some cases the cutting edge of the microtool was damaged (S9 – highest cutting speed and feed per tooth), in other cases the microtool was not able to withstand the cutting forces and broke close to the end of the slotting operation (S3 – lowest cutting speed, but highest feed per tooth).

The most severe tool wear was observed in experiments S8 (highest cutting speed and middle feed per tooth, Fig. 8): the cutting edge is clearly rounded both from top and from lateral views. Furthermore, the flank of the tool shows evident effects of abrasion. The detail shown in Fig. 8 was captured with the SEM-BSED detector and the dark agglomerate suggests that material from the workpiece adhered on the tungsten carbide tool flank surface.

3.4 Chip morphology

The samples of chips that were collected during the micromachining experiments were inspected through SEM analysis. Some examples of chips are shown in Fig. 9, where S7 and S8 correspond to the process parameters setting named S7 (highest cutting speed, lowest feed per tooth) and S8 (highest spindle speed, middle feed per tooth), respectively, while S1a and S1b represent two different samples both related to the experimental conditions named S1 (lowest cutting speed and feed per tooth).

The morphology of some of the collected chips shown in Fig. 9 is segmented, even if the level of segmentation is different: while the S7 chip morphology is similar to that of the S8 experimental conditions, there is a pronounced difference in the case of S1 conditions.

The chip morphology is in general the combination of the chip formation mechanisms and the machining process dynamics. It is worth to note that the chips S7 and S8 in Fig. 9 are the results of the same cutting speed but with different feed per tooth, while the chips S1 and S7 were produced with the same feed per tooth with the S1 conditions characterized by a lower cutting speed. At lower cutting speed (S1) the chips look more segmented than at the highest tested cutting speed (S7, S8). To be noted that the surface analysis relative to the process parameter settings S1 revealed the presence of tool vibrations during the micromilling process.

3.5 Microstructure

The microstructure analysis required dedicated experiments in order to avoid any influence of the WEDM cutting process and flattening milling operation. To this aim, a small portion of raw EBM Ti6Al4V was machined with a fresh 0.3 mm dia. microtool in order to produce a slot deep about 300 µm by means of a slotting operation and an axial depth of cut of 20 µm.

The machined workpiece was then sectioned perpendicularly to the top surface and to the slots at about half of the slot length. The section was then prepared for metallurgical analysis. Once polished, the surface containing the sections of the slots was etched using the Kroll's reagent and inspected by using an optical microscope.

Fig. 10 shows the microstructure after machining on the side wall and bottom surface, respectively (C is a detail of the bottom surface, roughly in the middle of the slot). These micrographs show that the slotting operation affected only a very thin substrate layer and that the alteration of the microstructure along the boundary surface is not homogeneous. In general, the acicular microstructure layer affected by the micromilling process presents distorted and smaller grains as a consequence of the shear deformation.

4 DISCUSSION

The results regarding surface quality reported in Table 3 show that the surface roughness is proportional to the chip thickness and inversely proportional to the cutting speed. The best surface finish was achieved in the experiments S7 (highest cutting speed and lowest feed per tooth) and S8 (highest cutting speed and middle feed per tooth). Cutting conditions with higher cutting speeds and smaller chip thickness should be further investigated to find the optimal values after which a further increment in the

cutting speed and reduction of the chip thickness would cause a worse surface finish [Jahanmir 2011].

Experiments S7 (highest cutting speed and lowest feed per tooth, Fig. 7) are also characterized by large and discontinuous burrs on both sides of the slots, while the experiment S9 (highest cutting speed and highest feed per tooth) is almost burrs free. The trend suggests that a better surface finish can be achieved at the expense of more and larger burrs. Indeed, the experiment S8 (highest cutting speed and middle feed per tooth) is characterized by medium sized burrs.

For this reason, the set of process parameters named S8 was selected as the optimal choice for the combination of micromilling machine, microtools, workpiece material and application considered in this paper.

SEM images of the microtools used in experiments S8 show the consequences of severe tool wear. However, it has to be considered that with proper coatings the wear resistance of the microtools can be greatly improved [Thepsonthi 2013]. The process parameters settings named S3 (lowest cutting speed and highest feed per tooth) led to the tool breakage after a few millimetres and thus should be avoided.

5 CONCLUSIONS

In this paper the machinability of the Ti6Al4V titanium alloy produced by the Electron Beam Melting additive manufacturing was investigated. The main aim of this work was a preliminary evaluation of the influence of process parameters on the part surface finish, burrs, chip morphology, tool wear and material microstructure.

The experimental results show that it is possible to achieve a surface roughness S_a lower than 50 nm by increasing the cutting speed, at the expenses of an increase of tool wear and burrs size. The microtools used for this work require a proper coating to increase the tool wear resistance and thus obtain an acceptable tool life.

Some process parameter settings selected for the experimental campaign of this paper showed an unexpected dynamic behaviour of the system composed by the machine, spindle and tool that affected the cutting results of some experiments and that needs further investigation.

The morphology of the collected chips proved to be segmented for each cutting condition, but with different levels of segmentation depending on the process parameters. The alteration of the material microstructure due to the micromilling process was evidenced, showing distorted and smaller grains than the as-received material; the microstructural alteration will be further studied in future works, together with the relationship between the chip morphology and process parameter settings.

6 REFERENCES

[Aramcharoen 2009] Aramcharoen, A. and Mativenga, P.T. Size effect and tool geometry in micromilling of tool steel. Precis. Eng., October 2009, Vol.33, No.4, pp. 402–407.

[ARCAM 2014] ARCAM. Ti6Al4V Titanium alloy. Catalogue. [on line] Available at <http://www.arcam.com/technology/products/metal-powders/catalogue> (consulted 05/05/2014).

[Dornfeld 2006] Dornfeld, D., et al. Recent advances in mechanical micromachining. CIRP Ann. Technol., January 2006, Vol.55, No.2, pp. 745–768.

[Dhanorker 2007] Dhanorker, A., et al. Micromilling Process Planning and Modeling for Micromold Manufacturing. ASME 2007 Int. Manuf. Sci. Eng. Conf., 2007, pp. 759–769.

[Fachcini 2010] Fachcini, L. Microstructure and mechanical properties of biomedical alloys produced by Rapid Manufacturing techniques. Thesis. Italy: Univeristy of Trento, January 2010.

[Filiz 2007] Filiz, S., et al. An experimental investigation of micro-machinability of copper 101 using tungsten carbide micro-endmills. Int. J. Mach. Tools Manuf., June 2007, Vol.47, No.7–8, pp. 1088–1100.

[Harrysson 2008] Harrysson, O.L., et al. Direct metal fabrication of titanium implants with tailored materials and mechanical properties using electron beam melting technology. Mater. Sci. Eng. C, Aprile 2008, Vol.28, No.3, pp. 366–373.

[Jahanmir 2011] Jahanmir, S. Surface Integrity in Ultrahigh Speed Micromachining. Procedia Eng., January 2011, Vol.19, pp. 156–161.

[Liu 2006] Liu, X., et al. An Analytical Model for the Prediction of Minimum Chip Thickness in Micromachining. J. Manuf. Sci. Eng., 2006, Vol.128, No.2, pp. 474.

[Milan 2010] Mian, J.A., et al. A comparative study of material phase effects on micro-machinability of multiphase materials. Int. J. Adv. Manuf. Technol., January 2010, Vol.50, No.1–4, pp. 163–174.

[Murr 2009a] Murr, L.E., et al. Microstructure and mechanical behavior of Ti-6Al-4V produced by rapid-layer manufacturing, for biomedical applications. J. Mech. Behav. Biomed. Mater., January 2009, Vol.2, No.1, pp. 20–32.

[Murr 2009b] Murr, L.E., et al. Microstructures and mechanical properties of electron beam-rapid manufactured Ti–6Al–4V biomedical prototypes compared to wrought Ti–6Al–4V. Mater. Charact., February 2009, Vol.60, No.2, pp. 96–105.

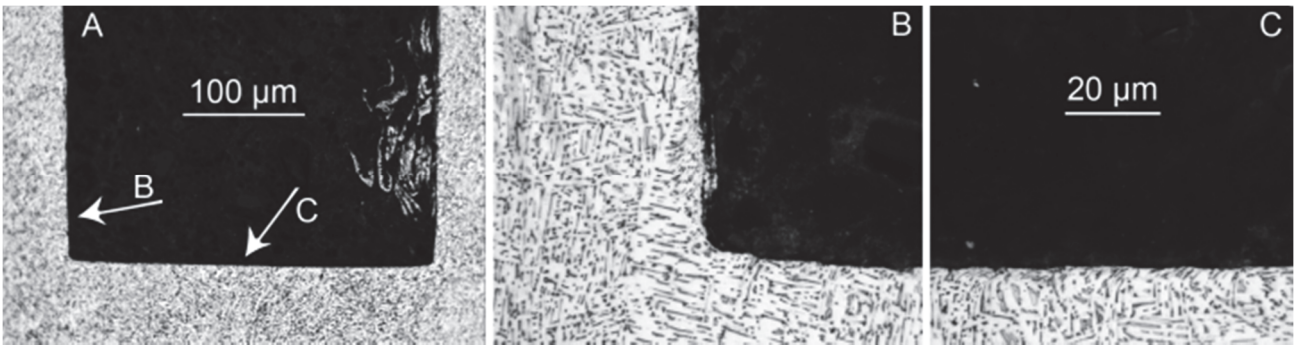

Fig. 10: Alteration of the Ti6Al4V microstructure after the slotting operation

[Özel 2007] Özel, T., et al. Modelling and simulation of micro-milling process. New Jersey, U.S.A.: Rutgers University, Piscataway, Dept. of Industrial & Systems Engineering, Manufacturing Automation and Research Laboratory, 2007.

[Özel 2011] Özel, T., et al. Experiments and finite element simulations on micro-milling of Ti–6Al–4V alloy with uncoated and cBN coated micro-tools. CIRP Ann. - Manuf. Technol., January 2011, Vol.60, No.1, pp. 85–88.

[Parthasarathy 2010] Parthasarathy, J., et al. Mechanical evaluation of porous titanium (Ti6Al4V) structures with electron beam melting (EBM). J. Mech. Behav. Biomed. Mater., Aprile 2010, Vol.3, No.3, pp. 249–59.

[Thepsonthi 2012] Thepsonthi, T., et al. Multi-objective process optimization for micro-end milling of Ti-6Al-4V titanium alloy. Int. J. Adv. Manuf. Technol., March 2012, Vol.63, No.9–12, pp. 903–914.

[Thepsonthi 2013] Thepsonthi, T. and Özel, T. Experimental and finite element simulation based investigations on micro-milling Ti-6Al-4V titanium alloy: Effects of cBN coating on tool wear. J. Mater. Process. Technol., Aprile 2013, Vol.213, No.4, pp. 532–542.

[Yan 2013] Yan, Y., et al. Effect of density and pore morphology on fatigue properties of sintered Ti–6Al–4V. Int. J. Fatigue, October 2013, Vol.55, pp. 81–91.

Process parameters optimization for micro-milling of EBM Ti6Al4V titanium alloy

4M/ICOMM 2015 No.

Z. Rysava[1] G. Tristo[1] S. Bruschi[1]

[1] *University of Padua, department of Industrial Engineering, Padua, Italy*

Abstract

The development and use of new processes, in particular Additive Manufacturing (AM) technologies, are increasingly applied thanks to the advantages they offer in the fabrication of parts made of difficult-to-cut metals, such as titanium and cobalt alloys. However, the surface quality and dimensional accuracy of the functional surfaces assured by AM technologies are not always satisfactory, often requiring subsequent finishing or semi-finishing operations to ensure the surface integrity requirements. While there is a wide literature dealing with the influence of the AM process parameters on the parts obtainable characteristics, the machinability of metal alloys obtained by AM has not been deeply studied yet, especially when micro-geometrical features have to be machined. This paper analyses the machinability under micro-milling operating conditions of the Ti6Al4V titanium alloy obtained by Electron Beam Melting (EBM) AM technology. Micro-milling tests were conducted on a high-precision 5-axis micro-milling center under dry conditions, by using uncoated, two fluted, flat-end-square tungsten carbide tools with a diameter of 300 microns. The micro-machined surface roughness, tool wear and burrs were analyzed as a function of cutting speed and feed per tooth process parameters.

Keywords: Titanium, machinability, micro-milling.

1. Introduction

With the increasing longevity and the aging of the population, the need and importance of biomedical industry are increasing every year. Considering medical implants, in the USA the number of knee joint replacements exceeds 300'000 surgeries per year [1]. Titanium alloys, and in particular the Ti6Al4V alloy, are the metal alloys most typically used for biomedical applications because of their distinctive properties, such as excellent biocompatibility, high ratio between the strength and mass (density around 4.4 g/cm^3), corrosion resistance, human allergic repose, osseo-integration, which make these alloys extremely suitable for manufacturing knees, hips and dental implants [1,2,3]. Despite titanium alloys are very well known and have been used since many tens of years, their machining remains still highly troublesome because of the high tool wear, chemical reactivity and low thermal conductivity [4,5]. Moreover, the high cost of the raw material forces to limit the material waste as much as possible [6]. Although the conventional manufacturing chain, which is very long and consists of the forming process, usually carried out at elevated temperature, machining, polishing, and finally cleaning, has been optimized as much as possible, it still leads, in particular the machining steps, to significant material waste [6,1] and long production time. To this end, the emerging Additive Manufacturing (AM) technologies are highly promising in the field of biomedical applications because they allow the production of near-net-shape parts characterized by tailored mechanical properties, being the latter a strong request in biomedical applications [3]. However, usually it is still necessary to machine parts that have been produced by AM to remove the rest material and to fine-finish the functional surfaces; finishing or semi-finishing operations are generally sufficient to obtain the desired features and thus limiting the waste of the costly material. This process chain including AM and machining operations could be also applied to micro-sized biomedical components, such as dental implants.

Since the performances of micro-machining processes can be influenced by the substrate microstructure of the workpiece material [7,8], the micro-machinability of materials produced by AM technologies should be investigated. Works dealing with micro-sized components or components showing micro-sized features produced either by AM technologies or micromachining can be found in literature [9] but information on the micro-machining of components produced by AM technologies are missing to a greater extent. The aim of this paper is to evaluate the machinability of the Ti6Al4V titanium alloy produced by the Electron Beam Melting (EBM) AM process under micro-milling process conditions. Experiments were conducted in order to study the influence of the cutting speed and feed per tooth on the machined surface roughness, the presence of burrs and the tool wear.

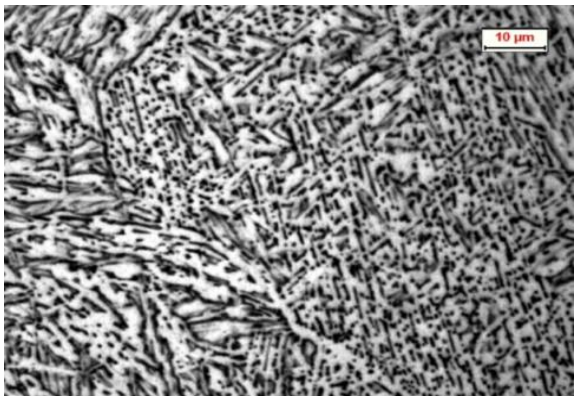

Fig. 1. EBM Ti6Al4V microstructure.

Table 1
Spindle speed (N), feed rate (V_f), cutting speed (V_c) and feed per tooth (F_z) selected for the experiments.

Setting Index	N (RPM)	V_f (mm/min)	V_c (m/min)	F_z (µm/th)
S1	67000	13.4	63	0.1
S2	67000	67	63	0.5
S3	67000	201	63	1.5
S4	67000	402	63	3.0
S5	98000	19.6	92	0.1
S6	98000	98	92	0.5
S7	98000	294	92	1.5
S8	98000	588	92	3.0
S9	154000	30.8	145	0.1
S10	154000	154	145	0.5
S11	154000	462	145	1.5
S12	154000	924	145	3.0

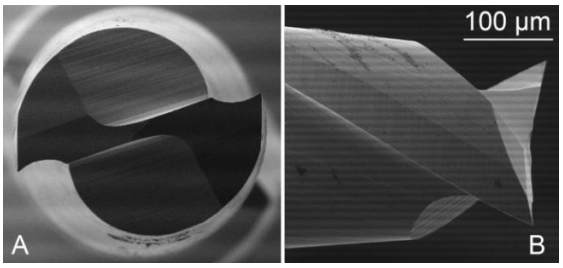

Fig. 2. SEM images of an uncoated, end-mill micro-tool with a diameter of 0.3 mm, as received from the tool manufacturer (Kyocera).

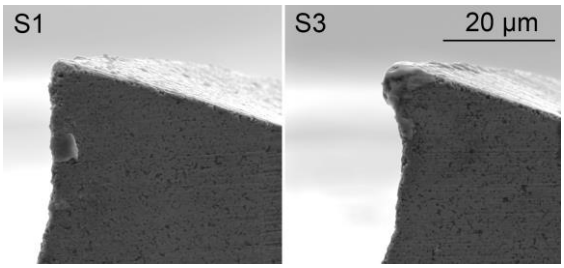

Fig. 3. SEM images of two worn-out tools with negligible workpiece material adhesion (S1) and built-up edge (S3).

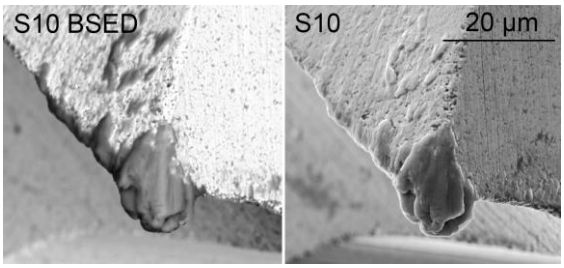

Fig. 4. Back-scattered electrons (left) and secondary electron (right) SEM images of the tool with the most evident Built-Up Edge (process parameters S10).

2. Experimental setup

2.1. Equipment and tools

The experiments were carried out on a Kugler™ Micromaster 5-axis ultra-precision micromilling machine, which provides an all-over positional error of 0.3 µm and a maximum linear axis speed of 6'000 mm/min. The machine was equipped with an air bearing spindle suitable for micro-machining that can reach 180'000 RPM.

One tool per test was used for the experiments, for a total of 24 uncoated flat-end-square two-fluted micro-tools made of tungsten carbide with a diameter of 0.3 mm. Each tool was inspected with a FEI™ Quanta 400 Scanning Electron Microscope (SEM) before (Fig. 2) and after (Fig. 3-4) machining to verify the cutting edges integrity and to estimate the tool wear.

A block of Ti6Al4V titanium alloy fabricated by EBM process was used as workpiece. Before performing the experiments, the top surface layer of the workpiece was flattened and polished by means of a laboratory polishing machine.

Machining was performed in dry conditions: a jet of compressed air without any cutting fluid was used during the experiments to cool the temperature of the tool and workpiece, and to clear the chips from the working area.

2.2. Design of experiments

The machining strategy chosen for the experiments was the full immersion slotting. The tool achieved full acceleration before engaging the workpiece from the side and then machined a straight slot, 0.3 mm wide and 0.030 mm deep, through the 25 mm long workpiece.

The experimental campaign followed the scheme of a full factorial design, consisting of two factors, namely the cutting speed V_c and the feed per tooth F_z, respectively with three and four levels. The experiments were repeated twice. The nominal values of the process parameters selected for the experimental plan are reported in Table 1.

The vibrations affecting the machine-tool-spindle system were evaluated in static conditions by means of accelerometers throughout the range of the available spindle speeds. These critical spindle speeds were thus avoided during the design of the experiments, though tool chatter affected some tests. The run-out of the tool tip was not investigated in this study.

The axial depth of cut was set equal to 30 µm and kept constant during all the experiments by the on-line spindle expansion compensation of the machine. The consistency of the axial depth of cut through the experiments was verified by measuring the depth of the slots by means of an optical profilometer.

3. Experimental results

3.1. Surface roughness

The machined surface topographies were sampled by using a Sensofar™ PLµ Neox confocal optical profilometer. The instrument was equipped with a 100x lens characterized by a field of view of 127x97 µm^2 and a vertical resolution of about 5 nm.

Table 2
Parameters for the surface roughness measurements, results are reported in terms of Ra for both repetitions, average and gap between the two repetitions (range). Built-Up Edge and burrs ratings[a,b] are also reported.

ID	Sample area (mm^2)	λ_c (mm)	N° of cut-off	Ra (nm) rep. 1	Ra (nm) rep. 2	Ra (nm) average	Ra (nm) range	BUE (rating[a])	Burrs (rating[b])
S1	5.0x0.1	0.8	5	133	172	153	39	5	3
S2	2.0x0.1	0.25	5	47	57	52	10	4	3
S3	2.0x0.1	0.25	5	47	44	45	3	2	5
S4	2.0x0.1	0.25	5	60	78	69	18	4	3
S5	5.0x0.1	0.8	5	152	169	161	17	4	2
S6	2.0x0.1	0.25	5	53	64	58	11	4	3
S7	5.0x0.1	0.8	5	138	158	148	20	3	4
S8	5.0x0.1	0.8	5	240	186	213	54	2	3
S9	5.0x0.1	0.8	5	220	189	204	31	3	1
S10	2.0x0.1	0.25	5	83	46	65	37	1	2
S11	2.0x0.1	0.25	5	48	64	56	16	2	3
S12	5.0x0.1	0.8	5	120	115	118	3	2	3

[a]Qualitative analysis through SEM images of the tool tip after machining, the presence of workpiece material adhesion was rated from 1 (evident Build-Up Edge BUE) to 5 (negligible).
[b]Qualitative analysis through SEM images of the burrs produced at the left-hand side of the slots, ratings range from 1 (extremely bad) to 5 (extremely good).

Roughness was evaluated following the ISO 25178 standard and the arithmetic mean value Ra was used to quantify the surface quality of the machined surfaces. Depending on the estimated surface roughness, the profile analysis was performed by using cut-off values λ_c of 0.25 mm or 0.8 mm in a number of 5. To this end, respectively 21x1 and 51x1 stitched images with 25% of overlap were acquired along the bottom of the slots, close to the middle in order to avoid the entrance and exit areas. Average Ra values were calculated on 10 different roughness profiles.

The correlation between the feed per tooth, cutting speed and surface roughness is represented in Figure 5. The results shows that the best surface finish is achieved with feeds per tooth close to 1.5 µm and that in these conditions the influence of the cutting speed is less relevant. It is possible to achieve an acceptable surface finish even with higher feeds per tooth by reducing the cutting speed, but in this case results are very sensitive to tool vibrations. The lower limit in the choice of feed rates for the best surface finish is given by the ploughing mechanism that affects the micro-machining process [7,8,9,10] when the uncut chip thickness is smaller than the minimum chip thickness [7,11,12,13,14]. The minimum chip thickness in case of machining of multi-phase metals can be estimated to be 0.3 - 0.4 times the cutting edge radius [5]. The cutting edge radius of the micro-tools used in these experiments was estimated to be about 1.1 µm by means of SEM and confocal images, thus the critical feed per tooth can be expected to be between 0.33 and 0.44 µm. The experimental results are in good agreement with the estimation of the critical feed per tooth, in particular the sharp change in slope of all the curves in Figure 5 when the feed per tooth is between 0.1 and 0.5 µm. Interestingly, the slight tool vibrations that were affecting experiments S5 to S8 produced unacceptable surface finishes in all the cutting conditions except when the feed per tooth was close to this critical value.

3.1. Tool wear analysis

Tool wear in micro-milling can manifest mainly as a reduction of the tool tip diameter and as an increase of the cutting edge radius, thus affecting both the dimensional accuracy and the surface quality of the machined micro-features. In this work, the estimation of the tool wear was carried out by inspecting the tool tip before and after the experiments by means of SEM analysis.

The tool inspection revealed an appreciable difference in tool conditions as a result of the different process parameter settings, although it was not possible to quantify the amount of tool wear because of the substantial workpiece material adhesion affecting all the tools except the one used in experiment S1 (Figure 3). The formation of the Built-Up Edge (BUE) was evident in most of the experiments (Table 2) and in particular in experiment S10 (Figure 4). The presence of adhered workpiece material on the tool tip was verified through Back-Scattered Electron Detector

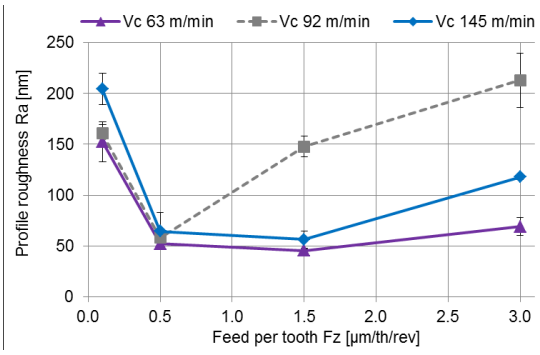

Fig. 5. Effects of the process parameters on the surface quality, represented by average Ra and range between the two repetitions (error bars).

(BSED) images (Figure 4) and energy-dispersive X-ray spectroscopy.

3.2. Burrs

Given the complex geometrical characteristics and small dimensions of the burrs, a qualitative analysis by using SEM images is usually carried out, using for instance the burrs maximum or average length as a mean of comparison [15]. In this paper, the presence of the burrs was qualified through SEM inspection. Ratings from extremely bad (1) to extremely good (5) were attributed to each process parameter setting used in the experiments by considering their dimensions and shape, as reported in Table 2.

Experimental results show that a minimum quantity of burrs is always present, but on the right side of the slots, hence in down-milling conditions, these are very small independently of the feed per tooth or cutting speed as shown in Figure 6. In up-milling, instead, the minimum quantity of burrs was obtained with process parameters S3, while setting S9, S10 and S5 should be avoided when burrs removal after machining is not feasible.

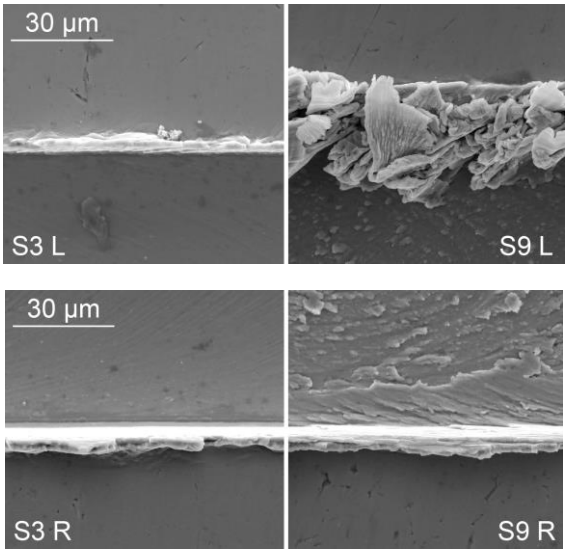

Fig. 6. SEM images of the burrs on the left-hand (L) and right-hand side (R) of the slot, relatively to two sets of process parameters characterized with minimum (S3) and maximum (S9) quantity of burrs.

4. Conclusions

In this paper the micro-machinability of the Ti6Al4V titanium alloy produced by the Electron Beam Melting additive manufacturing technology was studied. The main aim of this work was the evaluation of the influence of process parameters on the part surface finish, burrs formation, and tool wear.

SEM images show that workpiece material adhesion on the uncoated micro-tools was present in almost all the experiments, with the formation of evident build up edge.

For the range of process parameters considered in this work, relatively to slot machining with 0.3 mm end-mills, surface quality can be improved by reducing the feed per tooth and the cutting speed; however, when the feed per tooth is smaller than the minimum chip thickness, both surface roughness and the amount of burrs increase rapidly. According to the experimental results, it is possible to achieve a surface roughness Ra lower than 50 nm and at the same time to minimize the burrs formation on both sides of the slot (Table 2, experiment S3).

Tool vibrations and high cutting speeds can produce a poor surface finish, especially when these are combined with high feed rates.

References

[1] L.E. Murr et al., “Microstructure and mechanical behavior of Ti-6Al-4V produced by rapid-layer manufacturing, for biomedical applications,” J. Mech. Behav. Biomed. Mater., 2009; Vol.2: pp. 20–32.

[2] J. Parthasarathy et al., “Mechanical evaluation of porous titanium (Ti6Al4V) structures with electron beam melting (EBM),” J. Mech. Behav. Biomed. Mater., 2010; vol. 3: pp. 249–59.

[3] O.L. Harrysson et al., “Direct metal fabrication of titanium implants with tailored materials and mechanical properties using electron beam melting technology,” Mater. Sci. Eng. C, 2008; vol. 28: pp. 366–373.

[4] T. Thepsonthi et al., “Multi-objective process optimization for micro-end milling of Ti-6Al-4V titanium alloy,” Int. J. Adv. Manuf. Technol., 2012; vol. 63: pp. 903–914.

[5] T. Thepsonthi et al., “Experimental and finite element simulation based investigations on micro-milling Ti-6Al-4V titanium alloy: Effects of cBN coating on tool wear, “ J. Mater. Process. Technol., 2013; vol. 213: pp. 532–542.

[6] Y. Yan et al., “Effect of density and pore morphology on fatigue properties of sintered Ti–6Al–4V,” Int. J. Fatigue, 2013; vol. 55: pp. 81–91.

[7] D. Dornfeld et al.,”Recent advances in mechanical micromachining,” CIRP Ann. Technol., 2006; vol. 55: pp. 745–768.

[8] M.A. Câmara et al., “State of the Art on Micromilling of Materials, a Review,” J. Mater. Sci. Technol., 2012; vol. 28: pp. 673–685.

[9] P.A. Kobryn et al., "The laser additive manufacture of Ti-6Al-4V," JOM, 2001; vol. 53: pp. 40-42.

[10] A. Dhanorker et al., “Micromilling Process Planning and Modeling for Micromold Manufacturing,” ASME 2007 Int. Manuf. Sci. Eng. Conf.: 2007, pp. 759–769.

[11] T. Özel et al., “Modelling and simulation of micro-milling process,” Manufacturing Automation and Research Laboratory, Dept. of Industrial & Systems Engineering, Rutgers University, Piscataway, New Jersey, U.S.A: 2007.

[12] T. Özel et al., “Experiments and finite element simulations on micro-milling of Ti–6Al–4V alloy with uncoated and cBN coated micro-tools,” CIRP Ann. - Manuf. Technol., 2011; vol. 60: pp. 85–88.

[13] S.M. Afazov et al., “Effects of micro-milling conditions on the cutting forces and process stability,” J. Mater. Process. Technol., 2013; vol. 213: pp. 671–684.

[14] X. Liu et al., “An Analytical Model for the Prediction of Minimum Chip Thickness in Micromachining,” J. Manuf. Sci. Eng., 2006; vol. 128: pp. 474.

[15] S. Filiz et al., “An experimental investigation of micro-machinability of copper 101 using tungsten carbide micro-endmills,” Int. J. Mach. Tools Manuf., 2007; vol. 47: pp. 1088–1100.

Materials Science Forum
ISSN: 1662-9752, Vols. 836-837, pp 177-184
doi:10.4028/www.scientific.net/MSF.836-837.177

Submitted: 2015-06-01
Revised: 2015-07-24
Accepted: 2015-07-28
Online: 2016-01-05

Comparison between EBM and DMLS Ti6Al4V machinability characteristics under dry micro-milling conditions

RYSAVA Zdenka[1,a*] and BRUSCHI Stefania[1,b]

[1]Departement of Industrial Engineering, University of Padua, Via Venezia 1, 35131 Padua, Italy

[a] zdenka.rysava@studenti.unipd.it, [b] stefania.bruschi@unipd.it

Keywords: micro-milling, micro-machinability, surface integrity, titanium alloys, additive manufacturing

Abstract. This paper is aimed at evaluating the micro-machinability of the Ti-6Al-4V titanium alloy made by the means of two different Additive Manufacturing (AM) technologies. AM comprises promising technologies, widely used especially to produce parts made of difficult-to-cut materials, such as the titanium alloys. Titanium alloys represent one of the most widely used materials in the biomedical field, thanks to the high biocompatibility and excellent mechanical characteristics. Even if near-net-shape parts can be produced through AM, semi-finishing and/or finishing machining operations may be necessary to obtain the required surface finish and geometrical tolerances. Micro-milling technique is a soliciting solution for this kind of application due to its high flexibility, elevated material removal rate and direct contact between the tool geometry and work piece. Nevertheless, there are deficiencies in the literature regarding the study of micro-machinability of materials produced by means of AM technologies. In this paper, the micro-machinability of the Ti-6Al-4V alloy obtained by two different AM technologies, namely Electron Beam Melting (EBM) and Direct Metal Laser Sintering (DMLS), was studied and compared in order to assess the influence of the material as-delivered condition. Micro-milling tests were conducted on a high-precision 5-axis Kugler™ micro-milling centre under dry cutting conditions, by using uncoated, two fluted, flat-end-square, tungsten carbide tools with a diameter of 300 microns. The full immersion slotting strategy was chosen under full factorial design of experiments with two factors (cutting speed and feed per tooth). The micro-machinability was evaluated in terms of burr formation, surface integrity (surface topography and surface defects), tool damage and microstructure alterations.

Introduction

The number of biomedical prostheses that are implanted is increasing more and more every year and has reached millions of units at a worldwide level [1]. Despite the long tradition of using implants (the first hip surgery was realized in the 18th century), a high number of replacements fail, especially in the case of young patients, where the implant's life time ranges from 10 to 15 years [2]. When a high modulus material is used for the implant, the stress transferred to the bones is low, which can lead to bone resorption. In fact, it is a natural process that when the mature bone tissue is removed, the minerals are released, the calcium is transferred from the bone to the blood, and in the case of implants, it could eventually lead to aseptic loss. This difference in stiffness is called stress shielding. Because the bones are naturally remodelled in live bodies, when the stress transferred to the bones is low, the re-modelling naturally reacts to this change and the bones become weaker [2, 3].

Another lack of a standard implant can be found in the case of a patient's abnormalities requiring highly specific replacement, for example in the case of cranioplasty when a large amount of bone is missing [1]. In this case, tailored implants would improve the surgery and consecutive healing. They would fulfil the patient' specific needs and improve the contact between the implant and the bone. A possible alternative to conventional manufacturing processes is the use of Additive Manufacturing (AM) technologies for producing metal prostheses, as they can ensure the possibility of creating highly tailored components [1,2,3] since the metal powder is added layer by layer (in

ranges of few tens of microns depending on the particular process). The usual way to produce the metallic implants consists of a multi-step process chain, starting from casting or forging at elevated temperature, rough and finish machining, polishing, and in case heat treatments and ageing. In the case of a typical knee implant the waste of material due to machining operations can reach 80%. On the contrary, the AM technologies, which are nearly net-shape processes, require only finishing and/or semi-finishing machining steps, just to finish the workpiece with large material savings compared to the standard process chain [1].

Ti-6Al-4V is one of the most widely used metal alloys in the biomedical field, thanks to its properties, such as biocompatibility, osseo-integration, corrosion resistance and specific strength [1, 4]. However, its attitude to be machined is quite low [4], especially when produced by AM, as a consequence of its peculiar microstructure, which is function of the AM process parameters. Therefore, particular attention must be paid in choosing the correct cutting parameters to reduce the tool wear and assure a proper surface integrity at the same time.

This is emphasized when micro-cutting processes have to be carried out: an unsuitable choice of the process parameters may lead to the prevailing of the ploughing mechanisms over shearing. In the ploughing regime, due to the high elastic recovery once the tool has passed, the final surface quality is reduced in terms of topography and geometrical accuracy [5,6,7]. To avoid the ploughing regime, the so-called uncut chip thickness criterion must be respected. The appropriate choice of the feed per tooth, which is directly linked to the uncut chip thickness, being also the ratio of the feed per tooth to the cutting edge radius, is therefore crucial [7,8,9]. It was found that in multi-phase materials the minimum uncut chip thickness is about 0.3 – 0.4 times the cutting edge radius [9].

In addition, biomedical applications require clean production, which means the need to eliminate as much as possible the subsequent costly and time-consuming cleaning steps. Therefore, the use of cutting fluids should be avoided if possible, making the impact of dry cutting on the material machinability worth investigating. The aim of the paper is to evaluate and compare the machinability of the Ti6-Al-4V obtained by means of two different AM technologies, namely Electron Beam Melting (EBM) and Direct Metal Laser Sintering (DMLS), under dry micro-milling cutting conditions. The machinability is evaluated in terms of surface topography, burrs formation, microstructural alterations and tool damage.

Experimental

Material. In this study the biomedical alloy Ti-6Al-4V was used, produced by two different AM technologies, namely Electron Beam Melting (EBM) and Direct Metal Laser Sintering (DMLS), which were used to produce a cylinder of Ti-6Al-4V that was subsequently cut into specimens with approximate dimensions of 30x25x8mm^3. The specimen surfaces to be micro-milled were prepared in the same way as metallographic samples: they were polished by using different abrasive papers to ensure flat surfaces but without introducing any possible residual stresses or changes in the microstructure.

In Fig. 1, the microstructures of the EBM and DMLS Ti-6Al-4V samples in the as-delivered conditions are shown. The EBM microstructure is acicular-type and very fine. Its morphology is the result of a very fast solidification and consecutive annealing due to the high working zone temperature. Preheating of material ensures less severe thermal gradient thus lower residual stress in material. The preheating also causes the formation of the β−phase. When compared to the wrought annealed material structure, which is generally globular, the acicular structure results in lower fatigue resistance. On the other hand, the DMLS microstructure is finer, but not in equilibrium, as it consists of martensite at room temperature, as a consequence of the very high temperature gradient characterizing the process. The DMLS microstructure provokes higher strength but lower ductility [1, 3, 5].

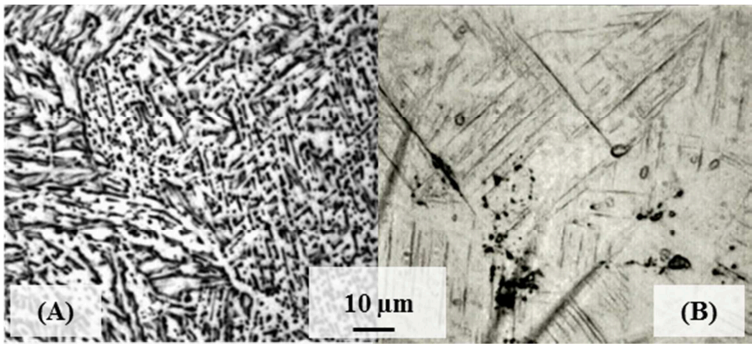

Fig. 1. *As-delivered microstructure of the Ti-6Al-4V produced by means of (A) EBM and (B) DMLS*

Design of experiments and set-up. The experiments were carried out on an ultra-precision, Kugler™ Micromaster 5-axis micro-milling machine, equipped with a granite structure, in an air-conditioned room, to ensure constant temperature conditions. The machine is also equipped with an eddy current sensor that permits on-line control and compensation of the possible expansion of the air bearing spindle, which can reach speeds up to 180 000 RPM. The chosen machining strategy was the full immersion slotting with a slot width of 0.3 mm, length 25 mm and constant depth of the cut equal to 30 µm. The scheme of the slot geometry is shown in Fig. 2. All the experiments were conducted under dry lubrication conditions, which is particularly interesting for biomedical applications, to favour the component cleanliness. A full factorial design of experiments was used with two factors, namely the cutting speed and feet per tooth with two and four levels, respectively (see Table 1). Each experiment was repeated twice.

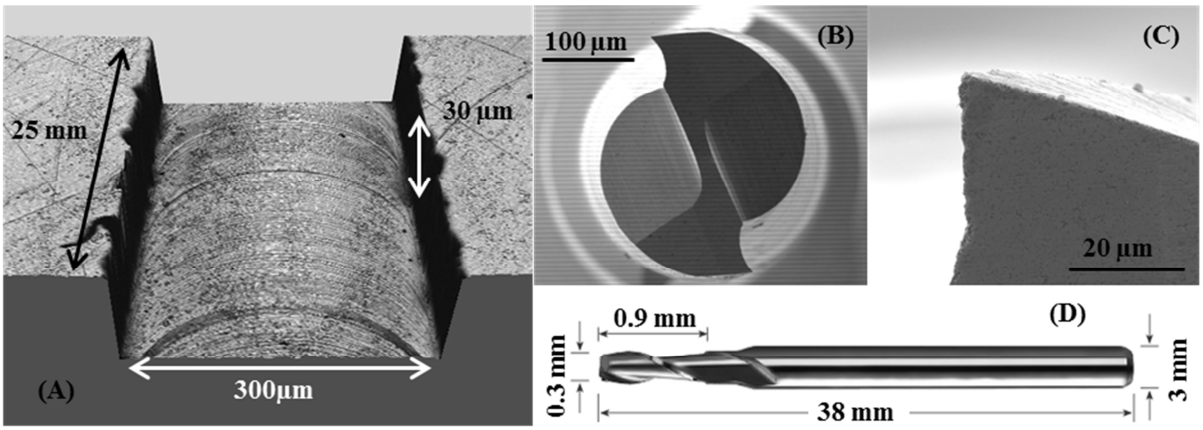

Fig. 2. *(A) Machining strategy: full immersion slotting with constant depth of cut equal to 30 µm; tool geometry: (B) top view, (C) detail of the cutting edge radius, (D) tool dimensions*

Table 1 *Cutting conditions used during the micro-milling experiments*

	Level 1	Level 2	Level 3	Level 4
Factor A – cutting speed v_c [m/min]	63	145	-	-
Factor B – feed per tooth f_z [µm/tooth]	0.1	0.5	1.5	3.0

Uncoated tungsten carbide tools were used, with a square flat-end geometry, two flutes, a diameter of 0.3 mm and cutting edge radius of about 1.1 µm, which leads to the critical feed per tooth of 0.33–0.44 µm/tooth (see Fig. 2). Each tool was inspected before machining to avoid any possible defects due to its fabrication.

Results

Surface topography and roughness. Fig. 3 shows images of the slots bottom acquired by using a FEI™ Quanta 400 SEM and a Sensofar™ PLμ Neox confocal optical profiler. Regardless of the cutting speed and material microstructure, we can appreciate the same trend in the surface topography as a function of the feed per tooth. For the lowest value of the feed per tooth, the surface quality is very poor, due to the ploughing mechanism that prevails over shearing, whereas, when increasing the feed per tooth, the feed marks become more regular. The roughness values were measured with the confocal optical profiler, using a 100x lens characterized by a field of view of 127x97 μm^2 and vertical resolution of about 5 nm, at a distance of 12.5 mm from the edge, following the ISO 25178 standard. Stitching of 21x1 or 51x1 images was acquired with 25% of overlapping, while the values of the cut-offs λ_c were 0.25 and 0.8 mm, considering the arithmetic mean of 10 different profiles. Fig. 4 shows the profile roughness as a function of the cutting parameters and initial material microstructure: the lowest feed per tooth always produces high roughness, because of the ploughing mechanism, whereas at increasing feed per tooth the roughness first decreases, then increases again at the highest feed per tooth, as it happens in the case of macro-machining.

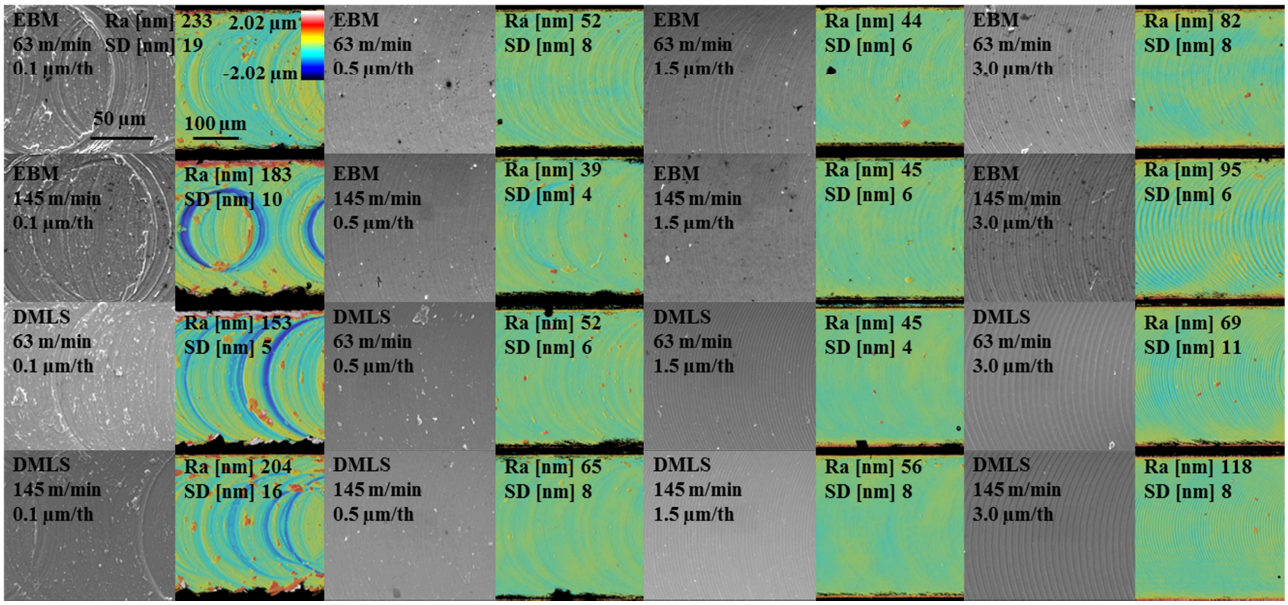

Fig. 3. *Images of the bottom of the slots acquired using SEM and optical confocal profiler*

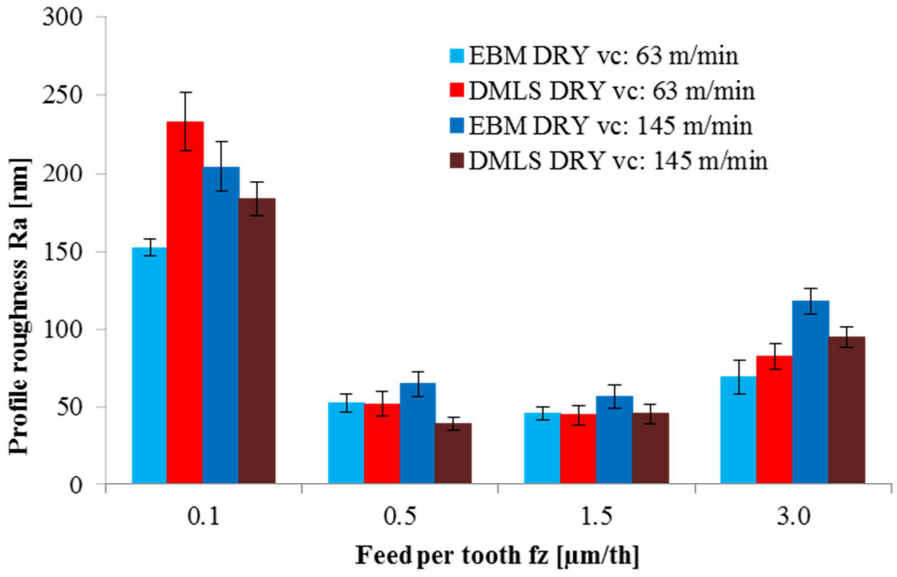

Fig. 4. *. Profile roughness as a function of the feed per tooth for different cutting speeds and material microstructure*

Surface defects. Fig. 5 shows the surface defects revealed at the bottom of the slots after micro-milling. We can see mainly smeared material at the highest value of the feed per tooth and a few chips debris. In the case of the lowest feed per tooth, being the ploughing predominant, the surface is highly perturbed, with a significant amount of defects.

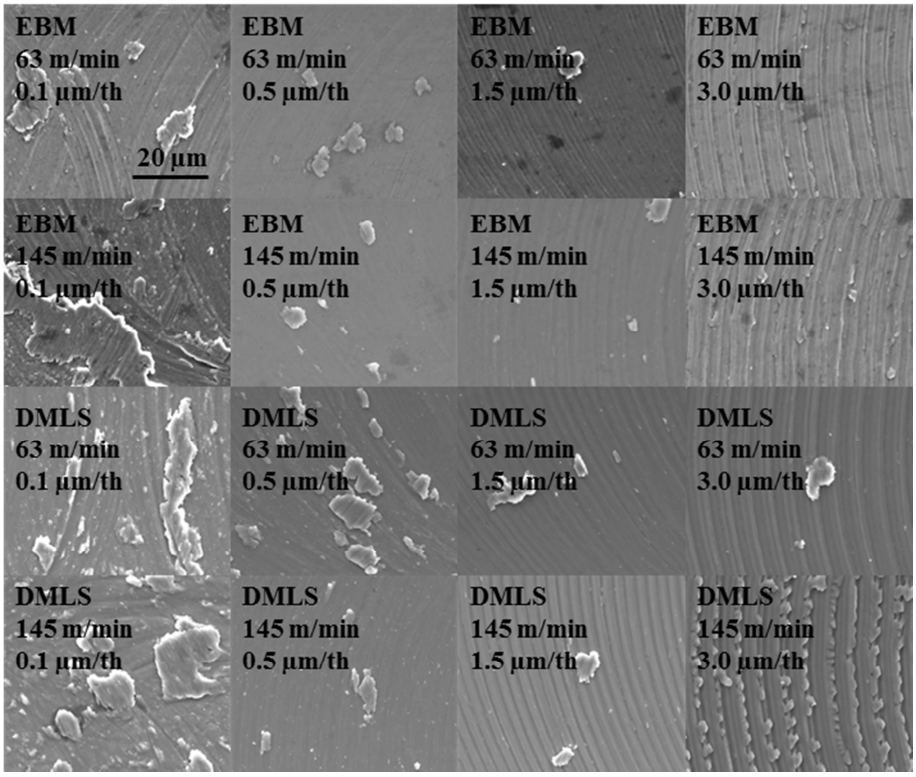

Fig. 5. *Surface defects at the bottom of the slots after micro-milling*

Burrs formation. Burrs can be found for all the combinations of the cutting parameters. Since their removal is highly complicated in micro-components, they should be minimised as much as possible by choosing the most appropriate cutting conditions. Fig. 6 shows the top burrs of the slots after micro-milling: again, it can be seen that the influence of the feed per tooth is predominant over the cutting speed. A minimum amount of burrs is evident at increasing feed per tooth regardless of the material initial microstructure. Fig 7 shows the associated burr height: the trend is similar, since at increasing feed per tooth the burr height decreases. The burr height was measured at the base of 1 mm long scans acquired by the optical confocal profiler. Then, ten random and independent cross sections were measured and their mean value was calculated.

Tool state. All the tools were inspected before and after the micro-milling experiments to evaluate their state. In all the cases, adhesion of the workpiece material to the tool can be found, to a different extent on the basis of the specific cutting conditions. Fig. 8 shows an example of two tools that machined EBM and DMLS Ti-6Al-4V at 63 m/min and 1.5 µm/tooth: the material adhesion on the cutting edge is evident, as witnessed by the EDS analysis.

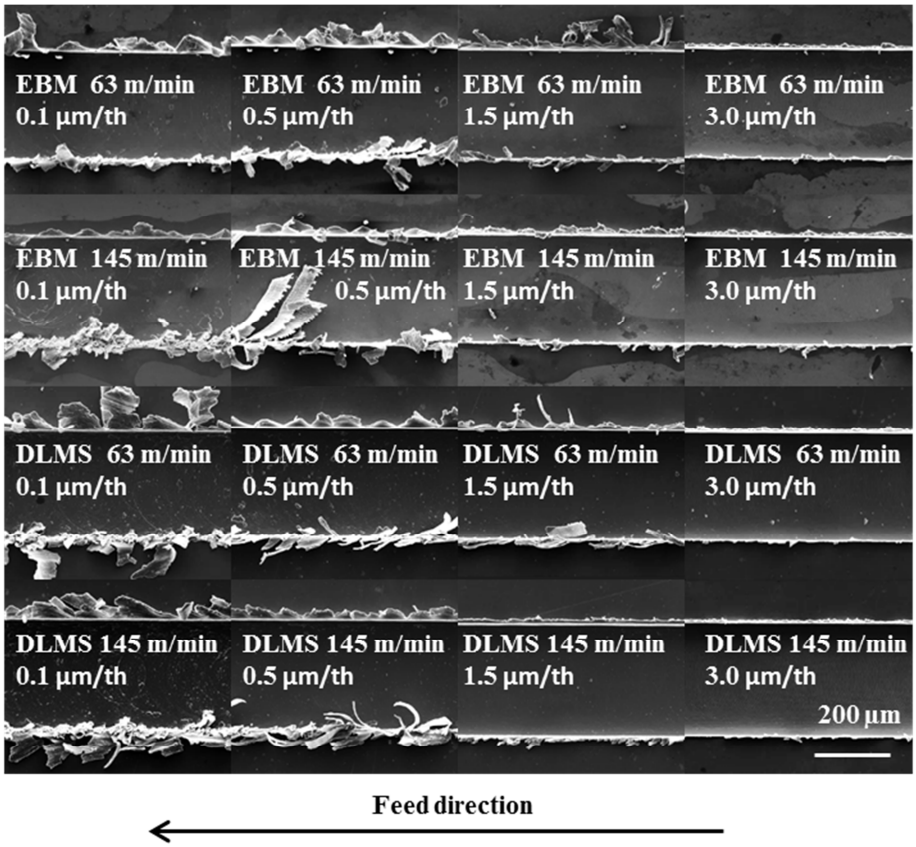

Fig. 6. *Burrs shape for difference cutting conditions*

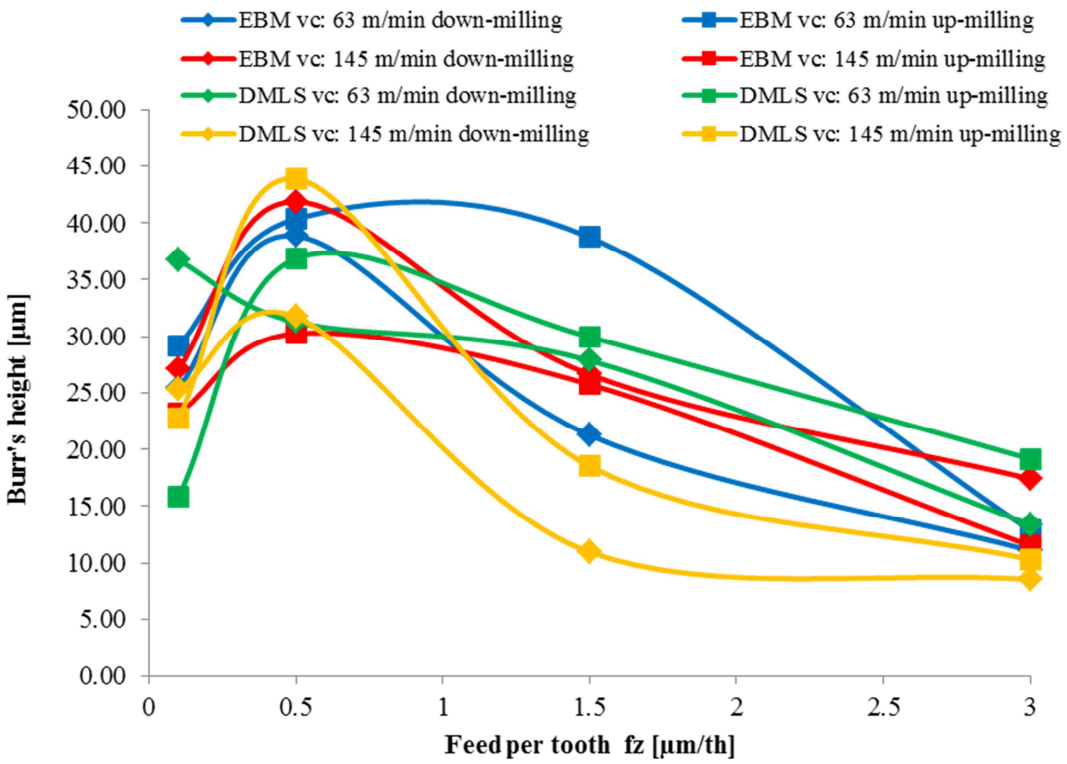

Fig. 7. *Burr height as a function of the feed per tooth*

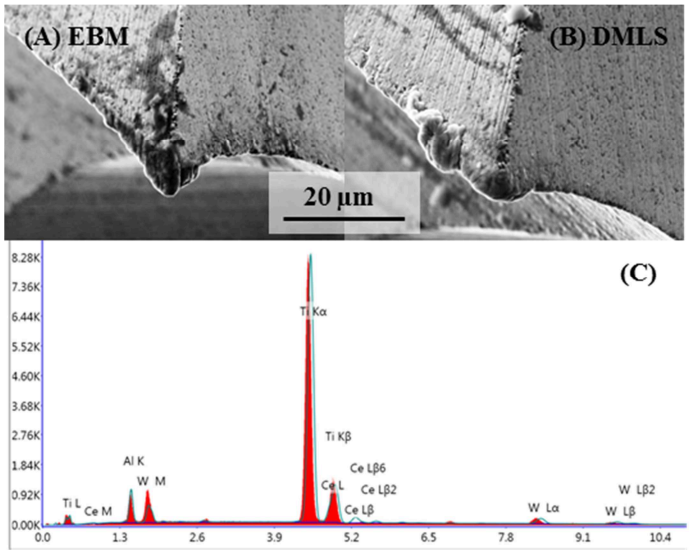

Fig. 8. *Cutting edges after machining at 63 m/min and 1.5 µm/tooth (A) EBM sample and (B) DMLS sample, (C) EDS analysis of the material adhered on the cutting edge*

Microstructure alterations. Metallographic samples after machining were prepared by polishing using different abrasive papers, grinding by using colloidal silica and chemical etching by using the Kroll's reagent. The microstructural observations were carried out using both the optical microscope Leica™ and the FEI™ Quanta 400 SEM. No changes in the microstructure or evidence of recrystallization were found; only some bending of the EBM lamellas near to the slots walls can be appreciated. The absence of microstructural alterations can be explained by the fact that both the temperatures and forces generated during micro-milling are lower than in macro-machining [15]. Fig. 9 shows the microstructures at the slots cross-section, which were machined at 63 m/min and 1.5 µm/tooth: in case (A) the machined material was the EBM and in case (B) the DMLS.

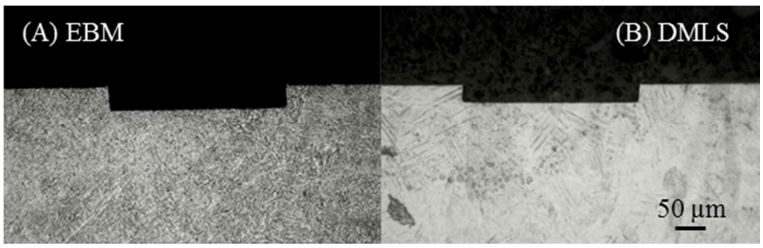

Fig. 9.*Cross section of slots machined at 63 m/min and 1,5 µm/tooth in (A) EBM workpiece and (B) corresponds to DMLS workpiece*

Concluding remarks

Micro-milling characteristics of EBM and DMLS Ti-6Al-4V alloy were compared in terms of surface topography, roughness, burrs formation, surface defects, tool damage and microstructural alterations.

- The most important cutting parameter is the feed per tooth that directly influences the final surface roughness and burrs formation. For the higher values of the feed per tooth the burrs are minimal but the surface roughness starts to increase. Within the range of the tested values of the feed per tooth, the optimal one with regard to the best possible surface roughness and minimal burrs was 1.5 µm/tooth, regardless of the material initial microstructure.
- Concerning the cutting speed, for the lowest value of 63 m/min there are nearly no differences in roughness for the different microstructures, but at the highest cutting speed, the DMLS Ti-6Al-4V presents a smoother surface. Also for the highest cutting speed combined with low feed per tooth, the amount of burrs is higher, especially in the case of up-milling conditions.

- No microstructure alterations were observed.
- The occurrence of surface defects is mainly influenced by the feed per tooth and they are analogous in both the microstructural cases.
- Mainly adhered material on the tool edges was observed, rather than abrasion wear.

References

[1] L. E. Murr, S. a Quinones, S. M. Gaytan, M. I. Lopez, a Rodela, E. Y. Martinez, D. H. Hernandez, E. Martinez, F. Medina, and R. B. Wicker, Microstructure and mechanical behavior of Ti-6Al-4V produced by rapid-layer manufacturing, for biomedical applications., J. Mech. Behav. Biomed. Mater., vol. 2, no. 1, pp. 20–32, Jan. 2009.

[2] O. L. a. Harrysson, O. Cansizoglu, D. J. Marcellin-Little, D. R. Cormier, and H. a. West, Direct metal fabrication of titanium implants with tailored materials and mechanical properties using electron beam melting technology, Mater. Sci. Eng. C, vol. 28, no. 3, pp. 366–373, Apr. 2008.

[3] T. Traini, C. Mangano, R. L. Sammons, F. Mangano, a Macchi, and a Piattelli, Direct laser metal sintering as a new approach to fabrication of an isoelastic functionally graded material for manufacture of porous titanium dental implants., Dent. Mater., vol. 24, no. 11, pp. 1525–33, Nov. 2008.

[4] T. Özel, T. Thepsonthi, D. Ulutan, and B. Kaftanoğlu, Experiments and finite element simulations on micro-milling of Ti–6Al–4V alloy with uncoated and cBN coated micro-tools, CIRP Ann. - Manuf. Technol., vol. 60, no. 1, pp. 85–88, Jan. 2011.

[5] T. Masuzawa, State of the Art of Micromachining, CIRP Ann. - Manuf. Technol., vol. 49, no. 2, pp. 473–488, 2000.

[6] S. Filiz, C. M. Conley, M. B. Wasserman, and O. B. Ozdoganlar, An experimental investigation of micro-machinability of copper 101 using tungsten carbide micro-endmills, Int. J. Mach. Tools Manuf., vol. 47, no. 7–8, pp. 1088–1100, Jun. 2007.

[7] T. Özel, X. Liu, and A. Dhanorker, Modelling and simulation of micro-milling process, ... Exhib. Des. Prod. ..., 2007.

[8] D. Dornfeld, S. Min, and Y. Takeuchi, Recent advances in mechanical micromachining, CIRP Ann. Technol., vol. 55, no. 2, pp. 745–768, Jan. 2006.

[9] X. Liu, R. E. DeVor, and S. G. Kapoor, An Analytical Model for the Prediction of Minimum Chip Thickness in Micromachining, J. Manuf. Sci. Eng., vol. 128, no. 2, p. 474, 2006.

[10] S. A. Lawal, I. A. Choudhury, and Y. Nukman, A critical assessment of lubrication techniques in machining processes: A case for minimum quantity lubrication using vegetable oil-based lubricant, J. Clean. Prod., vol. 41, pp. 210–221, 2013.

[11] K. M. Li and S. Y. Chou, Experimental evaluation of minimum quantity lubrication in near micro-milling, J. Mater. Process. Technol., vol. 210, no. 15, pp. 2163–2170, 2010.

[12] E. Vazquez, J. Gomar, J. Ciurana, and C. a. Rodríguez, Analyzing effects of cooling and lubrication conditions in micromilling of Ti6Al4V, J. Clean. Prod., vol. 87, pp. 906–913, 2015.

[13] M. Sarıkaya and A. Güllü, Multi-response optimization of minimum quantity lubrication parameters using Taguchi-based grey relational analysis in turning of difficult-to-cut alloy Haynes 25, J. Clean. Prod., vol. 91, pp. 347–357, 2015.

[14] L. Facchini, Microstructure and mechanical properties of biomedical alloys produced by Rapid Manufacturing techniques, Univeristy of Trento, Italy, 2010.

[15] K. Yang, Y. Liang, K. Zheng, Q. Bai, and W. Chen, Tool edge radius effect on cutting temperature in micro-end-milling process, Int. J. Adv. Manuf. Technol., vol. 52, no. 9–12, pp. 905–912, Jun. 2010.

12th International Conference on High Speed Machining
10.4028/www.scientific.net/MSF.836-837

Comparison between EBM and DMLS Ti6Al4V Machinability Characteristics under Dry Micro-Milling Conditions
10.4028/www.scientific.net/MSF.836-837.177

DOI References
[1] L. E. Murr, S. a Quinones, S. M. Gaytan, M. I. Lopez, a Rodela, E. Y. Martinez, D. H. Hernandez, E. Martinez, F. Medina, and R. B. Wicker, Microstructure and mechanical behavior of Ti-6Al-4V produced by rapid-layer manufacturing, for biomedical applications., J. Mech. Behav. Biomed. Mater., vol. 2, no. 1, pp.20-32, Jan. (2009).
10.1016/j.jmbbm.2008.05.004
[2] O. L. a. Harrysson, O. Cansizoglu, D. J. Marcellin-Little, D. R. Cormier, and H. a. West, Direct metal fabrication of titanium implants with tailored materials and mechanical properties using electron beam melting technology, Mater. Sci. Eng. C, vol. 28, no. 3, pp.366-373, Apr. (2008).
10.1016/j.msec.2007.04.022
[3] T. Traini, C. Mangano, R. L. Sammons, F. Mangano, a Macchi, and a Piattelli, Direct laser metal sintering as a new approach to fabrication of an isoelastic functionally graded material for manufacture of porous titanium dental implants., Dent. Mater., vol. 24, no. 11, pp.1525-33, Nov. (2008).
10.1016/j.dental.2008.03.029
[4] T. Özel, T. Thepsonthi, D. Ulutan, and B. Kaftanoğlu, Experiments and finite element simulations on micro-milling of Ti-6Al-4V alloy with uncoated and cBN coated micro-tools, CIRP Ann. - Manuf. Technol., vol. 60, no. 1, pp.85-88, Jan. (2011).
10.1016/j.cirp.2011.03.087
[5] T. Masuzawa, State of the Art of Micromachining, CIRP Ann. - Manuf. Technol., vol. 49, no. 2, pp.473-488, (2000).
10.1016/s0007-8506(07)63451-9
[6] S. Filiz, C. M. Conley, M. B. Wasserman, and O. B. Ozdoganlar, An experimental investigation of micro-machinability of copper 101 using tungsten carbide micro-endmills, Int. J. Mach. Tools Manuf., vol. 47, no. 7-8, pp.1088-1100, Jun. (2007).
10.1016/j.ijmachtools.2006.09.024
[8] D. Dornfeld, S. Min, and Y. Takeuchi, Recent advances in mechanical micromachining, CIRP Ann. Technol., vol. 55, no. 2, pp.745-768, Jan. (2006).
10.1016/j.cirp.2006.10.006
[9] X. Liu, R. E. DeVor, and S. G. Kapoor, An Analytical Model for the Prediction of Minimum Chip Thickness in Micromachining, J. Manuf. Sci. Eng., vol. 128, no. 2, p.474, (2006).
10.1115/1.2162905
[10] S. A. Lawal, I. A. Choudhury, and Y. Nukman, A critical assessment of lubrication techniques in machining processes: A case for minimum quantity lubrication using vegetable oil-based lubricant, J. Clean. Prod., vol. 41, pp.210-221, (2013).
10.1016/j.jclepro.2012.10.016
[11] K. M. Li and S. Y. Chou, Experimental evaluation of minimum quantity lubrication in near micro-milling, J. Mater. Process. Technol., vol. 210, no. 15, pp.2163-2170, (2010).
10.1016/j.jmatprotec.2010.07.031

[12] E. Vazquez, J. Gomar, J. Ciurana, and C. a. Rodríguez, Analyzing effects of cooling and lubrication conditions in micromilling of Ti6Al4V, J. Clean. Prod., vol. 87, pp.906-913, (2015). 10.1016/j.jclepro.2014.10.016
[13] M. Sarıkaya and A. Güllü, Multi-response optimization of minimum quantity lubrication parameters using Taguchi-based grey relational analysis in turning of difficult-to-cut alloy Haynes 25, J. Clean. Prod., vol. 91, pp.347-357, (2015). 10.1016/j.jclepro.2014.12.020
[15] K. Yang, Y. Liang, K. Zheng, Q. Bai, and W. Chen, Tool edge radius effect on cutting temperature in micro-end-milling process, Int. J. Adv. Manuf. Technol., vol. 52, no. 9-12, pp.905-912, Jun. (2010). 10.1007/s00170-010-2795-z

11th International Conference on Micro Manufacturing
Orange County, California, USA, March 2016

Paper# 5

Process parameters optimisation in micro-milling DMLS Ti6Al4V

Zdenka Rysava[1] Stefania Bruschi[1] Giovanni Lucchetta[1] Marco Sorgato[1]

[1] *Department of Industrial Engineering, University of Padova, Italy*

Abstract

This paper is aimed at optimising the parameters of micro-milling in order to improve the part surface integrity when the micro-machining operation is conducted on the Ti6Al4V Titanium alloy produced by means of Direct Metal Laser Sintering (DMLS), an Additive Manufacturing (AM) technology. This AM technology is widely used in the biomedical sector to produce near-net-shape prostheses with tailored properties, while reducing the material waste and manufacturing steps compared to the traditional process chains. As the machined surface finish after AM may not meet the requirements, finishing or semi-finishing machining operations can be necessary. The DMLS Ti6Al4V surface integrity was studied in terms of surface roughness, burrs, and surface defects as a function of the cutting speed and feed per tooth.

Keywords: Micro-milling, Titanium alloy, Additive manufacturing.

1. Introduction

The Ti6Al4V titanium alloy is used in a very wide range of applications thanks to its high strength-to-weight ratio, corrosion and mechanical resistances. Furthermore, its outstanding biocompatibility makes it one of the most used metal alloys for manufacturing prostheses. The biomedical components requirements are high as they are implanted into alive bodies and remain in contact with the human tissues. In the ISO 5832 standard (Implants for surgery € Metallic materials) chemical composition and mechanical characteristics with suggested, not suggested and rejected microstructures are listed. [1] Additive Manufacturing (AM) includes highly attractive technologies to produce Ti6Al4V implants and its popularity and use are increasing in recent years. [2] The AM advantages include the reduction of material waste, possibility to obtain tailored properties, and reduction of the manufacturing steps compared to the traditional long process chains, by producing near-net-shape products, which, however, may still need finishing or semi-finishing machining operations on the functional surfaces. [1, 3] On the other hand, the microstructures obtained after AM are very peculiar and far different from the ones obtained in standard production processes. Lamellar, very fine acicular or metastable martensitic microstructures can be mostly found [1], which can significantly affect the material machinability and the machined surface integrity compared to the wrought ones that are traditionally used. A proper evaluation of the machined surface integrity is particularly crucial as is the characteristic that mainly ensures the in-vivo functionalities of the implants (contact between implants and tissues, transferring of loads etc.). [4, 5] The paper focuses on the optimization of the cutting parameters to improve the machined surface integrity in case of micro-milling Ti6Al4V obtained by Direct Metal Laser Sintering (DMLS) and it is continuation of a previous research study conducted on another AM material. [6] This specific AM technology is used to manufacture dental implants, which present some miniature features (e.g. internal features such as threading, hexagon for spanner, etc.) in the order of hundreds microns to few millimetres that cannot be produced by AM and need to be later on machined; furthermore, some functional surfaces, such as the upper face of the dental pin, need to be machined in order to reach the required tolerances and surface finish for subsequent assembly. Whereas in literature some records about the micro-

milling process on the wrought Ti6Al4V can be found [5€7], the micro-milling performances on titanium alloys produced by AM remain still almost unexplored. The machined surface integrity of DMLS Ti6Al4V is here evaluated in terms of surface topography and defects, as well as burrs characteristics in order to identify the set of cutting parameters guaranteeing the best compromise between the different performances.

2. Experimental

2.1. Material

The Ti6Al4V titanium alloy used for this study was produced by DMLS, an AM technique able to create a fully dense material with a very fine martensitic microstructure consisting of only • (hcp) grains. [1] As this microstructure is not accepted by the ISO 5832 standard, a subsequent heat treatment was carried out on the DMLS Ti6Al4V samples, by increasing the material temperature above the β-transus temperature, and then cooling down in order to obtain a final microstructure consisting of α and β coarse lamellas as shown in Fig. 1.

Fig. 1. DMLS Ti6Al4V coarse lamellar microstructure after the heat treatment

2.2. Micro-machining experiments

The micro-milling experiments were carried out on a high-precision 5-axis micro-milling centre Kugler, . The machine is equipped with air-bearing spindle that can reach up to 180000 RPM. The thermal extension of the spindle axis is measured by built-in eddy current sensor and is compensated in real time.

Two fluted flat-end-square, uncoated, tungsten carbide tools (Kyocera € solid round € square end mill € series 1610) were used for all the experiments. The tool dimensions are shown in Fig. 2 with the detail of the cutting edge. Each tool was checked through SEM observations before machining to evaluate any possible imperfection.

Table 1. Experimental plan for the micro-milling experiments

#	Cutting speed v_c (m/min)	Feed per tooth fz (µm)
S01	63	0.1
S02	63	0.5
S03	63	1.5
S04	63	3.0
S05	149	0.1
S06	149	0.5
S07	149	1.5
S08	149	3.0

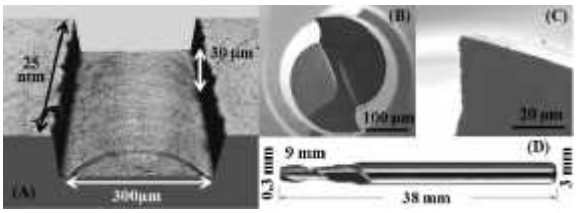

Fig. 2 (a) Geometry of the machined slot, (b) Detail of the tool diameter, (c) Detail of the cutting edge, (d) Tool dimensions

A full factorial design of experiments was chosen for carrying out the micro-machining experiments, using two factors, the cutting speed and feed per tooth with two and four levels, respectively. Each experiment was repeated twice.

The full immersion slotting was applied as machining strategy; the radial depth of cut corresponded to the tool diameter and the axial depth of the cut was set constant for all the experiments and equal to 30 µm, which is a suitable value for semi-finishing/finishing cutting. The machining was carried out under dry cutting conditions, and compressed air was sprayed on the tool and into the slot to facilitate the chips removal. The schematic geometry of the slot is shown in Fig. 2 (a) while the cutting parameters are listed in Table 1. Two factors of two and four levels were considered in the experimental plan, namely the cutting speed and the feed per tooth, whose lowest value was chosen to evidence the occurrence of the ploughing phenomenon and its influence on the machined surface integrity.

3. Results

3.1. Surface topography

In order to evaluate the surface integrity, the machined surface topography was measured. Topographies were sampled by using a Sensofar, PL*f* Neox confocal optical profiler. The instrument was equipped with a 100x lens characterized by a field of view of 127x97 fm^2 and a vertical resolution of about 5 nm. The profile roughness was evaluated on the basis of the ISO 4288 standard. Depending on the expected mean width of profile elements (RSm parameter) values, different length was acquired; in this way, stitching respectively of 21x1 and 51x1 images was applied and later cut-off λ_c value 0.08 mm was used. Ten values of the profile roughness, at different random locations along the sampled length, were taken and their mean value calculated.

In Fig. 3 the graph of the profile roughness as a function of the feed per tooth is represented. For the lowest value of the feed per tooth the profile roughness is quite high, as a consequence of the ploughing regime that prevails over shearing, because the criterion of the minimum uncut chip thickness is not respected, and, therefore, the material is mainly plastically deformed rather than cut [8-9].

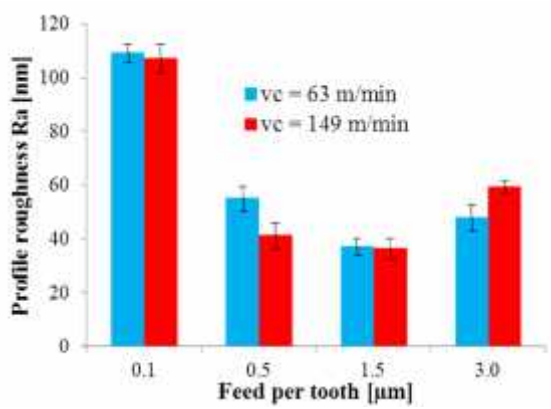

Fig. 3 Influence of the feed per tooth on the profile roughness

Once the minimum uncut chip thickness criterion is fulfilled, the roughness values drop down, to increase again with increasing the feed per tooth as it is observed in conventional macro-machining. The same figure shows that the influence of the cutting speed is negligible compared to the one of the feed per tooth.

Fig. 4 shows the surface scans acquired by the SEM and confocal optical profiler. In agreement with the results shown in Fig. 3, the lowest feed per tooth provokes a highly perturbed surface as discussed before, regardless the cutting speed.

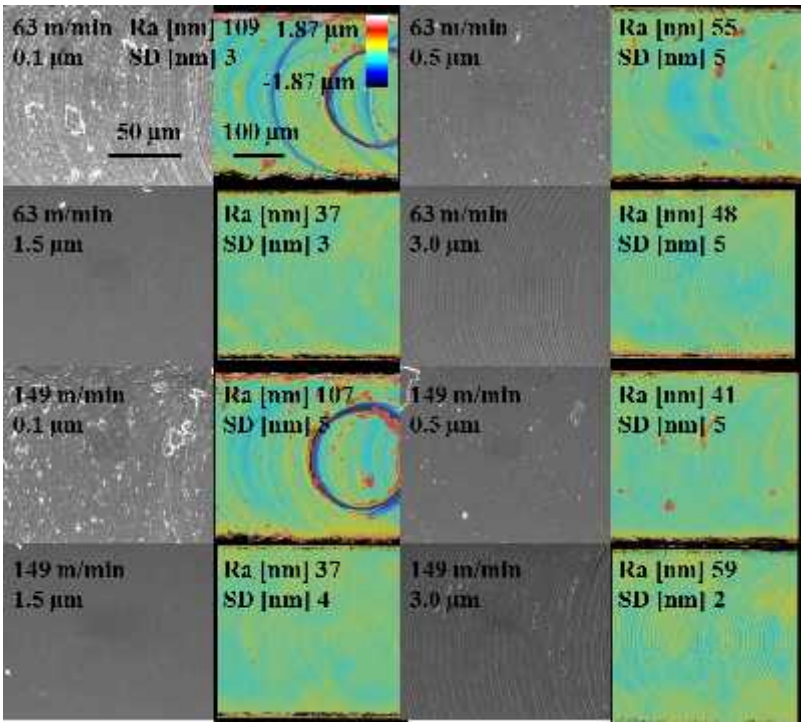

Fig. 4 Surface scans acquired by SEM and confocal optical profiler

3.2.Burrs analysis

The evaluation of burrs occurrence and their quantification is fundamental as their presence can lead to reduction of functionalities especially in assembly and the process of deburring is challenging particularly in case of micro-sized parts. Burrs are characterised as deviation from the ideal edge. [11] A qualitative analysis was first based on SEM images (Fig. 5): it is clearly visible that at increasing the feed per tooth, burrs seem to be minimised, regardless the cutting speed.

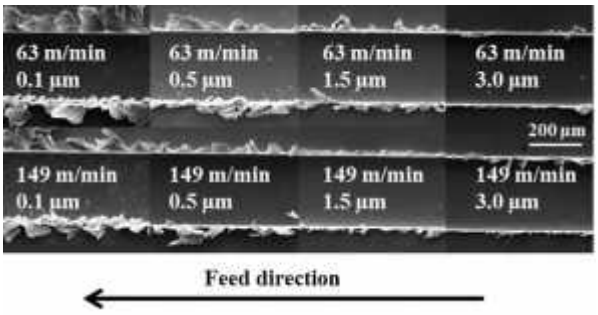

Fig. 3 Burrs after micro-milling as a function of the cutting parameters

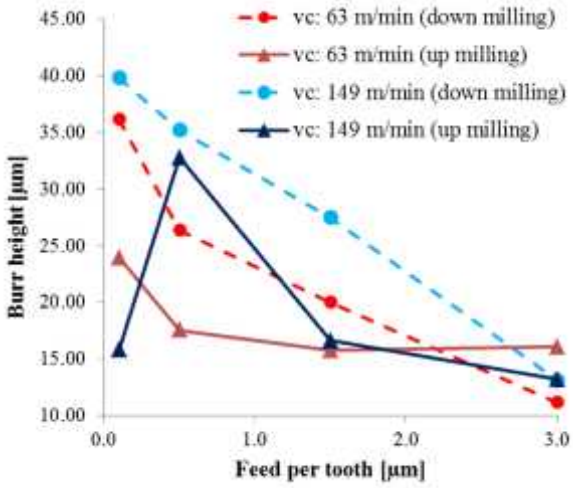

Fig. 4 Burrs height as a function of the feed per tooth (overall Std of 11µm)

Fig. 6 shows the graph of the burrs height as a function of the feed per tooth. Scans of the burrs were acquired using the confocal optical profiler for both the milling conditions (up and down milling). 1mm long scans were taken, and the acquired clouds of points analysed through a newly developed Matlab, script. From the cloud of points the surface was reconstructed. At each coordinate (acquired along the slot length), from the surface profile the mean burr height was calculated in order to obtain a profile of mean burrs height along the acquired slot length; finally, from these values the overall mean burr height was calculated. From the graph of Fig. 6 it can be seen that at increasing the feed per tooth, the burr height decreases, which is in accordance with the qualitative analysis of Fig. 5.

3.3. Surface defects

In this case study, mainly some chips debris were found on the machined surface for the lowest values of the feed per tooth (0.5 and 1.5 µm) and some smeared material for the highest feed per tooth (3.0 µm). At the lowest feed per tooth, as the ploughing mechanism prevails over shearing, the surface is highly perturbed as shown in Fig. 7.

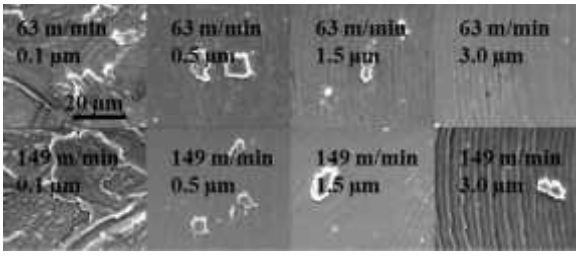

Fig. 5 Surface defects as a function of the cutting parameters

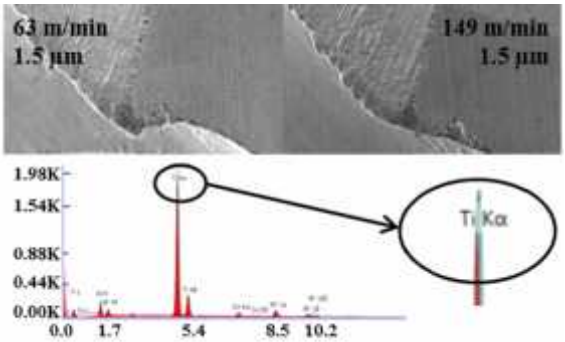

Fig. 6 Tool state after machining and proof of the adhesion of the workpiece material on the cutting edge

3.4. Tool state

Every tool was checked before machining and once again after machining. For each cutting condition a fresh tool was used to minimise the effect of the tool

state on the surface integrity evaluation. The tool state was qualitatively evaluated through SEM observations and the EDS analysis was used to verify the origin of the material adhered on the tool. It is proven that material from the workpiece adhered on the cutting edge as shown in the Fig. 8.

3.5. ANOVA analysis

An ANOVA analysis was carried out to verify the significance of the cutting parameters on the machine surface integrity characteristics. As regards the profile roughness, the most significant parameter is feed per tooth (P=0.000) compared to the cutting speed (P=0.721), moreover the model is covering about 97% of cases, which is in accordance with the results shown in Fig. 3. and Fig. 4.

In the case of the mean burr height in up milling, the feed per tooth appears to be more significant (P=0.046) than the cutting speed (P=0.301), whereas the case of down milling both the factors feed per tooth (P=0.340) and cutting speed (P=0.764) seem to be not significant, as the related models cover a quite low percentage of cases, 65% and 51% respectively. This can be explained by the fact that the process of burr formation is very complex and more factors may influence it than the sole cutting speed and feed per tooth. More tests are needed to develop a model than can satisfactorily explain burr formation. The results of the ANOVA analysis are shown in Fig. 9.

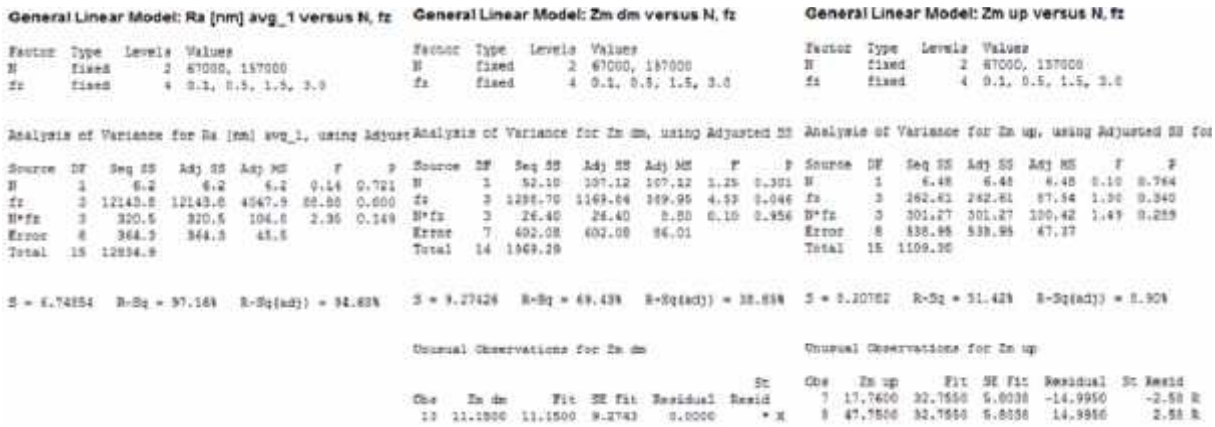

Fig. 9 ANOVA analysis for the profile roughness and mean height of burr (down/up milling) as a function of the cutting speed and feed per tooth

4. Concluding remarks

Titanium alloys fabricated by AM techniques exhibit different microstructures compared to the wrought material, which may affect the machinability and machined surface integrity as a function of the cutting parameters. In case of micro-milling, it is proved that the feed per tooth is the cutting parameter that mostly affects the machined surface integrity, being related to the minimum uncut chip thickness criterion. The feed increase leads to the burr size minimization, but, on the other hand, increases the surface roughness. Therefore, the best cutting conditions must be a trade-off between the surface topography and the burrs characteristics as a function of the final application: in the presented research, the best trade-off between minimal burr size and minimal profile roughness is achieved when using a feed per tooth equal to 1.5 μm. Finally, it is proved that the cutting speed has a negligible impact compared to the feed per tooth. This statement is supported by the ANOVA analysis, which shows the effect of the feed per tooth on the surface roughness (P=0.000) compared to the one of the cutting speed (P=0.721). In the case of the mean burr height, the difference between the feed per tooth and cutting speed is not evident; furthermore, the model does not cover all the cases, due to the complexity of the burr formation, which may be influenced by more factors than the sole cutting speed and feed per tooth.

References

[1] L. Facchini, „Microstructure and mechanical

properties of biomedical alloys produced by Rapid Manufacturing techniques,… Univeristy of Trento, Italy, 2010.

[2] P. Bartolo, J.-P. Kruth, J. Silva, G. Levy, A. Malshe, K. Rajurkar, M. Mitsuishi, J. Ciurana, and M. Leu, „Biomedical production of implants by additive electro-chemical and physical processes,… *CIRP Ann. - Manuf. Technol.*, vol. 61, no. 2, pp. 635€655, Jan. 2012.

[3] L. E. Murr, S. M. Gaytan, a. Ceylan, E. Martinez, J. L. Martinez, D. H. Hernandez, B. I. Machado, D. a. Ramirez, F. Medina, and S. Collins, „Characterization of titanium aluminide alloy components fabricated by additive manufacturing using electron beam melting,..*Acta Mater.*, vol. 58, no. 5, pp. 1887€1894, Mar. 2010.

[4] I. S. Jawahir, E. Brinksmeier, R. M†Saoubi, D. K. Aspinwall, J. C. Outeiro, D. Meyer, D. Umbrello, and a. D. Jayal, „Surface integrity in material removal processes: Recent advances,..*CIRP Ann. - Manuf. Technol.*, vol. 60, no. 2, pp. 603€626, 2011.

[5] T. Thepsonthi and T. ‡zel, „Experimental and finite element simulation based investigations on micro-milling Ti-6Al-4V titanium alloy: Effects of cBN coating on tool wear,..*J. Mater. Process. Technol.*, vol. 213, no. 4, pp. 532€542, Apr. 2013.

[6] Z. Rysava, G. Tristo, and S. Bruschi, „Process parameters optimization for micro-milling of EBM Ti6Al4V titanium alloy,..*Proc. 4M/ICOMM2015 Conf.*, 2015.

[7] T. ‡zel, T. Thepsonthi, D. Ulutan, and B. Kaftanoˆlu, „Experiments and finite element simulations on micro-milling of Ti€6Al€4V alloy with uncoated and cBN coated micro-tools,..*CIRP Ann. - Manuf. Technol.*, vol. 60, no. 1, pp. 85€88, Jan. 2011.

[8] T. Thepsonthi and T. ‡zel, „Multi -objective process optimization for micro-end milling of Ti-6Al-4V titanium alloy,…*Int. J. Adv. Manuf. Technol.*, vol. 63, no. 9€12, pp. 903€914, Mar. 2012.

[9] T. ‡zel, X. Liu, and A. Dhanorker, „Modelling and simulation of micro-milling process,…*€ Exhib. Des. Prod. €* , 2007.

[10] X. Liu, R. E. DeVor, and S. G. Kapoor, „An Analytical Model for the Prediction of Minimum Chip Thickness in Micromachining,..*J. Manuf. Sci. Eng.*, vol. 128, no. 2, p. 474, 2006.

[11] L. Piln‰, L. De Chiffre, M. PŠ‹ka, and M. F. Villumsen, „Hole quality and burr reduction in drilling aluminium sheets,…*CIRP J. Manuf. Sci. Technol.*, vol. 5, no. 2, pp. 102€107, Jan. 2012.

Available online at www.sciencedirect.com

ScienceDirect

Procedia CIRP 46 (2016) 583 – 586

www.elsevier.com/locate/procedia

7th HPC 2016 – CIRP Conference on High Performance Cutting

Micro-drilling and threading of the Ti6Al4V titanium alloy produced through Additive Manufacturing

Zdenka Rysava[a]*, Stefania Bruschi[a], Simone Carmignato[b], Fabrizio Medeossi[a], Enrico Savio[a], Filippo Zanini[a,b]

[a]*Departement of Industrial Engineering, University of Padua, Via Venezia 1, Padova 35131, Italy*
[b]*Department of Management and Engineering, University of Padua, Stradella San Nicola, Vicenza 36100, Italy*

* Corresponding author. Tel.: +39-3246278654; fax: +39-0498276818. *E-mail address:* zdenka.rysava@studenti.unipd.it

Abstract

The paper presents the evaluation of the drillability characteristics of the Ti6Al4V titanium alloy produced through the Additive Manufacturing (AM) technology called Direct Metal Laser Sintering (DMLS). Holes of 1.6 mm diameter were drilled on a 5-axis high-precision micro-milling machine under dry cutting conditions at varying cutting speed and feed rate. A specific measurement procedure was developed to quantify and compare the most representative geometrical features (diameter and perpendicularity) of the machined holes as well as the quantification of burrs. The influence of the AM material on the geometrical quality of high precision holes is discussed, taking into account the requirements of the following threading operations. Finally, thread milling experiments were carried out to prove the threading feasibility and performance based on the previous drilling experiments. From the results, within the tested range of cutting conditions, the lowest values of the cutting speed and feed rate seem to be the best trade-off for achieving the required hole quality.

Peer-review under responsibility of the International Scientific Committee of 7th HPC 2016 in the person of the Conference Chair Prof. Matthias Putz

Keywords: Drilling; Titanium alloys; High precision; Additive manufacturing

1. Additive manufacturing of Titanium alloys

In the recent years the studies about Additive Manufacturing (AM) of metallic materials are increasing [1], as AM is being used for a wide range of applications and in different sectors, being the biomedical one of the main. AM can in fact overcome many of the problems usually encountered during the service life of metallic implants. AM parts can be porous and therefore capable of ameliorating the contact with the tissues, reducing the stress shielding, and improving the osseointegration [1-4]. Complex shapes can be also produced making possible the substitution of large parts of missing specifically shaped bones, as in the case of cranioplasty. From the manufacturing point of view, the main advantage of AM is the capability of simplifying the conventional process chain of producing implants, which in general consists of forming processes at elevated temperature, rough and finishing machining, heat treatments, and final polishing. On the contrary, AM can produce near-net-shape parts where just semi-finishing or finishing machining operations are applied to mating surfaces, thus significantly reducing the material waste and manufacturing costs [5]. For example, in case of a knee implant machined from the wrought bar, the material waste due to the machining can reach up to 80% [4]).

The most used material for biomedical applications is the Ti6Al4V titanium alloy thanks to its outstanding properties of biocompatibility, osseointegration, corrosion resistance, specific strength [1,4]. However, its machinability is quiet low [6], especially when produced by AM where the obtained microstructure is very peculiar compared to the wrought material [7], making the choice of appropriate cutting

Peer-review under responsibility of the International Scientific Committee of 7th HPC 2016 in the person of the Conference Chair Prof. Matthias Putz
doi:10.1016/j.procir.2016.04.030

conditions a crucial point in the manufacturing process design.

The case study on which this paper is based is a Ti6Al4V dental pin produced by the Direct Metal Laser Sintering (DMLS) AM technique, which has to be further machined to assure the subsequent assembly with the abutment, crown or as a support for the bridge. First, the drillability of Ti6Al4V samples produced by means of DMLS is evaluated under dry cutting conditions in terms of geometrical accuracy of the drilled holes and the burr formation in order to choose the most suitable cutting parameters to reach the required hole quality. Later on, these drilling parameters are applied to the dental pin and then the threading operation is carried out, proving the capability to obtain accurate geometrical features of the machined thread

2. Micro-drilling and threading

2.1. Case study – dental pins

The CAD model of the final dental pin ready for subsequent assembly and an image of the preformed dental pin produced by DMLS are shown in Fig. 1. The rough surface of the external thread is suitable to be implanted as it is, but both the pin top surface and internal features have to be machined, the latter employing first a drilling operation and then a threading one. The function of the dental pin is to ensure the connection between the jaw, where the pin is screwed in, and the upper part of the implant (abutment and crown); thus, it is mandatory to machine a high precision hole and thread. Since the geometrical quality of the thread depends on the accuracy of the previous drilling operation, drillability tests have to be first performed to choose the best possible combination of cutting speed and feed rate, in order to prepare geometrically adequate holes for the subsequent threading (M2x0.4 into the hole with a depth of 5.8 mm) and final assembly.

2.2. The Ti6Al4V alloy and AM process

The Ti6Al4V Titanium alloy studied in this work was produced by DMLS, which permits to create fully dense material with a very fine martensitic microstructure consisting of only α (hcp) grains as a consequence of the large undercooling undergone by the material during the DMLS process [7].

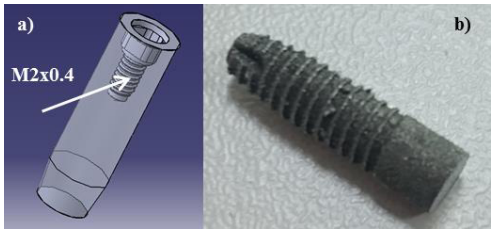

Fig. 1 (a) CAD model of the dental pin (for better visibility the external threading was removed from the visualisation), (b) image of the dental pin after the DMLS process

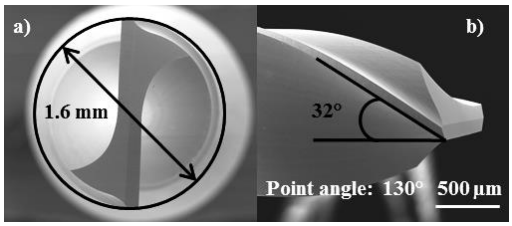

Fig. 2 SEM detail of the drill bit (a) diameter and (b) helix angle

2.3. Micro-drilling experiments

The drilling and threading experiments were carried out on the 5-axis high precision micro-milling machine Micromaster Kugler™, equipped with two spindles, mechanical (100 – 60 000 RPM) and air bearing (20 000 – 180 000 RPM) and with built-in eddy current sensor, which is able to online measure and compensate the spindle axes expansion.

The drilling experiments were carried out on samples of DMLS Ti6Al4V using tungsten carbide uncoated drill bits of 1.6 mm diameter. Fig. 2 shows the geometry of the tool. Each tool was inspected by means of FEI™ Quanta 400 Scanning Electron Microscope (SEM) before machining, to avoid any possible manufacturing defect. For each experiment a new tool was used, to minimize the influence of wear on the results of interest.

A full factorial design of the experiment was chosen, including two factors (the cutting speed and feed per tooth), both with two and three levels, respectively (Table 1). Each experiment was repeated three times.

Dry cutting conditions were used and a jet of compressed air was applied to facilitate the chips removal from the cutting zone. The hole depth was set constant for all the experiments and equal to 5.8 mm. The peck drilling strategy was chosen with constant One-Step-Feed-Length (OSFL) in order of tenth of the tool diameter as suggested by Kim [8] to improve the tool life and stability of micro-drilling.

2.4. Threading experiments

For the threading operation on the DMLS dental pins a solid micro single point thread mill was used with a diameter of 1.5 mm and 4 flutes. The cutting speed was set to 49 m/min and feed per tooth 2 µm. The two passes strategy was chosen to ensure better geometrical and surface quality under dry lubrication condition.

Table 1. Experimental plan for the drilling experiments.

Cutting speed v_c [m/min]	Feed per tooth f_z [µm]
60	10
60	15
60	20
110	10
110	15
110	20

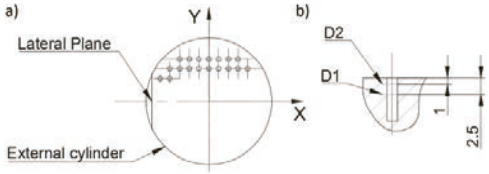

Fig. 3 Sketch of workpiece used for the drillability tests and measuring points D1 / D2 for the hole diameter and cylindricity .

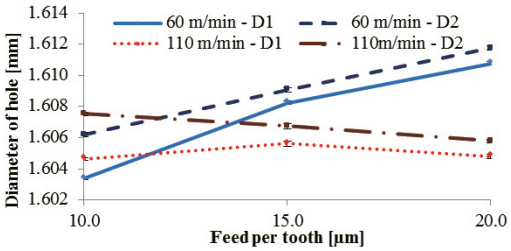

Fig. 4 Diameter of the drilled holes as a function of the feed per tooth.

2.5. Testing methods and standards

With regards to the subsequent threading step and final functionality of the dental pin, the diameter and perpendicularity of the drilled holes are chosen as the most important geometrical parameters to be evaluated, because any deviation would affect the feasibility and final precision of the threading operation. For this reason, a preliminary drillability study was carried out on samples made of DMLS Ti6Al4V whose geometry is shown in Fig. 3a.

The geometry of the drilled holes was measured using a Zeiss Prismo 7 VAST coordinate measuring machine featuring a maximum permissible error (MPE) for length measurements, of 2.2+L/300 µm (L in mm). A single stylus with a 0.6 mm rubidium tip was used. The measurements were carried out in a temperature-controlled room at a nominal temperature of 20°C. Moreover, the workpiece temperature stability was ensured by laying it the measuring room for 24 hours before measuring. To understand the trajectory of the tool during machining and the geometrical quality of the final drilled part the following characteristics were selected: diameter of two different circles (1 mm and 2.5 mm from the top plane, see Fig. 3b), and perpendicularity between the hole axis and the top plane of the workpiece.

The least squares method was used for the extraction of the fitting circles. The alignment was made using the lateral plane (specifically machined for this reason), top plane and external cylinder, as described in Fig. 3a. Mean values and standard deviation were calculated on 5 repetitions.

Due to the small dimensions and internal features, the threaded holes studied in this work were not measurable with conventional measuring systems (e.g. CMMs). Therefore, an innovative measuring procedure was developed for this task by exploiting the internal measurement capabilities of micro-X-ray computed tomography (CT) [9]. Three selected specimens were scanned using a metrological CT system, Nikon MCT225, with micro-focus X-ray source (focal spot resolution down to 3 µm), and temperature-controlled cabinet. The maximum permissible error (MPE) for length measurements, evaluated by tests in accordance to the guideline VDI/VDE 2630-13, is MPE = 9 + L/50 µm (where L is the length in mm).

3. Accuracy of drilling and threading operations

3.1. Drilling performances

In Fig. 4 the measured values of the hole diameters for different cutting speed as a function of the feed per tooth are shown. The maximal standard deviation for all the measurements is in order of hundreds of nanometers. Regardless the cutting speed, D2 appears to be slightly higher than D1. This could be caused by some shape error of the tool (conical shape instead of perfect cylinder) or tool tip runout, in any case further investigations are necessary to confirm or reject any of the theories.

Fig. 5 shows the measured values of the holes perpendicularity for the different cutting conditions. Except for the feed per tooth equal to 10 µm, the cutting speed of 60 m/min assures slightly better results than the highest cutting speed. Drilling and burrs

A qualitative analysis of the burrs was made acquiring the entrance burrs through SEM. In drilling operations the generated exit burrs are higher than the entrance ones and represent a bigger problem for the subsequent assembly operations [9,10]. The burr size is function of the workpiece material and cutting condition.

In the case proposed in the paper blind holes are drilled, therefore only the evaluation of the entrance burrs is required. Fig. 6 shows burrs obtained using different cutting conditions. From the figure it is evident that there are no significant differences in the burrs shape and size for all the tested cutting conditions.

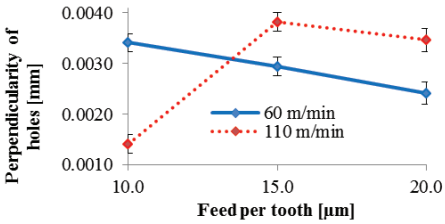

Fig. 5 Perpendicularity of the drilled holes as a function of the feed per tooth. Th maximal standard deviation for all measurements is in order of hundreds of nanom

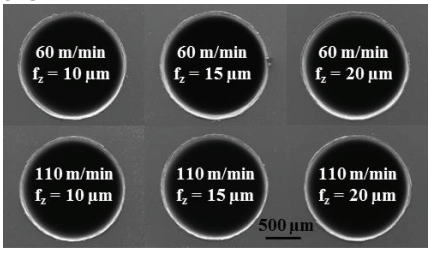

Fig. 6 Top burrs after drilling operation.

The confocal optical profiler Sensofar™ PLμ Neox was used to acquire the scans of burr height that were later measured at 10 independent cross sections and the mean value calculated. The height of the burrs is between 2.5 and 3 μm for all the cutting conditions, without any evident trend in the burr height as a function of the cutting conditions. This might be explained by the fact that during the peck drilling most of the burrs were removed.

3.2. Threading performances

The threading operation is the last machining step. The thread is a functional feature as it ensures the connection between the dental pin and the implant. If the thread is not correct the functionality of the pin can be deteriorated.

To ensure the best possible conditions for the final threading operation, the best cutting conditions for the drilling (cutting speed and feed) were chosen on the basis of the previously described drillability tests. In the case presented in the paper, a cutting speed of 60 m/min and a feed per tooth equal to 10 μm were chosen, which were considered to be the best trade-off between precision of the drilled diameter and perpendicularity of the hole. Regarding the burrs, as no significant difference can be appreciated for the different cutting conditions, they were not considered for the choice of the best drilling parameters.

Further work is needed to determine the CT measurement uncertainty for the specific measurement task. A previous study [12] has demonstrated that dimensional measurements using metrological CT systems can reach sub-voxel accuracy. The resolution related to the voxel size of the reconstructed volume (Fig. 7 (a)) is equal to (12 μm^3).

Table 2. Average results obtained by CT measurements of three specimens machined using the same process parameters (v_c = 60 m/min, f = 10 μm).

Measurand	Average
Minor diameter [mm]	1,617
Int. cylinder form error [mm]	0,033
Major diameter [mm]	1,953
Ext. cylinder form error [mm]	0,018
Depth [mm]	5,839
Pitch [mm]	0,400
Angle [deg]	59,84

From the CT reconstructed volume, the quality assessment of internal thread machining was achieved by performing dimensional measurements of depth, minor and major diameters, pitch and angle as shown in Fig. 7 (b). For each specimen, the internal and external cylinders were created by least-squares fitting and a total of 16 pitches and 16 angles were measured considering two different sections (0° and 90°) of the CT volume. The alignment was done with respect to the internal cylinder axis. The obtained average measurement results are reported in Table 2.

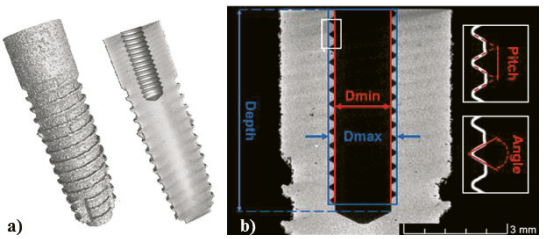

Fig. 7 (a) 3D volume obtained by X-ray computed tomography (b) Schematic representation of the dimensional measurements performed in the CT .

4. Concluding remarks

Drillability experiments were carried out on samples of DMLS Ti6Al4V, in order to qualify the best cutting conditions for drilling high precision holes, which were identified in a cutting speed of 60 m/min and feed per tooth of 10 μm. These parameters were used to drill high precision holes before threading, being the latter needed to manufacture the functional feature that ensure the fixture between upper part of a dental pin implant and the human jaw. It is proved that by choosing a proper set of drilling parameters, the subsequent threading can assure high accuracy geometrical quality.

References

[1] P. Bartolo, J.-P. Kruth, J. Silva, G. Levy, A. Malshe, K. Rajurkar, M. Mitsuishi, J. Ciurana, and M. Leu, "Biomedical production of implants by additive electro-chemical and physical processes," *CIRP Ann. - Manuf. Technol.*, vol. 61, no. 2, pp. 635–655, Jan. 2012.

[2] T. Traini, C. Mangano, R. L. Sammons, F. Mangano, a Macchi, and a Piattelli, "Direct laser metal sintering as a new approach to fabrication of an isoelastic functionally graded material for manufacture of porous titanium dental implants.," *Dent. Mater.*, vol. 24, no. 11, pp. 1525–33, Nov. 2008.

[3] O. L. a. Harrysson, O. Cansizoglu, D. J. Marcellin-Little, D. R. Cormier, and H. a. West, "Direct metal fabrication of titanium implants with tailored materials and mechanical properties using electron beam melting technology," *Mater. Sci. Eng. C*, vol. 28, no. 3, pp. 366–373, Apr. 2008.

[4] L. E. Murr, S. a Quinones, S. M. Gaytan, M. I. Lopez, a Rodela, E. Y. Martinez, D. H. Hernandez, E. Martinez, F. Medina, and R. B. Wicker, "Microstr. and mech. beha.of Ti-6Al-4V prod. by rapid-layer manuf., for biomed. applic.," *J. Mech. Behav. Biomed. Mater.*, vol. 2/1, pp.20–32, 2009.

[5] Y. Yan, G. L. Nash, P. Nash, "Effect of density and pore morph.on fatigue properties of sintered Ti–6Al–4V," *Int. J. Fatigue*, vol. 55, pp.81–91, 2013.

[6] T. Özel, T. Thepsonthi, D. Ulutan, B. Kaftanoğlu, "Experiments and finite elem. sim. on micro-milling of Ti–6Al–4V alloy with uncoated and cBN coated micro-tools," *CIRP Ann. - Manuf. Tech.*, vol. 60/1, pp. 85–88, 2011.

[7] L. Facchini, "Microstructure and mechanical prop. of biomedical alloys produced by Rapid Manu.techniques," Univeristy of Trento, Italy, 2010.

[8] D. W. Kim, Y. S. Lee, M. S. Park, and C. N. Chu, "Tool life improvement by peck drilling and thrust force monitoring during deep-micro-hole drilling of steel," *Int. J. Mach. Tools Man.*, vol. 49/3–4, pp. 246–255, 2009.

[9] J.-P. Kruth, M. Bartscher, S. Carmignato, R. Schmitt, L. De Chiffre, and A. Weckenmann, "Computed tomography for dimensional metrology," *CIRP Ann. - Manuf. Technol.*, vol. 60, pp. 821–842, 2011.

[10] L. Pilný, L. De Chiffre, M. Píška, and M. F. Villumsen, "Hole quality and burr red.in drilling al sheets," *CIRP J. Manuf. Sci. Technol.*, vol. 5/ 2, pp. 102–107, 2012.

[11] D. A. Dornfeld, J. S. Kim, H. Dechow, J. Hewson, and L. J. Chen, "Drilling Burr Formation in Titanium Alloy, Ti-6Al-4V," *CIRP Annals - Manufacturing Technology*, vol. 48, no. 1. pp. 73–76, 1999.

[12] S. Carmignato, "Accuracy of industrial computed tomogr. meas. experim.results from an internat.comparison," *CIRP Ann.*, vol. 61/1, pp 491–494, 2012.

Performances of precision drilling carried out on wrought and Additive Manufactured Ti6Al4V

Z. Rysava[1], S. Bruschi[1], F. Medeossi[1], E. Savio[1]
[1] University of Padua, Padua, Italy

Abstract
In this study, blind holes of 1.6 mm diameter and 5.8 mm depth were drilled on wrought and DLMS (direct metal laser sintered) AM (additive manufactured) Ti6Al4V under dry cutting conditions. A full factorial design of experiments with two factors, cutting speed and feed per tooth, was used. Geometrical features influencing consequent operations (diameter and perpendicularity) were measured. Burrs formation is evaluated as well. The influence of the Ti6Al4V initial state (AM versus wrought) on the holes geometrical quality is discussed. Results prove that the lowest values of the cutting speed and feed rate are the best trade-off regardless the Ti6Al4V as-delivered conditions.

Keywords:
Precision drilling, Additive manufacturing, Ti6Al4V

1 INTRODUCTION

The biomedical industry is a market touching the everyday life as it produces prostheses to improve the human life quality. Starting from the 18th century (first hip implant), the history of medical implants is long and characterized by continual improvements as the science and knowledge are developing too. Nevertheless, the current life time of an implant is only about 10–15 years [1]. Stress shielding is in fact one of the major problems leading to the implant failure, being characteristic when high modulus materials are used, the stresses transferred to bone are low and, thus, due to the bone resorption (natural process of bone remodelation), the new bones become weaker, which can finally lead to the aseptic loss of the implant [2–4].

Some of the above mentioned issues can be partially overcomed using titanium alloys, in particular the Ti6Al4V, which is one of the mostly used metal alloys for biomedical applications, thanks to its excellent biocompatibility, osseointegration, corrosion resistance and specific strength [1,4]. Ti6Al4V implants are usually produced through forming processes at elevated temperature followed by rough and finishing machining operations, polishing and heat treatment. However, this conventional manufacturing procedure builds on high material use requirements and costs. Furthermore, it cannot accomplish the increasing demand for customized implants. On the contrary, the emerging Additive Manufacturing (AM) technologies can represent a suitable way to simplify the conventional process chain of producing implants, being also able to tailor either full dense or porous structures to ameliorate the contact between the human tissues and the implant surface [1–4]. Parts made by AM are net- or near-net shape, needing only semi-finishing or finishing machining operations on functional surfaces, therefore reducing the material waste and costs [6] (in the case of a knee implant, the material waste due to machining can reach up to 80% [2]).

In this paper the drillability of Ti6Al4V samples produced by means of the Direct Metal Laser Sintering (DMLS) AM technique was studied under dry cutting conditions, as ideally no cutting fluid should be used to assure the highest cleanliness of the final product. Precision drilling experiments were carried on a micro-milling machine using the drillability of the wrought Ti6Al4V as a baseline. Both the geometry of the generated holes and their surfaces were measured as well as the burrs formation was evaluated. A microstructural analysis of the machined surface layer was carried out in order to evidence any microstructural refinement compared to the as-delivered structure.

2 EXPERIMENTS

2.1 Case study – dental pins

The case study this research refers to is the machining of high precision geometrical features on dental pins manufactured through the DMLS technology (Figure 1 (B) on the right). As the dental pins are to be screwed directly into the jaw, their function is to ensure the connection between the jaw and the upper part of the implant (abutment and crown). The CAD model of a dental pin ready for the assembly is shown in Figure 1 (A) on the left: on the as-built DMLS part a high-precision hole has to be machined whose quality will influence the precision of the following internal threading and final assembly, thus the overall functionality of the dental pin. The surface of the external thread produced by DMLS does not require any machining, as its rough surface will ensure a good osseointegration.

In particular, the precision drilling of blinded holes that are preparatory holes for the following threading will be studied in the paper, using different cutting parameters.

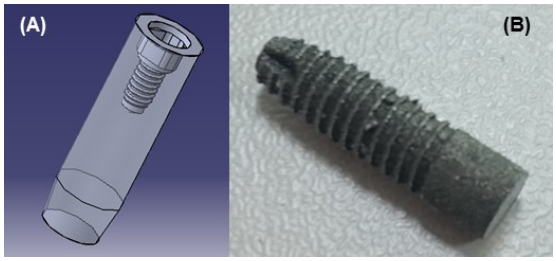

Figure 1: (A) CAD model of the dental pin before assembly, (B) as-built DMLS dental pin

2.2 DMLS versus wrought Ti6Al4V

The Ti6Al4V titanium alloy studied in this work was delivered in two conditions, namely wrought and produced by the DMLS technology. The latter permits to create a fully dense material with a very fine martensitic microstructure consisting of only α (hcp) grains as a consequence of the large undercooling undergone by the material during the process itself. The wrought materials presents a globular structure with α (hcp) and β (bcc) grains [7]. Figure 2 shows both the microstructures.

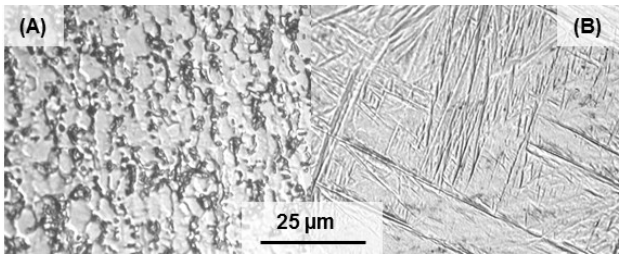

Figure 2: As-delivered microstructures: (A) wrought, (B) as-built DMLS

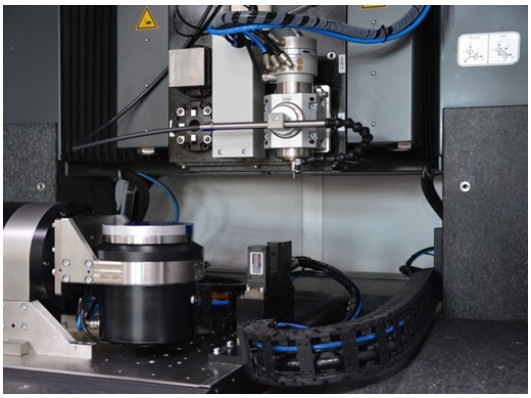

Figure 3: Detail of high precision micro milling machine Micromaster Kugler™

2.3 Precision drilling experiments

The precision drilling experiments were carried out on the 5-axis high precision micro-milling machine Micromaster Kugler™ (Figure 3). The experiments were carried out on both DMLS and wrought Ti6Al4V samples. Tungsten carbide uncoated drill bits of 1.6 mm diameter were used for all the experiments (details of the geometry in Figure 4). Each tool was inspected before machining, to avoid the effect of any possible manufacturing defect on the experiments outcomes. For each experiment a new tool was used, to minimize the influence of its wear.

For each tested material, a full factorial design of experiments was chosen, consisting of two factors, namely the cutting speed and feed per tooth, with two and three levels, respectively (Table 1). Each experiment was repeated three times. Dry cutting conditions were used for all the experiments, with the application of a jet of compressed air to facilitate the chips removal during drilling. The holes depth was set constant for all the experiments and equal to 5.8 mm. The peck drilling strategy was chosen with constant One-Step-Feed-Length (OSFL) in order of tenth of the tool diameter as suggested by Kim [8] to improve the tool life and drilling stability.

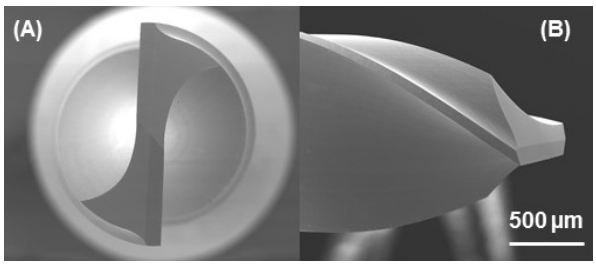

Figure 4: (a) Top view and (b) side view of the uncoated tungsten carbide drill bit

Table 1: Experimental plan carried out on both the as-delivered Ti6Al4V microstructures

	v_c [m/min]	f_z [µm]
S1	60	10
S2	60	15
S3	60	20
S4	110	10
S5	110	15
S6	110	20

3 RESULTS

3.1 Geometrical features of the drilled holes

After drilling, the holes geometrical features were measured, namely their diameter and perpendicularity with respect to a reference plane, having these two geometrical features the highest impact on the precision of the consecutive threading operation and final assembly.

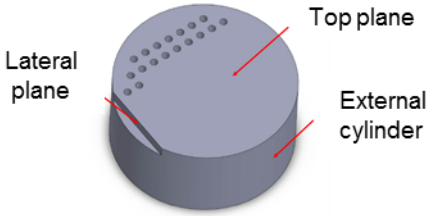

Figure 5: Sketch of the workpiece used for the tests and references used for the measurements

The geometry of the drilled holes were checked using a coordinate measuring machine (Zeiss Prismo 7 VAST with a Maximum Permissible Error of 2.2+L/300 µm, L in mm). A single stylus with a 0.6 mm rubidium tip was used. Thermal stability was ensured by laying the workpiece in the measuring room for a minimum of 12 hours before inspection. The temperature inside the measuring room was controlled and fixed at the standard reference temperature value of 20 °C to minimize measuring uncertainty. To check the geometrical quality of the holes the following characteristics were selected: the hole diameter (measured as cylinder, acquiring points in three circles at 1 mm, 2.5 mm and 4 mm from the top plane of the workpiece, see Figure 5) and the perpendicularity between the cylinder axis and the top plane of the workpiece. On the basis of the ratio between the radius of the tip and the measured diameter, according with the relevant ISO standards [9], a UPR (Undulation Per Revolution) filter parameter of 50 was applied. The least squares method was used for the extraction of the fitting cylinder.

Part alignment was based on the lateral plane, top plane and external cylinder (see Figure 5). The mean values and standard deviations were calculated on the basis of 5 repetitions.

Figure 6 shows the graph of the hole diameter as a function of the cutting conditions and Ti6Al4V as-delivered conditions. It is visible that the for the lowest value of the feed per tooth the variation in between measured values is only in order of 0.002 mm for the different material samples and cutting speeds. The difference between nominal and measured values is between 4 and 6 µm. Once the feed per tooth increases, the difference between the nominal and measured hole diameters increases too in the case of the DMLS material at the lowest cutting speed, whereas at the highest cutting speed the difference remains almost constant. In the case of the wrought material, the difference decreases at increasing feed per tooth regardless the cutting speed.

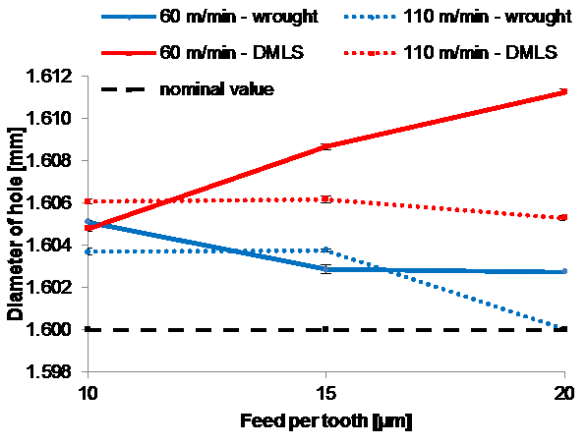

Figure 6: Diameter of the drilled holes as a function of the feed per tooth, cutting speed and Ti6Al4V as-delivered condition

Figure 7 shows the perpendicularity of the drilled holes with respect to the top plane as a function of the cutting conditions and Ti6Al4V as-delivered conditions. The hole drilled on the wrought Ti6Al4V at a cutting speed of 60 m/min exhibits the highest deviation from perpendicularity compared to the other tested combinations. Except for the latter case, the influence of the feed per tooth appears negligible, being the cutting speed the most significant factor. The best combination of cutting conditions in the range of the tested values includes the lowest feed per tooth and highest cutting speed, regardless the Ti6Al4V as-delivered conditions.

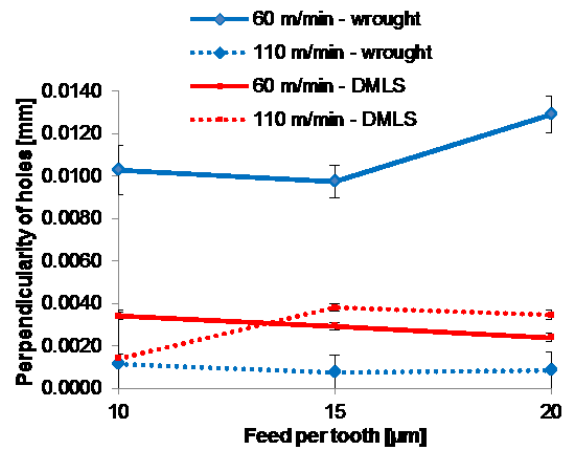

Figure 7: Perpendicularity of the drilled holes as a function of the feed per tooth, cutting speed and Ti6Al4V as-delivered condition

3.2 Burrs analysis

As deburring is a complicated operation especially in case of small features and the presence of burrs is problematic for assembly, the presence of burrs represents a major issue to be faced [10,11]. Therefore, it is highly recommended to minimise burrs formation by choosing appropriate cutting conditions.

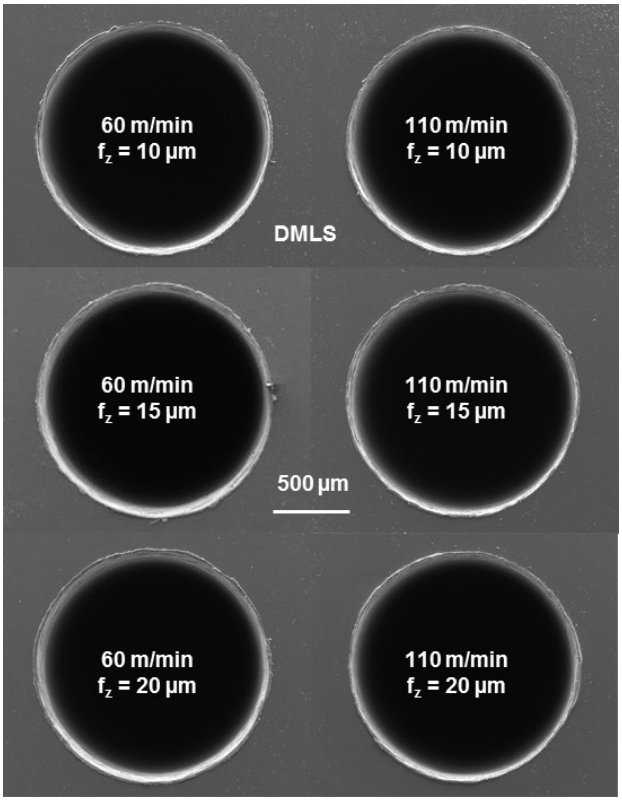

Figure 8: Entrance burrs after drilling the DMLS Ti6Al4V

The burrs were qualitatively analyzed by means of the FEI™ Quanta 400 Scanning Electron Microscope (SEM). Figs. 8 and 9 shown the entrance burrs after drilling the holes for the DMLS and wrought Ti6Al4V, respectively. The reported images clearly show that there are no significant differences in the burrs shape and size for all the tested conditions.

Besides the qualitative analysis, the burrs height was acquired by means of the confocal optical profiler Sensofar™ PLµ Neox. Ten independent cross sections were measured and the mean values calculated. The height of the burrs was found to be between 2.5 and 3.4 µm in the case of the DMLS material and between 1.2 - 2.0 µm in the case of the wrought one.

There is not any evident trend in the burrs height, shape or distribution as a function of the cutting parameters. This might be explained by the fact that the peck drilling approach was used in this study, which might remove most of the burrs.

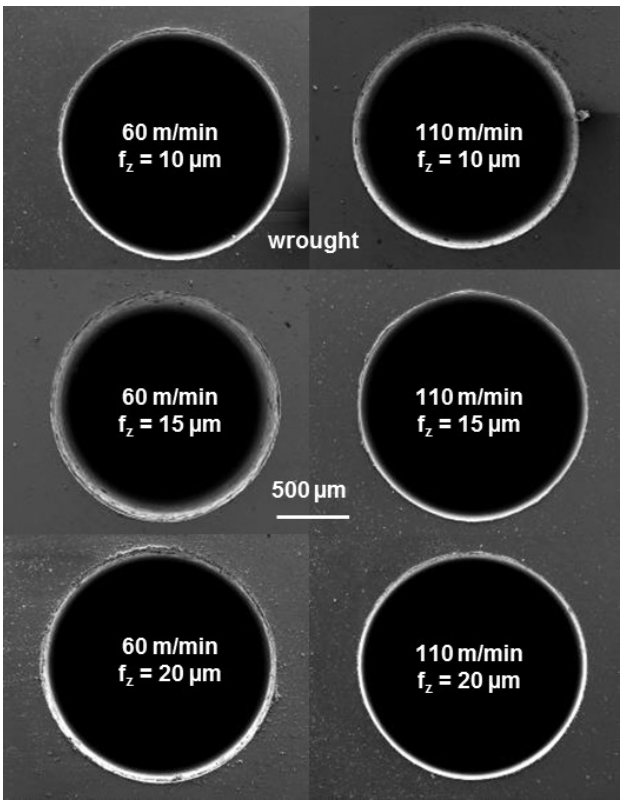

Figure 9: Entrance burrs after drilling the wrought Ti6Al4V

3.3 Profile roughness of the drilled holes

For the evaluation of the surface finish the sample was machined again (the workpiece was cut to open the drilled holes for further roughness measurements) after the evaluation of the geometrical quality. The holes were sectioned parallel to their axis in order to check their surface roughness with the Sensofar™ PLµ Neox. A confocal objective with a magnification of 20x and numerical aperture of 0.5 was used. In order to check most part of the hole surface, two topographies were acquired for each hole, one at 1 mm and the other at 3 mm from the top plane. The roughness parameters were extracted selecting 5 different profiles for each topography. The evaluation of the surface parameters was made with SPIP™ software from Image Metrology and the choice of filter parameters was developed according to ISO standards [12]. Figure 10 shows an example of the obtained surface topography after form correction, while in Figure 11 an extracted profile is shown.

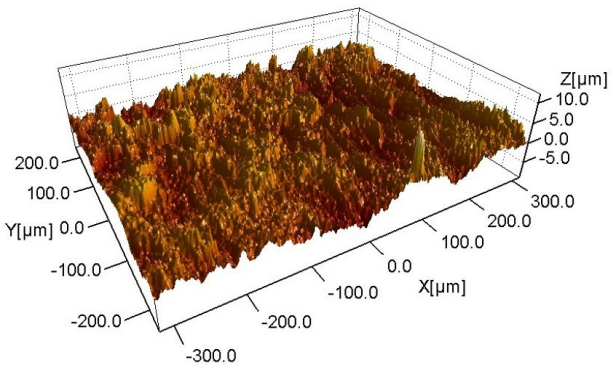

Figure 10: Example of a measured topography processed with the SPIP™ software

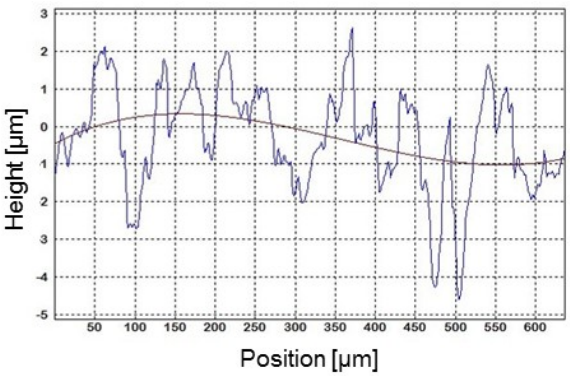

Figure 11: Example of an extracted roughness profile processed with the SPIP™ software

Figure 12 shows the roughness Ra for both the tested microstructure (wrought and DMLS) as a function of the cutting conditions. All the values are situated between 43 – 60 µm and no clear trend can be found as a function of the cutting conditions. The strategy of peck drilling with the choice of one-step feed-length could have impact on Ra through the feed rate and further investigations of OSFL's importance should be carried out.

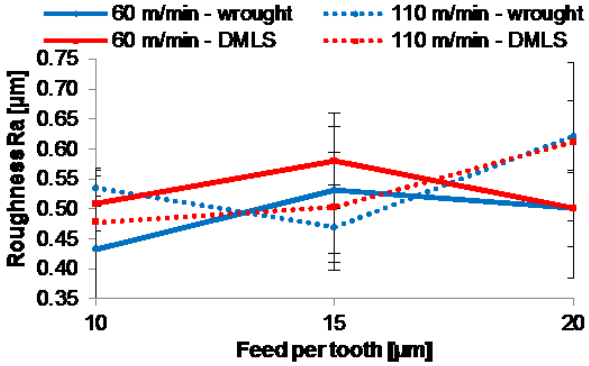

Figure 12: Roughness Ra as a function of the feed per tooth, cutting speed and Ti6Al4V as-delivered condition

3.4 Microstructure analysis

Finally, the samples were metallographically prepared, to observe the microstructure of the layer under the machined surface. The samples were ground using sandpapers, polished using solution of silica and finally etched using the Kroll's reagent.

Figure 13 shows the microstructures of the drilled hole wall. In the case of the wrought sample, some refining of the grains close to the edge can be seen, being the machined-affected layer in order of few tens of microns. On the other hand, in the case of the DMLS sample, there is not any evident affected layer. The rough appearance of the wall edges is likely due to the grinding, which provoked the breaking and falling apart of the grains of martensitic DMLS microstructure.

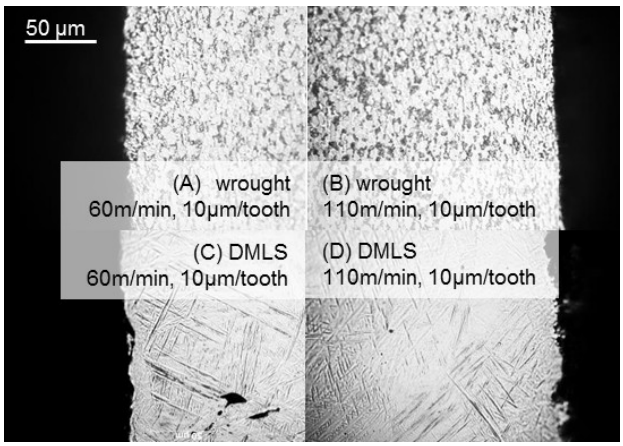

Figure 13: Microstructure after drilling, in the case of the lowest feed per tooth (10µm). (A) wrought material, v_c=60m/min, (B) wrought material, v_c=110m/min, (C) DMLS, v_c=60m/min, (D) DMLS, v_c=110m/min

4 CONCLUDING REMARKS

This paper presented and compared the performances of precision drilling carried out on the Ti6Al4V titanium alloy delivered in two microstructural states, namely wrought and DMLS. As the drilled hole diameter and its perpendicularity with respect to the reference plane are the geometrical parameters mostly affecting the subsequent threading operation and final assembly, they were measured and analysed together with the burrs formation, profile roughness and microstructure alteration of the sub-surface layer after drilling. Given the strategy of peck drilling with one-step feed-length, the best combination of cutting parameters was represented by the lowest feed per tooth and cutting speed within the investigated ranges. Regarding the Ti6Al4V initial microstructure, the wrought material showed slightly better performances compared to the DMLS one. This was expected, as the DMLS material is characterised by martensitic microstructure that is expected to have poor machinability characteristics.

5 REFERENCES

[1] O. L. a. Harrysson, O. Cansizoglu, D. J. Marcellin-Little, D. R. Cormier, and H. a. West, “Direct metal fabrication of titanium implants with tailored materials and mechanical properties using electron beam melting technology,” *Mater. Sci. Eng. C*, vol. 28, no. 3, pp. 366–373, Apr. 2008.

[2] L. E. Murr, S. a Quinones, S. M. Gaytan, M. I. Lopez, a Rodela, E. Y. Martinez, D. H. Hernandez, E. Martinez, F. Medina, and R. B. Wicker, “Microstructure and mechanical behavior of Ti-6Al-4V produced by rapid-layer manufacturing, for biomedical applications.,” *J. Mech. Behav. Biomed. Mater.*, vol. 2, no. 1, pp. 20–32, Jan. 2009.

[3] T. Traini, C. Mangano, R. L. Sammons, F. Mangano, a Macchi, and a Piattelli, “Direct laser metal sintering as a new approach to fabrication of an isoelastic functionally graded material for manufacture of porous titanium dental implants.,” *Dent. Mater.*, vol. 24, no. 11, pp. 1525–33, Nov. 2008.

[4] P. Bartolo, J.-P. Kruth, J. Silva, G. Levy, A. Malshe, K. Rajurkar, M. Mitsuishi, J. Ciurana, and M. Leu, “Biomedical production of implants by additive electro-chemical and physical processes,” *CIRP Ann. - Manuf. Technol.*, vol. 61, no. 2, pp. 635–655, Jan. 2012.

[5] T. Özel, T. Thepsonthi, D. Ulutan, and B. Kaftanoğlu, “Experiments and finite element simulations on micro-milling of Ti–6Al–4V alloy with uncoated and cBN coated micro-tools,” *CIRP Ann. - Manuf. Technol.*, vol. 60, no. 1, pp. 85–88, Jan. 2011.

[6] Y. Yan, G. L. Nash, and P. Nash, “Effect of density and pore morphology on fatigue properties of sintered Ti–6Al–4V,” *Int. J. Fatigue*, vol. 55, pp. 81–91, Oct. 2013.

[7] L. Facchini, “Microstructure and mechanical properties of biomedical alloys produced by Rapid Manufacturing techniques,” Univeristy of Trento, Italy, 2010.

[8] D. W. Kim, Y. S. Lee, M. S. Park, and C. N. Chu, “Tool life improvement by peck drilling and thrust force monitoring during deep-micro-hole drilling of steel,” *Int. J. Mach. Tools Manuf.*, vol. 49, no. 3–4, pp. 246–255, 2009.

[09] ISO 12181-2:2011, Geometrical Product Specification (GPS) - Roundness, Part 2: Specification operators. ISO, Geneva, 2011.

[10] L. Pilný, L. De Chiffre, M. Píška, and M. F. Villumsen, “Hole quality and burr reduction in drilling aluminium sheets,” *CIRP J. Manuf. Sci. Technol.*, vol. 5, no. 2, pp. 102–107, Jan. 2012.

[11] D. A. Dornfeld, J. S. Kim, H. Dechow, J. Hewson, and L. J. Chen, “Drilling Burr Formation in Titanium Alloy, Ti-6Al-4V,” *CIRP Annals - Manufacturing Technology*, vol. 48, no. 1. pp. 73–76, 1999.

[12] ISO 4288:1996, Geometrical Product Specification (GPS) - Surface Texture: rules and procedures for the assessment of surface texture. ISO, Geneva, 1996.